The Detection and Management of Space Resources

by

Kevin M. Hubbard

A Dissertation Presented in Partial Fulfillment
of the Requirements for the Degree
Doctor of Philosophy

Approved March 2023 by the
Graduate Supervisory Committee:

Linda Elkins-Tanton, Chair
Philip Christensen
Steven Semken
Thomas Sharp
Joseph O'Rourke
Melissa De Zwart

ARIZONA STATE UNIVERSITY

May 2023

ABSTRACT

Identifying space resources is essential to establish an off-Earth human presence on the Moon, Mars, and beyond. One method for determining the composition and mineralogy of planetary surfaces is thermal infrared emission spectroscopy. I investigated this technique as a potential tool to explore for magmatic Ni-Cu±PGE sulfide deposits by producing and measuring a 100% sulfide (pyrrhotite) sample derived from the Stillwater Complex. Pyrrhotite violates key assumptions used to calibrate thermal infrared emission data, making extraterrestrial sulfides "appear colder" than their actual physical temperature, and their spectra will contain a negative slope. To derive the absolute emissivity of graybody minerals more accurately, I developed a new measurement technique, which demonstrates that pyrrhotite is spectrally featureless in the mid-infrared and has a maximum emissivity of ~0.7.

Magmatic sulfide deposits are commonly associated with silicates. Thus, emissivity spectra of sulfide/silicate mixtures were acquired to further understand how sulfide prospecting would be conducted on rocky bodies such as Mars. I demonstrate that as sulfide increases, the apparent brightness temperature decreases linearly and, if left unaccounted for, will contribute a negative spectral slope in their emissivity spectra. The presence of sulfide also reduces the magnitude of all the silicate's diagnostic spectral features, which is linear as sulfide increases. A linear retrieval algorithm was also applied to the mixture spectra, demonstrating that sulfide could be detected at abundances of ≥10 modal %.

The main resource being targeted for mining on the Moon is water ice. Thus, a mining map tool of the Lunar South Pole that incorporates temperature, illumination,

Earth visibility, and slope data was developed to identify the most suitable locations for water ice mining and establishing bases for operations. The map is also used to assess the mining potential of the Artemis III candidate landing regions. Finally, space mining must be governed, but no framework has yet to be established. I propose a governance structure, notification system, contract system, best mining practices, and area-based environmental regulations to manage water ice mining activities. The Lunar Mining Map Tool's block system is used as a spatial planning tool to administer the governance framework and facilitate management.

ACKNOWLEDGMENTS

The work presented in this dissertation is a culmination of nearly eight years as a student at Arizona State University. I started my Ph.D. journey as a political scientist at the School of Politics and Global Studies and will leave ASU as an expert in geology and planetary science. Throughout this journey, I have met and have been impacted by so many people that I would like to acknowledge. I'd first like to thank my advisor, Linda Elkins-Tanton, for believing in me and supporting interdisciplinarity in academia. Over the course of my Ph.D. experience, I have witnessed an entire NASA mission unfold, geeked out with astronauts, space experts, artists, and lawyers, walked through an exposed magmatic intrusion, studied volcanoes in Mexico, explored lava tubes, lava flows, and impact craters, partook in space design charrettes, and moved to Europe to work for a foreign space industry. None of this would have happened without you giving me a chance to indulge in my curiosities. Need I remind you about pouring that glass of water on the Moon? We have seven more years to meet that goal!

I'd also like to thank Philip Christensen for shaping me as an infrared spectroscopist. I will never forget the day I saw my first remotely sensed image and I will forever cherish Granite Wash and our 7:00am breakfasts at the Normal Diner. Your teaching inspired me to stick with science and actually made feel like I could learn. I'd also like to express my sincerest gratitude to the rest of my committee (Steven Semken, Thomas Sharp, Joe O'Rourke, Melissa de Zwart) for shaping me into the scientist that I am today. Steve, our trip to the Stillwater Complex was life changing, and my grandfather will forever remember his experience at the Grand Canyon. Tom, please never stop wearing that octahedron. Gosh, your mineralogy class was hard and eye

opening. Joe, thank you for being a great cat dad and a great academic role model. Melissa, thank you for stepping up late in the game.

I'd like to also express my thanks and love to my family who supported me throughout this arduous process. Dad and Mary – Thank you for being great role models and supporting me when I needed it most. I know I haven't always been the easiest son to raise. Lexi and Matt – You are the best siblings ever. Lovins. Aunt Trish and Papa – Thank you for being my foundation for all these years. Molly – You're the best cousin. Good luck in Kansas. Cindy – Thank you for bringing a new light to our family. Finally, to my partner Blake and our family, Nyah and Gerald. I love you so much.

Finally, I am grateful to the following peers, mentors, collaborators, and friends that supported me throughout my PhD: Chris Haberle, Meghan Guild, Steve Dibb, Jon Hoh, Josh Thompson, Roxanne Rodriguez, Lena Heffern, Travis Gabriel, Jon Hoh, Grace Carlson, Matt Steber, Hannah Kerner, Jake Adler, Hannah Bercovici, Mitch Phillips, Nivedita Mahesh, Dylan Gagler, Alireza Bahremand, Bella Breen, Alex Huff, Ed Buie II, Cassie Bowman, Taryn Struck, Sona Seely, Tess Calvert, Steve Ruff, Pete Worden, Jessy-Kate Schingler, Timiebi Aganaba-Jeanty, Becca Dial, Scott Dickenshied and the rest of the JMars team, JAMSA (huzzah!), all my friends and colleagues at Open Lunar, Team Magrathea, Overburden Drilling Management, and my friends in Luxembourg (Liz, Cat, Natalie, and Sven). I'd also like to express a special thanks to Ennis Geraghty, who provided me with priceless knowledge on economic geology, sulfide mineralization, and the Stillwater Complex's J-M Reef. I owe each and every one of you a personal thank you for being there for me. You helped me maintain my self-belief and happiness throughout this journey.

TABLE OF CONTENTS

Page

CHAPTER Page

CHAPTER Page

CHAPTER Page

LIST OF TABLES

LIST OF FIGURES

Figure Page

Figure Page

CHAPTER 1

INTRODUCTION

In the same way that humans on Earth have had to identify, recover, and process local resources for their survival, the identification and utilization of space resources will be even more paramount for the development of a permanent and sustainable human presence on other planetary bodies such as the Moon, Mars, and asteroids. The work presented in this dissertation is motivated by the concept of in-situ resource utilization (ISRU), or the generation of consumables for autonomous or human activities from extraterrestrial materials found on the Moon, Mars, and or other planetary bodies (Anand et al., 2010). If techniques can be developed to identify and process resources in-situ, off-Earth human settlement would become less dependent on supplies from Earth. ISRU is critical because the main barrier to equitable human space exploration and settlement in space is the cost of launching equipment and supplies out of Earth's gravity well. For example, while the cost of liquid oxygen and liquid hydrogen–the two primary components to make rocket fuel–is $1/kg on Earth, transporting that same propellant to the Moon increases its cost by a factor of 36,000 (Kornuta et al., 2019). While companies like SpaceX are reducing the costs of delivering cargo to space, ISRU will also dramatically reduce the costs of off-Earth human settlement because the production of in-situ materials to produce commodities such as propellant, water, and fertilizer will free up space on launch and delivery vehicles for supplies that cannot be produced in space in the near-term.

This dissertation is also motivated by the fact that the development of ISRU will require the same amount of human effort and technological advancement as was required

to successfully send humans to the Moon during the Apollo era. However, if successful, ISRU could accelerate the development of a new space economy. The utilization of space resources is contingent upon the development of an interconnected chain of numerous technologies and processes, including those related to prospecting, site planning, excavation, beneficiation, extraction, purification, additive manufacturing and construction, product storage, power generation delivery, site planning and construction, and waste storage/recycling. The first stage of the ISRU chain, prospecting, is essential since this step identifies the resources that the downstream processes will utilize. In a way, this step has been maturing since the dawn of the space age vis-à-vis orbital and in-situ remote sensing technologies deployed on missions that have characterized our Solar System.

In Chapters 2 and 3, I contribute knowledge to the prospecting stage of ISRU by investigating whether or not it is possible to detect magmatic sulfide ore deposits using a technique known as thermal infrared (TIR) emission spectroscopy. TIR-emission spectroscopy has already been used to map the composition and mineralogy of the surface of Mars, the Moon, asteroid 101955 Bennu, and will soon be used to investigate the surfaces of Jupiter's Moon Europa and the Trojan asteroids. Yet, even though magmatic sulfide deposits are a critical source of the world's iron, nickel, copper, and platinum group metals, very little research has been conducted to determine whether or not sulfide deposits are present on Mars and whether or not they can be identified spectrally. Our experiments only cover the mid-infrared range of the electromagnetic spectrum from 2000-200 cm^{-1} (5–50 μm). I chose to investigate the mid-IR as a potential prospecting tool because at these wavelengths, the emitted energy of the components in

view of an infrared spectrometer is linearly additive (Ramsey and Fink, 1999; Ramsey and Christensen, 1998; Ramsey 1996; Christensen et al., 2000). Thus, if an exposed sulfide ore body can be identified, one may be able to remotely estimate the abundance of sulfide ore bodies on the surfaces of planets.

In Chapter 2, I introduce the Reference Temperature Method, which was developed to estimate the absolute emissivity of graybody minerals, a class of minerals that do not exhibit spectral features in the mid-infrared. The method was developed because this unique class of minerals violates the assumptions inherent in the calibration routines conventionally used in space applications (Ruff et al., 1997). For example, our experiments in chapter 2 demonstrate that the low emissivity of pyrrhotite results in temperature errors and spectral slopes resulting from the physical properties of pyrrhotite, though such errors can be used to differentiate them from other common rock-forming minerals in space. I also demonstrate that using reference samples, the RTM can accurately produce an absolute emissivity spectrum for virtually any mineral, as long as the sample has the same volume and particle size.

Building off our knowledge gained in Chapter 2, Chapter 3 presents a series of laboratory experiments more representative of sulfide prospecting on rocky bodies by acquiring spectral measurements of two physically constructed suites of sulfide/silicate mixtures with varying amounts of sulfide. This chapter demonstrates that while pyrrhotite does not exhibit spectral features, this "ghost mineral" can be detected using TIR-emission spectroscopy at abundances of ≥10 modal %. The experiments demonstrate that one can explore for such deposits spectrally by searching for anomalously cold mafic/ultramafic surfaces whose emissivity spectra exhibit a spectral slope from high to

low wavenumbers. In addition, the spectral features of coexisting silicates will all have severely reduced spectral contrast, and the magnitude of the silicate features decreases linearly as the proportion of sulfide increases.

In Chapter 4, I shift the focus from prospecting for sulfides on Mars to water ice mining on the Moon. A necessary step in the valorization of space resources is reconnaissance and site planning. On the Moon, mining locations are driven by the Moon's environmental conditions. Due to the Moon's topography and small spin axis obliquity relative to the Sun (Hayne et al., 2021), large areas at the poles remain in permanent shadow. These areas are termed 'cold traps' because their temperatures are low enough for volatiles to accumulate and be retained for longer than the age of the Solar System (Watson et al., 1961). Such areas are being targeted in the near future for exploration to determine the lateral and vertical extent of the volatiles (Colaprete et al., 2019; Colaprete, 2021). If the ices are indeed present in economic quantities, value chains will emerge for water ice and other volatiles for in-situ production of O_2 and H_2O for life support and liquid H_2 and O_2 for rocket propellant.

To support an industrial-scale mining venture, operations bases must also be established to supply power, establish communications with Earth, manage a landing complex to deliver mining equipment, and maintain habitats for astronaut crews who will be in charge of maintenance. However, the optimal environmental conditions and geographic locations for establishing an operations base are completely different to mining locations. Such locations must have moderate temperatures, continuous line-of-sight with Earth, and super illumination conditions. Thus, in Chapter 4, I introduce the Lunar Mining Map Tool, which utilizes a "block system" to divide the Lunar South Pole

into a grid of 1 km x 1km blocks. The blocks classify areas on the lunar south pole according to their average slope, maximum summer temperature, percent illumination, and percent Earth visibility. Blocks with suitable temperature conditions to trap volatiles and average slopes navigable by rovers were considered suitable for mining. The blocks with high average percent illumination and Earth visibility, and terrain with average slopes that are flat enough to enable infrastructure construction without significant site planning were considered the best for operations. I also use the map to analyze the mining potential of the Artemis III candidate landing regions.

While ISRU is contingent upon the capacity to detect and access resources and develop the necessary technologies to process them into functional commodities and consumables, the largest obstacles in the development and utilization of space resources are likely social and political in nature. The Moon is an area beyond national jurisdiction, where no sovereign authority's laws and rules apply. However, no intergovernmental governance regime has been proposed to manage lunar mining activities. Without a governance regime to manage lunar resources, universally agreed-upon rules, regulations, and best mining practices and procedures will not be established, increasing the propensity for disputes, degradation of the lunar environment, and depletion of resources. Thus, in Chapter 5, I propose the development of an intergovernmental regime–the Lunar Resource Management Authority (LRMA)–which would be responsible for developing the Moon's resources, safeguarding and sustaining the lunar environment, and ensuring equitable access. To fulfill its management responsibilities, I propose that the LRMA develop a Lunar Mining Code comprised of a notification system to manage prospecting activities, a contract system for issuing temporary but exclusive exploration licenses,

area-based environmental measures to safeguard the lunar environment, regulations to ensure equitable access, and best practices to guide the behavior of future mining operators. The regime is based on the International Seabed Authority, the only intergovernmental regime on Earth responsible for overseeing the development of resources and regulating mining activities beyond national jurisdiction.

Throughout human history, governments have used block systems to divide up and allocate territory to companies in extractive industries (Reina, 2022; Valle, 2023; Daintith and Gault, 1977; Parviainen et al., 2019). While the Lunar Mining Map Tool is used in Chapter 4 to identify the best locations for mining and bases for operations, I demonstrate in Chapter 5 that the block system of the tool can be applied to oversee water ice mining activities and administer our recommended Lunar Mining Code and associated area-based regulations. This governance framework can be a potential solution to encourage investment in lunar resources, standardize how resource rights are afforded to lunar contractors, safeguard the lunar environment, and ensure equitable access.

References

Anand, M., Crawford, I.A., Balat-Pichelin, M., Abanades, S., van Westrenen, W., Péraudeau, G., Jaumann, R., & Sebolt, W. (2010) A brief review of chemical and mineralogical resources on the Moon and likely initial in situ resource utilization (ISRU) applications. *Planetary and Space Science*, 74,42–48.

Christensen, P.R., Bandfield, J.L., Smith, M.D., Hamilton, V.E., & Clark, R.N. (2000). Identification of a basaltic component on the Martian surface From Thermal Emission Spectrometer Data. *Journal of Geophysical Research*, 105(E4),9609-9621.

Colaprete, A., Andrews, D., Bluethmann, W., Elphic, R.C., Bussey, B., Trimble, J., Zacny, K. and J.E. Captain. (2019). An Overview of the Volatiles Investigating Polar Exploration Rover (VIPER) Mission. American Geophysical Meeting, Fall Meeting 2019, ab. #P34B-03.

Colaprete, A. (2021). Volatiles Investigating Polar Exploration Rover (VIPER). NASA.

Daintith, T., & Gault, I. (1977). Pacta Sunt Servanda and the Licensing and Taxation of North Sea Oil Production. *Cambrian Law Review*, 8,27–44.

Hayne, P.O., Aharonson, O., & Schörghofer, N. (2021). Micro cold traps on the Moon. *Nature Astronomy*, 5,169-175.

Kornuta, D., Abbud-Madrid, A., Atkinson, J., Barr, J., Barnhard, G., Bienhoff, D., Blair, B., Clark, V., Cyrus, J., deWitt, B., Dreyer, C., Finger, B., Goff, J., Ho, K. Kelsey, L., Keravala, J., Kutter, B., Metzger, P., Montgomery, L., Morrison, P., Neal, C., Otto, E., Roesler, G., Schier, J., Seifert, B., Sowers, G., Spudis, P., Sundahl, M., Zacny, K., & Zhu, G. (2019). Commercial lunar propellant architecture: A collaborative study of lunar propellant production. *Reviews in Human Space Exploration*, 129(100026),1-77.

Parviainen, T., Lehikoinen, A., Kuikka, S., & Happasaari, P. (2019). Risk frames and multiple ways of knowing: Coping with ambiguity in oil spill risk governance in the Norwegian Barents Sea. *Environmental Science and Policy*, 98,95–111.

Ramsey, M. (1996). Quantitative analysis of geological surfaces: A deconvolution algorithm for midinfrared remote sensing data, Ph.D. dissertation. Pp. 276. Arizona State University.

Ramsey, M. (2004). Quantitative geological surface processes extracted from infrared spectroscopy and remote sensing. In: Molecules to Planets: Infrared Spectroscopy in Geochemistry, Exploration Geochemistry and Remote Sensing. *Mineralogical Association of Canada*, 33,1-17.

Ramsey, M., & Christensen, P.R. (1998). Mineral abundance determination: Quantitative deconvolution of thermal emission spectra. *Journal of Geophysical Research*, 103(B1),577–596.

Ramsey, M., & Fink, J.H. (1999). Estimating silicic lava vascularity with thermal remote sensing: A new technique for volcanic mapping and monitoring. *Bull. Volcanol*, 61,32–39.

Reina, P. (2022). UK Government Expands Offshore Oil Leases in North Sea. Energy News-Record, October 9, 2022. Available at: https://www.enr.com/articles/54953-uk-government-expands-offshore-oil-leases-in-north-sea. Accessed (February 24, 2023).

Ruff, S.W., Christensen, P.R., Barbera, P.W., & Anderson, D.L. (1997). Quantitative thermal emission spectroscopy of minerals: A laboratory technique for measurement and calibration. *Journal of Geophysical Research*, 102(B7),14899–14913.

Valle, B. (2023). Guyana to complete new oil contract model by Q2 as auction looms. Reuters, February 14, 2023. Available at: https://www.reuters.com/business/energy/guyana-kicks-off-oil-conference-exxon-mulls-adding-more-blocks-2023-02-14/. Accessed (February 24, 2023).

Watson, K., Murray, B.C., & Brown, H. (1961). The behavior of volatiles on the lunar surface. *Journal of Geophysical Research*, 66(9),3033–3045.

CHAPTER 2

THERMAL INFRARED EMISSION SPECTROSCOPY OF GRAYBODY MINERALS (SULFIDE): IMPLICATIONS FOR EXTRATERRESTRIAL EXPLORATION FOR MAGMATIC ORE DEPOSITS

Kevin M. Hubbard[1*], Christopher W. Haberle[2], Linda T. Elkins-Tanton[1], Philip R. Christensen[1], and Steven Semken[1]

[1]School of Earth and Space Exploration, Arizona State University, Tempe, AZ, USA,

[2]Department of Astronomy and Planetary Science, Northern Arizona University, Flagstaff, AZ, USA

*Corresponding author. E-mail: k.m.h@asu.edu

Hubbard, K. M., Haberle, C. W., Elkins-Tanton, L. T., Christensen, P. R., & Semken, S. (2023). Thermal infrared emission spectroscopy of graybody minerals (sulfide): Implications for extraterrestrial exploration for magmatic ore deposits. *Earth and Space Science*, 10, e2022EA002641. https://doi.org/10.1029/2022EA002641.

Abstract

Graybody materials exhibit systematically low emissivity across their spectrum. This characteristic violates the key assumption of unit emissivity at some wavenumber in the spectrum used to calibrate thermal infrared emission data. This assumption makes graybody materials "appear colder" than their actual physical temperature and imparts a slope in emission spectra that is non-physical in nature, both of which affect interpretations of planetary surfaces. Pyrrhotite derived from the Stillwater Complex's J-M Reef in Montana, USA exhibits systemic graybody behavior across its mid-infrared

spectrum and thus has a steep negative spectral slope from high to low wavenumbers when calibrated using conventional methods. A new measurement technique is introduced for deriving the absolute emissivity of graybody materials using reference samples with known Christiansen Frequencies during calibration. The reference temperature method significantly reduces the spectral slope of and provides a more accurate estimation of the absolute emissivity of graybody materials. After correcting the temperature of pyrrhotite using results from a series of reference experiments, we conclude that the emission spectrum of pyrrhotite is spectrally featureless and has a maximum emissivity of ~0.7. If sulfide mineral deposits are exposed on Mars, they will not be identified using spectral features found in the mid-infrared (5–40 μm). However, they could be located by identifying basaltic terrain that appears colder than their surroundings and with apparent emissivity spectra that exhibit negative spectral slopes from high to low wavenumbers and are spectrally neutral.

2.1 Introduction

For decades, TIR-emission spectroscopy has proven valuable for analyzing geologic materials from remote platforms and in laboratory settings. Laboratory applications using high-resolution benchtop infrared spectrometers enabled detailed investigations of mineralogy, geochemistry, and the physical properties of rocks, minerals, and soils (Conel, 1969; Christensen, Bandfield, Hamilton, 2000; Hunt & Vincent, 1968; King et al., 2004; Lane, 1999; Maturilli et al., 2008; McMillan, 1985; Moersch, 1992; Moersch & Christensen, 1995; Salisbury, 1993; Salisbury & Estes, 1985; Salisbury & D'Aria, 1992; Salisbury et al., 1991; Shirley & Glotch, 2019; Hamilton,

2000,2010). Results of these studies have been used to constrain ground-truth observations of planetary surfaces acquired by TIR instruments onboard orbiting and landed spacecraft (e.g., Earth (Abrams, 2000; Palluconi & Meeks, 1985), Mars (Altunaiji et al., 2017; Badri et al., 2018; Bandfield, 2002; Christensen, Bandfield, Smith, et al., 2000, 2001; Christensen, Jakosky, et al., 2004; Christensen et al., 1992; Ehlmann & Edwards, 2014; Glotch & Christensen, 2005; Glotch et al., 2004, 2016; Hamilton et al., 2000; Ruff et al., 2022), the Moon (Donaldson Hanna et al., 2014; Greenhagen et al., 2010; Page, 2010; Paige et al., 2010; Shirley & Glotch, 2019; Williams et al., 2017, 2019), Mercury (Hiesinger et al., 2010, 2020), asteroid (101,955) Bennu (Breitenfeld et al., 2021, 2022; Christensen et al., 2018; Hamilton et al., 2019, 2021; Okada et al., 2017), and on the martian surface (Ashley, 2011, Christensen, Wyatt, et al., 2004; Christensen et al., 2003; Hamilton & Ruff, 2012; Haberle et al., 2019; Ruff & Farmer, 2016; Ruff & Hamilton, 2017; Ruff et al., 2006, 2008)).

This research paper presents the results of an investigation to determine if TIR-emission spectroscopy can serve as a prospecting tool for identifying extraterrestrial resource deposits, specifically concentrations of sulfide minerals. On Earth, magmatic sulfide deposits are primary targets for mining since they concentrate critical elements such as Ni, Cu, Co, and the platinum-group elements (PGEs). Because Mars is also a basaltic planet and is predicted to be enriched in S relative to Earth, its extensive magmatic history has also likely exhibited the appropriate conditions to segregate and accumulate sulfides at crustal levels (Greeley & Schneid, 1991; Baumgartner et al., 2015; Burns & Fisher, 1990; West & Clarke, 2010). A lack of thorough investigations for sulfides using remote sensing data might be due to the presumption that they are

challenging to detect because of their lack of deep, narrow absorption bands and that they are susceptible to rapid oxidation from chemical weathering processes. However, in-situ and orbital reconnaissance of impact crater ejecta, central peaks, and bedrock exposures in canyon floors and walls could identify exhumed or exposed sulfide reservoirs for future prospecting. Moreover, future in-situ exploration missions may be able to identify subsurface sulfide deposits via drilling, excavation, or burrowing techniques (Zacny et al., 2008, 2013, 2014; Zhang et al., 2019), where TIR-emission spectroscopy could be used for ore detection, grading, and reserve estimates (Rivard et al., 2001).

This paper also introduces the reference temperature method (RTM), a new calibration and sample measurement methodology for acquiring absolute emissivity measurements of low-emissivity materials and materials lacking the principal Christiansen Frequency (CF). The CF feature is related to the real and imaginary indices of refraction n and k (often referred to collectively as optical constants) and is associated with the Restrahlen Band, the strongest vibrational band of the material (Ruff et al., 1997; Salisbury, 1993; Salisbury & Walter, 1989). It occurs in a wavenumber region where the sample's refractive index (n) undergoes rapid change and approaches that of the surrounding medium (i.e., atmosphere, vacuum) and where the extinction coefficient (k) reaches a local minimum (i.e., atmosphere, vacuum; Conel, 1969). At this location in the electromagnetic spectrum, minimum surface scattering occurs and absorption is low (Conel, 1969), allowing infrared radiation to easily pass through the mineral (Salisbury & Walter, 1989). This results in an emissivity maximum (i.e., reflectance minimum) that is close or equal to unity.

The RTM was initially developed to mitigate issues for measuring highly reflective minerals such as sulfides that exhibit systemic graybody behavior in the mid-infrared, a characteristic that presents difficulties in accurately determining the sample's actual kinetic temperature as well as its emissivity (Bandfield, 2009; Ruff et al., 1997). However, the new technique can also be utilized to estimate the absolute emissivity of virtually any granular material. The RTM effectively reduces uncertainties in sample temperature determination associated with the one-temperature method (OTM) (Christensen & Harrison, 1993; Ruff et al., 1997) by incorporating natural reference samples with known CF features during calibration. After describing the RTM, we present a brief error analysis, examining how the temperature input parameters in our calibration procedure affect the certainty of our absolute emissivity measurements.

Following this analysis, we present newly acquired mid-infrared emissivity spectra from 2,000 to 250 cm^{-1} (5–40 μm) of beneficiated magmatic sulfide derived from the J-M Reef of the Stillwater Complex, a Neoarchean (~2.7 Ga) differentiated mafic to ultramafic layered intrusion located along the northern front of the Beartooth Mountains in south-central Montana (Jenkins et al., 2020; Todd et al., 1982; Zientek et al., 1985). The sample consists of nearly 100% pyrrhotite ($Fe_{(1-x)}S$), which is the most common constituent in magmatic sulfide deposits (Barnes et al., 2017; Vaughan & Lennie, 1991) and thus an appropriate analog sample to use as a reference in future extraterrestrial resource exploration campaigns. The sulfide spectra were calibrated using both the OTM and the RTM to determine how the physical and chemical properties of the material, coupled with assumptions inherent to the OTM, affect the derivation of sample temperature and absolute emissivity. The paper concludes with a discussion of the

implications of these results for future extraterrestrial sulfide mineral deposit exploration and a brief discussion concerning future work.

2.2 The Significance of Sulfide Minerals

Critical elements required to manufacture space electronics, satellite components and alloys used in rocketry systems are found in nearly all rock-forming minerals and will be accessible on all rocky bodies in some amount. However, they are often measured in trace amounts, sometimes at the parts per million/billion level. Under certain conditions, igneous processes create large-scale mineral deposits enriched in iron, nickel, copper, cobalt, and platinum group elements (PGEs; e.g., platinum, palladium, rhodium) that form during the cooling and crystallization of mafic to ultramafic magmas (Barnes & Fiorentini, 2012). These deposits are composed of important ore minerals such as sulfides, PGMs such as Pt-Fe alloys, and Pt-Pd tellurides (Arndt et al., 2005; Barnes, 2006; Cawthorne, 2010; Godel & Barnes, 2008; Lesher, 1989; Maier, 2005; Naldrett, 1999, 2010).

In order for magma to produce an appreciable amount of sulfide to form a mineral deposit, its sulfur budget must exceed the sulfur concentration at sulfide saturation, which is achieved through processes such as fractional crystallization, magma mixing, or the assimilation of crustal materials (e.g., volatiles, sulfur, or siliceous country rock) (Baumgartner et al., 2015; Ding et al., 2014; Jugo, 2009; Liu et al., 2007; Mavrogenes & O'Neill, 1999; Naldrett, 2010; Righter et al., 2009; Ripley & Li, 2013). Once achieved, an immiscible sulfide liquid forms, which scavenges the metals from its parent melt due to it highly chalcophile and siderophile nature (Naldrett, 1999, 2010). The partitioned

metals and sulfide segregate from the parent melt and subsequently accumulate and crystallize at the base of intrusive magma bodies, lava flows, and physical traps in magmatic plumbing systems to form the metal-rich sulfide mineral deposits that are targeted for mining (Arndt et al., 2005; Naldrett, 2010).

Terrestrial nickel-rich sulfide deposits are 5–10 times richer in Ni than the mantle (~1,960 ppm) and ~100–200 times more enriched than the crust (~105 ppm) (Barnes & Lightfoot, 2005; McDonough & Sun, 1995; Taylor & McClennan, 1985). The amount of Ni in nickel-sulfide deposits varies considerably and depends largely on the composition of the silicate magma from which the sulfide liquid segregated from (Barnes & Lightfoot, 2005). Generally, the average concentration of Ni in 100% sulfides derived from deposits with mafic host rocks ranges from ~1 to 6 wt%, while the average wt% Ni from deposits derived from deposits with ultramafic host rocks is in the range of 6–18 wt% (Barnes & Lightfoot, 2005, Table 2).

As is true on Earth, Martian melts also have the capacity to produce sulfide mineral deposits. The sulfur content in the primitive Martian mantle (700–2,000 ppm) (Gaillard et al., 2013; Gaillard & Scaillet, 2009) is estimated to be well above the sulfide content of Earth's mantle (250 ppm) (McDonough & Sun, 1995). However, Martian basalts are more FeO-rich, which increases the amount of sulfur required to induce saturation and produce the immiscible sulfide liquid that forms such deposits (Ding et al., 2014; Righter et al., 2009). While Martian melts are capable of transporting large amounts of sulfur to upper crustal levels, the relatively lower Ni and Cu abun-dances in the mantle compared to Earth may lead to sulfide deposits with lower Ni and Cu tenors (Baumgartner et al., 2015; Wänke et al., 1994).

Due to their highly chalcophile and siderophile nature, the enrichment factor for the PGEs is even more drastic: approximately 1,000 times that of Earth's crust (Barnes & Lightfoot, 2005). The average Pd and Pt concentrations in the upper continental crust are ~0.51 and ~0.52 ppb (Rudnick & Gao, 2003), whereas the Pd and Pt concentra-tions in the upper mantle exhibit ranges of 0.5–6.3 ppb 0.8–7.3 of ppb respectively (Lorand & Alard, 2001; Maier et al., 2012). Reported median values for Pd and Pt in the Upper Critical Zone of the Merensky Reef (Bushveld Complex) are 78 and 21 ppb (Maier & Barnes, 1999; Naldrett et al., 2009), while the average grade of Pd and Pt in the J-M Reef of the Stillwater Complex are 14 and 5 ppm (Ripley et al., 2017; Zientek et al., 2017).

Metals sourced from magmatic sulfide ores have many use cases on Earth (Zientek, 2012), which together generated ~$70 billion in 2013, representing ~7% of total global metal and mineral mine output (Peck & Huminicki, 2016). Moreover, ~60% of the world's nickel (Ni), 23% Cobalt, ~3% Copper (Cu), and >99% of the PGEs (PGE) in the global market are produced from the exploitation and recovery of Ni-Cu-(PGE) magmatic sulfides (Le Vaillant et al., 2016; Naldrett, 2010; Song et al., 2011; Slack et al., 2017). The total value of the metal in the 157 Ni-Cu-PGE major sulfide mining operations has been estimated to be $6.15 trillion (Peck & Huminicki, 2016). Thus, sulfide deposits should make for enticing targets for prospecting, exploration, and extraction as we expand our human presence to Mars.

Orbital and in-situ measurements suggest that the Martian surface is dominated by rocks derived from the mantle that exhibit physical-chemical commonalities with high-temperature komatiitic and ferropicritic volcanism on Earth (Burns & Fisher, 1990: Baumgartner et al., 2015; Filiberto, 2008; Hamilton & Christensen, 2005; Reyes &

Christensen, 1994). Ni-Cu ± PGE sulfide ores are commonly associated with such magmatic rocks (Arndt et al., 2005; Barnes & Fiorentini et al., 2012; Barnes & Lightfoot, 2005; Maier, 2005; Naldrett, 1999, 2010). However, compositional mapping using the Mars Odyssey Thermal Emission Imaging System also identified a diversity of more evolved magmatic materials with higher silica contents, inferring that pyrrhotite-pentlandite-chalcopyrite sulfides might be conceivably found in both mafic and ultramafic rocks at or near the Martian surface (Burns, 1988; Christensen et al., 2005). Because Martian magmas are enriched in FeO, they can transport large amounts of dissolved sulfur to the surface and subsurface (Ding et al., 2014; Haughton et al., 1974; Liu et al., 2007; Righter et al., 2009; Wykes et al., 2015). If Martian mafic to ultramafic magma became saturated in sulfur, immiscible metal-rich sulfide liquids could form, segregate, and crystalize to produce disseminated and massive Ni-Cu ± (PGE) sulfide ore bodies.

2.3 Background on Thermal infrared Emission

Because contact measurements are challenging to make remotely on planetary surfaces and impossible to make from orbit, radiometric techniques have been implemented to estimate the temperature of objects observed in space. These “brightness” temperature observations are crucial to producing TIR-emissivity spectra for characterizing planetary surfaces and will be paramount when prospecting for space resources. The brightness temperature is not the same as the actual physical temperature but instead is a value derived from a material's spectral radiance. In most cases, it is lower than the kinetic temperature measured using a contact measurement such as a

thermometer or a thermocouple due to planetary materials exhibiting non-unit emissivity. To calculate the brightness temperature of an object (i.e., laboratory sample or planetary surface) from its calibrated radiance, one must assume that the material exhibits unit emissivity (ε = 1.0) somewhere in its radiance spectrum. This assumption holds at every wavenumber for a blackbody, meaning its physical temperature can be determined at any wavenumber. For naturally occurring materials, this assumption holds at discrete locations in its spectrum.

In planetary thermal infrared emission spectroscopy, a brightness temperature (T_{bright}) is calculated for a pre-defined wavenumber pair using Equation 1:

$$T_{bright} = \frac{\left(\frac{hc}{k}\right)\tilde{\nu}}{ln[1+\frac{2hc^2\tilde{\nu}^3}{B_{samp}}]} \quad \text{(Equation 1)}$$

where h is Planck's constant, c is the speed of light, k is Boltzmann's constant, $\tilde{\nu}$ represents the wavenumber interval, and B_{samp} represents the observed calibrated radiance value at the corresponding wavenumber. If the object's composition is unknown, a brightness temperature can be calculated across the entire spectral range of the instrument, and the highest derived brightness temperature value is considered the temperature (Ruff et al., 1997).

The highest brightness temperature is commonly found at the CF, which for most rock-forming minerals is a location that satisfies the assumption of unit emissivity ($\varepsilon \cong 1.0$, $R \cong 0.0$). For silicates, the CF is commonly found between ~1,400 and 900 cm^{-1} and is associated with the Reststrahlen Band (Ramsey, 2004). If the CF also coincides with a low extinction coefficient (k), thermal energy easily propagates into and out of the material, leading to an emissivity (ε) maximum at or close to 1.0. This means that the spectral

radiance value at the CF is at or near the blackbody value and is appropriate for approximating the kinetic temperature. But naturally occurring materials are not blackbodies; they can be understood as "selective" radiators that exhibit blackbody character in spectral regions where no fundamental vibrations are present and graybody character when they are present. A material exhibits graybody character when it does not absorb 100% of incident radiation. Thus, a material with systematic graybody radiation follows a Planck function with a constant emissivity that is less than 1.0 (Michelsen et al., 2020).

CF features are present for >95% of the rock-forming minerals in the mid-IR (Salisbury, 1993). They are particularly useful for analyzing planetary surfaces since they are diagnostic of mineralogy, composition, and remain present (though their position does shift slightly) as particle size decreases (Maturilli et al., 2008; Moersch & Christensen, 1995). The CF can be used to distinguish between compositions within a solid solution series and is used to map the silicate mineralogy of planetary surfaces (Ehlmann & Edwards, 2014; Greenhagen et al., 2010; Nash et al., 1993; Rogers & Christensen, 2007). For example, Donaldson Hanna et al. (2012) demonstrate that for plagioclase, the wavenumber position of the CF shifts linearly as a function of composition (An#), suggesting that TIR-emission spectroscopic observations can be employed to map the purity, compositional variation, and abundance of regolith materials derived from the Moon's anorthositic crust (Donaldson Hanna et al., 2014; Hecker et al., 2010; Logan et al., 1973). Hamilton (2010) showed that the CF in emission spectra of the olivine solid solution series shifts to lower wavenumbers with increasing substitution of

Fe for Mg in olivine, further supporting the ability of the technique to detect differences in mineral structure and composition.

An object's emissivity, defined as the ratio between its spectral radiance and a blackbody at the same temperature (Petty, 2006), is determined radiometrically by fitting a Planck radiance spectrum to its calibrated radiance value at the CF. Doing so enables comparison and interpretation of its spectral properties to other measured materials. Figure 2.1 displays the average calibrated radiance of 500–710 μm quartz (SiO_2) and forsteritic olivine (Mg_2SiO_4), which are accompanied by blackbody radiance curves at the derived brightness temperature calculated at their respective CFs. The principal CF positions for quartz and olivine were calculated to be 1,358 and 1,174 cm^{-1} respectively, agreeing with calculations stated in previous research (Bramble et al., 2019; Hamilton, 2010; Salisbury & D'Aria, 1992; Salisbury et al., 1991). Because quartz and forsterite exhibit near-blackbody behavior at their CFs, the brightness temperatures estimated at that region are at or close to their kinetic temperatures, resulting in emissivity spectra devoid of a slope. As seen in Figure 2.2, if the Planck radiance was derived from a wavenumber position that exhibits graybody behavior, such as at locations where a spectral absorption is present, the derived brightness temperature will not represent the physical temperature of the material. This temperature offset would ultimately introduce a systemic negative slope in its derived emissivity spectrum from high to low wavenumbers, complicating interpretations of mineralogy, chemical composition, and grain size (see Section 2.6 below).

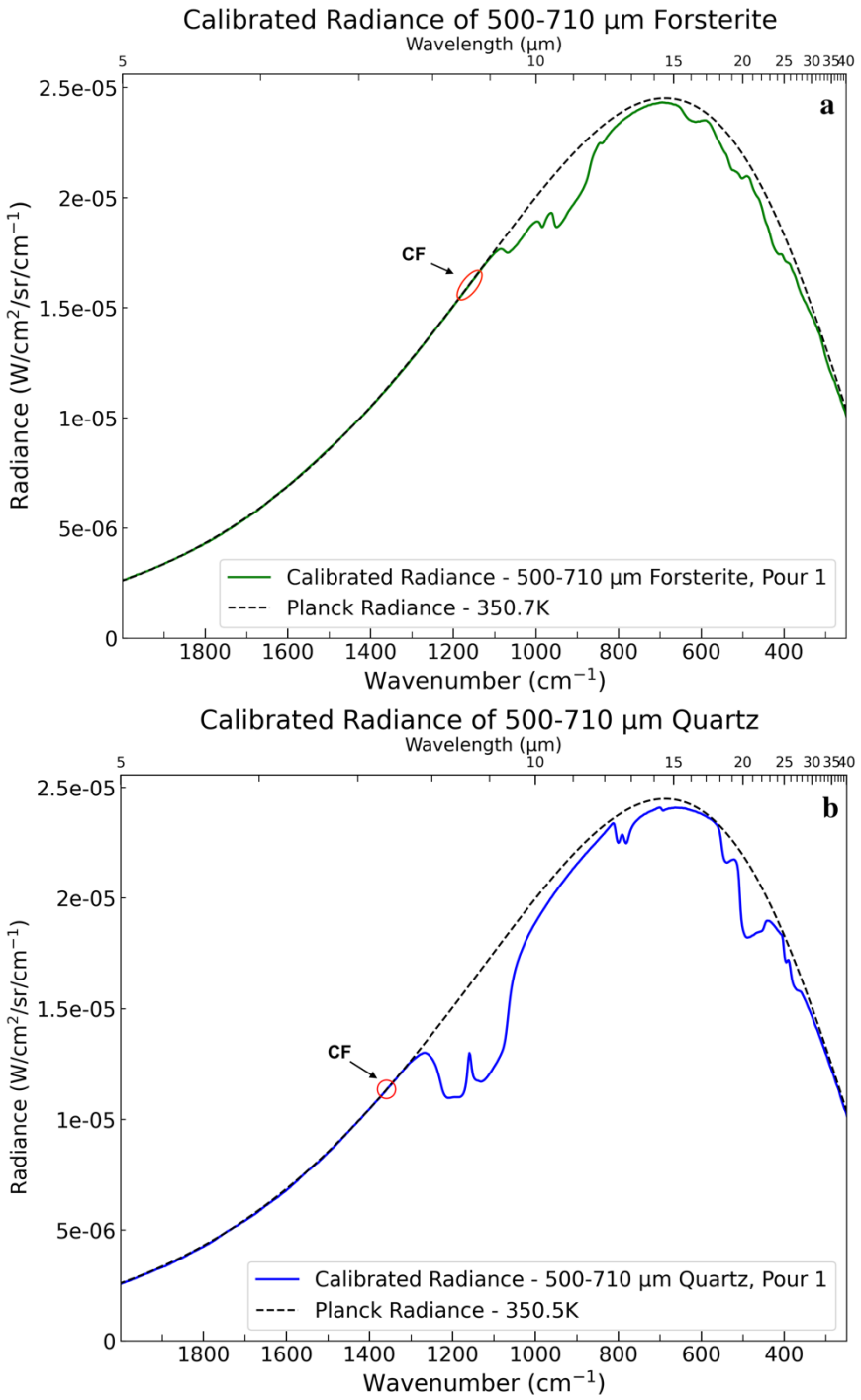

Figure 2.1 – Calibrated radiance and corresponding Planck radiance for forsteritic olivine (a) and quartz (b). The area enclosed in red indicates the wavenumber interval where the CF is present. At this value, the temperature of the sample is estimated by fitting a blackbody radiance spectrum to the calibrated radiance of the mineral. The calibrated radiance spectrum is divided by the blackbody spectrum at the estimated temperature of the sample to compute emissivity.

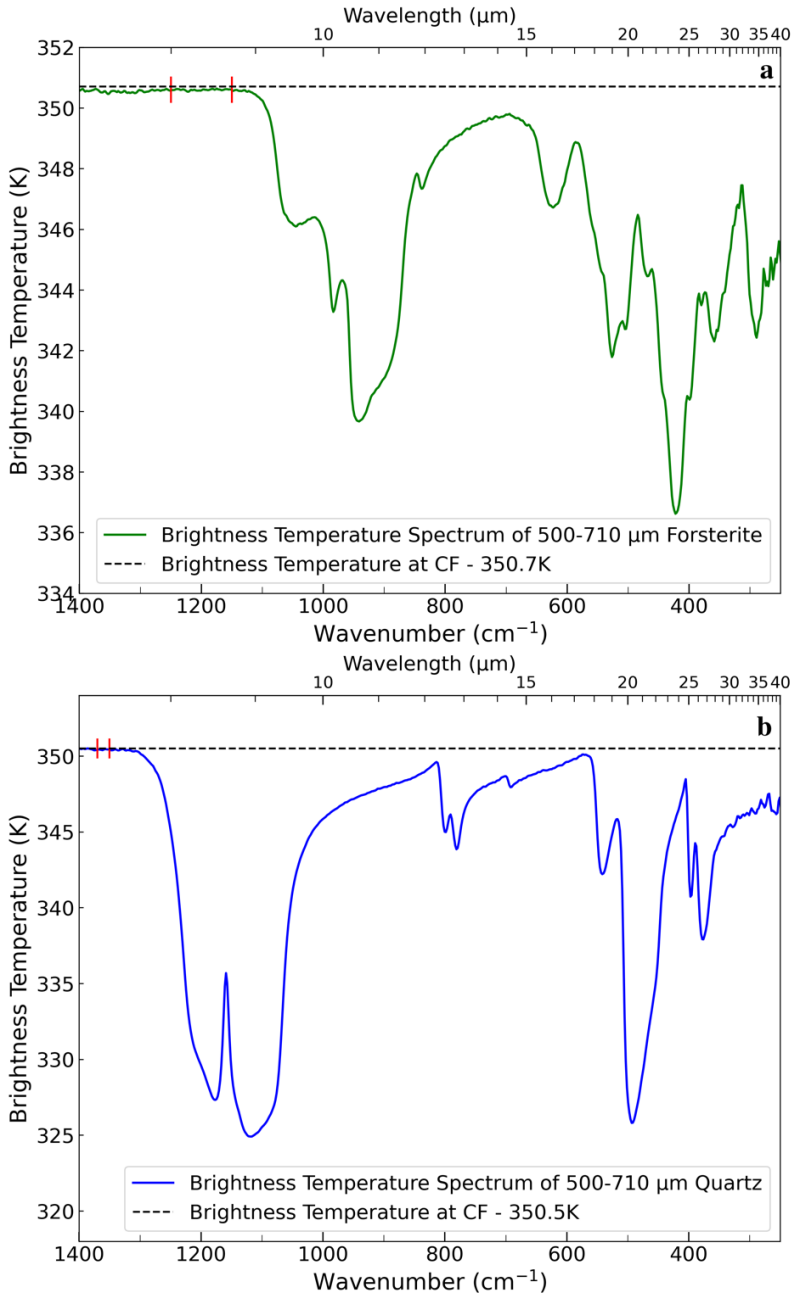

Figure 2.2 – Brightness temperature spectra (in Kelvin) for forsterite (a) and quartz (b). The vertical red lines indicate the wavenumber region where the Christiansen Frequency (CF) was estimated, and the kinetic temperature of the sample was determined. The horizontal black line represents a blackbody's brightness temperature spectrum at the estimated kinetic temperature of the sample determined at the CF. The difference in temperature estimated at the CF versus at a graybody region in the spectrum reveals the significance of a CF for accurately determining the physical temperature of the sample. Without a CF, it would be impossible to remotely determine the kinetic temperature in space.

2.4 Sample Preparation

2.4.1 Sulfide Endmember

On Earth, pyrrhotite (Fe1-xS) is the most abundant sulfide mineral found in mafic and ultramafic sulfide ore deposits. It typically co-exists with pentlandite ((Fe,Ni)9S8), chalcopyrite (CuFeS2), and in some cases, concentrations of PGE-rich sulfides (Jenkins et al., 2020; Vaughan & Corkhill, 2017). Thus, it is a likely indicator mineral for detecting a sulfide ore body.

We prepared a 100% sulfide sample from ~4.3 kg of rock collected from the J-M Reef, a thin layer of disseminated sulfide composed mainly of pyrrhotite, pentlandite, and minor amounts of chalcopyrite primarily mined for the platinum and palladium that accompany these base-metal sulfides. This deposit can be traced for over 40 km along strike, averaging approximately 1.75 m in thickness. The rock was collected at the 4,100 West level, #14,100 stope, a mining location of the Troctolite-Anorthosite Zone I of the Lower Banded Series, a stratabound plagioclase-olivine cumulate unit hosting the J-M Reef. The J-M Reef itself is located in Olivine-Bearing Zone I, the basal contact of the complex marked by the first appearance of cumulus olivine (Jenkins et al., 2020), and contains a small volume (~3 vol%) of sulfide (Jenkins et al., 2020), meaning that the sample must be processed to concentrate the sulfide. The sample resided at depth, which is preferred to limit contamination from oxidation products.

There were four requirements for the sulfide sample.

1. It must be nearly 100% pure (e.g., free of its silicate host rock),
2. The grain size should be sufficiently large as to eliminate transparency features,

3. The sample must match the same particle size as the silicate reference samples so that the calibration experiments (described below) for the RTM are valid,

4. The original shape and form of the sulfide grains should be preserved so that the particles represent a natural sample.

Because typical crushing methods may not completely liberate sulfide from its silicate host rock and would likely comminute the grains to a size fraction too fine for use in this study, the Stillwater samples were processed at Overburden Drilling Management in Ontario, Canada utilizing an electric pulse disaggregator. Electric pulse disaggregation is a comminution technique that applies high-voltage pulses of electric current to a sample in a water bath, sundering the rock into its mineral constituents irrespective of lithology or grain-size distribution (Cabri et al., 2008). The current travels preferentially along zones of weakness in the rock (i.e., along grain boundaries), resulting in undamaged mineral grains that can be recovered for analysis. The technique works particularly well when mineral phases have different electrical conductivities (e.g., sulfide and silicate; Cabri et al., 2008).

The post-disaggregation sample was first sieved to recover particle-size fractions of 1.0 mm or less and then processed on a shaker table to obtain ~1.1 kg of heavy-mineral separates. The heavy-mineral separates were then passed through a methylene iodide heavy liquid with a specific gravity of 3.3 to concentrate the sulfide further, yielding 490.5 g. A paramagnetic separation was then performed on the remaining mass in a series of ordered steps. First, a handmagnet was passed over the sample (~0.1 Amp equivalent) to isolate the magnetic sulfide fraction. A second pass was then performed to account for minerals that may have been trapped between magnetic grains. A visible

inspection was then performed to remove any identified non-sulfide components (i.e., magnetite, rutile), though very few were observed. The purity and composition of the beneficiated fraction of the J-M Reef sulfide were confirmed with X-ray diffraction, which showed the presence of pyrrhotite, pentlandite, and minor chalcopyrite. The sulfide was then hand-sieved to the desired size-fraction (500–710 μm) and washed in ethanol to remove any clinging fines (Figure 2.3a).

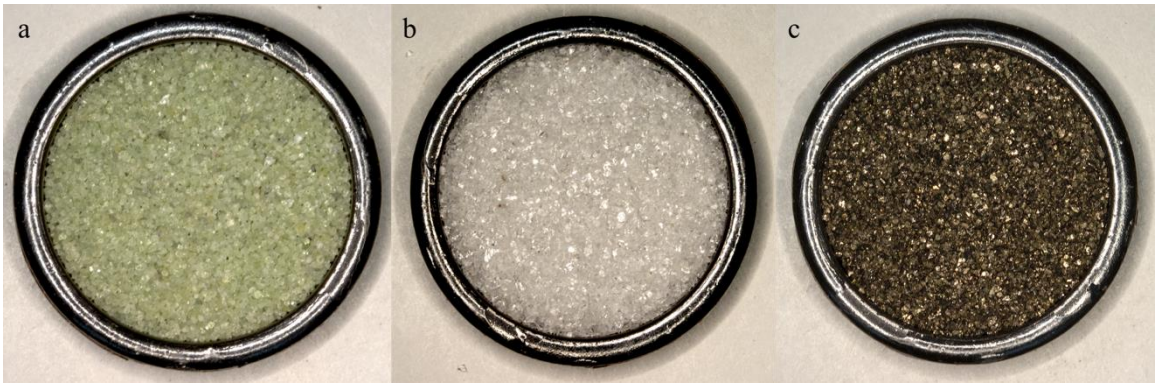

Figure 2.3 – 500–710 μm samples of (a) forsteritic olivine, (b) quartz, and (c) pyrrhotite.

2.4.2 Silicate Reference Samples

Quartz (ASU ID: BUR4120) was selected as a reference sample (Figure 2.3b) because its optical constants are well known, its infrared spectrum is relatively simple and well-characterized (e.g., it only has seven assigned lattice vibrations), and it is often used as a calibration material due to its strongly varying optical properties in the mid-infrared (Bramble et al., 2019; Edwards & Christensen, 2013; Moersch & Christensen, 1995; Wenrich & Christensen, 1996). Additionally, the emissivity at the CF is extremely close to 1.0 (Ruff et al., 1997; Salisbury & D'Aria, 1992), allowing for an accurate determination of the kinetic temperature of the sample with minimal error.

Forsteritic olivine (ASU ID: BUR3720A) was selected (Figure 2.3c) because, like quartz, its spectral characteristics are well characterized and its CF exhibits near unit emissivity (Burns & Huggins, 1972; Hamilton, 2000, 2010; Hamilton et al., 2020; Salisbury et al., 1991). Moreover, olivine is abundant in mafic and ultramafic igneous rocks commonly associated with Ni-Cu-PGE sulfide ore deposits (Arndt et al., 2005; Averill, 2011; Barnes Fiorentini et al., 2012; Jenkins et al., 2020; Naldrett et al., 2008, 2010). The PGE-enriched J-M Reef of the Stillwater Complex, for example, is associated with the first occurrence of olivine-bearing plagioclase in the Lower Banded Series (Page et al., 1985; Todd et al., 1982). Compositional information for both references can be found in Arizona State University's online spectral library (https://speclib.asu.edu/).

Before measurement, the samples were inspected for contaminants and washed with diluted ethanol to remove clinging fines (Christensen et al., 2000). The 500–710 μm size fraction was used to eliminate the possibility of volume scattering effects introduced from small size fractions (Maturilli & Helbert, 2014; Wenrich & Christensen, 1996).

2.5 The Reference Temperature Method Experiment: A New Sample Calibration and Measurement Methodology

2.5.1 Instrument Apparatus

Spectral data were acquired at Arizona State University using a Nicolet iS50R Fourier-Transform Infrared Spectrometer equipped with a deuterated triglycine sulfate detector and CsI beam splitter. The spectral range is from 2,000 to 200 cm^{-1} (~5–50 μm) with a spectral sampling of 2 cm^{-1} (4 cm^{-1} resolution). Initially designed for transmission, the spectrometer was modified for emission measurements by incorporating an external

collimated emission source port and an external off-axis parabolic gold-plated mirror to focus the optical path on the sample housed inside the blackbody chamber (Christensen & Harrison, 1993; Ruff et al., 1997). This allows the energy reaching the detector to be from the sample itself.

The apparatus was assembled such that the spectrometer and Plexiglas glovebox housing the blackbody targets, sample heater, mirror assembly, and the temperature-controlled sample chamber are continuously purged with dry air that has been scrubbed of CO_2 using a Parker Balston purge-gas generator to "scrub" the air of dust particles, H_2O, and CO_2. This allows repeated measurements to be acquired in a controlled, dry, and ambient environment, significantly reducing water vapor and carbon dioxide from imparting spectral features in the measured spectra.

2.5.2 Experimental Method

The methods for converting spectral radiance data to emissivity as well as their applications have progressed over time and differ mainly in how they determine sample kinetic temperature (Bramble et al., 2019; Christensen & Harrison, 1993; Edwards & Christensen, 2013; Maturilli & Helbert, 2014; Maturilli et al., 2006, 2016; Ruff et al., 1997). The OTM is advantageous for orbital and surface remote sensing applications because it is a contactless measurement that derives a brightness temperature at the CF from the sample or planetary surface's spectral radiance (Ruff et al., 1997). The RTM begins by measuring blackbody reference targets at 100 and 70ºC before measuring the sample to establish the instrument's response function and instrument energy (Ruff et al., 1997). The conical blackbodies are coated with Krylon Ultra Flat Black 1,602 paint,

which results in an average $\varepsilon \geq 0.95$ (Ruff et al., 1997). After the calibration targets are measured, the sample is then measured. In the OTM, samples are heated in an oven for several hours and then placed onto a sample heating platform. The sample is left to equilibrate for several minutes before measurement with the intention of reaching an equilibration temperature between that of the blackbody calibration targets. The RTM eliminates the preheating step by incorporating a custom-built sample heater that brings the sample to an equilibrium temperature between the blackbody targets within 5 min. The structural configuration of the sample heater (Figure 2.4) is based on the design of laboratory blackbody targets (Ruff et al., 1997). The heater is made of aluminum and cylindrical in shape, with a conical cavity coated with high-emissivity paint. It is equipped with two thermocouples connected to a temperature controller at a setpoint of 120ºC. While the heater's internal thermocouples reach this temperature, the surface temperature of a sample reaches ~80ºC (see reference experiments below), which falls between the range of the calibration targets. The higher temperature set point was also selected to ensure that the radiant energy emitting from a low-emissivity sample such as iron metal or pyrrhotite is easily distinguished from the energy emitted by the instrument and the surrounding environment.

After measuring the blackbodies, a pre-measured amount of 500–710 μm sample is poured into a sample cup, gently packed to reduce porosity, and left to equilibrate for 5 min in the sample heater inside the purged Plexiglas glovebox. The five-minute time span was determined after repeated tests using the sample heater, where we carefully monitored the intensity of our quartz and olivine samples for 30 min. After 5 min, the sample is inserted into the blackbody chamber for measurement.

When employing the OTM, 256 interferograms are collected in ~3–4 min during one measurement depending on the resolution, which are averaged by the spectrometer to produce a raw spectrum. The number of spectral scans was optimized to maximize the signal-to-noise ratio. The RTM collects and averages 64 interferograms in 55 s during one measurement. This results in a slight reduction in the signal-to-noise as a tradeoff to characterize the capacity of the sample heater to maintain a consistent and repeatable temperature over time. Additionally, reducing the number of interferograms during each spectral measurement enables us to monitor time-dependent fluctuations in sample temperature.

The final emissivity spectrum calibrated using the RTM is an average of 14 consecutive measurements, where each measurement is produced by an average of 64 interferograms collected consecutively. If a sample is measured multiple times, it is re-poured and re-measured to eliminate any effects of crystal orientation. Because we are constantly monitoring the temperatures of each component using a Keithley multimeter, this methodology also tests the sample heater's capacity to bring a sample to the same temperature. Between measurements, the sample was removed from the sample cup and left to equilibrate with the lab environment before being re-poured into the sample cup. This was done to ensure that the environmental chamber–which can slightly increase in temperature over time if a sample is left in the chamber–was at the same temperature each time before inserting a sample into the chamber for measurement.

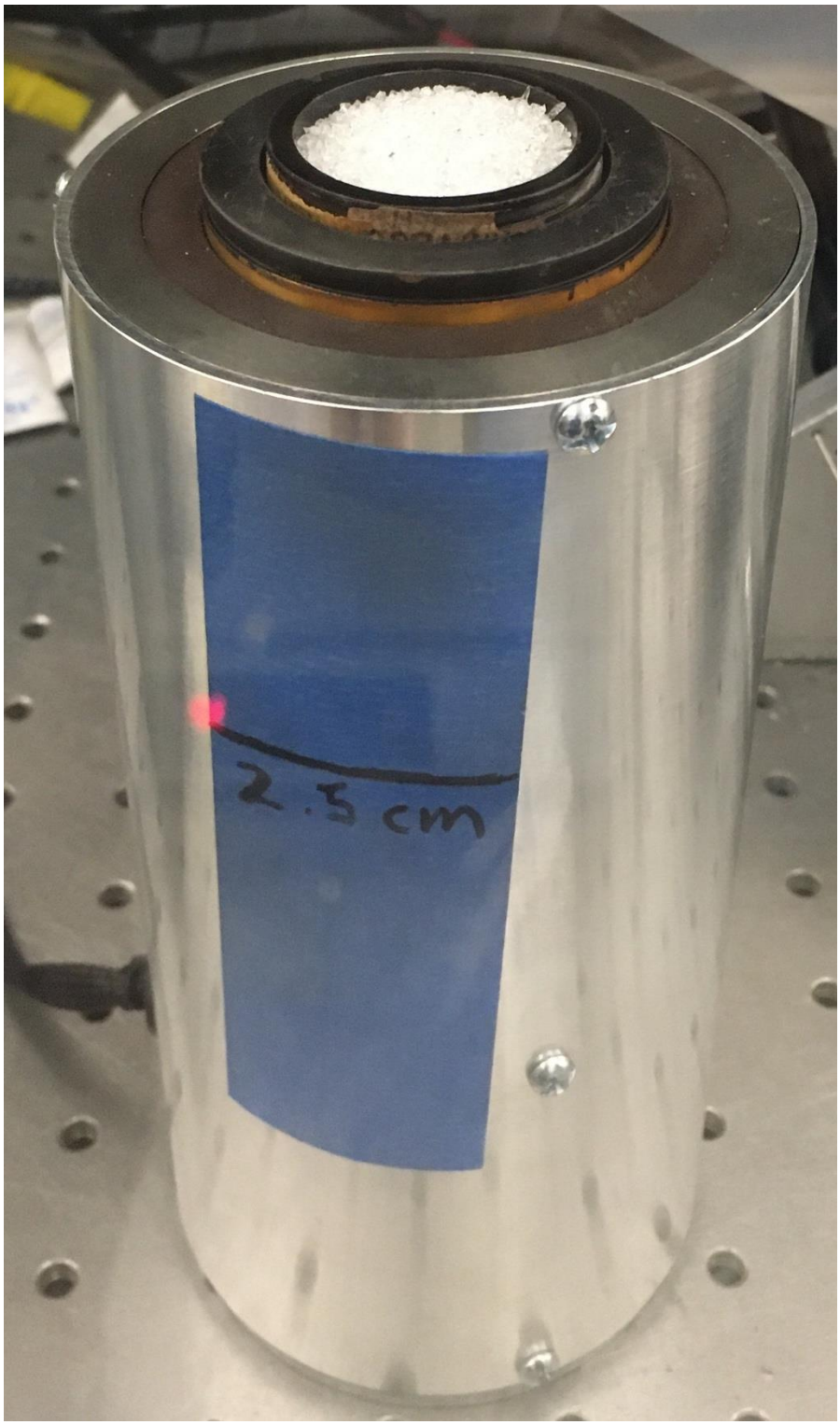

Figure 2.4 – Photograph of the sample heater developed for measuring the absolute emissivity of graybody materials.

2.5.3 Spectral Measurements of J-M Sulfide Using the One Temperature Method

In general, every percentage departure from unity of the CF results in an equal percentage of error in sample emissivity (Ruff et al., 1997). Because >95% of rock-forming minerals exhibit emissivity maxima of ~0.98 or higher at their CF, the assumption of unit emissivity does not impart significant errors in downstream emissivity calculations for the vast majority of rocks (Salisbury et al., 1991). However, certain minerals such as chlorides (Osterloo et al., 2008, 2010), iron metal (Ashley, 2011; Bramble et al., 2021a, 2021b), and some sulfides (e.g., pyrrhotite, this study) exhibit systematic graybody behavior in the mid-infrared, presenting difficulties in accurately determining the true kinetic temperature and emissivity of the sample.

Figure 2.5 displays the 42 calibrated radiance spectra from three separate "pours" of the J-M Reef sulfide, along with the average apparent brightness temperature spectrum for each measurement assuming unit emissivity. Each brightness temperature spectrum is an average of 14 spectral measurements taken consecutively, with each measurement consisting of 64 spectral scans. A temperature was estimated for each sulfide measurement by calculating a brightness temperature across the entire spectral range and within a 250 cm^{-1} band near 1,150 cm^{-1} that is typically used in planetary science applications since the CFs of most rock-forming minerals are located in this region (Figure 2.5b). The brightness temperatures and one standard deviation from the mean for each measurement are reported in Table 2.1.

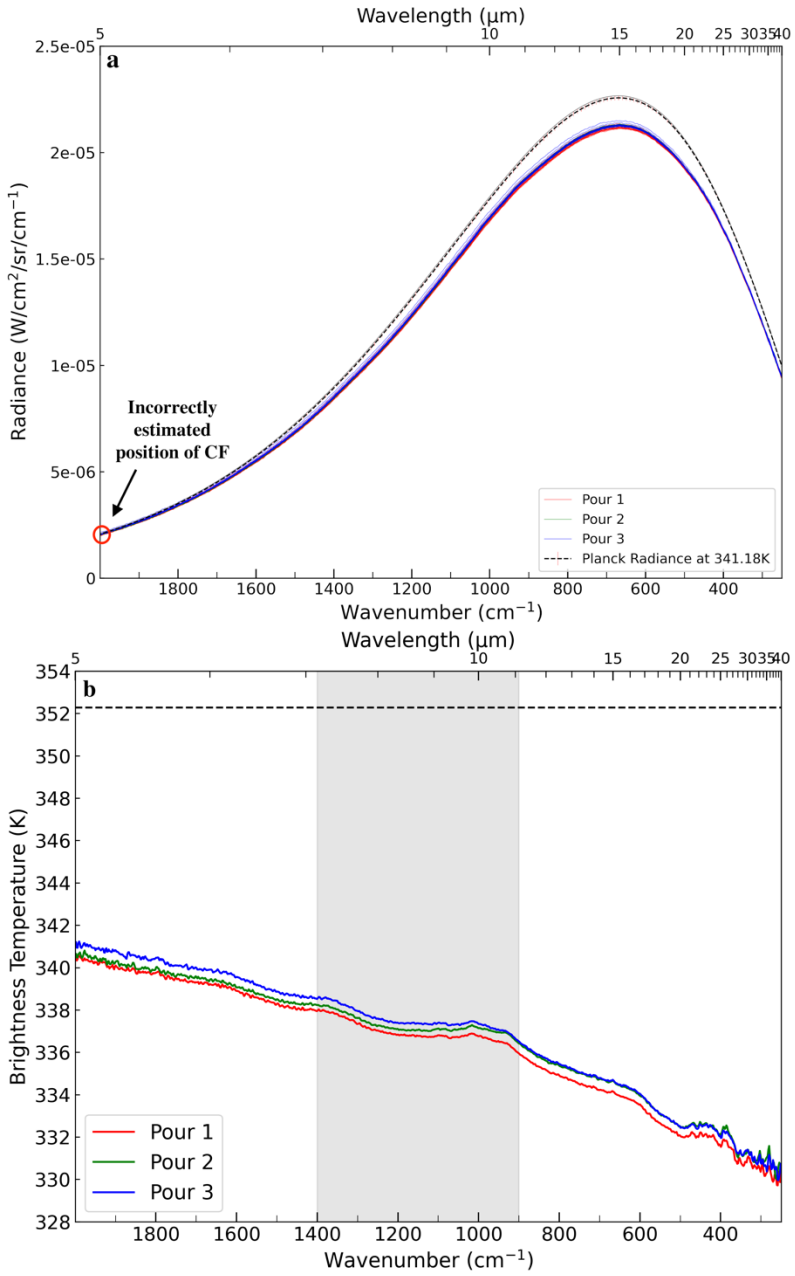

Figure 2.5 – (a) Forty-two calibrated radiance spectra of the J-M Reef sulfide collected during three separate measurements. Planck radiance spectra at the average estimated maximum brightness temperature (341.18 K) and ±1 standard deviation from the mean (0.49 K) of the 42 measurements are also displayed. (b) Average apparent brightness temperature spectra of the J-M Reef sulfide using the custom-built sample heater. The region shaded in gray represents the wavenumber region (1,400–900 cm^{-1}) typically utilized to estimate planetary surface temperatures. The horizontal black dashed line represents the estimated kinetic temperature of the sulfide determined from our reference experiments.

Regardless of the wavenumber interval used to estimate pyrrhotite's kinetic temperature, the maximum brightness temperature was always determined at the highest wavenumber (i.e., 2,000 and 1,400 cm^{-1}). For silicates, the maximum brightness temperature is determined at the CF feature due to the optical properties of the material as a function of wavenumber. Here, the selection of the highest wavenumber suggests that a CF is not present and/or that the material exhibits systemic graybody emissivity ($\varepsilon < 1.0$) across its spectrum. There is no wavenumber within the spectral range of the instrument where pyrrhotite exhibits minimal scattering and little absorption. Thus, while the results in Table 2.2 suggest that the OTM is extremely precise (i.e., repeatable), the results in Table 2.1 demonstrate that it is inaccurate for materials lacking a CF.

Table 2.1 – Estimated Sample Temperature (K) of the J-M Reef Pyrrhotite Assuming Unit Emissivity, Where the Maximum Brightness Temperature Was Determined Across the Entire Spectral Range (i.e., Unconstrained From 2000 to 250 cm^{-1}) and Within the Silicate Region (1,400–900 cm^{-1}). Std represents one standard deviation from the mean brightness temperature.

	Unconstrained				Silicate Region			
Pour	**1**	**2**	**3**	**Avg***	**1**	**2**	**3**	**Avg***
Mean	340.88	341.04	341.6	341.18	338.09	338.32	338.67	338.36
Std	0.44	0.2	0.46	0.49	0.36	0.16	0.43	0.41

*Represents the average maximum brightness temperature and standard deviation of all sulfide measurements.

2.5.4 Reference Sample Experiments

To accurately determine the kinetic temperature of the J-M Reef sulfide, a series of reference test experiments were conducted using quartz and forsterite at approximately the same size-fraction and volume as the J-M Reef sulfide sample. The rationale behind these tests is that because quartz and forsterite contain CFs that exhibit blackbody character, they can be measured to monitor temperature stability of the sample heater to itself as well as

to determine the sample temperature error resulting from the assumption of unit emissivity inherent in the OTM. If the temperature is repeatable and accurate, the samples can be used as reference targets before measuring a graybody, so long as the material is similar in grain size and volume. The maximum brightness temperature of the reference targets can then be used as the kinetic temperature of the graybody, rather than the inappropriate brightness temperature to provide a more accurate absolute emissivity spectrum.

Table 2.2 – Average maximum brightness temperature (K) of the 500–710 µm quartz and forsterite reference sample measurements taken over the course of nine days.

	Quartz Measurements							
Pour	1	2	3	4	5	6	7	8
Date	10-Feb-20	10-Feb-20	10-Feb-20	11-Feb-20	11-Feb-20	11-Feb-20	16-Feb-20	19-Feb-20
Mean	350.50	350.99	350.67	353.46	355.70	353.21	353.31	350.72
Std	0.59	0.27	0.52	0.21	0.35	0.52	0.43	0.20
	Forsterite Measurements						**Totals**	
Pour	1	2	3	4	5	6	Quartz	Forsterite
Date	12-Feb-20	12-Feb-20	12-Feb-20	13-Feb-20	13-Feb-20	13-Feb-20		
Mean	350.71	353.88	354.54	351.83	351.39	350.89	352.32	352.20
Std	0.34	0.31	0.33	0.47	0.55	0.40	1.81	1.53

The experiment consisted of collecting reference sample measurements 14 times over 9 days. Each reference sample measurement consists of 15 consecutive spectral measurements collected back-to-back, with each spectral measurement consisting of 64 interferometric scans averaged by the spectrometer. Each consecutive spectral measurement was then calibrated using the method described by Ruff et al. (1997) to determine the temperature of the sample over time.

We observed that when the sample was transferred from the purged glovebox to the sample chamber, the sample would re-equilibrate with its new environment, resulting in a small “temperature spike.” Because this phenomenon was observed during each

measurement, the first spectral measurement was dropped from each spectral measurement, bringing our total number spectral measurements to 196.

2.5.5 Reference Experiment Results

The results of our reference experiments are displayed in Figure 2.6. The average sample temperature for the forsterite measurements determined at the CF of their calibrated radiance curves is 352.2 ± 1.53 K, which is within ~0.1 K of the quartz measurements (352.32 ± 1.81 K). Overall, the temperature during a given pour remains stable, where one standard deviation from the mean temperature was ~0.4 K. While the difference between the minimum and maximum temperature of the 14 reference measurements was ~6.7 K, the standard deviation from the mean temperature of all the reference samples (352.27 K) was only 1.7 K. These results demonstrate that the heater brings granular samples at similar grain sizes and volumes to approximately the same temperature each time.

The magnitude of the temperature error for a graybody arising from the assumption of unit emissivity is reflected in Figure 2.7. Assuming the silicate reference tests represent the true kinetic temperature, the apparent maximum brightness temperature of the sulfide (341.18 ± 0.49 K) appears to be at least ~11.1 K less than its kinetic temperature of ~352.27 K as determined from the reference samples. However, based on the temperature determined between the wavenumber interval (900 and 1,400 cm^{-1}) often used during calibration in space applications, a massive sulfide detected in space might appear even colder.

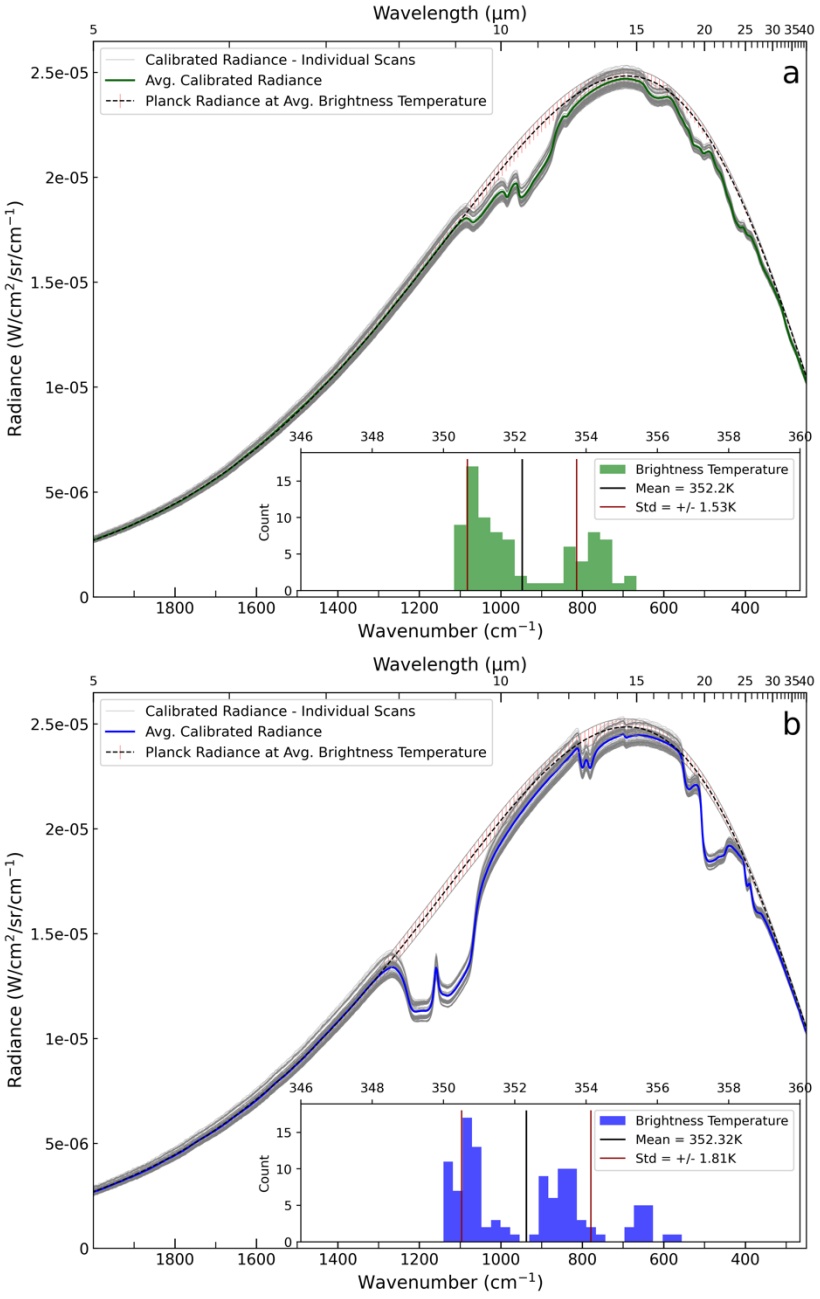

Figure 2.6 – (a) Calibrated radiance spectra of our forsterite reference measurements, with the average calibrated radiance in green. A Planck radiance spectrum at the average maximum brightness temperature of the forsterite measurements (352.2 K) and one standard deviation from the mean (1.53 K) is displayed in red. (b) Calibrated radiance spectra of the quartz reference measurements, with the average calibrated radiance in blue. A Planck radiance spectrum at the average maximum brightness temperature of the quartz measurements (352.32 K) and one standard deviation from the mean (1.81 K) are also displayed. The subplots in each figure show the estimated sample temperature for each spectral scan.

Because we demonstrate that samples can be maintained at a uniform and repeatable temperature, we can safely assume that this apparent temperature error is due to pyrrhotite exhibiting systemic graybody character, meaning that its emissivity is significantly less than 1.0 across its entire spectrum. As reflected in Figure 2.7, a significant amount of radiant energy is unaccounted for during calibration due to the incorrect estimation of pyrrhotite's temperature. This temperature error ultimately propagates into downstream emissivity calculations, manifesting as a severe negative spectral slope (see Section 2.6).

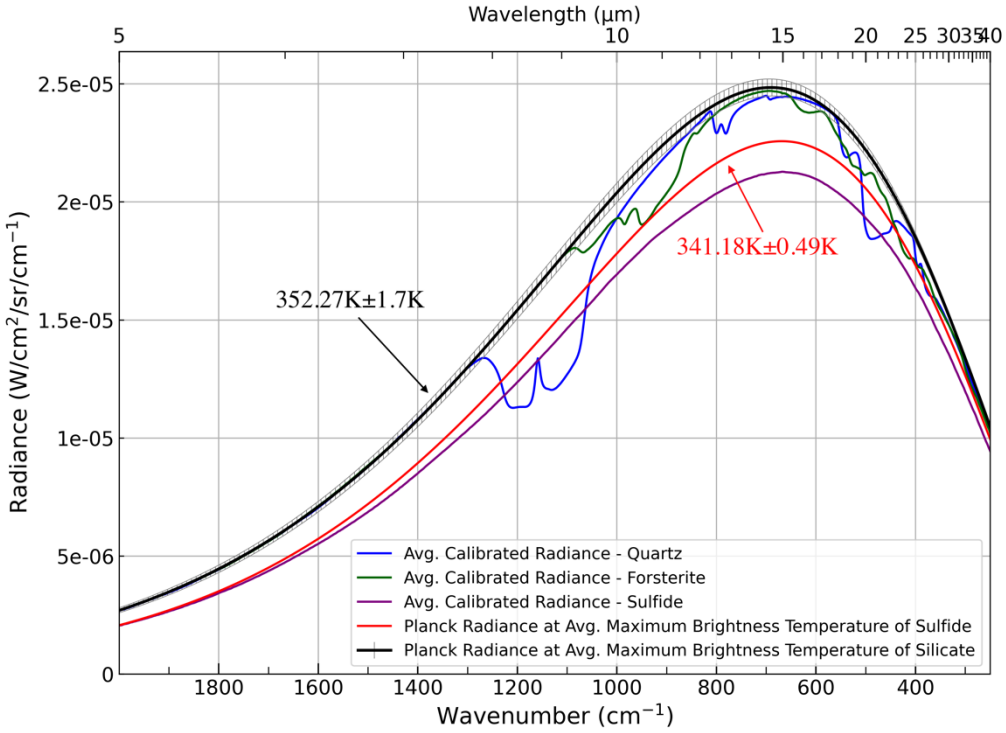

Figure 2.7 – Average calibrated radiance for the 112 quartz (blue), 84 forsterite (green), and 42 sulfide measurements (purple) measured for this study. Assuming unit emissivity, the temperature of the J–M Reef pyrrhotite is estimated to be 341.18±0.49K, which appears ~11.1K colder than its physical temperature. The spectral radiance curves demonstrate that much less radiant energy is emitted from a material exhibiting systemic graybody emissivity than selective radiators such as quartz and forsterite. Planck radiance curves at the average brightness temperatures of the silicate references (black) and the J–M Reef sulfide (red) are also displayed to provide context on how much reflected radiant energy was unaccounted for in downstream emissivity calculations.

2.6 Emissivity Results

Figure 8 compares the emissivity spectra of the quartz and forsterite reference measurements derived from both the OTM and the RTM. When converting to emissivity, the spectra calibrated using the OTM (Figures 2.8a and 2.8d) utilize a brightness temperature determined at their respective CFs (Table 2.2). In contrast, spectra calibrated using the RTM (Figures 2.8b and 2.8e) use the average brightness temperature of the reference measurements.

Because spectra calibrated using the RTM utilize the average brightness temperature of multiple reference sample measurements to compute emissivity, samples are calibrated using a Planck radiance curve at a brightness temperature that is either slightly warmer or colder than the actual kinetic temperature of the sample. Doing so systematically offsets the absolute emissivity spectrum. For example, if a sample's actual kinetic temperature was warmer than the average brightness temperature of the reference samples, the temperature difference manifests as a systematic reduction in emissivity across the spectrum. If the sample's kinetic temperature was colder than the reference temperature, it exhibits a systematic increase in emissivity across its spectrum (see Figure 2.8). The temperature error also imparts a slope on each spectrum, which is insignificant in these cases since the temperature error is marginal.

The average emissivity of multiple measurements of both quartz and forsterite calibrated using the RTM is nearly identical to the average emissivity spectra calibrated using the OTM (Figures 2.8c and 2.8f). As shown in Figure 2.9, the difference in average emissivity for the reference samples calibrated using the RTM and OTM is negligible.

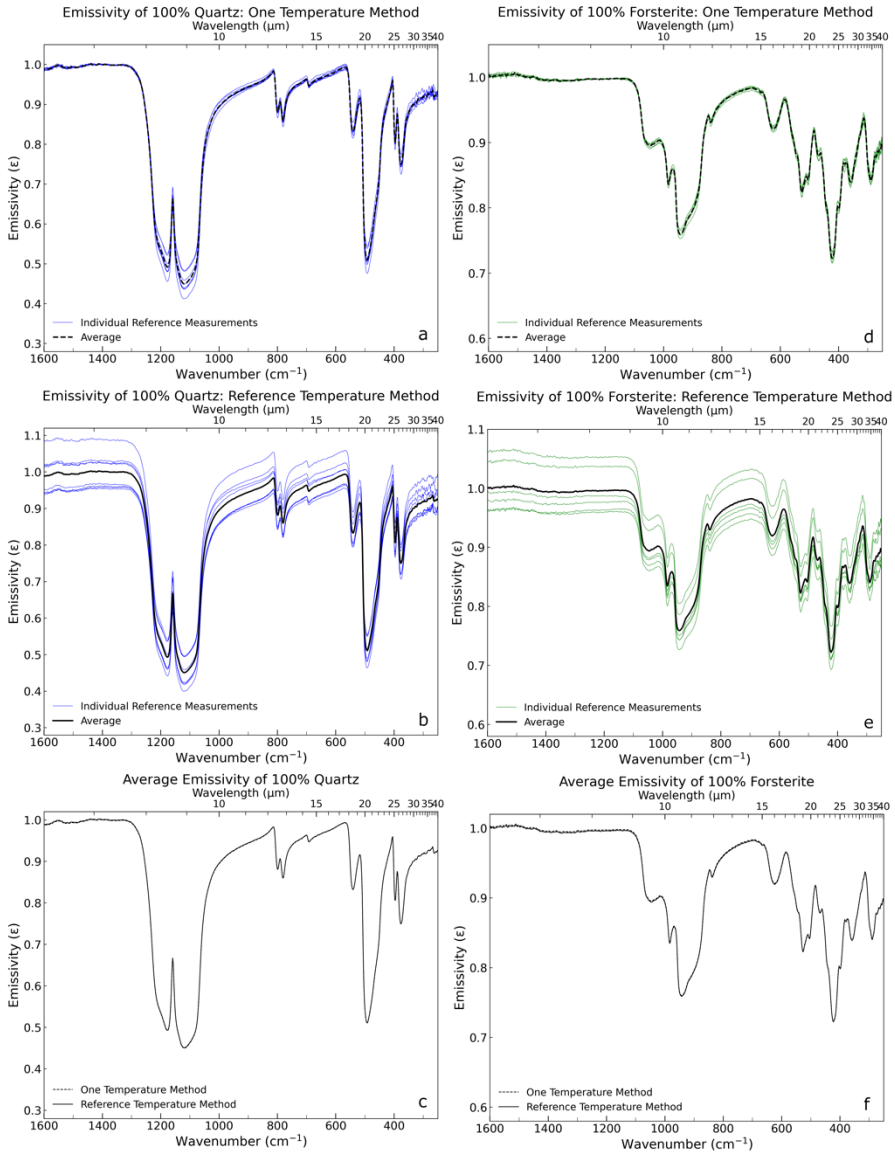

Figure 2.8 – Emissivity spectra of the reference sample measurements derived from the one-temperature method (OTM) and reference temperature method (RTM). Panels (a and d) display the quartz and forsterite measurements calibrated using the OTM, where each measurement was calibrated using a temperature determined at their respective CFs. Panels (b and e) display the same quartz and forsterite measurements derived using the RTM, where each spectrum was calibrated using the average temperature of the reference measurements. The average spectrum from each method is displayed in panels (c and f) for quartz and forsterite, respectively. The variation in band depth for the spectral absorptions in panels (a and d) is likely due to slight differences in the average grain size at the optical surface of the sample. The emissivity offset of the individual spectral measurements in panels (b and e) results from the difference between the reference sample temperature used during calibration from the sample's true kinetic temperature. Panels (c and f) demonstrate that the OTM and RTM are negligible.

As a rule of thumb, we suggest that an unknown sample calibrated using the RTM be measured at least three times and averaged to produce an accurate absolute emissivity spectrum to account for temperature variations between sample measurements.

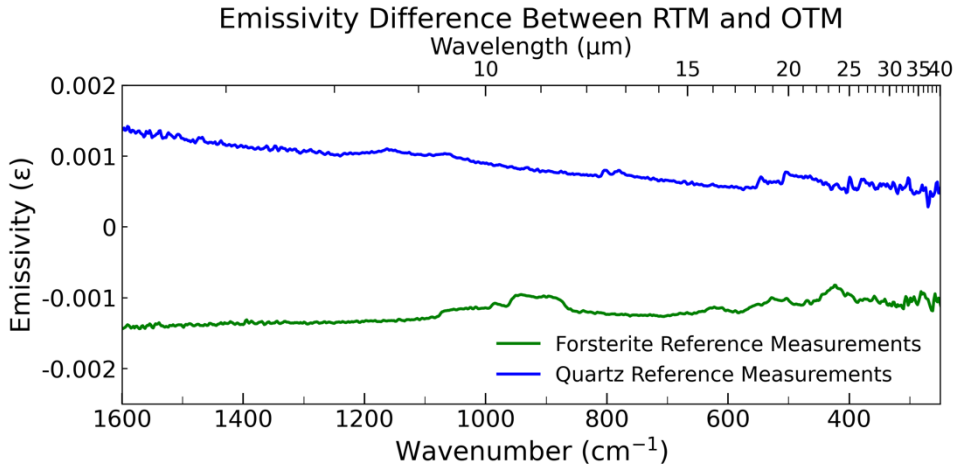

Figure 2.9 – Difference in average emissivity spectra for the quartz and forsterite reference measurements derived from the Reference Temperature Method and One-Temperature Method.

Figure 2.10a displays the average of 42 emissivity spectra of pyrrhotite ($Fe_{(1-x)}S$) from 2,000 to 250 wavenumbers (~5–40 μm) calibrated using the OTM and the RTM, where the maximum brightness temperature for calibration using the OTM was determined between 900 and 1,400 cm^{-1}. The spectrum calibrated using the OTM exhibits a severe negative slope from high to low wavenumbers, contains "non-physical" emissivity values >1.0 at wavenumbers greater than the estimated location of the CF, and is nearly spectrally featureless. Extremely low contrast spectral features at ~1,200, ~500, and ~350 cm^{-1} appear to be present, though the spectral slope makes them difficult to discern.

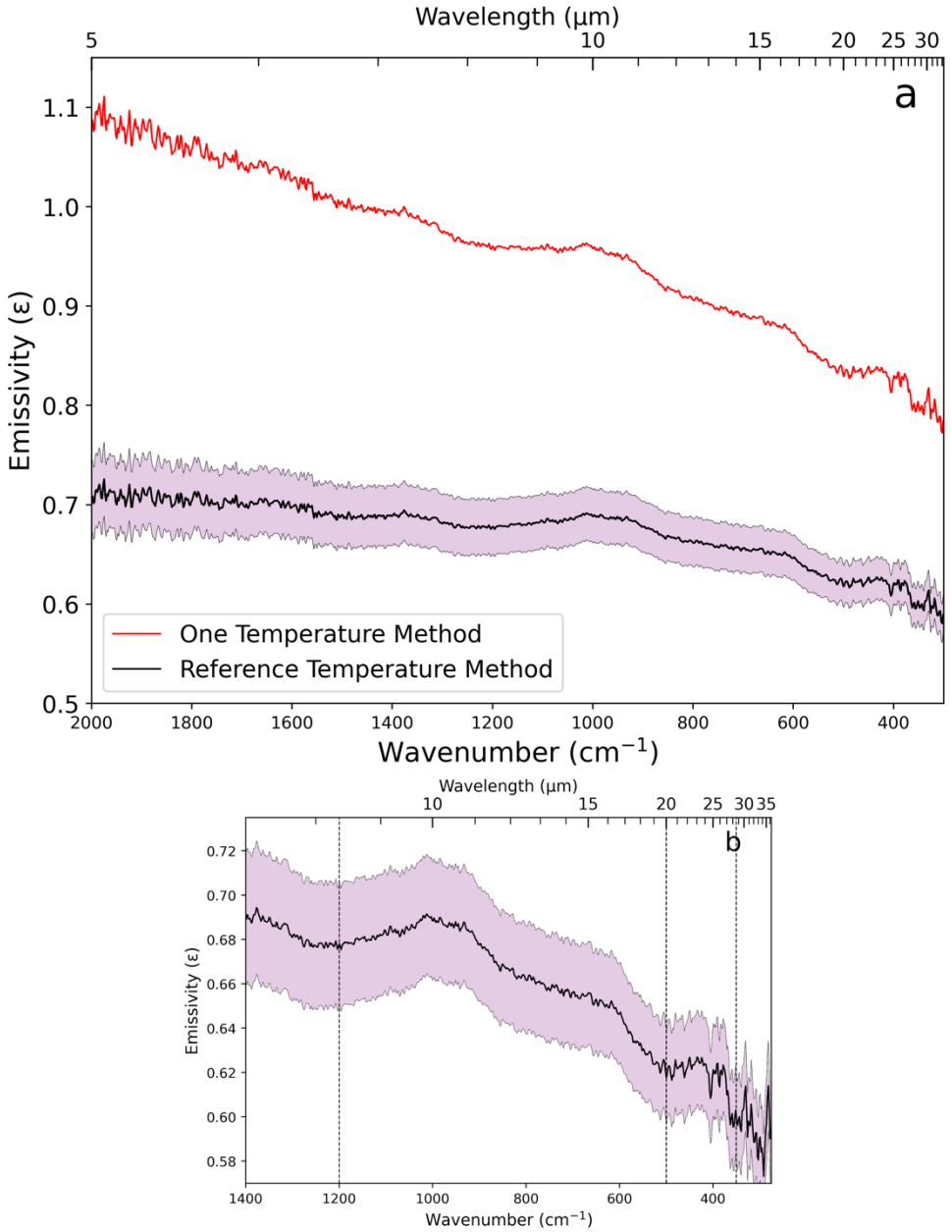

Figure 2.10 – (a) Thermal infrared emissivity spectra of the J-M Reef sulfide calibrated using the one-temperature method (red) and the reference temperature method (RTM) (black). The area shaded in purple represents one standard deviation from the mean emissivity spectrum of the J-M Reef sulfide. After correcting the sample temperature error, the slope imparted on the J-M Reef sulfide spectrum diminishes and likely represents the actual spectral shape. The J-M sulfide has a maximum absolute emissivity of ~0.7 and is spectrally neutral. (b) Zoomed in region of the RTM calibrated J-M Reef sulfide spectrum where severely low contrast spectral features potentially resulting from the Fe-S vibrational modes in pyrrhotite are present. The center of each potential feature is indicated with a dashed vertical line.

For a more accurate estimation of the absolute emissivity of the J-M Reef sulfide, we implement the RTM. After substituting B_{samp} with B_{ref} in Equation 1, the slope imparted on the J-M Reef sulfide emissivity spectrum shallows significantly, and the systemic graybody character of the J-M Reef sulfide becomes easily distinguishable. The absolute emissivity of the J-M Reef pyrrhotite is determined to be ~0.7–0.6 from high to low wavenumbers, with the difference in emissivity between the two calibration methods per unit wavenumber ranging from ~0.4 to 0.27 (Figure 2.11). This result demonstrates that the RTM significantly improves the accuracy of a graybody sample's absolute emissivity spectrum. Additionally, the difference between the two methods shows the substantial and non-linear effect of temperature errors on TIR-emissivity spectra.

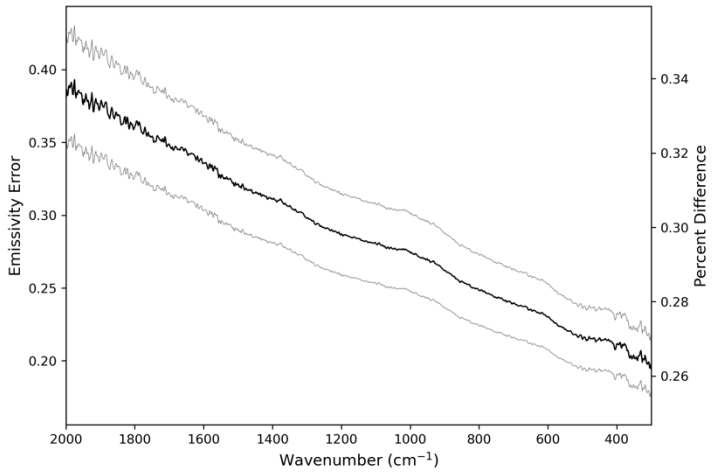

Figure 2.11 – Difference in the emissivity of the J–M Reef sulfide between the One-Temperature Method and the Reference Temperature Method. The gray curves represent one standard deviation from the mean.

Soong and Farmer (1978) previously attributed pyrrhotite's featureless far-infrared (420–90 cm^{-1}) transmittance spectrum to its metallic conductivity. Thus, it is reasonable to assume that the nearly featureless, low-emissivity character of the J-M Reef pyrrhotite spectrum reported in this study might be due to the Fe-Fe metallic bonds in

pyrrhotite's crystal lattice. Metallic bonding may manifest in mid-infrared emission spectra as a broad “absorption” feature rather than as a discrete spectral band, for these features arise in other minerals such as silicates since the bonds between individual diatomic pairs (e.g., Si and O) constituting their crystal lattices vibrate independently.

Similarly to the sulfides measured by Lane et al. (2009), the J-M Reef pyrrhotite is spectrally featureless at high wavenumbers. The low-contrast features centered at ~1,200, 500, and 350 cm^{-1} found in the OTM spectrum remain present in the RTM spectrum (Figure 2.10b). Previous research has shown that spectral features from contaminant phases are pronounced when the host medium is spectrally featureless and non-absorbing (Eastes, 1989; Lane & Christensen, 1998). Therefore, the features present in the J-M Reef sulfide spectrum may not correspond to the pyrrhotite itself, but volumetrically low amounts of minor sulfide phases in the sample such as pentlandite or chalcopyrite or an oxide component such as magnetite that may have been retained in the sample during magnetic beneficiation. The weak feature centered at ~1,200 cm^{-1} could be due to a silicate contamination that was not removed during processing. However, qualitative assessments of the band centers of spectral features in emissivity spectra of the J-M Reef silicates removed during processing do not align with the features found in the pyrrhotite spectrum. A qualitative assessment of spectra presented by Lane and Bishop (2019) suggests that the low frequency features are unlikely to be chalcopyrite and that the 500 cm^{-1} feature might be attributed to trace amounts of rutile (TiO_2).

The lower frequency features centered at 500 and 350 cm^{-1} may be diagnostic of weak Fe-S vibrational modes in pyrrhotite. It is also plausible that the Fe-S vibrational

modes are not “infrared active” and that the weak features are associated with the vibrational modes of other less common chalcophile elements that can substitute for Fe in the pyrrhotite structure such as Ni. This could explain why the features exhibit such low spectral contrast. Nonetheless, current planetary remote sensing instruments lack the signal to noise (e.g., the noise equivalent delta emissivity) to resolve the observed low contrast features required for diagnostic mineral detection. Thus, sulfide mineral deposits would likely be detected not from their spectral features, but from their low-emissivity and spectral slopes.

2.6.1 Error Analysis

The OTM has previously been validated by a robust analysis of potential errors associated with instrument, environment, blackbody, and sample temperature errors, with a conclusion that the derived emissivity is accurate in most cases to within 2% uncertainty and with the worst-case combination of errors to ~4% (Ramsey & Christensen, 1998; Ruff et al., 1997).

As shown in Figures 2.8b and 2.8e, slight errors in sample temperature can artificially offset a sample's absolute emissivity spectrum. To characterize the certainty of an absolute emissivity spectrum produced using the RTM, 1,000 emissivity spectra of the J-M Reef sulfide were computed using one calibrated radiance measurement of the sulfide sample and Planck radiance curves for the other input variables (e.g., sample temperature, hot blackbody, warm blackbody, environmental chamber) sampled from a normal distribution of temperatures based on the errors reported in Table 2.3. The average modeled emissivity spectrum and measurement uncertainty is shown in Figure 2.10. The measurement uncertainty–expressed as one standard deviation from the mean–

in absolute emissivity ranges from approximately ±2.1%–3.8% from low to high wavenumbers due to the nonlinear relationship between temperature and wavelength, with an average emissivity error across the spectrum of approximately ±2.8%.

Table 2.3 – Average temperature and one standard deviation from the mean for each input used to derive the absolute emissivity of the J–M sulfide.

Calibration Quantity	*T(K)*	σ
Hot Blackbody Target	372.7	0.09
Warm Blackbody Target	343.86	0.09
Environmental Chamber	299.91	0.29
Sample Temperature	352.27	1.7

2.7 Conclusion

Our spectral measurements of pyrrhotite derived from the J-M Reef demonstrate that the assumption of unit emissivity inherent in the OTM can result in significant errors in sample temperature and downstream emissivity calculations when a material lacks a CF and exhibits systematically low emissivity. The highly reflective nature of sulfide and other economically relevant materials such as metallic iron-nickel (Ashley, 2011; Bramble et al., 2021a, 2021b) result in an incorrect "colder" Planck radiance being fit to the sample's calibrated radiance, imparting a steep slope on its derived emissivity spectrum.

Past experiments suggest correcting this error via direct sample temperature measurement with a thermocouple (Ashley, 2011). We demonstrate that this temperature error can be significantly constrained using the RTM, which uses contactless measurements of reference samples with known CF features. Replacing the blackbody

radiance curve at the incorrect brightness temperature with one at the correct temperature of the graybody material significantly shallows the spectral slope, and the absolute emissivity spectrum from 2000 to 250 cm^{-1} for pyrrhotite was determined to be ~0.7–0.6 from high to low wavenumbers. The percent improvement on the J-M Reef sulfide calibrated using the OTM ranges from ~53% to 27% from high to low wavenumbers, highlighting the significance of sample temperature errors in emissivity calculations.

The primary features in TIR-emissivity spectra commonly used to determine the chemical composition, mineralogy, and grain size of a sample or planetary surface are the appearance and position of a CF, the position, shape, and intensity of absorption features, and the presence of transparency features. The J-M Reef pyrrhotite does not contain these features. Although the spectrally neutral character and systemic graybody behavior of pyrrhotite complicate the accurate determination of its temperature and spectral emissivity, these characteristics may be exploited to prospect for economically significant materials on other celestial bodies, similarly to the conventional features described above. Rather than searching for diagnostic absorption bands, detecting sulfide outcrops will require identifying regions in mafic/ultramafic terrain that exhibit anomalously cold apparent brightness temperatures and have relatively spectrally featureless infrared emissivity spectra with steep negative slopes from high to low wavenumbers. Additionally, after a temperature correction, the spectra should exhibit systematically low emissivity across its mid-IR spectrum.

Spectrally featureless infrared emissivity spectra exhibiting steep negative slopes similar to the sulfide spectra reported in this study have already been identified in over

640 locations on the Martian surface. These spectra have been interpreted based on geologic context as signatures of chloride-bearing materials (Osterloo et al., 2008). However, sulfides could not be entirely ruled out (Osterloo et al., 2010). Because intrusive and extrusive volcanism were dominant during martian evolution, it seems unlikely that igneous activity on Mars did not lead to the formation of Ni-Cu-PGE sulfide mineralization. Based on our experiments, we demonstrate that the previously identified featureless, sloped emissivity spectra could indeed be derived from a sulfide ore body. While the J-M reef sulfide spectra presented in this work contained ~100% sulfide, it is likely that magmatic sulfide mineralization on Mars will be detected alongside silicate minerals and will be highly variable in terms of its concentration. A companion paper addresses this hypothesis experimentally using suites of sulfide/silicate mixtures, exploring how the abundance of a sulfide ore affects the spectral characteristics of its silicate host rock, defining a detection limit of a spectrally featureless mineral, and to determine if the assumption of linear mixing is valid when a graybody material is present in a composite spectrum.

References

Abrams, M. (2000). The Advanced Spaceborne Thermal Emission and Reflection Radiometer (ASTER): Data products for the high spatial resolution imager on NASA's terra platform. *International Journal of Remote Sensing*, 21(5), 847–859.

Altunaiji, E., Edwards, C. S., Smith, M. D., & Christensen, P. R. (2017). Scientific payload of the Emirates Mars mission: Emirates Mars infrared spectrometer (EMIRS) overview. In *6th international workshop on the Mars atmosphere: Modelling and observations* (pp. 17–20).

Arndt, N., Lesher, C. M., & Czamanske, G. K. (2005). Mantle-derived magmas and magmatic Ni-Cu-(PGE) deposits. In *Economic Geology*, (pp. 5–24). 100th anniversary, Retrieved from https://hal.archives-ouvertes.fr/hal-00016864

Ashley, J. W. (2011). Meteorites on Mars as planetary research tools with special considerations for Martian weathering processes. Doctoral dissertation, Arizona State University (p.343).

Averill, S. A. (2011). Viable indicator minerals in surficial sediments for two major deposit types: Ni-Cu-PGE and porphyry Cu. *Geochemistry: Exploration, Environment, Analysis*, 11(4), 279–291.

Badri, K., Altunaiji, E., Edwards, C. S., Smith, M. D., Christensen, P. R., Almheiri, S., et al. (2018). Scientific payload of the Emirates Mars mission: Emirates Mars infrared spectrometer (EMIRS). In *European Planetary Science Congress* (pp. 1–3). Retrieved from https://meetingorganizer.copernicus.org/EPSC2018/EPSC2018-1007.pdf

Bandfield, J. (2002). Global mineral distributions on Mars. *Journal of Geophysical Research*, 107(E6), 1–20.

Bandfield, J. (2009). Effects of surface roughness and graybody emissivity on Martian thermal infrared spectra. *Icarus*, 202(2), 414–428.

Barnes, S. J. (2006). Komatiite-hosted nickel sulfide deposits: Geology, Geochemistry, and Genesis (Vol. 13, pp. 51–118). Society of Economic Geologists.

Barnes, S. J., & Fiorentini, M. I. (2012). Komatiite magmas and sulfide nickel deposits: A comparison of variability endowed Archean terranes. *Economic Geology*, 107(5), 755–780.

Barnes, S. J., Holwell, D. A., & Le Vaillant, M. (2017). Magmatic sulfide ore deposits. *Elements*, 13(2), 89–95.

Barnes, S. J., & Lightfoot, P. C. (2005). Formation of magmatic nickel-sulfide ore deposits and processes affecting their copper and platinum-group element contents. In *Economic geology*, 100th anniversary (pp. 179–213).

Baumgartner, R. J., Fiorentini, M. L., Baratoux, D., Micklethwaite, S., Sener, A. K., Lorand, J. P., & McCuaig, T. C. (2015). Magmatic controls on the Genesis of Ni–Cu±(PGE) sulphide mineralisation on Mars. *Ore Geology Reviews*, 65, 400–412.

Bramble, M. S., Milliken, R. E., & Patterson, W. R., III. (2021a). Thermal emission measurements of ordinary chondrite mineral analogs in a simulated asteroid environment: 1. Constituent mineral phases. *Icarus*, 369(114561), 1–22.

Bramble, M. S., Milliken, R. E., & Patterson, W. R., III. (2021b). Thermal emission measurements of ordinary chondrite mineral analogs in a simulated asteroid environment: 2. Representative mineral mixtures. *Icarus*, 369(114251), 1–24.

Bramble, M. S., Yang, Y., Patterson, W. R., Milliken, R. E., Mustard, J. F., & Donaldson Hanna, K. L. (2019). Radiometric calibration of thermal emission data from the asteroid and lunar environment chamber (ALEC). *Review of Scientific Instruments*, 90(093101), 1–20.

Breitenfeld, L. B., Rogers, A. D., Glotch, T. D., Hamilton, V. E., Christensen, P. R., Lauretta, D. S., et al. (2021). Machine learning mid-infrared spectral models for predicting modal mineralogy of CI/CM chondritic asteroids and Bennu. *Journal of Geophysical Research: Planets*, 126(12), e2021JE007035.

Breitenfeld, L. B., Rogers, A. D., Glotch, T. D., Kaplan, H. H., Hamilton, V. E., & Christensen, P. R. (2022). Mapping phyllosilicates on the asteroid Bennu using thermal emission spectra and machine learning model applications. *Geophysical Research Letters*, 49(20), e2022GL100815.

Burns, R. G. (1988). Gossans on Mars. In *The proceedings of the 18th Lunar and Planetary Science* (pp. 713–721).

Burns, R. G., & Fisher, D. S. (1990). Iron-sulfur mineralogy of Mars: Magmatic evolution and chemical weathering products. *Journal of Geophysical Research*, 95(B9), 14415–14421.

Burns, R. G., & Huggins, F. E. (1972). Cation determinative curves for Mg–Fe–Mn olivines from vibrational spectra. *American Mineralogist*, 57, 967–985.

Cabri, L. J., Rudashevsky, N. S., Rudashevsky, V. N., & Oberthür, T. (2008). Paper 14: Electric-pulse disaggregation (EPD), hydroseparation (Hs) and their use in combination for mineral processing and advanced characterization of ores. In *40th Annual Meeting of the Canadian Mineral Processors* (Vol. 14, pp. 211–235).

Cawthorne, R. G. (2010). The platinum group element deposits of the bushveld complex in South Africa. *Platinum Metals Review*, 54(4), 205–215.

Christensen, P. R., Anderson, D. L., Chase, S. C., Clark, R. N., Kieffer, H. H., Malin, M. C., et al. (1992). Thermal emission spectrometer experiment: Mars observer mission. *Journal of Geophysical Research*, 97(E5), 7719–7734.

Christensen, P. R., Bandfield, J. L., Hamilton, V. E., Howard, D. A., Lane, M. D., Piatek, J. L., et al. (2000). A thermal emission spectral library of rock-forming minerals. *Journal of Geophysical Research*, 105(E4), 9735–9739.

Christensen, P. R., Bandfield, J. L., Hamilton, V. E., Ruff, S. W., Kieffer, H. H., Titus, T. N., et al. (2001). Mars Global surveyor thermal emission spectrometer experiment: Investigation description and surface science results. *Journal of Geophysical Research*, 106(E10), 23823–23871.

Christensen, P. R., Bandfield, J. L., Smith, M. D., Hamilton, V. E., & Clark, R. N. (2000). Identification of a basaltic component on the Martian surface from thermal emission spectrometer data. *Journal of Geophysical Research*, 105(E4), 9609–9621.

Christensen, P. R., Hamilton, V. E., Mehall, G. L., Pelham, D., O'Donnell, W., Anwar, S., et al. (2018). The OSIRIS-REx thermal emission spectrometer (OTES) instrument. *Space Science Reviews*, 214(87), 1–39.

Christensen, P. R., & Harrison, S. T. (1993). Thermal infrared emission spectroscopy of natural surfaces: Application to desert varnish coatings on rocks. *Journal of Geophysical Research*, 98(B11), 19819–19834.

Christensen, P. R., Jakosky, B. M., Kieffer, H. H., Malin, M. C., McSween, H. Y., Jr., Nealson, K., et al. (2004). The thermal emission imaging system for the Mars 2001 Odyssey mission. *Space Science Reviews*, 110(1/2), 85–130.

Christensen, P. R., McSween Jr, H. Y., Bandfield, J. L., Ruff, S. W., Rogers, A. D., Hamilton, V. E., et al. (2005). Evidence for magmatic evolution and diversity on Mars from infrared observations. *Nature*, 436(7050), 504–509.

Christensen, P. R., Mehall, G. L., Silverman, S. H., Anwar, S., Cannon, G., Gorelick, N., et al. (2003). Miniature thermal emission spectrometer for the Mars exploration rovers. *Journal of Geophysical Research*, 108(E12), 1–23.

Christensen, P. R., Wyatt, M. B., Glotch, T. D., Rogers, A. D., Anwar, S., Arvidson, R. E., et al. (2004). Mineralogy at Meridiani Planum from the Mini-TES experiment on the opportunity rover. *Science*, 306(5702), 1733–1739.

Conel, J. E. (1969). Infrared emissivities of silicates: Experimental results and a cloudy atmosphere model of spectral emission from condensed particulate mediums. *Journal of Geophysical Research*, 74(6):1614–1634.

Ding, S., Dasgupta, R., & Tsuno, K. (2014). Sulfur concentration of Martian basalts at sulfide saturation at high pressures and temperatures–Implications for deep sulfur cycle on Mars. *Geochimica et Cosmochimica Acta*, 131, 227–246.

Donaldson Hanna, K. L., Cheek, L. C., Pieters, C. M., Mustard, J. F., Greenhagen, B. T., Thomas, I. R., & Bowles, N. E. (2014). Global assessment of pure crystalline plagioclase across the Moon and implications for the evolution of the primary crust. Journal of *Geophysical Research: Planets*, 119(7), 1516–1545.

Donaldson Hanna, K. L., Wyatt, M. B., Thomas, I. R., Bowles, N. E., Greenhagen, B. T., Pieters, C. M., et al. (2012). Thermal infrared emissivity measurements under a simulated lunar environment: Application to the Diviner Lunar Radiometer Experiment. *Journal of Geophysical Research*, 117(E12), 1–15.

Eastes, J. (1989). Spectral properties of halite-rich mineral mixtures: Implications for middle infrared remote sensing of highly saline environments. *Remote Sensing of Environment*, 27(3), 289–304.

Edwards, C. S., & Christensen, P. R. (2013). Microscopic emission and reflectance thermal infrared spectroscopy: Instrumentation for quantitative in situ mineralogy of complex planetary surfaces. *Applied Optics*, 52(11), 2200–2217.

Ehlmann, B., & Edwards, C. (2014). Mineralogy of the Martian surface. *Annual Review of Earth and Planetary Sciences*, 42(1), 291–315.

Filiberto, J. (2008). Similarities between the shergottites and terrestrial ferropicrites. *Icarus*, 197(1), 52–59.

Gaillard, F., Michalski, J., Berger, G., McLennan, S. M., & Scaillet, B. (2013). Geochemical reservoirs and timing of sulfur cycling on Mars. *Space Science Reviews*, 174(1–4), 25–300.

Gaillard, F., & Scaillet, B. (2009). The sulfur content of volcanic gases on Mars. *Earth and Planetary Science Letters*, 279(1–2), 34–43.

Glotch, T. D., Bandfield, J., Wolff, M., Arnold, J., & Che, C. (2016). Constraints on the composition and particle size of chloride salt-bearing deposits on Mars. *Journal of Geophysical Research: Planets*, 121(3), 454–471.

Glotch, T. D., & Christensen, P. R. (2005). Geologic and mineralogic mapping of Aram Chaos: Evidence for a water-rich history. *Journal of Geophysical Research*, 110(E9), E09006.

Glotch, T. D., Morris, R. V., Christensen, P. R., & Sharp, T. G. (2004). Effect of precursor mineralogy on the thermal infrared emission spectra of hematite: Application to Martian hematite mineralization. *Journal of Geophysical Research*, 109(E7), 0700311–E70118.

Godel, B., & Barnes, S.-J. (2008). Platinum-group elements in sulphide minerals and the whole rocks of the J-M Reef (Stillwater Complex): Implication for the formation of the reef. *Chemical Geology*, 248(3–4), 272–294.

Greenhagen, B. T., Lucey, P. G., Wyatt, M. B., Glotch, T. D., Allen, C. C., Arnold, J. A., et al. (2010). Global silicate mineralogy of the Moon from the Diviner Lunar Radiometer. *Science*, 329(5998), 1507–1509.

Haberle, C. W., Christensen, P. W., & Ruff, S. W. (2019). Interpreting the petrogenetic history of Martian volcanic rocks using thermal emission spectroscopy and thermodynamic calculations of phase equilibria. American Geophysical Union, Fall Meeting 2019, abs. #P33F-3494.

Hamilton, V. E. (2000). Thermal infrared emission spectroscopy of the pyroxene mineral series. *Journal of Geophysical Research*, 105(E4), 9701–9716.

Hamilton, V. E. (2003). Thermal infrared emission spectroscopy of titanium-enriched pyroxenes. *Journal of Geophysical Research*, 108(E8), 5095.

Hamilton, V. E. (2010). Thermal infrared (vibrational) spectroscopy of Mg-Fe olivines: A review and applications to determining the composition of planetary surfaces. *Chemie der Erde*, 70(1), 7–33.

Hamilton, V. E., & Christensen, P. R. (2005). Evidence for extensive, olivine-rich bedrock on Mars. *Geology*, 33(6), 433–436.

Hamilton, V. E., Christensen, P. R., Kaplan, H. H., Haberle, C. W., Rogers, A. D., Glotch, T. D., et al. (2021). Evidence for limited compositional and particle size variation on asteroid (101955) Bennu from thermal infrared spectroscopy. *Astronomy and Astrophysics*, 650, A120.

Hamilton, V. E., Christensen, P. R., McSween, H. Y., Jr., & Bandfield, J. L. (2000). Searching for the source regions of Martian meteorites using MGS TES: Integrating Martian meteorites into the global distribution of igneous materials on Mars. *Meteoritics & Planetary Sciences*, 38(6), 871–885.

Hamilton, V. E., Haberle, C. W., & Mayerhofer, T. G. (2020). Effects of small crystallite size on the thermal infrared (vibrational) spectra of minerals. *American Mineralogist*, 105(11), 1756–1760.

Hamilton, V. E., & Ruff, S. W. (2012). Distribution and characteristics of Adirondack-class basalt as observed by Mini-TES in Gusev crater, Mars and its possible volcanic source. *Icarus*, 218(2), 917–949.

Hamilton, V. E., Simon, A. A., Christensen, P. R., Reuter, D. C., Clark, B. E., Barucci, M. A., & OSIRIS-Rex Team. (2019). Evidence for widespread hydrated minerals on asteroid (101955) Bennu. *Nature Astronomy*, 3, 332–340.

Haughton, D. R., Roeder, P. L., & Skinner, B. J. (1974). Solubility of sulfur in mafic magmas. *Economic Geology*, 69(4), 451–467.

Hecker, C., van der Meijde, M., & van der Meer, F. D. (2010). Thermal infrared spectroscopy on feldspars–successes, limitations, and their implications for remote sensing. *Earth-Science Reviews*, 103(1–2), 60–70.

Hiesinger, H., & Helbert, J. (2010). The Mercury radiometer and thermal infrared spectrometer (MERTIS) for the BepiColombo mission. *Planetary and Space Science*, 58(1–2), 144–165.

Hiesinger, H., Helbert, J., Alemanno, G., Bauch, K. E., D'Amore, M., Maturilli, A., et al. (2020). Studying the composition and mineralogy of the hermean surface with the Mercury radiometer and thermal infrared spectrometer (MERTIS) for the BepiColombo mission: An update. *Space Science Reviews*, 216(110), 1–37.

Hunt, G. R., & Vincent, R. K. (1968). The behavior of spectral features in the infrared emission from particulate surfaces of various grain sizes. *Journal of Geophysical Research*, 73(18):6039–6046.

Jenkins, M. C., Mungall, J. E., Zientek, M. L., Holick, P., & Butak, K. (2020). The nature and composition of the J-M Reef, Stillwater Complex, Montana, USA. *Economic Geology*, 115(8):1799–1826.

Jugo, P. (2009). Sulfide content at sulfide saturation in oxidized magmas. *Geology*, 37(5): 415–418.

King, P. L., Ramsey, M. S., McMillan, P. F., & Swayze, G. (2004). Laboratory Fourier transform infrared spectroscopy methods for geologic samples. *Infrared Spectroscopy in Geochemistry, Exploration, and Remote Sensing*, 33:57–91.

Lane, M. (1999). Midinfrared optical constants of calcite and their relationship to particle size effects in thermal emission spectra of granular calcite. *Journal of Geophysical Research*, 104(E6):14099–14108.

Lane, M., & Bishop, J. (2019). Mid-infrared (thermal) emission and reflectance spectroscopy: Laboratory spectra of geologic materials. In J. Bishop, J. Bell III, & J. Moersch (Eds.), *Part I–Theory of remote compositional analysis techniques and laboratory measurements* (pp. 42–67). Cambridge University Press.

Lane, M., & Christensen, P. R. (1998). Thermal infrared emission spectroscopy of salt minerals predicted for Mars. *Icarus*, 136(2):528–536.

Lane, M. D., Bishop, J. L., Dyar, M. D., King, P. L., & Hyde, B. C. (2009). Iron sulfate and sulfide spectroscopy at thermal infrared wavelengths. In: *Workshop on modeling Martian hydrous environments.*

Lesher, C. M. (1989). Komatiite-associated nickel sulfide deposits. Chapter 5. In J. A. Whitney & A. J. Naldrett (Eds.), *Ore deposition associated with magmas* (Vol. 4, pp. 45–100). *Reviews in Economic Geology*.

Le Vaillant, M., Fiorentini, M. L., & Barnes, S. J. (2016). Review of lithogeochemical exploration tools for komatiite-hosted Ni-Cu-(PGE) deposits. *Journal of Geochemical Exploration*, 168, 1–19.

Liu, Y., Samaha, N.-T., & Baker, D. R. (2007). Sulfur concentration at sulfide saturation (SCSS) in magmatic silicate melts. *Geochimica et Cosmochimica Acta*, 71(7):1783–1799.

Logan, L.M., Hunt, G.R., Salisbury, J.W., & Balsamo, S.R. (1973). Compositional implications of Christiansen frequency minimums for infrared remote sensing applications. *Journal of Geophysical Research*, 78:4983–5003.

Lorand, J.-P., & Alard, O. (2001). Platinum-group element abundances in the upper mantle: New constraints from in situ and whole-rock analyses of Massi Central xenoliths. *Geochimica et Cosmochimica Acta*, 65(16), 2789–2806.

Maier, W. D. (2005). Platinum-group element (PGE) deposits and occurrences: Mineralization styles, genetic concepts, and exploration criteria. *Journal of African Earth Sciences*, 41(3), 165–191.

Maier, W. D., & Barnes, S.-J. (1999). Platinum-group elements in silicate rocks of the lower, critical and main zones at union section, Western Bushveld Complex. *Journal of Petrology*, 40(11), 1647–1671.

Maier, W. D., Peltonen, P., McDonald, I., Barnes, S. J., Barnes, S.-J., Hatton, C., & Viljoen, F. (2012). The concentration of platinum-group elements and gold in southern African and Karelian kimberlite-hosted mantle xenoliths: Implications for the noble metal content of the Earth's mantle. *Chemical Geology*, 302–303, 119–135.

Maturilli, A., & Helbert, J. (2014). Characterization, testing, calibration, and validation of the Berlin emissivity database. *Journal of Applied Remote Sensing*, 8, 1–12.

Maturilli, A., Helbert, J., Ferrari, S., Davidsson, B., & D'Amore, M. (2016). Characterization of asteroid analogues by means of emission and reflectance spectroscopy in the 1- to 100-μm spectral range. *Earth Planets and Space*, 68(1), 113–124.

Maturilli, A., Helbert, J., & Moroz, L. (2008). The Berlin emissivity database (BED). *Planetary and Space Science*, 56(3–4), 420–425.

Maturilli, A., Helbert, J., Witzke, A., & Moroz, L. (2006). Emissivity measurements of analogue materials for the interpretation of data from PFS on Mars Express and MERTIS on Bepi-Colombo. *Planetary and Space Science*, 54(11), 1057–1064.

Mavrogenes, J. A., & O'Neill, H. S. C. (1999). The relative effects of pressure, temperature and oxygen fugacity on the solubility of sulfide in mafic magmas. *Geochimica et Cosmochimica Acta*, 63(7–8), 1173–1180.

McDonough, W. W., & Sun, S. S. (1995). The composition of the Earth. *Chemical Geology*, 120(3–4), 223–253.

McMillan, P. (1985). Vibrational spectroscopy in the mineral sciences. In S. W. Kieffer & A. Navrotsky (Eds.), *Microscopic to macroscopic: Atomic environments to mineral thermodynamics* (Vol. 14, pp. 9–63). *Reviews in Mineralogy*.

Michelsen, H. A., Colket, M. B., Bengtsson, P. E., D'Anna, A., Desgroux, P., Haynes, B. S., et al. (2020). A review of terminology used to describe soot formation and evolution under combustion and pyrolytic condition. *ACS Nano*, 14(10), 12470–12490.

Moersch, J. E. (1992). Modeling particle size effects on the thermal emission spectra of minerals in the thermal infrared. M.S. thesis (pp. 1–77). Arizona State University.

Moersch, J. E., & Christensen, P. R. (1995). Thermal emission from particulate surfaces: A comparison of scattering models with measured spectra. *Journal of Geophysical Research*, 100(E4):7465–7477.

Naldrett, A. (1999). World-class Ni-Cu-PGE deposits: Key factors in their genesis. *Mineralium Deposita*, 34(3), 227–240.

Naldrett, A. (2010). *Magmatic sulphide deposits: Geology, geochemistry, and exploration* (p. 728). Oxford University Press.

Naldrett, A. J., Wilson, A., Kinnaird, J., & Chunnett, G. (2009). PGE tenor and metal ratios within and below the Merensky Reef, Bushveld Complex: Implications for its genesis. *Journal of Petrology*, 50(4), 625–659.

Naldrett, T., Kinniard, J. A., Wilson, A. H., & Chunnett, G. (2008). Concentration of PGE in the Earth's crust with special reference to the Bushveld Complex. *Earth Science Frontiers*, 15(5), 264–297.

Nash, D. B., Salisbury, J. W., Conel, J. E., Lucey, P. G., & Christensen, P. R. (1993). Evaluation of infrared emission spectroscopy for mapping the Moon's surface composition from lunar orbit. *Journal of Geophysical Research*, 98(E12):23535–23552.

Okada, T., Fukuhara, T., Tanaka, S., Taguchi, M., Imamura, T., Arai, T., et al. (2017). Thermal infrared imaging experiments of C-type asteroid 162173 Ryugu on Hayabusa2. *Space Science Reviews*, 208(1), 255–286.

Osterloo, M. M., Anderson, F. S., Hamilton, V. E., & Hynek, B. M. (2010). Geologic context of proposed chloride-bearing materials on Mars. *Journal of Geophysical Research*, 115(E10012), 1–29.

Osterloo, M. M., Hamilton, V. E., Bandfield, J. L., Glotch, T. D., Baldridge, A. M., Christensen, P. R., et al. (2008). Chloride-bearing materials in the southern highlands of Mars. *Science*, 319(5870), 1651–1654.

Page, N. J., Zientek, M. L., Lipin, B. R., Raedeke, L. D., Wooden, J. L., Turner, A. R., et al. (1985). Geology of the Stillwater complex exposed in the Mountain View area and on the west side of the Stillwater Canyon. In G. K. Czamanske & M. L. Zientek (Eds.), *The Stillwater Complex, Montana: Geology and guide. Special publication 92* (pp. 147–209).

Paige, D. A., Foote, M. C., Greenhagen, B. T., Schofield, J. T., Calcutt, S., Vasavada, A. R., et al. (2010). The lunar reconnaissance orbiter diviner lunar radiometer experiment. *Space Science Reviews*, 150(1–4), 125–160.

Paige, D. A., Lucey, P. G., Wyatt, M. B., Glotch, T. D., Allen, C. C., Arnold, J. A., et al. (2010). Global silicate mineralogy of the Moon from the Diviner lunar radiometer. *Science*, 329(5998), 1507–1509.

Palluconi, F. D., & Meeks, G. R. (1985). Thermal infrared multispectral scanner (TIMS): An investigator's guide to TIMS data (pp. 1–32). JPL Publication. Retrieved from https://ntrs.nasa.gov/api/citations/19850019974/downloads/19850019974.pdf

Peck, D. C., & Huminicki, M. A. E. (2016). Value of mineral deposits associated with mafic and ultramafic magmatism: Implications for exploration. *Ore Geology Reviews*, 72, 269–278.

Petty, G. W. (2006). *A first course in atmospheric radiation* (p. 459). Sundog Publishing.

Raedeke, L. D., & McCallum, I. S. (1980). A comparison of fractionation trends in the lunar crust and the Stillwater Complex. In *Conference on the lunar highlands crust* (Vol. 14, pp. 133–153). Pergamon Press.

Ramsey, M. (2004). Quantitative geological surface processes extracted from infrared spectroscopy and remote sensing. *Infrared Spectroscopy in Geochemistry, Exploration Geochemistry and Remote Sensing*, 33:197–224.

Ramsey, M., & Christensen, P. R. (1998). Mineral abundance determination: Quantitative deconvolution of thermal emission spectra. *Journal of Geophysical Research*, 103(B1): 577–596.

Reyes, D.P., & Christensen, P.R. (1994). Evidence for komatiite-type lavas on Mars from Phobos ISM data and other observations. *Geophysical Research Letters*, 21:887–890.

Righter, K., Pando, K. & Danielson, L.R. (2009). Experimental evidence for sulfur-rich martian magmas: Implications for volcanisms and surficial sulfur sources. *Earth and Planet. Sci.* 43:1709–1723.

Ripley, E. M., & Li, C. (2013). Sulfide saturation in mafic magmas: Is external sulfur required for magmatic Ni-Cu-(PGE) ore genesis? *Economic Geology*, 108(1):45–58.

Ripley, E. M., Wernette, B. W., Ayre, A., Li, C., Smith, J. M., Underwood, B. S., & Keays, R. R. (2017). Multiple S isotope studies of the Stillwater Complex and country rocks: An assessment of the role of crustal S in the origin of PGE enrichment found in the J-M Reef and related rocks. *Geochmica et Cosmochmica Acta*, 214, 226–245.

Rivard, B., Feng, J., Gallie, E. A., & Francis, H. (2001). Ore detection and grade estimation in the Sudbury mines using thermal infrared reflectance spectroscopy. *Geophysics*, 66(6), 1691–1698.

Rogers, A. D., & Christensen, P. R. (2007). Surface mineralogy of Martian low-albedo regions from MGS-TES data: Implications for upper crustal evolution and surface alteration. *Journal of Geophysical Research*, 112(E1), 1–18.

Rudnick, R. L., & Gao, S. (2003). Composition of the continental crust. In H. D. Holland & K. K. Tuekian (Eds.), *Treatise on geochemistry* (1st ed., pp. 1–64). Pergamon.

Ruff, S. W., Christensen, P. R., Barbera, P. W., & Anderson, D. L. (1997). Quantitative thermal emission spectroscopy of minerals: A laboratory technique for measurement and calibration. *Journal of Geophysical Research*, 102(B7), 14899–14913.

Ruff, S. W., Christensen, P. R., Blaney, D. L., Farrand, W. H., Johnson, J. R., Michalski, J. R., et al. (2006). The rocks of Gusev Crater as viewed by the mini-TES instrument. *Journal of Geophysical Research*, 111(E12), 1–36.

Ruff, S. W., Christensen, P. R., Glotch, T. D., Blaney, D. L., Moersch, J. E., & Wyatt, M. B. (2008). The mineralogy of Gusev crater and Meridiani Planum derived from the Miniature Thermal Emission Spectrometers on the Spirit and Opportunity rovers. In J. F. Bell III (Ed.), *The Martian surface: Composition, mineralogy, and physical properties* (pp. 315–338). Cambridge University Press.

Ruff, S. W., & Farmer, J. D. (2016). Silica deposits on Mars with features resembling hot spring biosignatures at El Tatio in Chile. *Nature Communications*, 7(13554), 1–10.

Ruff, S. W., & Hamilton, V. E. (2017). Wishtone to Watchtower: Amorphous alteration of plagioclase-rich rocks in Gusev crater, Mars. *American Mineralogist*, 102(2), 235–251.

Ruff, S. W., Hamilton, V. E., Rogers, D., Edwards, C. S., & Horgan, B. H. N. (2022). Olivine and carbonate-rich bedrock in Gusev crater and the Nili Fossae region of Mars may be altered ignimbrite deposits. *Icarus*, 380, 114974.

Salisbury, J. M., & Walter, L. S. (1989). Thermal infrared (2.5–13.5 μm) spectroscopic remote sensing of igneous rock types on particulate planetary surfaces. *Journal of Geophysical Research*, 94(B7), 9192–9202.

Salisbury, J. W. (1993). Mid-infrared spectroscopy: Laboratory data. Remote geochemical analysis: Elemental and mineralogical composition (pp. 79–98).

Salisbury, J. W., & D'Aria, D. M. (1992). Emissivity of terrestrial materials in the 8–14 μm atmospheric window. *Remote Sensing of Environment*, 42(2), 83–106.

Salisbury, J. W., & Estes, J. (1985). The effect of particle size and porosity on spectra in the mid-infrared. *Icarus*, 64(3), 586–588.

Salisbury, J. W., Walter, L. S., Vergo, N., & D'Aria, D. M. (1991). *Infrared (2.1–25 μm) spectra of minerals.* Johns Hopkins University Press.

Shirley, K. A., & Glotch, T. D. (2019). Particle size effects on mid-infrared spectra of lunar analog minerals in a simulated lunar environment. *Journal of Geophysical Research: Planets*, 124(4):970–988.

Slack, J. F., Kimball, B. E., Shedd, K. B., & Cobalt, C. F. (2017). Critical mineral resources of the United States–Economic and environmental geology and prospects for future supply. In K. J. Schulz, J. H. DeYoung Jr, R. R. Seal II, & D. C. Bradley (Eds.). *U.S. Geological survey professional paper 1802*. (pp.F1–F40).

Song, X., Wang, Y., & Chen, L. (2011). Magmatic Ni-Cu-(PGE) deposits in magma plumbing systems: Features, formation and exploration. *Geoscience Frontiers*, 2(3): 375–384.

Soong, R., & Farmer, V. C. (1978). The identification of sulphide minerals by infra-red spectroscopy. *Mineralogical Magazine*, 42(322), M17– M20.

Taylor, S. R., & McClennan, S. M. (1985). The continental crust: Its composition and evolution and examination of the geochemical record preserved in sedimentary rocks (p. 312). Blackwell Scientific Publication.

Todd, S. G., Keith, D. W., Le Roy, L. W., Schissel, D. J., Mann, E. L., & Irvine, T. N. (1982). The J-M platinum-palladium reef of the Stillwater Complex, Montana: I. Stratigraphy and petrology. *Economic Geology*, 77(6):1454–1480.

Vaughan, D., & Corkhill, C. (2017). Mineralogy of sulfides. *Elements*, 13(2):81–87.

Vaughan, D., & Lennie, A. R. (1991). The iron sulphide minerals: Their chemistry and role in nature. *Science Progress*, 75(3/4), 371–388.

Wänke, H., Dreibus, G., & Wright, I. P. (1994). Chemistry and accretion history of Mars. *Transactions of the Royal Society of London. A*, 349:285–293.

Wenrich, M., & Christensen, P. R. (1996). Optical constants of minerals derived from emission spectroscopy: Application to quartz. *Journal of Geophysical Research*, 101(B7):15921–15931.

West, M. D., & Clarke, J. D. A. (2010). Potential Martian mineral resources: Mechanisms and terrestrial analogues. *Planetary and Space Science*, 58(4):574–582.

Williams, J. P., Greenhagen, B. T., Paige, D. A., Schorghofer, N., Sefton-Nash, E., Hayne, P. O., et al. (2019). Seasonal polar temperatures on the Moon. *Journal of Geophysical Research: Planets*, 124(10):2505–2521.

Williams, J. P., Paige, D. A., Greenhagen, B. T., & Sefton-Nash, E. (2017). The global surface temperature of the Moon as measured by the diviner lunar radiometer experiment. *Icarus*, 283:300–325.

Wykes, J. L., O'Neill, H. S., & Mavrogenes, J. A. (2015). The effect of FeO on the sulfur content at sulfide saturation (SCSS) and the selenium content at selenide saturation of silicate melts. *Journal of Petrology*, 56(7):1407–1424.

Zacny, K., Bar-Cohen, Y., Brennan, M., Briggs, G., Cooper, G., Davis, K., et al. (2008). Drilling systems for extraterrestrial subsurface exploration. *Astrobiology*, 8(3):665–706.

Zacny, K., Betts, B., Hedlund, M., Long, P., Gramlich, M., Tura, K., et al. (2014). PlanetVac: Pneumatic regolith sampling system. *In 2014 IEEE Aerospace Conference*. (pp. 1–7). IEEE.

Zacny, K., Paulsen, G., McKay, C. P., Glass, B., Dav., A., Davila, A. F., et al. (2013). Reaching 1m deep on Mars: The icebreaker drill. *Astrobiology*, 13(12):1166–1198.

Zhang, T., Xu, K., Yao, Z., Ding, X., Zhao, Z., Hou, X., et al. (2019). The progress of extraterrestrial regolith-sampling robots. *Nature Astronomy*, 3(6):487–497.

Zientek, M. L. (2012). Magmatic ore deposits in layered intrusions–descriptive model for reef-type PGE and contact-type Cu-Ni-PGE deposits. *U.S. Geological Survey Open-File Report 2012-1010* (pp. 1–48).

Zientek, M. L., Czamanske, K., & Irvine, T. N. (1985). Stratigraphy and nomenclature for the Stillwater Complex. In G. K. Czamanske & M. L. Zientek (Eds.), *The Stillwater Complex, Montana: Geology and guide. Special publication 92* (pp. 21–38).

Zientek, M. L., Loferski, P. J., Parks, H. L., Schulte, R. F., & Seal II, R. R. (2017). Platinum-group elements, chap. N of Schulz. In K. J. Schulz, J. H. DeYoung Jr, R. R. Seal II, & D. C. Bradley (Eds.), *Critical mineral resources of the United States—economic and environmental geology and prospects for future supply (pp. N1–N91). U.S. Geological Survey. Professional Paper 1802*. https://doi.org/10.3133/pp1802N

CHAPTER 3

PROSPECTING FOR MAGMATIC SULFIDE ORE DEPOSITS USING THERMAL INFRARED EMISSION SPECTROSCOPY

Abstract

Thermal infrared emission spectroscopy has successfully detected many rock-forming minerals on planetary surfaces. However, it remains unclear whether the technique can be used as a tool to prospect for magmatic Ni-Cu±(PGE) sulfide ore deposits due to their lack of distinct spectral features. To clarify this uncertainty, we acquired thermal infrared emission measurements of two physically constructed suites of sulfide/silicate mixtures. The results demonstrate that as the abundance of sulfide increases, the apparent brightness temperature decreases linearly. If unaccounted, this temperature error contributes a negative spectral slope from high to low wavenumbers on the resultant emissivity spectrum, which becomes more pronounced as sulfide increases. Additionally, the presence of sulfide in a mixture with silicates reduces the magnitude of the diagnostic absorption features of the silicate mineral. This reduction in spectral contrast is linear as the proportion of sulfide increases. While this phenomenon is commonly attributed to a reduction in particle size, reductions in spectral contrast due to the contribution of a graybody component can be distinguished from particle size effects by the lack of Transparency Features. A linear retrieval (spectral deconvolution) algorithm was also applied to the emissivity spectra of our particulate mixtures, confirming that the assumption of linear mixing remains valid when a graybody component is present. Additionally, the model detected pyrrhotite at abundances of ≥10 modal %. These results provide a foundation for a resource prospecting campaign at one

of the previously identified “spectrally featureless” units on Mars that share similar spectral properties to the emissivity spectra presented in this study.

3.1 Introduction

Most magmatic Ni-Cu-PGE sulfide deposits form through segregation, concentration, and crystallization of a metal-rich (i.e., Ni, Cu, Co, platinum-group elements) sulfide melt which forms when a mafic to ultramafic magma produced from high degrees of partial melting becomes saturated in sulfur (Arndt et al., 2005; Barnes et al., 2005). The factors that lead to the saturation of mafic to ultramafic magmas in iron sulfide include: (1) an increase in pressure, (2) a decrease in temperature, (3) a change in magma composition (notably, a decrease in FeO content through the addition of crustal silica), (4) an increase in sulfur through assimilation of S-rich country rock, (5) water content, and (6) an increase in oxygen fugacity (Mavrogenes & O’Neil. 1999; Righter et al., 2009; Ding et al., 2015; Ripley & Li, 2013; Li & Ripley, 2005,2009; Liu et al., 2007; Liu et al., 2021). Because the phase with the highest partition coefficient for the metals in a silicate-rich magma is the immiscible sulfide melt, the economically desirable metals are preferentially concentrated in the melt as it interacts with its parent magma (Campbell & Naldrett, 1979; Patten et al., 2013; Barnes & Lightfoot, 2005; Barnes et al., 2017). Depending on the geologic setting, the sulfide melt (initially forming as individual droplets) eventually segregates and coalesces at the bottom of magma chambers, at the base of channels and in feeder tubes within lava-flow fields, and in other structural traps in magmatic plumbing systems (Song et al., 2011; Perring, 2015). The sulfides then

accumulate and crystallize in sufficient quantities at these locations to form an economic ore deposit (Righter et al., 2009).

Information derived from orbital remote sensing instruments (Reyes & Christensen, 1994; Christensen et al., 2001,2004; Bandfield, 2002; Bibring et al., 2005; Murchie et al., 2007), in-situ observations of the martian surface (Christensen et al., 2003,2004; Klingelhöfer et al., 2004; Squyres et al., 2004; McSween et al., 2006; Blake et al., 2012), and examinations of martian meteorites (Nyquist et al., 2001; Papike et al., 2009) indicate that Mars exhibited widespread igneous activity with physicochemical characteristics analogous to terrestrial mantle-derived mafic to ultramafic magmatism. These terrestrial magmas produced large concentrations of disseminated to massive Ni-Cu-PGE sulfides, leading scholars to question whether Mars produced similar economically viable ore deposits (Burns & Fisher, 1990). Recent research has concluded that martian magmas do indeed have the capacity to form sulfide deposits (Baumgartner et al., 2015;2017). Additionally, the many impact events on Mars may also produce sulfide mineralization events similar to the Sudbury impact structure found on Earth (West & Clarke, 2010). Thus, it is conceivable that primitive sulfide ore deposits exist on Mars. The question remains as to how we can explore for such deposits.

The first step in developing a space resources economy is determining the resources' locations, quantities, distributions, and accessibility of the resources. This step can be performed by deploying orbital and roving remote sensing instruments capable of characterizing the surface and near subsurface. Subsurface terrestrial exploration techniques for sulfide orebodies include airborne aeromagnetic surveys, in-situ electromagnetic surveys, seismic surveys, and mapping gravity anomalies (Blakely &

Zientek, 1985; Zientek et al., 2012; Le Vaillant et al., 2016). In the case of Mars, gravity anomalies beneath Tyrrhena Patera, Hadriaca Patera, and Amphitrites Patera, along with magnetic signatures and gravity anomalies of Syrtis Major, are consistent with the existence of solidified magma chambers analogous to terrestrial layered intrusions such as the Stillwater and Bushveld Complex (Kiefer, 2004; Lillis et al., 2015).

Building from the work of Hubbard et al. (2023), we report on the results of a series of experiments using physically constructed sulfide/silicate mixtures to investigate whether thermal infrared emission spectroscopy could be utilized as a prospecting tool for extraterrestrial ore deposits containing Ni-Cu-PGM sulfides. The lack of research on remote detection of sulfide minerals on Mars may be attributed to their lack of remotely identifiable optical features and their susceptibility to rapid oxidation. In fact, recent thermal infrared emissivity measurements demonstrate that pyrrhotite–the most common constituent in magmatic sulfide ore deposits–lacks the diagnostic spectral features commonly used when interpreting the composition of planetary surfaces (Hubbard et al., 2023).

Similar to chloride (Osterloo et al., 2008,2010), the systematic low emissivity of pyrrhotite in the mid-infrared (e.g., a "graybody) leads to incorrect temperature estimations and the addition of spectral slopes, which can further complicate mineralogical interpretations (Hubbard et al., 2023). However, this work demonstrates that the distinctive spectral characteristics described above can be exploited to prospect for sulfide ore bodies. In this paper, we describe the effects of magmatic pyrrhotite ($Fe_{1-x}S$) on the estimation of sample temperature and how the presence of a graybody component alters the spectral features of other components present in a composite

emissivity spectrum. We also provide a quantitative investigation of the limits and applicability of spectral deconvolution on thermal emission spectra containing a graybody end member to determine how much sulfide would be required for an ore deposit to be detectable. We conclude with a brief discussion on a future prospecting campaign to investigate a compositional unit on Mars exhibiting similar spectral features to our sulfide mixtures.

3.2. Materials and Experimental Method

3.2.1 Sample Selection and Preparation

The sample suites consist of 1 cm^3 of 500–710 μm physically constructed mixtures containing magmatic pyrrhotite and quartz (ASU ID: BUR4120) or forsteritic olivine (ASU ID: BUR3720A). Because the density of pyrrhotite (~4.61 g/cm^3) is much higher than the density of quartz (2.65 g/cm^3) and forsteritic olivine (3.27 g/cm^3), each mixture was constructed by filling the sample cup with pre-determined volume percentages considering the mineral densities. The amount of sulfide in each mixture ranges from 0 to 100 volume percent in increments of 10 percent, with an additional mixture containing 5 volume percent sulfide to test the sensitivity of the technique. Assuming that the samples are well-mixed at depth, the areal (modal) fraction of each component in a mixture measured by the spectrometer equates to the volume fraction of each component. Two sample suites containing different silicate end members were constructed to validate the spectral effects of sulfide on emissivity spectra.

Sample preparation for the silicate end members follows the method presented in Christensen et al. (2000). The preparation method of the pyrrhotite ($Fe_{1-x}S$) end member

consists of several stages and is described in detail in Hubbard et al. (2023). Compositional information for the silicate end members can be found in the online spectral library at Arizona State University (https://speclib.asu.edu/).

Pyrrhotite was selected for this study because nearly all unaltered magmatic sulfide ores have a characteristic assemblage of pyrrhotite–pentlandite–chalcopyrite–platinum-group minerals (Vaughn & Lennie, 1991; Barnes et al., 2017). Because it is the most abundant phase in magmatic sulfide deposits, pyrrhotite is the most likely sulfide phase to be detectable if an orebody were exposed on the surface of Mars. Silicates were utilized as end members in our mixture experiments because any magmatic sulfide orebody found on Mars will likely be co-associated with silicate minerals. Thus, mixing sulfide with a silicate component allows us to understand better how a sulfide orebody might appear spectrally.

3.2.2 Laboratory Procedure

Spectral data were collected from 2000–200 cm^{-1} (5–50 μm) using a Nicolet iS50R Fourier-Transform Infrared Spectrometer modified for emission with a spectral sampling of 2 cm^{-1} (4 cm^{-1} resolution). Each spectrum was calibrated using the conventional One Temperature Method (OTM; Ruff et al., 1997) and the Reference Temperature Method (RTM; Hubbard et al., 2023). While the OTM estimates the temperature of the sample by assuming that somewhere in the spectrum that the emissivity is equal to 1.0, the Reference Temperature Method utilizes the average brightness temperature of multiple reference sample measurements with known CFs to compute emissivity. The technique was specifically developed to produce more accurate

emissivity spectra of samples that violate the assumption of unit emissivity (Hubbard et al., 2023)

Each emissivity spectrum is an average of 14 consecutive spectral radiance measurements. Each spectral radiance measurement is the average of 64 spectral scans acquired in 55 seconds. Each mixture was re-mixed and re-measured three times to improve the likelihood that the mineral grains exposed at the optical surface were proportionate to the mixed percentages. Photographs of one of the three measurements for each mixture are shown in Figure 3.1.

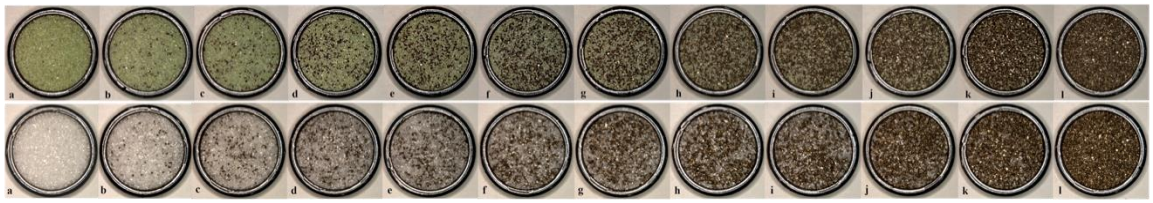

Figure 3.1 – 500-710 μm (top) sulfide/forsterite and sulfide/quartz (bottom) mixture suites used in this study. To make the mixtures, the density of each component was utilized to determine how much mass of each component was required to achieve the pre-determined volumes. From left to right: (a) 100% silicate, (b) 5% sulfide / 95% silicate, (c) 10% sulfide / 90% silicate, (d) 20% sulfide / 80% silicate, (e) 30% sulfide / 70% silicate, (f) 40% sulfide / 60% silicate, (g) 50% sulfide / 50% silicate, (h) 60% sulfide / 40% silicate, (i) 70% sulfide / 30% silicate, (j) 80% sulfide / 20% silicate, (k) 90% sulfide / 10% silicate, (l) 100% sulfide.

The advantage of thermal infrared emission spectroscopy for resource prospecting is that the composite emission spectrum of a target surface or sample is a linear combination of each component at the optical surface (Gillespie, 1992; Ramsey and Christensen, 1998; Ramsey, 2004), which is not the case for other spectral regions. The assumption of linearity is made possible by the high absorption coefficients of coarse particulate samples that minimize nonlinear scattering effects (Hamilton & Christensen, 2000). Coarse particles such as those used in this study have diameters ~25-50x the TIR

wavelengths, assuring that volumetric scattering is minimized (Ramsey & Christensen, 1998). Because photons have a much shorter path length relative to the grain size of coarse particulates and rocks, photons can only interact with one particle before they are either completely absorbed or return to the detector (Ramsey, 2004). Therefore, linear spectral deconvolution methods can be used to "unmix" the emitted thermal energy that reaches the detector to derive the modal abundance of the target resource present on the optical surface.

3.3 Results

3.3.1 Calibrated Radiance and Brightness Temperature Results

The kinetic temperature of a planetary surface or laboratory sample is estimated remotely by deriving a brightness temperature from its measured calibrated radiance. The brightness temperature is not the same as the actual physical temperature. Rather, it is the temperature at which a blackbody in thermal equilibrium with its surroundings would have to be to emit the observed radiance at a discrete wavenumber. To calculate the brightness temperature of a laboratory sample or planetary surface, it must be assumed that there is an emissivity maximum at or very close to unity over some portion of the spectrum (Christensen & Harrison, 1993; Ruff et al., 1997; Christensen et al., 2001; Bandfield, 2009; Hubbard et al., 2023), an assumption that holds at the Christiansen Frequency (CF) feature for >95% of the rock-forming minerals constituting rocky planetary bodies (Salisbury et al., 1991; Hook et al., 1992; Kealy & Hook, 1993; Ruff et al., 1997; Gillespie et al., 1998). When the CF coincides with a low extinction coefficient (*k*), thermal energy easily propagates into and out of the material, leading to an emissivity

maximum at or very close to 1.0. This means that the emitted energy at this wavenumber exhibits blackbody character and can be used to estimate the kinetic surface temperature using the Planck equation.

Pyrrhotite lacks a CF feature and exhibits a uniform, systematically low emissivity of ~0.7 in the mid-infrared, making it a graybody mineral within the spectral range of the instrument (Hubbard et al., 2023). This characteristic makes its estimated brightness temperature appear much cooler than its physical temperature (Hubbard et al., 2023). While this is unusual, Osterloo et al. (2008, 2010) previously identified compositional units on Mars with similar spectral characteristics to pyrrhotite, which were interpreted to be chlorides based on morphological characteristics.

One possible way to detect an extraterrestrial sulfide orebody using thermal infrared spectroscopy is from the difference in its apparent brightness temperature relative to the surrounding country rock. We demonstrate this by acquiring calibrated radiance measurements of samples containing 100% silicate and samples containing silicate and a range of sulfide abundances. While removing temperature effects from spectral measurements is typically done to isolate the temperature-independent spectral properties utilized to compositionally map planetary surfaces (Gillespie et al., 1998), the apparent temperature can also serve as a tool to identify low-emissivity, graybody minerals.

The systematic graybody behavior of pyrrhotite means that the amount of energy emitted from the surface, and observed at the detector, is significantly lower than that of a blackbody emitter. Because of this, the classical assumption of unit emissivity is no longer valid, and will result in errors when deriving surface kinetic temperature. A

fundamental principle of thermal infrared remote sensing is that the emitted energy from a multi-mineralic surface is a linear combination of the energy radiated from each component in proportion to its areal percentage (Ramsey & Christensen, 1998). Thus, if a sulfide-enriched location were detected on the surface of Mars, the energy of the sulfide component would linearly combine with that of the silicate components. Doing so results in a systematic reduction in the total amount of radiant energy relative to an area on the surface composed entirely of silicate (Figure 3.2). Moreover, the apparent brightness temperature of the sulfide-enriched surface will *appear* lower because the presence of the low-emissivity component reduces the emitted radiance at the silicate's Christiansen Frequency. As demonstrated in Figure 3.2, as the abundance of sulfide increases in our mixtures, the emitted radiance decreases systematically across the spectrum even though the sample kinetic temperature remains constant.

The emitted radiance of mixtures containing predominantly pyrrhotite exhibit a spectral shape similar to a blackbody. We attribute this to the graybody and nearly spectrally featureless nature of pyrrhotite (Hubbard et al., 2023). When radiance of the sulfide end member is higher than the radiance values at wavenumber intervals where the silicate end member exhibits spectral absorptions (i.e., the quartz doublet at ~1150 cm^{-1} and the feature at ~500 cm^{-1}), the combined energy from the two components results in an increase in radiance and a simultaneous reduction in the spectral contrast of the spectral feature. At wavenumbers where the amount of energy radiating from the sulfide component is less than the graybody regions of the silicate component (i.e., the forsterite feature from ~1100-900 cm^{-1}), the silicate features similarly reduce in spectral contrast,

but the emitted spectral radiance decreases. These effects intensify proportionally as the sulfide component increases.

The brightness temperatures for both mixture suites determined at the CF feature of the silicate end member are shown in Figure 3.3. Brightness temperatures were determined assuming unit emissivity between 1350-1360 cm^{-1} for the quartz mixture suite and 1150-1250 cm^{-1} for the forsterite suite. Assuming each sample has equilibrated to the experimental reference surface temperature of ~352.3 ± 1.7K during measurement (Hubbard et al., 2023), the results show that brightness temperature decreases linearly with increasing sulfide abundance because the sulfide (graybody) component reduces the emission at the CF of the silicate component. When fitting a blackbody curve to the CF, the estimated temperature is lower than the actual physical temperature, making sample's with significant amounts of sulfide appear colder than their true physical temperature. Put differently, as sulfide increases, the estimated apparent brightness temperature becomes less indicative of the true physical temperature of the sample. Thus, assuming unit emissivity somewhere in the spectrum during calibration (Ruff et al., 1997), we observe a temperature error that increases linearly as the abundance of sulfide increases.

If a prospecting campaign were to exploit such temperature errors to prospect for sulfide orebodies, they would have to be distinguished from other variations in surface temperature previously described in the literature, such as those related to thermal inertia, topography, or surface roughness (Christensen, 1986; Colwell & Jakosky, 2002; Bandfield & Edwards, 2008; Bandfield, 2009; Kieffer, 2013).

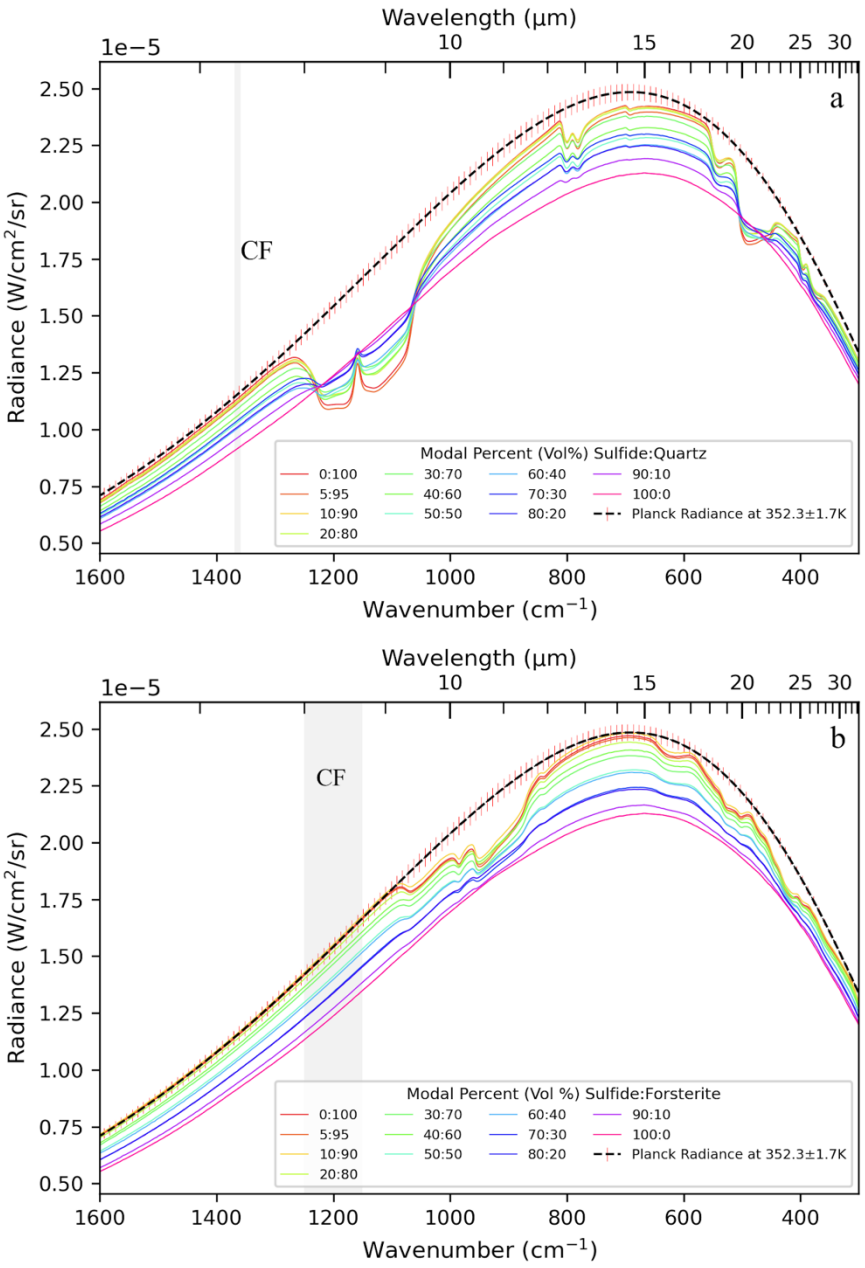

Figure 3.2 – Average emitted radiance for each sample in the (a) quartz/sulfide and (b) forsterite/sulfide mixture suites, demonstrating how the addition of a graybody material (e.g., pyrrhotite) reduces the total emitted radiance, despite each sample reaching approximately the same physical temperature. The actual temperature of each sample was determined by repeatedly measuring reference samples with known Christiansen Frequencies (CF; Chapter 2), which is represented by a dashed Planck curve. As sulfide increases in our mixtures, the spectral radiance curves appear to take on the shape of a blackbody radiance curve. This is due to the spectrally neutral character of the sulfide component. Sample temperatures were estimated at the CF, which was determined for each mixture in the wavenumber interval indicated in gray.

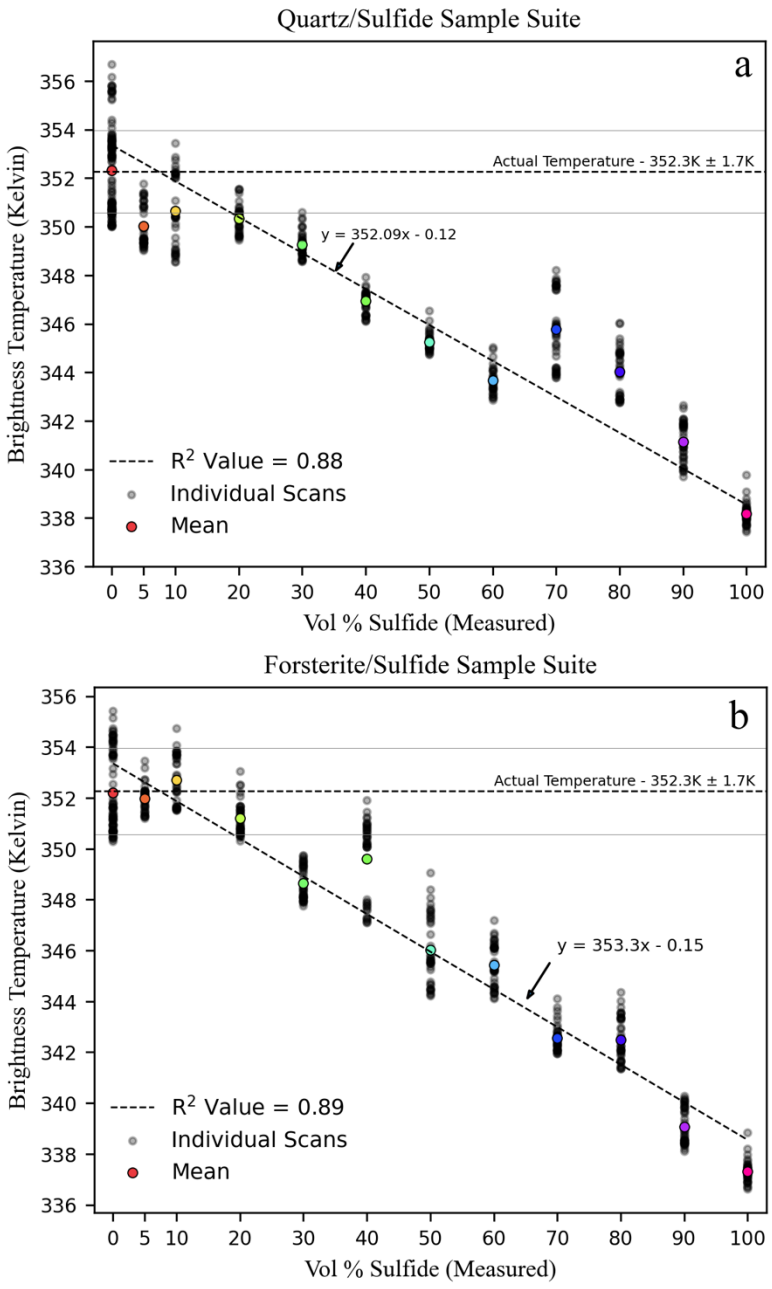

Figure 3.3 – Relationship between sulfide abundance and apparent brightness temperature in the (a) quartz/sulfide and (b) forsterite/sulfide mixture suites. Each gray dot represents a single brightness temperature measurement. The colored dots represent the average for each mixture. Dot colors correspond to the average emitted radiance shown in Figure 3.2. The diagonal dashed lines are linear fits demonstrating the linear relationship between sulfide abundance and a decrease in apparent brightness temperature. The horizontal dashed lines represent the actual physical temperature of the samples and the gray lines represent the standard error derived from experiments reported in Chapter 2.

3.3.2 Emissivity Results Using the One-Temperature Method

Thermal emissivity is the efficiency with which a surface emits its stored heat as thermal infrared radiation (Gillespie, 2014) The collection of thermal infrared emissivity spectra is useful because it contains compositional information about the radiating surface that can be quantified using spectral deconvolution algorithms. The exact locations, shapes, and intensities of spectral absorptions (i.e., spectral bands) in TIR-emissivity spectra depend on the relative masses, radii, distance, bond angles, and bond strengths between atoms (e.g., Nash et al., 1993). Such parameters are governed by the structural arrangement of the anions (i.e., their polymerization) and the location and composition of the associated cations. In the TIR, spectral bands are caused by the stretching and bending motions in bound atoms when interacting with incident electromagnetic radiation. Thus, each mineral produces a diagnostic suite of spectral features in the mid-infrared that allow for mineral groups such as silicates, carbonates, sulfates, phosphates, oxides, and hydroxides to be discriminated from one another and be readily identified on planetary surfaces (Christensen et al., 2000). The Reststrahlen Bands are the most prominent spectral signatures found in the thermal infrared region at approximately 8–12μm for silicates (~1250–714 cm^{-1}) (Salisbury & Walter, 1989; Ramsey, 2004). Additional features resulting from the metal-oxygen and lattice vibrations are typically found at lower wavenumbers (Salisbury & Walter, 1989; Hamilton, 2010).

When calibrating a spectrum of 100% pyrrhotite, the incorrect assumption of unit emissivity inherent in the conventional OTM (Ruff et al., 1997) not only results in an inaccurate temperature estimation but also imparts a significant slope from high to low

wavenumbers in emissivity spectra (Hubbard et al., 2023). The spectrum will also exhibit non-physical emissivity values ($\varepsilon > 1.0$) at wavenumbers higher than the location incorrectly assumed to be unity. Such spectral slopes previously observed in martian remote sensing data (Osterloo et al. 2008, 2010; Bandfield, 2009) also appear in the emissivity spectra of our sulfide/silicate mixtures (Figure 3.4). The slope steepens as the modal percent of sulfide increases.

Moreover, magmatic pyrrhotite does not exhibit distinct Reststrahlen Bands or other spectral absorptions in the mid-infrared region (~5-50 μm) typically used in mineral characterization (Hubbard et al., 2023). While this "spectrally flat" characteristic might suggest that it would be difficult to identify that the sulfide component is present, when the emitted energy of pyrrhotite combines with the emitted energy of the silicate host rock, it reduces the spectral contrast (i.e., shallower features) of all silicate features across the composite spectra linearly with increasing sulfide abundance.

Depending on whether the emissivity of the silicate absorptions is higher or lower than the apparent emissivity of pyrrhotite, the silicate spectral band will either increase or decrease in emissivity while also reducing in spectral contrast. This phenomenon is evident in Figure 3.4 when the known sulfide abundance is ≥10%. Regardless of the wavenumber position of the absorption feature, the band depth of the silicate absorption features decreases as the abundance of sulfide increases. While spectral slopes in emissivity spectra present difficulties in interpreting the composition and mineralogy of a sample, a spectral slope from high to low wavenumbers coupled with spectral features with severely reduced contrast may be used alongside brightness temperature errors to prospect for sulfide ore deposits.

The morphological characteristics of emissivity spectra are affected by the scattering of energy within the mineral sample. Scattering effects depend upon the differences in the wavelength-dependent optical properties (*n*) and (*k*) between the grains and the surrounding medium, as well as the size and shape of the particle itself (Moersch & Christensen, 1995). When the index of refraction (*n*) of the material is small, and the absorption coefficient (*k*) is large, surface (Fresnel) scattering dominates (Moersch & Christensen, 1995). Because *k* is large, a considerable amount of energy propagating within the mineral grain will be reflected back into the grain at the first grain/surface interface (Lane, 1999). For large particles, this prevents very little energy from passing through the grain boundary and escaping the sample (Moersch & Christensen, 1995). Instead, most of the energy at that location in the electromagnetic spectrum is absorbed and reemitted, manifesting in emissivity spectra as strong spectral absorption features (i.e., low emissivity). This "Type 1" behavior (Hunt & Vincent, 1968) is responsible for all the absorption features present in the emissivity spectra displayed in Figure 3.4.

Many scholars have previously described the significance of particle size on emissivity spectra (Lyon, 1965; Conel, 1969; Salisbury & Eastes, 1985; Salisbury et al., 1987; Salisbury & Walter, 1989; Shirley & Glotch, 2019). In particular, Moersch & Christensen (1995), Mustard & Hays (1997), and Maturilli et al. (2008) describe these effects for the silicate end members used in this study. As grain size decreases, the number of interfaces for photons to interact with increases. This leads to an increase in the fraction of energy that is refracted (absorbed) and subsequently re-emitted by the sample. Multiple reflections decrease the magnitude of the reflectivity, increasing

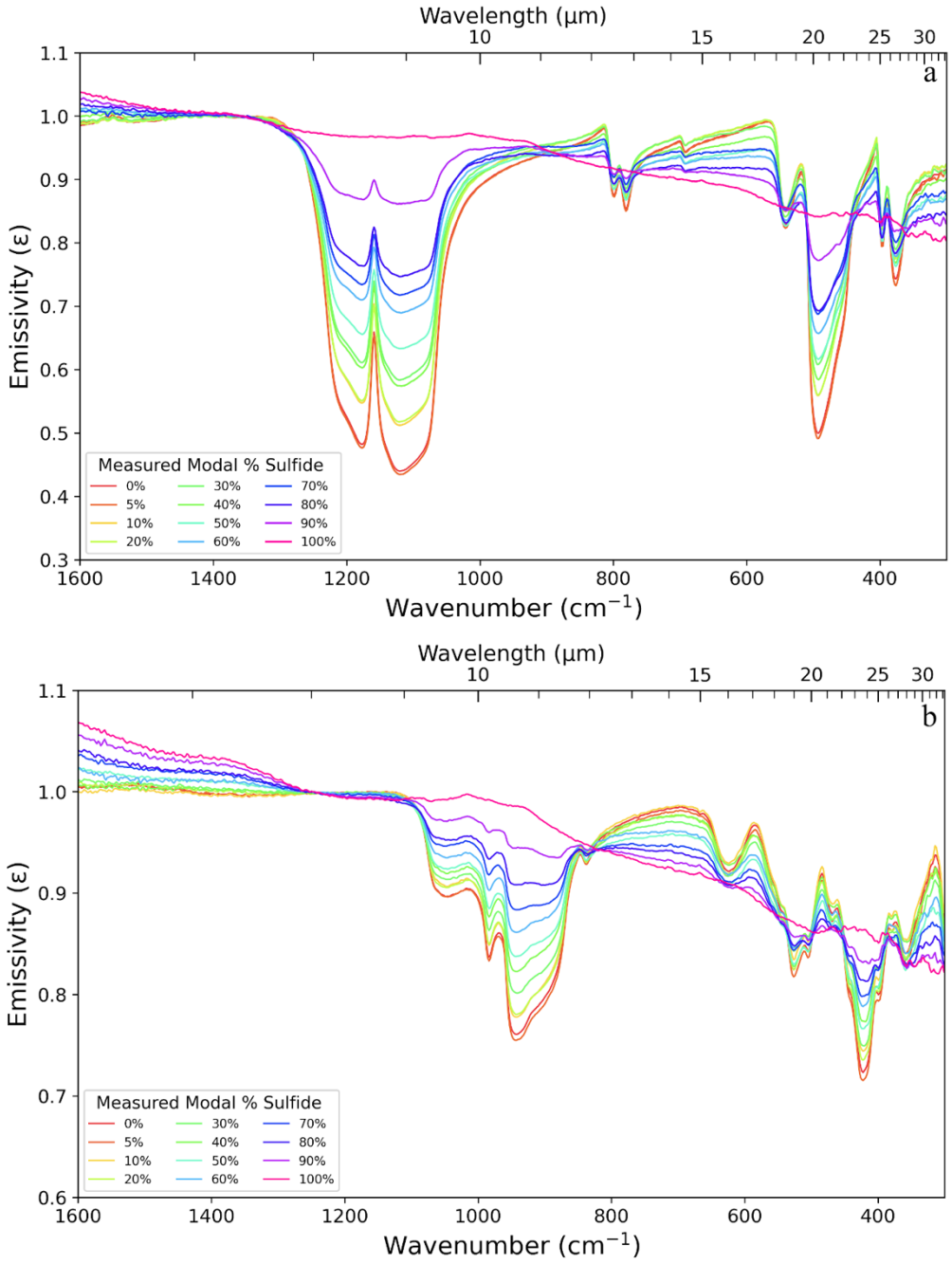

Figure 3.4 – Emissivity spectra of the quartz/sulfide (a) and forsterite/sulfide (b) mixtures from 1600-300 cm^{-1} calibrated using the OTM. Each spectrum represents an average of at least three spectral measurements of the physical mixture. We assume unit emissivity between 1350-1370 cm^{-1} for the quartz mixtures and 1150-1250 cm^{-1} for the forsterite/sulfide mixtures. Data collected >1600cm^{-1} are not shown because there are no absorption features in that range. The figures illustrate how an increase in sulfide content imparts a negative slope from high to low wavenumbers and reduces the spectral contrast of the coexisting silicate components in the mixture.

emissivity (e.g., a decrease in spectral contrast) at the principal vibrational modes (Lane 1999).

Furthermore, Transparency Features (TFs) appear in regions of a spectrum where the mineral is weakly absorbing (*k* is small) and n is moderate (Moersch & Christensen, 1995). This "Type 3" behavior results in little surface scattering, allowing propagating energy to easily pass through a mineral grain and for true absorption processes (e.g., volume scattering effects) to dominate how much energy is leaving the sample or planetary surface (Salisbury and Wald, 1992; Moersch & Christensen, 1995). A decrease in particle size results in a longer path length and more optical surfaces for energy to travel through, leading to more absorption and a decrease in emitted energy in these regions of the spectrum (Hunt & Vincent, 1968). As shown in Figure 3.5, TFs emerge in the intraband regions at ~1550 cm^{-1}, ~900 cm^{-1}, ~775 cm^{-1}, and ~625cm^{-1} for the fine-grained quartz spectra contain.

The decrease in spectral contrast at the Restrahlen Bands due to a decrease in grain size (Figure 3.5) appears similar to the decrease in spectral contrast resulting from an increase in sulfide in our mixtures (Figure 3.4a). While this reduction in spectral contrast could easily be misinterpreted in remote sensing data as a decrease in the grain size of the silicate component, there are apparent differences in the spectral shapes between the sulfide/quartz mixture spectra in Figure 3.4 and the fine-grained quartz emissivity spectra displayed in Figure 3.5. Additionally, the TFs do not exist in the sulfide/silicate mixture spectra. Coupled with the reduction in the spectral contrast at the RBs of the silicate features, the lack of such features can be used to distinguish between a sulfide-enriched silicate ore body from a fine-grained surface composed of only silicates.

While an increase in the abundance of sulfide and a decrease in the particle size of the silicate end member both lessen the intensity of the Reststrahlen Bands, the morphology of the principal Reststrahlen Band in Figure 3.5 becomes distorted as the particles become very fine, an observation also apparent in olivine spectra (Maturilli et al., 2008). Thus, a sulfide ore body could be distinguished from a fine-grained sulfide-barren surface through qualitative examination of the intraband regions for TFs, the spectral contrast of the absorption features of the coexisting silicate, and the spectral shape of the principal Reststrahlen Bands of the coexisting silicates.

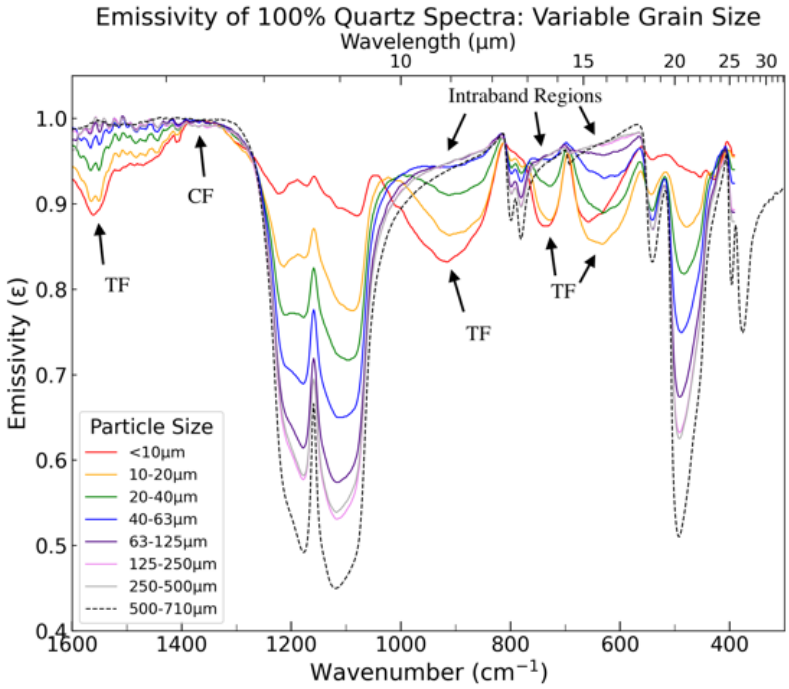

Figure 3.5 –Measured emissivity spectra of particulate quartz for a range of size fractions in an ambient environment, depicting how a reduction in grain size significantly alters the spectral morphology. Unlike our sulfide/quartz mixture suite, TFs centered at ~1550 cm^{-1}, ~900 cm^{-1}, ~775 cm^{-1}, and ~625 cm^{-1} appear in the intraband regions of quartz' emissivity spectrum as particle size decreases. Reststrahlen Bands decrease in spectral contrast, and their spectral shape is distorted due to volume scattering effects at very fine particle sizes. The blackbody character ($\varepsilon = 1.0$) at the Christiansen Frequency remains present regardless of particle size. Spectra with solid lines are data from Wenrich & Christensen (1996). The dashed spectrum was derived from measurements collected by the authors at the Mars Spectral Laboratory at Arizona State University.

3.3.3 Emissivity Results Using the Reference Temperature Method

Spectra of the sulfide/silicate mixture suites calibrated using the Reference Temperature Method (Hubbard et al., 2023) are shown in Figures 3.6 and 3.7. Generally, the absolute emissivity of the sulfide/silicate mixtures systematically decreases as the sulfide's abundance increases. Begemann et al. (1994) report extremely high indices of refraction but low extinction coefficients from 1000-250 cm^{-1} for synthetic pyrrhotite. Thus, the systemically high reflectivity (low-emissivity) of mixtures with high abundances of pyrrhotite may result from the high refractive indices of pyrrhotite across the spectral range.

Similar to the spectra calibrated using the OTM, the silicate absorption features reduce in spectral contrast. However, the spectral slope is no longer present, which we attribute to the RTM not assuming unit emissivity during calibration. Removing this assumption means that the RTM generates absolute emissivity spectra rather than apparent emissivity spectra.

Unlike the conventional OTM, the absolute emissivity spectra derived from the RTM provide a visualization of the reflected energy of the sulfide component in our mixtures and why our temperature estimates are incorrect when unit emissivity was assumed. In the intraband regions of the silicate spectral features, the low emissivity of pyrrhotite linearly combines with the near-blackbody energy of the silicate component, resulting in lower emissivity values relative to the pure silicate endmember spectrum. If the Restrahlen Bands and other spectral features derived from the silicate end members exhibit higher or lower emissivity values than the pyrrhotite spectrum, the Reststrahlen

Bands will either decrease or increase in emissivity as sulfide abundance increases.

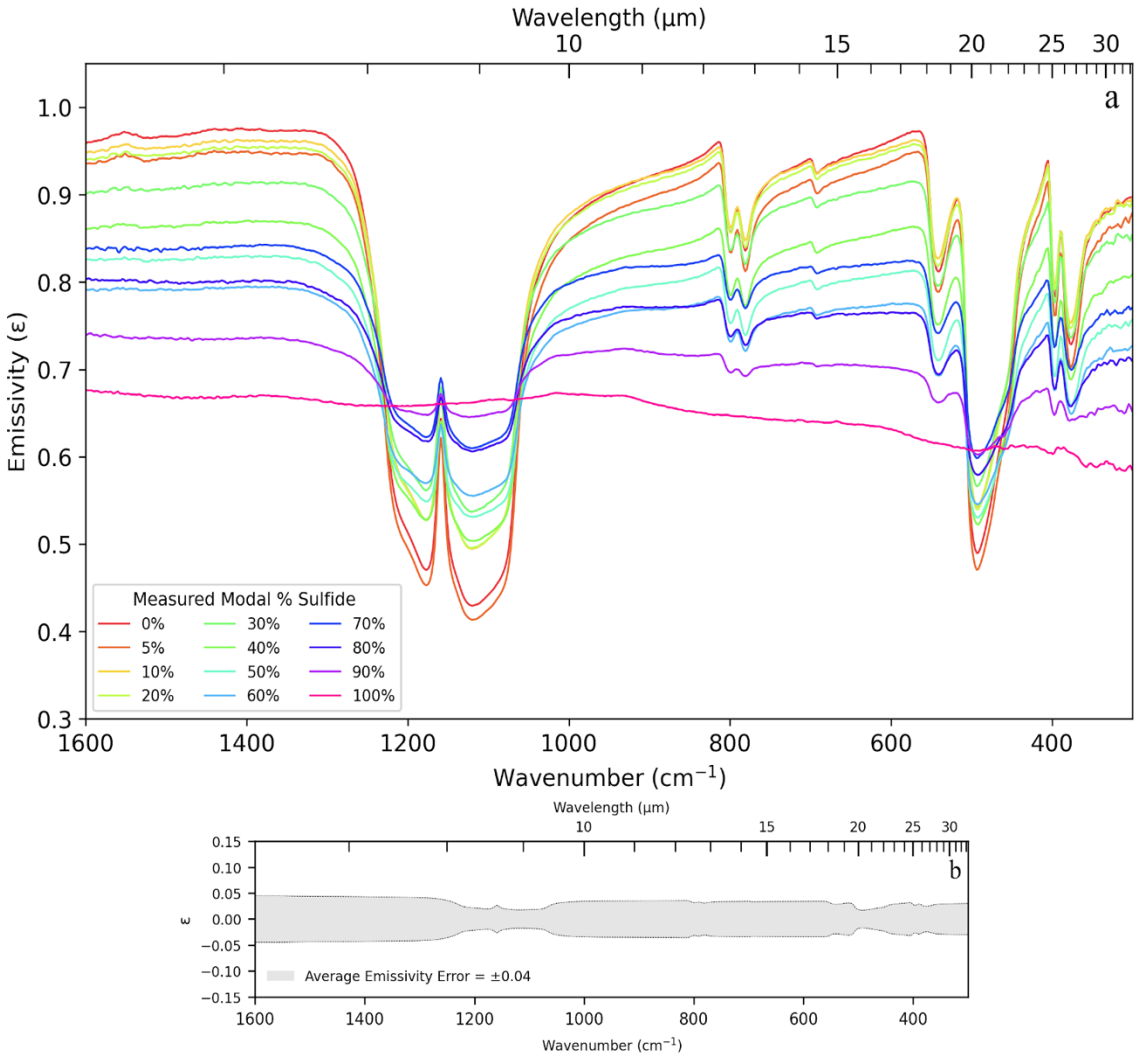

Figure 3.6 – (a) Emissivity spectra of the sulfide/quartz mixture suite calibrated using the Reference Temperature Method, demonstrating how a more accurate sample temperature produces absolute emissivity spectra with systematically low emissivity across the spectrum when sulfide is present. (b) The emissivity error shown is the standard error from the mean for the 100% quartz spectra measured for this study.

The effects of all known sources of error for a spectrum calibrated using the RTM are reported in Hubbard et al. (2023), with the most significant contribution resulting from the uncertainty in sample temperature due to the use of a reference sample during calibration. The emissivity error per unit wavenumber for spectral measurement of 100%

quartz and 100% forsterite silicate samples are shown in Figures 3.6 and 3.7. Due to the non-linear relationship between temperature and wavenumber, the emissivity error decreases from high to low wavenumbers. We also observe slightly smaller errors in regions where spectral absorptions are present.

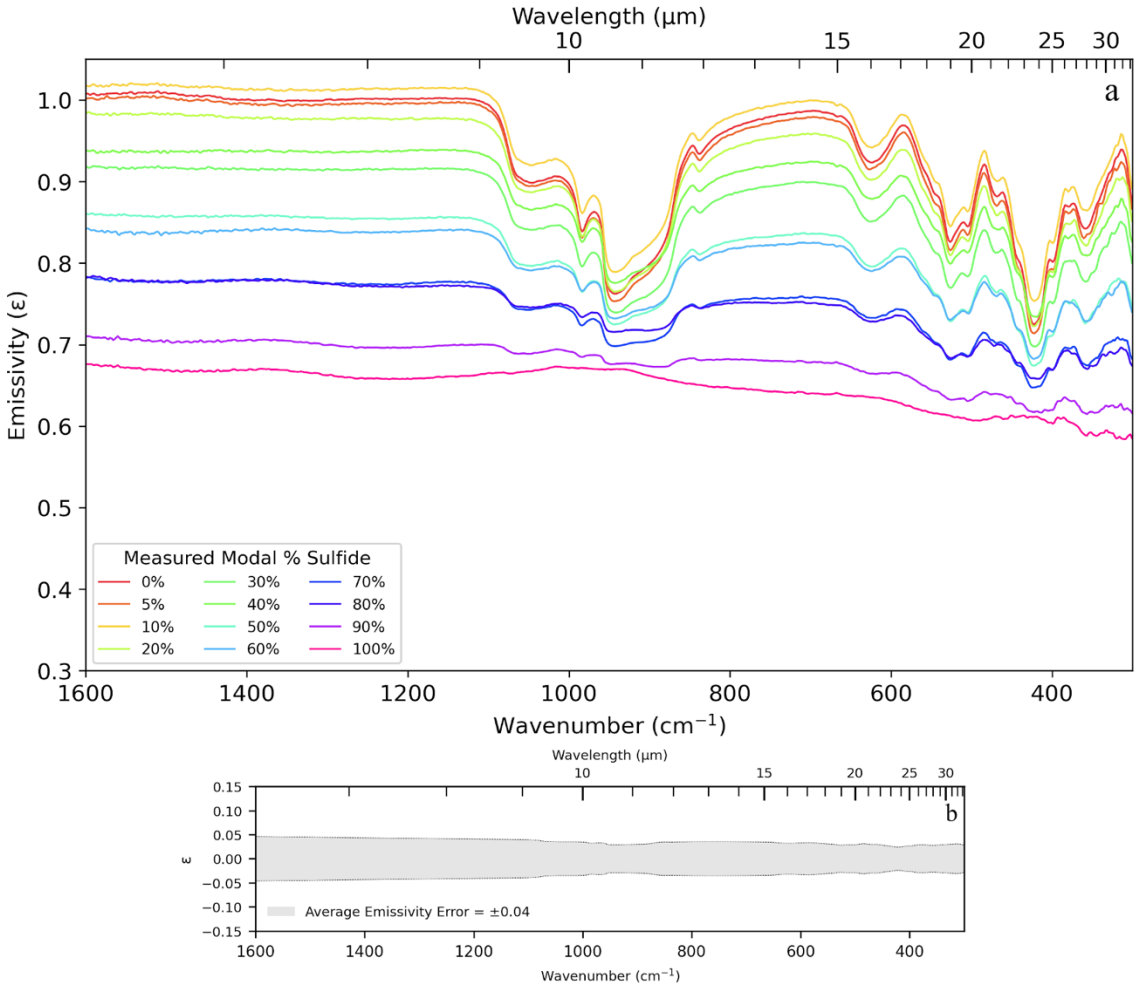

Figure 3.7 – (a) Emissivity spectra of the sulfide/forsterite mixture suite calibrated using the Reference Temperature Method, demonstrating how a more accurate sample temperature produces absolute emissivity spectra with systematically low emissivity across the spectrum when sulfide is present. (b) The emissivity error is the standard error from the mean for the 100% forsterite spectrum.

The position of the CF feature has been used to estimate the composition of laboratory samples and planetary surfaces (Conel, 1969; Logan et al., 1973; Salisbury & Walter, 1989; Donaldson Hanna et al., 2012, 2014; Hamilton, 2010). For silicates, the wavenumber position of the CF shifts to lower wavenumbers as the material becomes more mafic and is strongly dependent on the degree of polymerization of minerals (Nash et al., 1993; Greenhagen et al., 2010; Salisbury & Walter, 1989; Shirley and Glotch, 2019). Additionally, the wavenumber position of the CF also has trends as a function of solid solution composition (e.g., Hamilton, 2010).

So long as the physical temperature is accurate when computing emissivity, we show that the emissivity at the CF can also be used to estimate the abundance of a graybody component. Figure 3.8 shows a strong linear correlation between sulfide abundance and the emissivity at the CF for both the quartz/sulfide ($R^2 = 0.918$) and the forsterite/sulfide mixtures ($R^2 = 0.958$). As the graybody component increases, the emissivity at the CF feature of the silicate end member relative to the pure silicate spectrum decreases linearly.

3.3.4 Continuum Removal

To alleviate issues inherent in both the OTM (e.g., spectral slopes) and the RTM (e.g., emissivity offsets), a continuum removal process was applied to each sulfide/silicate emissivity spectrum in our mixture; these results are presented in Figures 3.9 and 3.10. Regardless of the wavenumber position, each silicate spectral feature increases emissivity as sulfide abundance increases. The linear relationship between the band depth of a silicate spectral feature and sulfide content is not apparent until the sulfide abundance approaches ~10 vol %. This is likely due to uncertainty in the sample's

temperature. Because each spectrum is an average of three individual measurements, it is also possible that averaging the spectral measurements could make it difficult to decipher a small amount of contrast reduction resulting from a small volume of a graybody component.

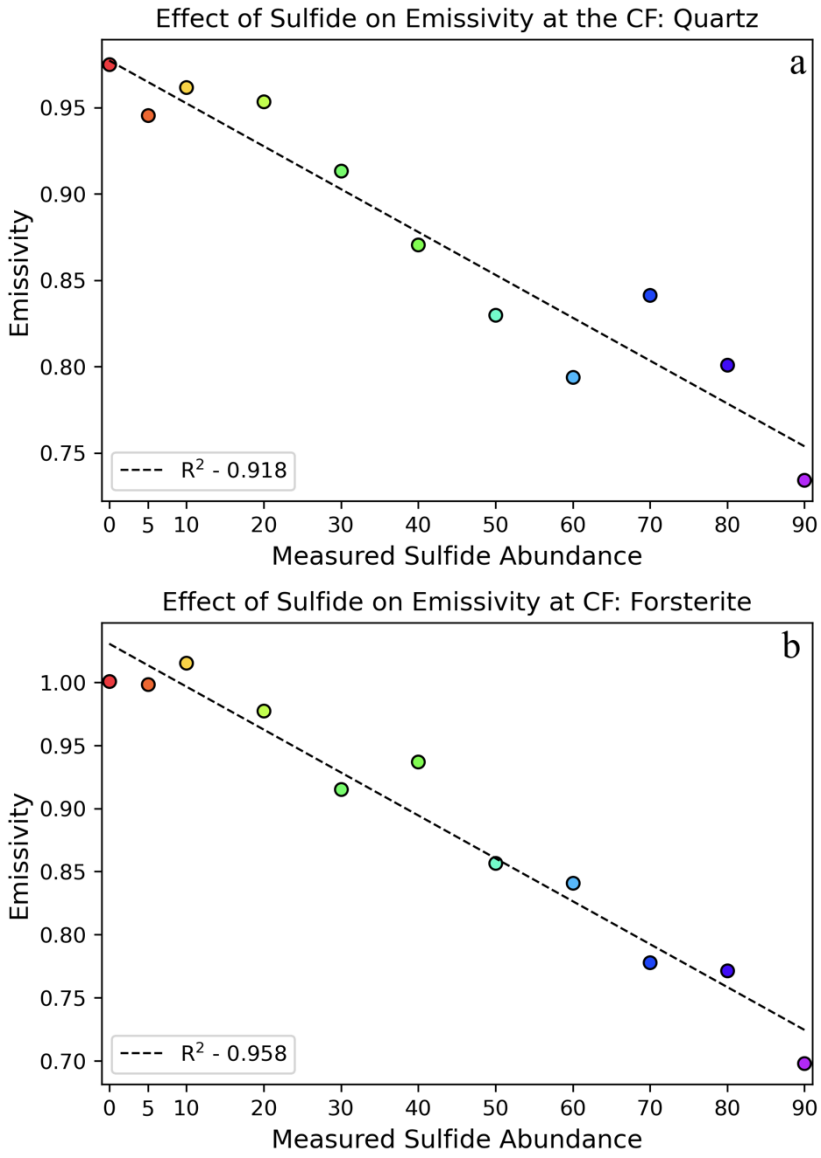

Figure 3.8 – Emissivity at the Christiansen Frequency feature for the (a) quartz /sulfide and (b) forsterite/sulfide (right) mixtures calibrated using the Reference Temperature Method. This figure shows that as sulfide increases at the optical surface, the absolute emissivity at the Christiansen Frequency decreases relative to the pure silicate sample. It

is this behavior that causes the temperature error demonstrated in Figure 3.3 and slope in Figure 3.4. Dot colors correspond to the legend in Figure 3.4.

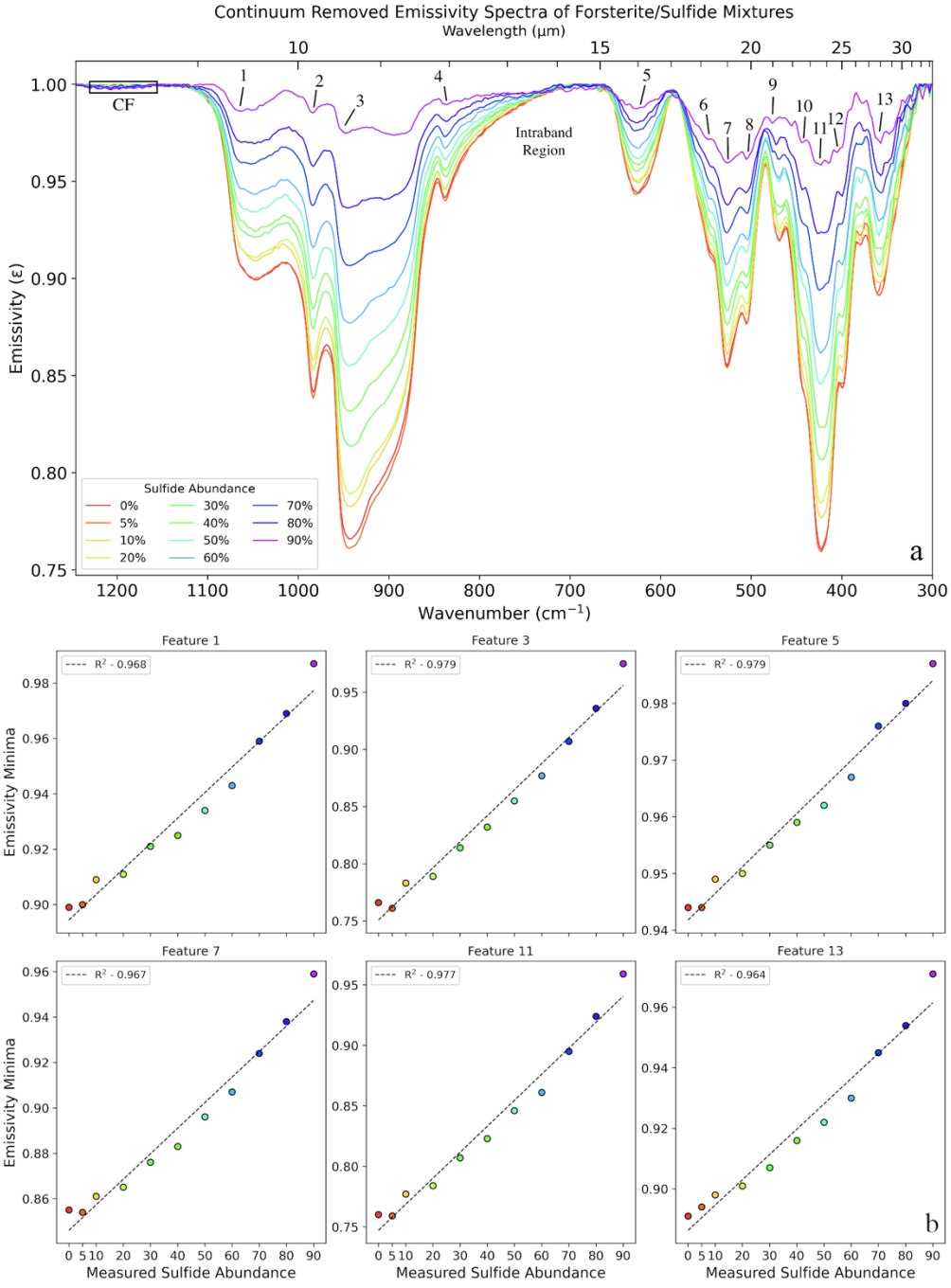

Figure 3.9 – (a) Continuum removed emissivity spectra of the forsterite/sulfide mixture suite from 1250-300 cm^{-1} showing the relationship between sulfide abundance and the reduction in spectral contrast of the spectral features of forsterite. The wavenumber position of the CF of forsterite is labeled along with the intraband region where TFs

would reside if the reduction in spectral contrast were due to small particle sizes. The assigned band numbers are defined in Burns & Huggins (1972) and Hamilton (2010). Each dot in the subplots (b) represent the emissivity minima for the corresponding spectral feature. Dot colors correspond to the spectrum with the same color in (a).

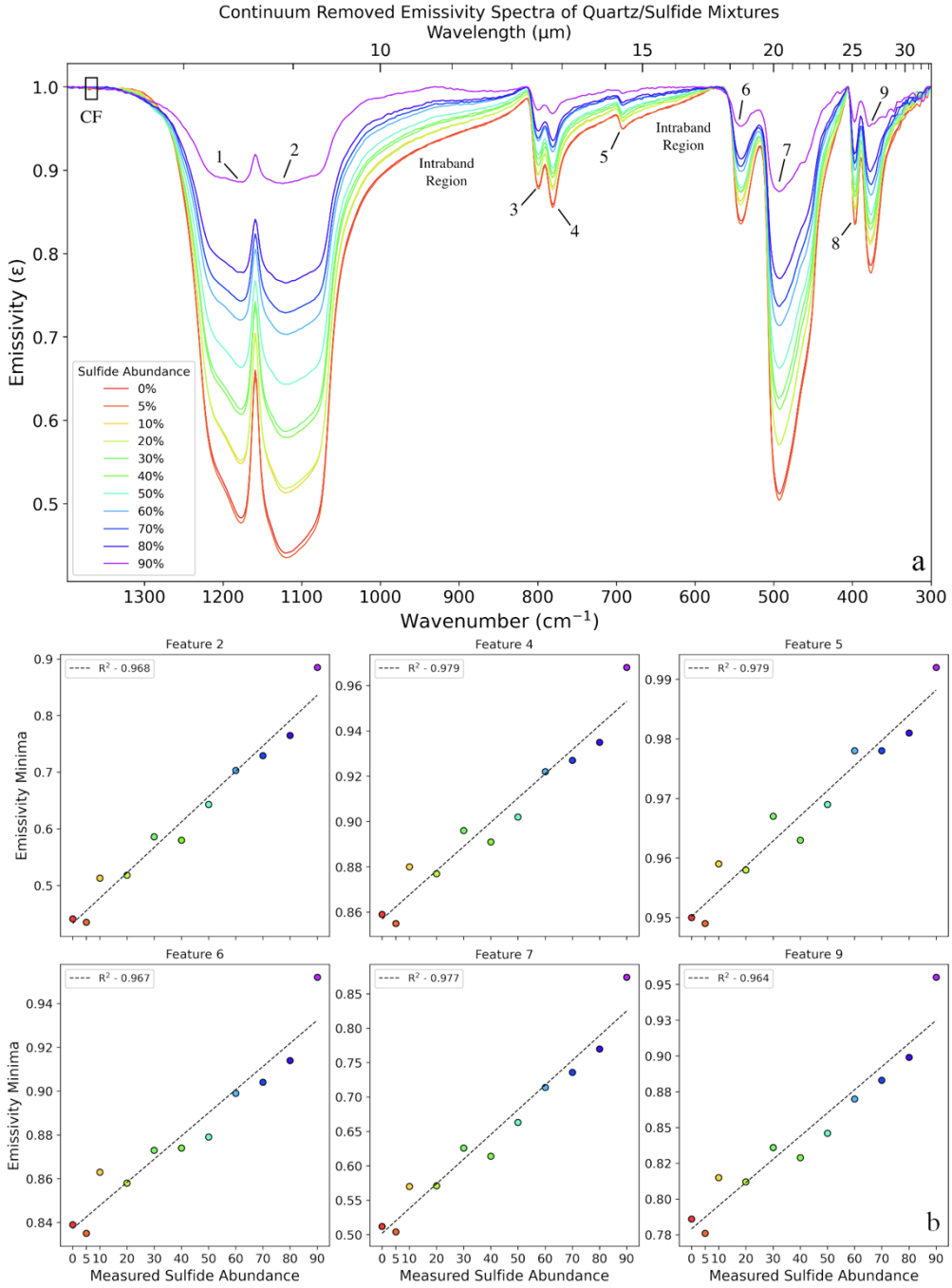

Figure 3.10 – (a) Continuum removed emissivity spectra of the quartz/sulfide mixture suite from 1400-300 cm^{-1} showing the relationship between sulfide abundance and the reduction in spectral contrast of the spectral features of quartz. The wavenumber position

of the CF of quartz is labeled along with the intraband region where Transparency Features would reside if the reduction in spectral contrast were due to small particle sizes. Band assignments are defined in Moersch & Christensen (1995). Each dot in the subplots (b) represent the emissivity minima for the corresponding spectral feature. Dot colors correspond to the spectrum with the same color in (a).

3.3.5 Modal Analysis by Spectral Deconvolution

Previous research has demonstrated that thermal infrared spectra of mineral mixtures can be approximated by the linear combination of the end members present in the composite spectrum and that the fraction of each component matches the volume abundance of each component in the sample (e.g., Ramsey & Christensen, 1998). To determine whether the assumption of linearity is valid when a low-emissivity, spectrally featureless component (e.g., pyrrhotite) is present, two spectral libraries were constructed using only the end members comprising the mixture. The first library contained the pyrrhotite end member calibrated using the OTM (i.e., a sloped spectrum) and was used to deconvolve spectra calibrated using the OTM. The second library contained the pyrrhotite spectrum calibrated using the RTM, which was used to deconvolve the mixture spectra calibrated using the RTM. Deconvolution results for both mixture suites calibrated using both methods are reported in Tables 3.1-3.4. We attempt to quantify the uncertainties in the predicted mineral abundances using the mean, standard deviation, median, and absolute range of the differences between each end member's modeled and measured abundances (Table 3.5).

When the OTM-calibrated spectra are deconvolved using the OTM library, the average percent difference between the modeled and measured abundances is 12 ± 6 vol % for both end members in the forsterite/sulfide mixture suite and 12 ± 7 vol % for both end members in the quartz/sulfide mixture suite. The agreement between the modeled

and measured abundances improves when the RTM-calibrated emissivity spectra are deconvolved using the RTM library. For the sulfide/forsterite mixture suite, the average difference between the modeled and measured abundance is 6 ± 4 vol % for forsterite and 5 ± 4 vol % for the sulfide component, each with error ranges of ~14%. The average percent differences in the quartz/sulfide mixture suite calibrated using the RTM are 6 ± 5 vol % for the quartz end member and 7 ± 5% for the sulfide end member.

The median value provides a measure of the systematic differences between the modeled and measured abundances shown in Figure 3.11. For the silicate component in the forsterite/sulfide suite, the median percent difference was +12% for OTM spectra and +5% for RTM spectra. We observe an inverse relationship for the sulfide component, where the median percent difference was -12% for the OTM spectra and -5% for the RTM spectra. The same patterns emerge for the spectral deconvolution results of the quartz/sulfide suite. The median percent difference between the modeled and known values for quartz was +10% when the mixture suite was calibrated using the OTM and +4% when calibrated using the RTM. For the sulfide component, the median percent difference was -10% for the OTM spectra and -4% for the RTM spectra. Thus, regardless of the calibration routine, the spectral deconvolution results contain a significant systematic bias, where the silicate component is consistently overestimated, and the graybody component is consistently underestimated (Tables 3.1–3.4). The bias is considerably reduced in the RTM relative to the OTM.

The RMS error is a single error value summed over all wavenumbers and describes how well the modeled emissivity spectrum reproduces the measured spectrum (Feely & Christensen, 1999). The RMS error ranged was ~0.1–1.3% for the RTM-

calibrated mixtures and ~0.2–1.3% for the OTM-calibrated mixtures, demonstrating that spectral slopes imparted on spectra as a result of an inaccurate temperature estimation do not greatly affect the accuracy of the model fit.

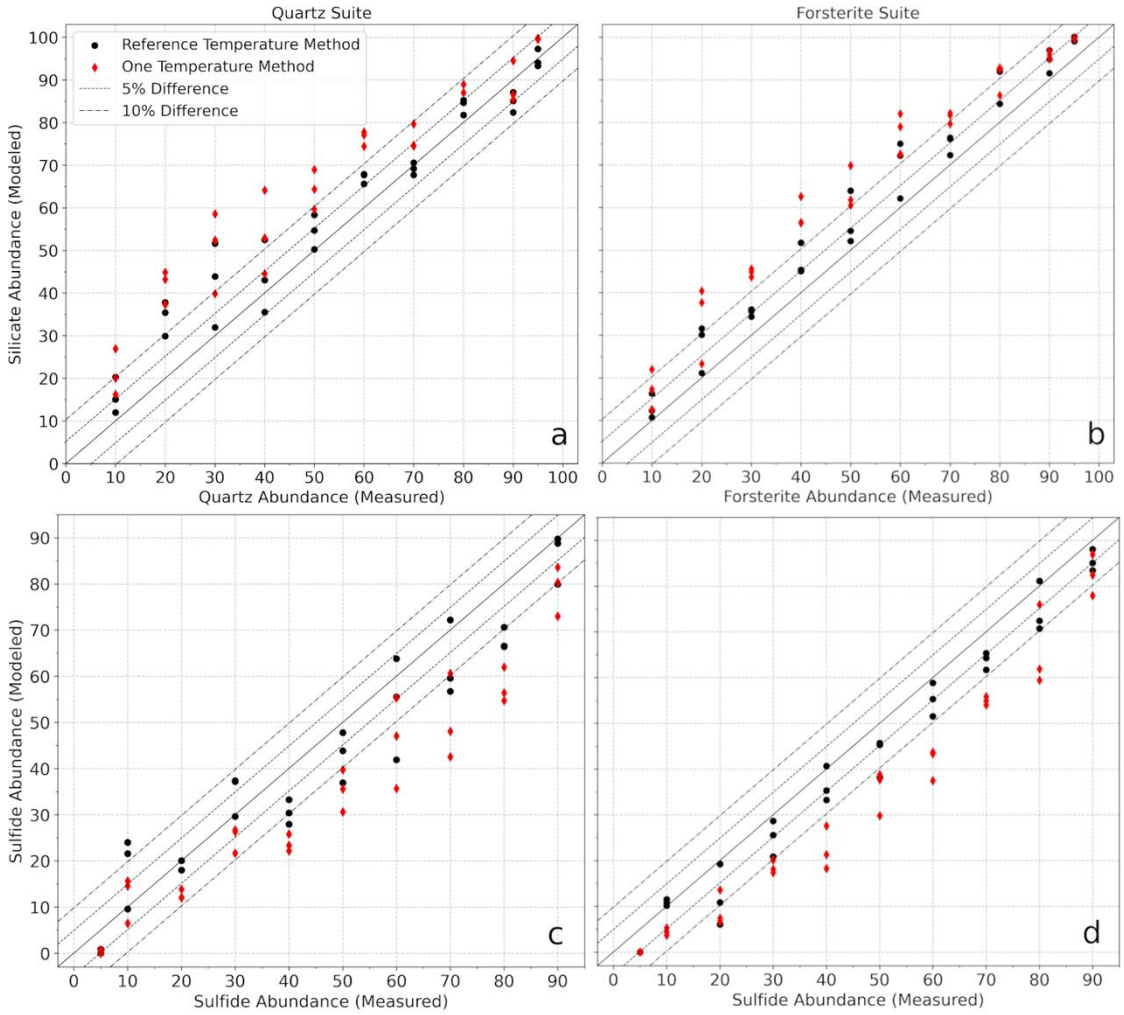

Figure 3.11 – Comparing the measured versus modeled abundances of the sulfide and silicate end members in the quartz/sulfide (a and c) and forsterite/sulfide (b and d) mixture suites. Black dots are results calibrated using the OTM, and red diamonds are calibrated using the RTM. The solid diagonal line represents a 1-1 relationship between the measured and modeled abundances, the dashed line represents a 5% difference, and the dotted-dashed line represents a 10% difference. The figure shows that the modal percentage of the silicate components are overestimated and the sulfide abundances are underestimated in both mixture suites. The percentage errors between the modeled and measured spectrum are larger for spectra calibrated using the OTM.

Combining the results of both mixture suites, the average absolute difference between the modeled and predicted abundance of sulfide is 12 ± 7 vol % for the OTM and 6 ± 4 vol % for the RTM. The improvement on the agreement between the modeled and measured abundances of both components in our mixture suites calibrated using the RTM compared to the OTM suggests that a more accurate temperature estimation will increase the accuracy of spectral deconvolution.

Table 3.1 - Spectral deconvolution results for the forsterite/sulfide mixture suite calibrated using the OTM. Measurements and modeled abundances are in volume percent. The percent difference is the difference between the measured and modeled values.

Measured		Meas. No	Modeled Modal Abundance			% Difference	
% Forsterite	% Sulfide		% Forsterite	% Sulfide	RMS Error	Forsterite	Sulfide
		1	99.7 ± 0.0	0.0 ± 0.0	0.4	5	-5
95	5	2	99.6 ± 0.2	0.0 ± 0.2	0.4	5	-5
		3	99.8 ± 0.0	0.0 ± 0.0	0.3	5	-5
		1	94.9 ± 0.3	5.3 ± 0.3	0.4	5	-5
90	10	2	96.7 ± 0.3	3.7 ± 0.3	0.6	7	-6
		3	95.9 ± 0.4	4.4 ± 0.4	0.6	6	-6
		1	86.4 ± 0.1	13.6 ± 0.1	0.2	6	-6
80	20	2	92.6 ± 0.1	7.4 ± 0.1	0.2	13	-13
		3	92.9 ± 0.2	6.7 ± 0.2	0.4	13	-13
		1	81.7 ± 0.1	18.1 ± 0.1	0.2	12	-12
70	30	2	79.7 ± 0.2	20.1 ± 0.2	0.3	10	-10
		3	82.2 ± 0.3	17.3 ± 0.3	0.5	12	-13
		1	72.6 ± 0.3	27.6 ± 0.3	0.5	13	-12
60	40	2	79.0 ± 0.4	21.3 ± 0.4	0.7	19	-19
		3	82.1 ± 0.5	18.2 ± 0.5	0.9	22	-22
		1	61.8 ± 0.2	37.7 ± 0.2	0.4	12	-12
50	50	2	60.6 ± 0.3	38.8 ± 0.3	0.5	11	-11
		3	69.9 ± 0.1	29.8 ± 0.1	0.2	20	-20
		1	56.5 ± 0.2	43.4 ± 0.2	0.4	17	-17
40	60	2	56.4 ± 0.3	43.7 ± 0.3	0.6	16	-16
		3	62.6 ± 0.3	37.5 ± 0.3	0.5	23	-23
		1	45.6 ± 0.2	54.0 ± 0.2	0.3	16	-16
30	70	2	43.7 ± 0.2	55.9 ± 0.2	0.3	14	-14
		3	44.9 ± 0.1	54.9 ± 0.1	0.3	15	-15
20	80	1	40.4 ± 0.2	59.4 ± 0.2	0.4	20	-21

		2	37.7	±	0.2	61.9	±	0.2	0.3	18	-18
		3	23.3	±	0.3	76.0	±	0.3	0.6	3	-4
		1	22.0	±	0.1	77.9	±	0.1	0.2	12	-12
10	90	2	12.6	±	0.3	86.9	±	0.3	0.4	3	-3
		3	17.3	±	0.1	82.4	±	0.1	0.3	7	-8

Table 3.2 - Spectral deconvolution results for the forsterite/sulfide mixture suite calibrated using the RTM. Measurements and modeled abundances are in volume percent. The percent difference is the difference between the measured and modeled values.

Measured		Meas. No	Modeled Modal Abundance							% Difference	
% Forsterite	% Sulfide		% Forsterite			% Sulfide			RMS Error	Forsterite	Sulfide
		1	99.3	±	0.0	0.0	±	0.0	0.3	4	-5
95	5	2	100.1	±	0.0	0.0	±	0.0	0.4	5	-5
		3	99.1	±	0.0	0.0	±	0.0	0.3	4	-5
		1	91.5	±	0.2	11.5	±	0.3	0.3	2	2
90	10	2	94.9	±	0.2	10.1	±	0.3	0.3	5	0
		3	96.9	±	0.1	10.8	±	0.1	0.1	7	1
		1	84.3	±	0.1	19.3	±	0.2	0.2	4	-1
80	20	2	92.0	±	0.1	10.9	±	0.2	0.2	12	-9
		3	92.5	±	0.2	6.1	±	0.3	0.3	13	-14
		1	76.1	±	0.1	25.6	±	0.2	0.2	6	-4
70	30	2	72.3	±	0.2	28.7	±	0.2	0.3	2	-1
		3	76.4	±	0.2	20.8	±	0.2	0.3	6	-9
		1	62.2	±	0.3	40.7	±	0.4	0.5	2	1
60	40	2	72.2	±	0.2	35.3	±	0.3	0.4	12	-5
		3	75.0	±	0.3	33.3	±	0.4	0.5	15	-7
		1	54.5	±	0.2	45.7	±	0.2	0.3	5	-4
50	50	2	52.1	±	0.2	45.3	±	0.3	0.3	2	-5
		3	64.0	±	0.1	38.2	±	0.2	0.2	14	-12
		1	45.1	±	0.2	55.3	±	0.4	0.4	5	-5
40	60	2	45.4	±	0.2	58.8	±	0.4	0.4	5	-1
		3	51.7	±	0.3	51.5	±	0.4	0.5	12	-9
		1	36.1	±	0.1	61.7	±	0.2	0.2	6	-8
30	70	2	35.7	±	0.1	64.3	±	0.1	0.2	6	-6
		3	34.4	±	0.2	65.3	±	0.3	0.3	4	-5
		1	31.6	±	0.1	72.4	±	0.2	0.3	12	-8
20	80	2	30.1	±	0.1	70.7	±	0.2	0.2	10	-9
		3	21.2	±	0.3	81.1	±	0.4	0.5	1	1
		1	16.3	±	0.1	83.4	±	0.1	0.1	6	-7
10	90	2	10.8	±	0.1	88.0	±	0.2	0.2	1	-2
		3	12.3	±	0.1	85.1	±	0.1	0.2	2	-5

Table 3.3 - Spectral deconvolution results for the quartz/sulfide mixture suite calibrated using the OTM. Measurements and modeled abundances are in volume percent. The percent difference is the difference between the measured and modeled values.

Measured		Meas. No	Modeled Modal Abundance			% Difference	
% Quartz	% Sulfide		% Quartz	% Sulfide	RMS Error	Quartz	Sulfide
		1	99.6 ± 0.0	0.0 ± 0.0	0.8	5	-5
95	5	2	99.8 ± 0.0	0.0 ± 0.0	0.4	5	-5
		3	99.5 ± 0.0	0.7 ± 0.0	0.2	4	-4
		1	94.5 ± 0.2	6.5 ± 0.2	0.7	4	-4
90	10	2	86.5 ± 0.2	14.6 ± 0.2	1.0	-4	6
		3	85.4 ± 0.2	15.6 ± 0.2	0.9	-5	6
		1	88.9 ± 0.2	12.1 ± 0.2	0.9	9	-8
80	20	2	89.0 ± 0.2	12.0 ± 0.2	0.9	9	-8
		3	87.0 ± 0.2	13.8 ± 0.2	0.9	7	-6
		1	74.5 ± 0.3	26.7 ± 0.3	1.3	4	-3
70	30	2	79.7 ± 0.3	21.7 ± 0.3	1.2	10	-8
		3	74.7 ± 0.2	26.3 ± 0.2	1.1	5	-4
		1	77.1 ± 0.2	23.4 ± 0.1	0.7	17	-17
60	40	2	74.4 ± 0.1	25.8 ± 0.1	0.4	14	-14
		3	77.8 ± 0.1	22.1 ± 0.1	0.4	18	-18
		1	69.0 ± 0.1	30.6 ± 0.1	0.5	19	-19
50	50	2	59.6 ± 0.2	39.8 ± 0.1	0.7	10	-10
		3	64.3 ± 0.1	35.6 ± 0.1	0.4	14	-14
		1	53.0 ± 0.1	47.0 ± 0.1	0.5	13	-13
40	60	2	64.1 ± 0.1	35.7 ± 0.1	0.6	24	-24
		3	44.5 ± 0.1	55.3 ± 0.1	0.5	5	-5
		1	52.4 ± 0.2	48.1 ± 0.2	0.7	22	-22
30	70	2	39.9 ± 0.2	60.6 ± 0.1	0.7	10	-9
		3	58.6 ± 0.3	42.5 ± 0.2	1.2	29	-27
		1	37.3 ± 0.1	62.0 ± 0.1	0.6	17	-18
20	80	2	44.9 ± 0.1	54.7 ± 0.1	0.5	25	-25
		3	43.2 ± 0.1	56.4 ± 0.1	0.4	23	-24
		1	20.0 ± 0.1	80.3 ± 0.1	0.5	10	-10
10	90	2	16.2 ± 0.1	83.6 ± 0.1	0.3	6	-6
		3	26.9 ± 0.1	73.0 ± 0.1	0.4	17	-17

Table 3.4 – Spectral deconvolution results for the quartz/sulfide mixture suite calibrated using the RTM. Measurements and modeled abundances are in volume percent. The percent difference is the difference between the measured and modeled values.

Measured		Meas. No	Modeled Modal Abundance			% Difference	
% Quartz	% Sulfide		% Quartz	% Sulfide	RMS Error	Quartz	Sulfide
		1	93.3 ± 0.0	0.0 ± 0.0	0.8	-2	-5
95	5	2	94.0 ± 0.0	0.0 ± 0.0	0.3	-1	-5
		3	97.3 ± 0.0	0.9 ± 0.1	0.2	2	-4
		1	87.1 ± 0.3	9.5 ± 0.4	1.1	-3	0
90	10	2	82.4 ± 0.2	21.6 ± 0.2	0.8	-8	12
		3	85.0 ± 0.1	24.0 ± 0.1	0.4	-5	14
		1	84.6 ± 0.2	18.0 ± 0.3	0.8	5	-2
80	20	2	85.2 ± 0.2	18.0 ± 0.2	0.8	5	-2
		3	81.8 ± 0.2	20.0 ± 0.3	0.9	2	0
		1	67.7 ± 0.2	37.3 ± 0.3	1.1	-2	7
70	30	2	70.6 ± 0.3	29.6 ± 0.4	1.3	1	0
		3	69.2 ± 0.2	37.2 ± 0.2	0.8	-1	7
		1	67.7 ± 0.2	30.4 ± 0.3	0.9	8	-10
60	40	2	65.6 ± 0.1	33.3 ± 0.2	0.6	6	-7
		3	67.9 ± 0.2	27.9 ± 0.2	0.6	8	-12
		1	58.3 ± 0.1	36.9 ± 0.2	0.5	8	-13
50	50	2	50.3 ± 0.1	47.8 ± 0.2	0.5	0	-2
		3	54.7 ± 0.1	43.8 ± 0.2	0.5	5	-6
		1	43.0 ± 0.1	55.5 ± 0.2	0.5	3	-4
40	60	2	52.5 ± 0.2	41.9 ± 0.2	0.6	12	-18
		3	35.6 ± 0.1	63.8 ± 0.1	0.4	-4	4
		1	43.9 ± 0.1	59.6 ± 0.2	0.6	14	-10
30	70	2	32.0 ± 0.1	72.2 ± 0.2	0.5	2	2
		3	51.6 ± 0.2	56.7 ± 0.2	0.8	22	-13
		1	29.9 ± 0.1	70.6 ± 0.1	0.4	10	-9
20	80	2	37.8 ± 0.1	66.4 ± 0.2	0.5	18	-14
		3	35.4 ± 0.1	66.5 ± 0.1	0.4	15	-13
		1	15.1 ± 0.1	89.8 ± 0.1	0.3	5	0
10	90	2	12.0 ± 0.1	88.8 ± 0.1	0.2	2	-1
		3	20.3 ± 0.1	79.9 ± 0.1	0.4	10	-10

Regardless of the calibration method, spectral deconvolution consistently fails to detect the sulfide end member in spectra containing 5% or less sulfide. This is not surprising, given that the average detection limit of the spectral deconvolution algorithm

has been estimated to be ~5% (Feely & Christensen, 1999; Ramsey & Christensen, 1998). However, the predicted percentage of sulfide in the mixture containing 10% sulfide was highly accurate, leading us to define a detection limit of ~10%. The higher model uncertainties for both end members derived from emissivity spectra calibrated using the OTM relative to spectra calibrated using the RTM leads us to conclude that errors in sample temperature determination and the addition of a spectral slope will decrease the certainty of retrieving the modes of a potential ore such as sulfide. Thus, when prospecting on other planetary surfaces, inaccurate surface temperature estimations could impede the detection of an exposed sulfide ore body.

Table 3.5 – Summary statistics comparing the percent differences between the modeled and measured abundances of the silicate/sulfide mixture suites when calibrated using the OTM and the RTM. Values are rounded to the nearest percent. We attribute the sizable error range to a sampling error, for the abundances of each end member at the optical surface may not be entirely representative of the measured abundances.

	Forsterite		Sulfide		Quartz		Sulfide	
	OTM	RTM	OTM	RTM	OTM	RTM	OTM	RTM
Average*	12	6	12	5	12	6	12	7
Std	6	4	6	4	8	7	9	8
Median	12	5	-12	-5	10	4	-10	-4
Range*	20	14	19	14	25	21	24	18

*The average percent difference and error range were determined by taking the absolute value of the difference of the measured and modeled abundance for each endmember.

3.4 Conclusions and Discussion

This research demonstrates for the first time that despite its lack of spectral features, pyrrhotite ($Fe_{1-x}S$), which the most common sulfide phase in magmatic sulfide ore deposits, can be identified based on its effects in multimineralic thermal infrared emission spectra. The calibrated radiance of our sulfide/silicate mixtures decreases in intensity as sulfide increases despite being at the same kinetic temperature, and its

radiance spectrum takes on the shape of a blackbody as sulfide increases. In addition, as the areal/volumetric abundance of sulfide increases, the apparent brightness temperature decreases linearly with increasing sulfide abundance. When calibrating the measured radiance spectra of our mixtures to emissivity using the conventional OTM, a spectral slope is observed from high to low wavenumbers when sulfide is present in our mixtures. The slope steepens as the volume of sulfide increases in the mixture. The severity of the slope results from the situationally erroneous assumption of unit emissivity and the resulting incorrectly estimated sample temperature, which we directly attribute to the systematically low emissivity of and broadband graybody behavior of pyrrhotite.

When calibrating using the RTM, the maximum emissivity at the principal Christiansen Frequency of the accompanying silicate component decreases linearly with increasing sulfide content. Moreover, every Restrahlen Band and spectral feature from the non-sulfide end member linearly reduces in spectral contrast as the sulfide component of the silicate end members increases. While this is a non-unique phenomenon since spectral features also reduce in contrast as grain size decreases, a reduction in spectral contrast due to the presence of a graybody component can be differentiated from a reduction in grain size because, along with a reduction in spectral contrast, small grains also produce Transparency Features and change the shape and relative depth of the spectral bands, which does not occur with the addition of a graybody component.

Our spectral deconvolution results demonstrate that pyrrhotite currently has a detection limit of ~10 vol % using thermal infrared emission spectroscopy, though improvements in the RTM methods sample temperature knowledge would improve on this threshold. The sulfide abundances derived from spectral deconvolution enabled

mineral percentage prediction to within 12 ± 7 vol % on average when calibrating using the conventional OTM and improved to within 6 ± 4 vol % of the measured abundance when calibrating using the new RTM. These differences are comparable to previous quantitative analyses using thermal emission spectroscopy (Ramsey & Christensen, 1998; Feely & Christensen, 1999; Bramble et al., 2021).

Martian exploration has primarily been driven by strategies to "Follow the Water" and to "Seek Signs of Life," with overarching goals of mapping the past and present distribution of water on Mars, assessing its habitability, and searching for signs of past microbial life. These goals reflect the science objectives, landing site selections, and instrument selection of previous and current Mars exploration architectures. With widening focus on the human settlement of Mars, particularly in the private sector, there is an emerging opportunity to develop new mission architectures with technological and scientific objectives geared toward meeting anthropocentric goals such as prospecting for and development of the critical resources required to enable a persistent and sustainable human and robotic presence on the martian surface.

We believe that a prospecting mission to search for magmatic Ni-Cu-PGE sulfide ore deposits would be a fruitful and exciting objective for a future Mars mission. Such a mission could utilize spectroscopic instruments with extensive flight heritage while also allowing the chance to test new technologies relevant to in-situ resource utilization and human habitability. For example, a prospecting rover equipped with an infrared spectrometer similar to the Mini-TES instrument aboard the Opportunity rover (Christensen et al., 2004) or the OSIRIS-REx Thermal Emission Spectrometer that observed the asteroid 101955 Bennu (Christensen et al., 2018) could prospect one of the

640 locations on Mars containing the featureless, sloping emissivity spectra observed in THEMIS and TES data (Osterloo et al. 2008, 2010; Bandfield, 2009) that are analogous to the spectral characteristics of our sulfide mixtures.

The units responsible for the featureless spectrum were argued to be chloride salts, though sulfides could not be entirely ruled out (Osterloo et al., 2010). Because magmatic pyrrhotite and chloride salts both exhibit featureless spectra in the mid-infrared, we recommend a complimentary X-ray fluorescence payload similar to those described in Le Vaillant et al. (2014) and Gellert et al. (2006) be deployed with an TIR-spectrometer in-situ to constrain the sample composition and detect the presence of S, Cl, and other key sulfide ore indicator elements (Cousin et al., 2022) to determine whether the featureless unit is a sulfide or chloride.

A prospecting campaign would gather meaningful data that could be used in tandem with existing orbital data products to make preliminary estimations on the extent of martian sulfide mineralization. Moreover, high-level ore grades and resource estimations of metals such as Ni, Cu, and the PGMs requisite for sustainable human habitation on Mars can also be calculated. Because estimating ore grades is labor-intensive and costly, the application of thermal infrared reflectance spectroscopy has previously been investigated for quantitative estimation of sulfide contents in core samples and rocks in the terrestrial mining industry (Rivard et al., 2001; Feng et al., 2006). To prepare for martian settlement, humans will likely rely heavily on robotic techniques to supplement the lack of a labor force. This increases the significance of testing the prospecting capabilities of remote spectroscopic methods such as thermal infrared emission spectroscopy to search for ore deposits.

If the spectrally featureless units are chlorides, they still have substantial value for human settlement. The deposit could be mined to produce an electrolyte used in Molten Salt Electrolysis, a process capable of reducing martian minerals and oxides in a bed of molten chloride salt to produce O^2 and metallic alloy byproducts (Fray et al., 1999; Chen et al., 2000; Lomax et al., 2020). If the chloride deposit could be used as a feedstock to produce the electrolyte, it would not have to be sourced from Earth, and the technique will not require a closed-loop process.

Because sulfides can also be reduced using Molten Salt Electrolysis (Ge et al., 2009; Liu et al., 2023; Guo et al., 2022; Li et al., 2007; Chen and Fray, 2020), a Molten Salt Electrolysis technology demonstration could be equipped on the prospecting rover investigating the spectrally featureless units. If the featureless unit is sulfide, it could be extracted and used as the input feedstock for processing using the payload. If the unit is chloride, it could be collected and processed for use as the electrolyte during demonstration of the technology to produce O^2 and metals from the martian regolith. Oxygen and a ferromagnetic alloy (Fe_3Si) byproduct with high heat resistance have already been made from martian regolith simulant using the Molten Salt Electrolysis process (Zheng and Qiao, 2022). Thus, regardless of the composition, a mission to explore one of the spectrally neutral units on Mars will help prepare humans for long-term exploration and habitation.

References

Arndt, N., Lesher, C. M., & Czamanske, G. K. (2005). Mantle-derived magmas and magmatic Ni-Cu-(PGE) deposits. *In Economic geology*, (pp. 5–24). 100th anniversary, Retrieved from https://hal.archives-ouvertes.fr/hal-00016864

Bandfield, J. (2002). Global mineral distributions on Mars. *Journal of Geophysical Research*, 107(E6), 1–20.

Bandfield, J. (2009). Effects of surface roughness and graybody emissivity on Martian thermal infrared spectra. *Icarus*, 202(2), 414–428.

Bandfield, J., & Edwards, C.S. Edwards. (2008). Derivation of martian surface slope characteristics from directional thermal infrared radiometry. *Icarus*, 193, 139–157.

Barnes, S. J., & Lightfoot, P. C. (2005). Formation of magmatic nickel-sulfide ore deposits and processes affecting their copper and platinum-group element contents. In *Economic geology*, 100th anniversary (pp. 179–213).

Barnes, S. J., Holwell, D. A., & Le Vaillant, M. (2017). Magmatic sulfide ore deposits. *Elements*, 13(2), 89–95.

Baumgartner, R.J., Baratoux, D., Gaillard, F., & Fiorentini, M.I. (2017). Numerical modeling of erosion and assimilation of sulfur-rich substrate by martian lava flows: Implications for the genesis of massive sulfide mineralization on Mars. *Icarus*. 296, 257–274.

Baumgartner, R. J., Fiorentini, M. L., Baratoux, D., Micklethwaite, S., Sener, A. K., Lorand, J. P., & McCuaig, T. C. (2015). Magmatic controls on the Genesis of Ni–Cu±(PGE) sulphide mineralisation on Mars. *Ore Geology Reviews*, 65, 400–412.

Begemannm D., Dorschner, J., Henning, T., Mutschke, H., & Thamm, E. (1994). A Laboratory Approach to the Interstellar Sulfide Dust Problem. *The Astrophysical Journal*, 423, L71–L74.

Bibring, J.-P., Langevin, Y., Gendrin, A., Gondet, B., Poulet, F., Berthé, M., Soufflot, A., Arvidson, R.., Mangold, N., Mustard, J., Drossart, P., & the OMEGA Team. (2005). Mars Surface Diversity as Revealed by the OMEGA/Mars Express Observations. *Science*, 307(5715), 1576–1581.

Blake, D., Vaniman, D., Achilles, C., Anderson, R., Bish, D., Bristow, T., Chen, C., Chipera, S., Crisp, J., Des Marais, D., Downs, R.T., Farmer, J., Feldman, S., Fonda, M., Gailhanou, M., Ma, H., Ming, D.W., Morris, R.V., Sarrazin, P., Stolper, E., Treiman, A., & Yen, A. (2012). Characterization and Calibration of the CheMin

Mineralogical Instrument on Mars Science Laboratory. *Space Science Reviews*. 170, 341–399.

Blakely, R.J., & Zientek, M.L. (1985). Magnetic Anomalies Over A Mafic Intrusion: The Stillwater Network. Ed: Czamanske, G.K. and M.L. Zientek *In: The Stillwater Complex, Montana: Geology and Guide. Special Publication 92*. pp. 39-46.

Bramble, M.S., Milliken, R.E., & Patterson III, W.R. (2021). Thermal emission measurements of ordinary chondrite mineral analogs in a simulated asteroid environment: 1. Constituent mineral phases. *Icarus*, 369(114561), 1-22.

Burns, R.G., & Huggins, F.E. (1972). Cation determinative curves for MG–Fe–Mn olivines from vibrational spectra. *American Mineralogist*, 57, 967–985.

Burns, R.G., & Fisher, D.S. (1990). Iron-Sulfur Mineralogy of Mars: Magmatic Evolution and Chemical Weathering Products. *Journal of Geophysical Research*. 95(B9), 14415–14421.

Campbell, I.H. & Naldrett. A.J. (1979). The influence of silicate: sulfide ratios on the geochemistry of magmatic sulfides. Economic Geology, 74(6), 1503–1506.

Chen, G., & Fray, D. (2020). Chapter 11 – Invention and fundamentals of the FFC Cambridge Process. *In: Extractive Metallurgy of Titanium*, 227-286.

Chen, G., Fray, D., & Farthing, T. (2000). Direct electrochemical reduction of titanium dioxide to titanium in molten calcium chloride. *Nature*, 407, 361–364.

Christensen, P.R. (1986). The spatial distribution of rocks on Mars. *Icarus*, 68, 217–238.

Christensen, P.R., Bandfield, J.L., Hamilton, V.E., Howard, D.A., Lane, M.D., Piatek, J.L., Ruff, S.W., & Stefanov, W.L. (2000). A thermal emission spectral library of rock-forming minerals. *Journal of Geophysical Research*, 105(E4), 9735–9739.

Christensen, P.R., Bandfield, J.L., Hamilton, V.E., Ruff, S.W., Kieffer, H.H., Titus, T.N., Malin, M.C., Morris, R.V., Lane, M.D., Clark, R.L., Jakosky, B.M., Mellon, M.T., Pearl, J.C., Conrath, B.J., Smith, M.D., Clancy, R.T., Kuzmin, R.O., Roush, T., Mehall, G.L., Gorelick, N., Bender, K., Murray, Dason, S., Greene, E., Silverman, S., & Greenfield, M. (2001). Mars Global Surveyor Thermal Emission Spectrometer experiment: Investigation description and surface science results. Journal of Geophysical Research, 106(E10), 23823–23871.

Christensen, P.R., Hamilton, V.E., Mehall, G.L., Pelham, D., O'Donnell, W., Anwar, S., Bowels, H., Chase, S., Fahlgren, J., Farkas, Z.., Fisher, T., James, O., Kubik, I., Lazbin, I., Miner, M., Rassas, M., Schulze, L., Shamordola, K., Tourville, T., West,

G., Woodward, R., & Lauretta, D. (2018). The OSIRIS-REx Thermal Emission Spectrometer (OTES) Instrument. *Space Science Reviews*, 214(87), 1–39.

Christensen, P. R., & Harrison, S. T. (1993). Thermal infrared emission spectroscopy of natural surfaces: Application to desert varnish coatings on rocks. *Journal of Geophysical Research*, 98(B11), 19819–19834.

Christensen, P.R., Mehall, G.L., Silverman, S.H., Anwar, S., Cannon, G., Gorelick, N., Kheen, R., Tourville, T., Bates, D., Ferry, S., Fortuna, T., Jeffreys, J., O'Donnell, W., Peralta, R., Wolverton, T., Blaney, D., Denise, R., Rademacher, J., Morris, R., & Squyres, S. (2003). Miniature Thermal Emission Spectrometer for the Mars Exploration Rovers. *Journal of Geophysical Research*, 108(E12-8064), 1–23. doi:10.1029/2003JE002117.

Christensen, P.R., Morris, R.V., Lane, M.D., Bandfield, J.L., & Malin, M.C. (2001). Global mapping of Martian hematite mineral deposits: Remnants of water-driven processes on early Mars. *Journal of Geophysical Research*, 106(E10), 23,873–23,885.

Christensen, P.R., Wyatt, M.B., Glotch, T.D., Rogers, A.D., Anwar, S., Arvidson, R.E. … Wolff, M.J. (2004). Mineralogy at Meridiani Planum from the Mini-TES Experiment on the Opportunity Rover. Science, 306, 1733–1739.

Conel, J.E. (1969). Infrared emissivities of silicates: experimental results and a cloudy atmosphere model of spectral emission from condensed particulate mediums. *Journal of Geophysical Research*, 74(6), 1614–1634.

Cousin, A., Sautter, V., Fabre, C., Dromart, G., Montagnac, G., Drounet, C. … & Wiens, R.C. (2022). SuperCam calibration targets on board the perseverance rover: Fabrication and quantitative characterization. Spectrochimica Acta Part B: *Atomic Spectroscopy*, 188(106341), 1–26.

Colwell, J.E., & Jakosky, B.M. (2002). Effects of topography on thermal infrared spectra of planetary surfaces. *Space Sci. Rev*. 110, 85–130.

Ding, S., Dasgupta, R., & Tsuno, K. (2014). Sulfur concentration of martian basalts at sulfide saturation at high pressures and temperatures – Implications for deep sulfur cycle on Mars. *Geochimica et Cosmochimica Acta*, 131, 227–246.

Donaldson Hanna, K.L., Cheek, L.C., Pieters, C.M., Mustard, J.F., Wyatt, M.B., & Greenhagen, B.T. (2012). Global indications of crystalline plagioclase across the lunar surface using M3 and Diviner data. *Proc. Lunar Planet. Sci. Conf*., 43,1968.

Donaldson Hanna, K.L., Cheek, L.C., Pieters, C.M., Mustard, J.F., Greenhagen, B.T., Thomas, I.R. and N.E. Bowles. (2014). Global assessment of pure crystalline

plagioclase across the Moon and implications for the evolution of the primary crust. *JGR Planets*, 119, 1516–1545.

Feely, K.C., & Christensen, P.R. (1999). Quantitative compositional analysis using thermal emission spectroscopy: Application to igneous and metamorphic rocks. *Journal of Geophysical Research*, 10(E10), 24195–24210.

Feng, J., Rivard, B., Gallie, E.A., & Sanchez, A. (2006). Quantifying total sulfide content of cores and cut-rock surfaces using thermal infrared reflectance. *Geophysics*, 71(3), M1-M9.

Fray, D.J., Farthing, T.W. and Z. Chen. (1999). Removal of oxygen from Metal Oxides and Solid Solutions by Electrolysis in a Fused Salt. WO/99/64638. Retrieved from: https://patentimages.storage.googleapis.com/02/ff/c2/090b10cc5e821e/WO1999064638A1.pdf

Ge, X.L., Wang, X.D., & Seetharaman, S. (2009). Copper extraction from copper ore by electro-reduction in molten $CaCl_2$–NaCl. *Electrochimica Acta*, 54, 4397–4402.

Gellert, R., Rider, R., Brückner, J., Clark, B.C., Dreibus, G., Klingelhöfer, G., Lugmair, G., Ming, D.W., Wänke, H., Yen, A., Zipfwl, J., & Squyres, S.W. (2006). Alpha Particle X-Ray Spectrometer (APXS): Results from Gusev crater and calibration report. *Journal of Geophysical Research: Planets*, 111(E2), 1-32.

Gillespie, A. (1992). Spectral mixture analysis of multispectral thermal infrared images. *Remote Sensing of Environment.* 42(2),137-145.

Gillespie, A. Land Surface Emissivity. (2014). In: *Encyclopedia of Remote Sensing*. Njoku, E.G., (Ed.). Springer New York: New York, NY, USA. (pp. 303-311).

Gillespie, A., Rokugawa, S., Matsunga, T., Cothern, J.S., Hook, J., & Kahle, A.B. (1998). A temperature and emissivity separation algorithm for Advanced Spaceborne Thermal Emission and Reflection Radiometer (ASTER) images. *IEEE Transactions on Geoscience and Remote Sensing*, 36(4), 1113-1126.

Greeley, R. &, Schneid, B.D. (1991). Magma generation on Mars: amounts, rates, and comparisons with Earth, Moon, and Venus. *Science*, 254(5034), 996-998.

Greenhagen, B.T., Lucey, P.G., Wyatt, M.B., Glotch, T.D., Allen, C.C., Arnold, J.A., Bandfield, J.L., Bowles, N.E., Donaldson Hanna, K.L., Hayne, P.O., Song, E., Thomas, I.R., & Paige, D.A. (2010). Global Silicate Mineralogy of the Moon from the Diviner Lunar Radiometer. *Science*, 329, 1507–1509.

Guo, Y.Y., Li, X.Y., Zhao, Z.Q., Qu, J.K., Ma, Q., Wang, D.H., & Yin, H.Y. (2022). The electrochemical reduction process of converting solid sulfides to liquid metals in molten salt: ZnS. *Journal of Electroanalytic Chemistry,* 922(116801), 1-8.

Hamilton, V.E. (2000). Thermal infrared emission spectroscopy of the pyroxene mineral series. *Journal of Geophysical Research*, 105, 9701–9716.

Hamilton, V.E. (2010). Thermal infrared (vibrational) spectroscopy of Mg-Fe olivines: A review and applications to determining the composition of planetary surfaces. *Chemie der Erde*, 70, 7–33.

Hamilton, V.E., & Christensen, P.R. (2000). Determining the modal mineralogy of mafic and ultramafic igneous rocks using thermal emission spectroscopy. *Journal of Geophysical Research,* 105(E40), 9717-9733.

Hook, S.J., Gabell, A.R., Green, A.A., & Kealy, P.S. (1992). A comparison of techniques for extracting emissivity information from thermal infrared data for geologic studies. *Remote Sensing of Environment*, 42(2), 123–135.

Hubbard, K.M., Haberle, C.W., Elkins-Tanton, L.T., Christensen, P.R., & Semken, S. (2023). Thermal infrared Emission Spectroscopy of Graybody Minerals (Sulfide): Implications for Extraterrestrial Exploration for Magmatic Ore Deposits. *Earth and Space Science.* 10, 1-24. DOI: 10.1029/2022EA002641.

Hunt, G.R., & Vincent, R.K. (1968). The behavior of spectral features in the infrared emission from particulate surfaces of various grain sizes. *Journal of Geophysical Research,* 73(18), 6039-6046.

Kealy, P.S., & Hook, S.J. (1993). Separating temperature and emissivity in thermal infrared multispectral scanner data: Implications for recovering land surface temperatures. *IEEE Transactions on Geoscience and Remote Sensing*. 31(6), 1155–1164.

Kiefer, W.S. (2004). Gravity evidence for an extinct magma chamber beneath Syrtis Major, Mars. A look at the magmatic plumbing system. *Earth Planet. Sci. Lett.*, 222(2), 349–361.

Kieffer, H.H. (2013). Thermal model for analysis of Mars infrared mapping. *Journal of Geophysical Research: Planets*. 118, 451–470.

Klingelhöfer, G., Morris, R.V., Bernhardt, B., Schröder, C., Rodionov, D.S., De Souza, P.A., Yen, A., Gellert, R., Evlanov, E.N., Zubkov, B., Foh, J., Bonnes, U., Kankeleit, E., Gütlick, P., Ming, D.W., Renz, F., Wdowiak, T., Squyres, S.W., & Arvidson, R.E. (2004). Jarosite and Hematite at Meridiani Planum From Opportunity's Mössbauer Spectrometer. *Science,* 306(5702), 1740–1745.

Lane, M. (1999). Midinfrared optical constants of calcite and their relationship to particle size effects in thermal infrared emission spectra of granular calcite. *Journal of Geophysical Research,* 104(E6), 14099–14108.

Le Vaillant, M., Barnes, S.J., Fisher, L., Fiorentini, M.I., & Caruso, S. (2014). Use and calibration of portable X-Ray fluorescence analysers: application to lithogeochemical exploration for komatiite-hosted sulphide deposits. *Geochemistry, Exploration, Environment, Analysis.* 14(3), 199.

Li, C., & Ripley, E.M. (2005). Empirical equations to predict the sulfur content of mafic magmas at sulfide saturation and applications to magmatic sulfide deposits. Mineralium Deposita, 40, 218–230.

Li, C. & Ripley, E.M. (2009). Sulfur Contents at Sulfide-Liquid or Anhydrite Saturation in Silicate Melts: Empirical Equations and Example Applications. Economic Geology, 104, 405–412.

Li, G.M., Wang, D.H., Jin, X.B., & Chen, G.Z. (2007). Electrolysis of solid MoS_2 in molten $CaCl_2$ for Mo extraction without emission. *Electrochemistry Communications*, 9, 1951–1957.

Lillis, R.J., Dufek, J., Kiefer, W.S., Black, B.A., Manga, M.., Richardson, J.A., & Bleacher, J.E. (2015). The Syrtis Major volcano, Mars: A multidisciplinary approach to interpreting its magmatic evolution and structural development. *J. Geophys. Res. Planets,* 120, 1476–1496.

Liu, J., Li, S., Lv, Z., Fan, Y., He, J., & Song, J. (2023). Electro-desulfurization of metal sulfides in molten salts. *Separation and Purification Technology*, 310(123109), 1-10.

Liu, K., Zhang, L., Guo, X., & Huaiwei, N. (2021). Effects of sulfide composition and melt H_2O on sulfur content at sulfide saturation in basaltic melts. *Chemical Geology*, 559(119913), 1-8.

Liu, Y., Samaha, N.-T., & Baker, D.R. (2007). Sulfur concentration at sulfide saturation (SCSS) in magmatic silicate melts. *Geochim. Cosmochim. Acta*, 71:1783–1799.

Logan, L.M., Hunt, G.R., Salisbury, J.W., Balsamo, S.R. (1973). Compositional implications of Christiansen frequency minimums for infrared remote sensing applications. *Journal of Geophysical Research*, 78:4983–5003.

Lomax, B.E., Conti, M., Khan, N., Bennett, N.S., Ganin, A.Y., & Symes, M.D. (2020). Proving the viability of an electrochemical process for the simultaneous extraction of oxygen and production of metal alloys from lunar regolith. *Planetary and Space Science*, 180(104748), 1–10.

Lyon, R.J.P. (1965). Analysis of rocks by spectral infrared emission (8 to 25 microns). *Economic Geology*, 60,715–736.

Maturilli, A., Helbert, J., & Moroz, L. (2008). The Berlin emissivity database (BED). *Planetary and Space Science*, 56(3–4), 420–425.

Mavrogenes, J.A. & O'Neill, H.S.C. (1999). The relative effects of pressure, temperature and oxygen fugacity on the solubility of sulfide in mafic magmas. *Geochim. Cosmochim. Acta*, 63,1173–1180.

McSween, H.Y., Wyatt, M.B., Gellert, R., Bell, J.F., Morris, R.V., Herkenhoff, K.E., Crumpler, L.S., Miliam, K.A., Stockstill, K.R., Tornabene, L.L., Arvidson, R.E., Bartlett, P., Blaney, D., Cabrol, N.A., Christensen, P.R., Clark, B.C., Crisp, J.A., Des Marais, D.J., Economou, T., Farmer, J.D., Farrand, W., Ghosh, A., Golombek, M., Gorevan, S., Greeley, R., Hamilton, V.E., Johnson, J.R., Joliff, B.L., Klingelhöfer, G., Knudon, A.T., McLennan, S., Ming, D., Moersch, J.E., Rieder, R., Ruff, S.W., Schröder, C., de Souza, P.A., Squyres, S.W., Wänke, H., Wang, A., Yen, A., & Zipfel, J. (2006). Characterization and petrologic interpretation of olivine-rich basalts at Gusev Crater, Mars. *JGR: Planets*, 111(E02S10), 1-17.

Moersch, J.E., & Christensen, P.R. (1995). Thermal emission from particulate surfaces: A comparison of scattering models with measured spectra. *Journal of Geophysical Research*, 100, 7465–7477.

Murchie, S., Arvidson, R., Bedini, P., Beisser, K., Bibring, J.-P., Bishop, J., Boldt, J., Cavender, P., Choo, T., Clancy, R.T., Darlington, E.H., Des Marais, D.D., Espiritu, R., Fort, D., Green, R., Guinness, E., Hayes, J., Hash, C., Heffernan, K., Hemmler, J., Heyler, G., Humm, D., Hutcheson, J., Izenberg, N., Lee, R., Lees, J., Lohr, D., Malaret, E., Martin, T., McGovern, J.A., McGuire, P., Morris, R., Mustard, J., Pelkey, S., Rhodes, E., Robinson, M., Roush, T., Schaefer, E., Seagrave, G., Seelos, F., Silverglate, P., Slavney, S., Smith, M., Shyong, W.-J., Strohbehn, K., Taylor, H., Thompson, P., Tossman, B., Wirzburger, M., & Wolff, M. (2007). Compact Reconnaissance Imaging Spectrometer for Mars (CRISM) on Mars Reconnaissance Orbiter (MRO). *JGR: Planets*, 112(E5), 1-53.

Mustard, J.F., & Hays, J.E. (1997). Effects of hyperfine particles on reflectance spectra from 0.3 to 25 μm. *Icarus*, 145–163.

Nash, D.B., Salisbury, J.W., Conel, J.E., Lucey, P.G., & Christensen, P.R. (1993). Evaluation of Infrared Emission Spectroscopy for Mapping the Moon's Surface

Composition From Lunar Orbit. *Journal of Geophysical Research*, 98(E12), 23535-23552.

Nyquist, L.E., Boggard, D.D., Shih, C.-Y., Greshake, A., Stöffler, D., & Eugster, O. (2001). Ages and Geological Histories of Martian Meteorites. *Space Science Reviews*, 96, 105–164.

Osterloo, M. M., Anderson, F. S., Hamilton, V. E., & Hynek, B. M. (2010). Geologic context of proposed chloride-bearing materials on Mars. *Journal of Geophysical Research*, 115(E10012), 1–29.

Osterloo, M. M., Hamilton, V. E., Bandfield, J. L., Glotch, T. D., Baldridge, A. M., Christensen, P. R., et al. (2008). Chloride-bearing materials in the southern highlands of Mars. *Science*, 319(5870), 1651–1654.

Patten, C., Barnes, S.-J., Mathes, E.A., & Jenner, F.E. (2013). Partition coefficients of chalcophile elements between sulfide and silicate melts and the early crystallization history of sulfide liquid: LA-CIP-MS analysis of MORB sulfide droplets. *Chemical Geology*. 358, 170–188.

Papike, J.J., Karner, J.M., Shearer, C.K., & Burger, P.V. (2009). Silicate mineralogy of martian meteorites. *Geochim. Cosmochim. Acta*, 73, 7443–7485.

Perring, C.S. (2015). Volcanological and Structural Controls on Mineralization at the Mount Keith and Cliffs Komatiite-Associated Nickel Sulfide Deposits, Agnew-Wiluna Belt, Western Australia–Implications for Ore Genesis and Targeting. *Economic Geology*, 110(7), 1669-1695.

Ramsey, M. (2004). Quantitative geological surface processes extracted from infrared spectroscopy and remote sensing. *Infrared Spectroscopy in Geochemistry, Exploration Geochemistry and Remote Sensing*, 33, 197–224.

Ramsey, M., & Christensen, P.R. (1998). Mineral abundance determination: Quantitative deconvolution of thermal emission spectra. *Journal of Geophysical Research*, 103(B1), 577–596.

Reyes, D.P., & Christensen, P.R. (1994). Evidence for Komatiite-type lavas on mars from Phobos ISM data and other observations. *Geophysical Research Letters*, 21, 887–890.

Righter, K., Pando, K. & Danielson, L.R. (2009). Experimental evidence for sulfur-rich martian magmas: Implications for volcanisms and surficial sulfur sources. *Earth and Planet. Sci.* 43, 1709–1723.

Ripley, E.M., & Li, C. (2013). Sulfide Saturation in Mafic Magmas: Is External Sulfur Required for Magmatic Ni-Cu-(PGE) Ore Genesis? *Economic Geology,* 108, 45–58.

Rivard, B., Feng, J., Gallie, E., & Francis, H. (2001). Ore detection and grade estimation in the Sudbury mines using thermal infrared reflectance spectroscopy. *Geophysics*, 66(6), 1691–1698.

Ruff, S.W., Christensen, P.R., Barbera, P.W., & Anderson, D.L. (1997). Quantitative thermal emission spectroscopy of minerals: A laboratory technique for measurement and calibration. *Journal of Geophysical Research*, 102(B7), 14899–14913.

Salisbury, J.W., & Wald, A. (1992). The role of volume scattering in reducing spectral contrast of Reststrahlen bands in spectra of powdered minerals. *Icarus*, 96:121–128.

Salisbury, J.W., & Eastes, J.W. (1985). The effect of particle size and porosity on spectral contrast in the mid-infrared. *Icarus*, 64:586–588.

Salisbury, J.W., Walter, L.S., & Vergo, N. (1987). Mid-infrared (2.1-25 μm) reflectance spectra of powdered stony meteorites. *Icarus*, 92:280–297.

Salisbury, J. W., Walter, L. S., Vergo, N., & D'Aria, D. M. (1991). *Infrared (2.1–25 μm) spectra of minerals.* Johns Hopkins University Press.

Salisbury, J.W., & Walter, L.S. (1989). Thermal infrared (2.5–13.5 μm) Spectroscopic Remote Sensing of Igneous Rock types on Particulate Planetary Surfaces. *Journal of Geophysical Research,* 94(B7), 9192–9202.

Shirley, K.A., & Glotch, T.D. (2019). Particle Size Effects on Mid-Infrared Spectra of Lunar Analog Minerals in a Simulated Lunar Environment. *JGR Planets*, 124. 970–988.

Song, X., Wang, Y., & Chen, L. (2011). Magmatic Ni-Cu-(PGE) deposits in magmatic plumbing systems: Features, formation and exploration. *Geoscience Frontiers*. 2(3), 375–385.

Squyres, S.W., Arvidson, R.E., Bell III, J.F., Bruckner, J., Cabrol, N.A., Calvin, W., … & Yen, A. (2004). The Spirit rover's Athena science investigation at Gusev crater, Mars. *Science,* 305(5685), 794–799.

Vaughan, D., & Lennie, A. R. (1991). The iron sulphide minerals: Their chemistry and role in nature. *Science Progress,* 75(3/4), 371–388.

Wenrich, M.L., & Christensen, P.R. (1996). Optical constants of minerals derived from emission spectroscopy: Application to quartz. *JGR: Solid Earth*, 101(B7), 15921–15931.

West, M.D., & Clarke, J.D. (2010). Potential martian mineral resources: Mechanisms and terrestrial analogues. *Planetary and Space Science*, 58, 574–582.

Zheng, W., & Qiao, G. (2022). Metal alloys obtained from solid martian regolith simulant by an electrochemical reduction process. *Advances in Space Research*, 70(4), 1175–1187.

Zientek, M. L. (2012). Magmatic ore deposits in layered intrusions–descriptive model for reef-type PGE and contact-type Cu-Ni-PGE deposits. *U.S. Geological Survey Open-File Report 2012-1010* (pp. 1–48).

Zientek, M. L., Czamanske, K., & Irvine, T. N. (1985). Stratigraphy and nomenclature for the stillwater complex. In G. K. Czamanske & M. L. Zientek (Eds.), *The stillwater complex, Montana: Geology and guide. Special publication 92* (pp. 21–38).

CHAPTER 4

A LUNAR WATER ICE MINING MAP TOOL FOR IDENTIFYING SUITABLE LOCATIONS FOR MINING AND BASES FOR OPERATIONS

Abstract

To reduce the cost of space exploration, establish a permanent human presence in space, and promote the sustainable development of our Solar System, it is essential to detect, identify, extract, and utilize resources in situ. The main resource being targeted on the Moon is water ice, for it is being considered for use in the near term to produce rocket propellant, oxygen, drinking water, mineral processing, and manufacturing. However, some locations on the Moon are more conducive to development than others. In this paper, we present a Lunar Water Ice Mining Map Tool that identifies suitable locations for large-scale surface and subsurface mining and for establishing bases for operations. The map divides the Lunar South Pole into a grid of blocks ~1 km x 1 km in size. A block is classified as suitable for surface or subsurface mining based on its potential to harbor water ice (average maximum temperature in the summer) and its navigability (average slope). Blocks suitable for establishing bases for operations were identified based on their access to power (average percent illumination), communications with Earth (average percent Earth visibility), and terrain with slopes flat enough to enable the construction of infrastructure with minimal site preparation (average slope). In addition, we use the map's block system to assess the potential of the Artemis III candidate landing regions for mining and for constructing bases to support a mine site.

4.1 Introduction

To establish a permanent human presence on the Moon, Mars, and beyond, we will need to obtain the essentials for life in part from the Moon, rather than from Earth, including water, food, fuel, and the materials for building and manufacturing. Our current solution is to bring these resources with us, which is costly since we have to transport these resources on rockets out of Earth's gravity well. However, if we can locate and extract the raw materials in-situ to produce these resources, we can substantially lower the cost of space travel, reduce our dependence on Earth-based resources, and promote sustainable development of our Solar System.

Even before the Apollo era, scientists hypothesized that volatile compounds, including water ice, might be in minable quantities in the Moon's polar regions (Watson et al., 1961a,b; Arnold, 1979; Hodges, 1981). Owing to the Moon's low axial tilt and topography at the poles, certain areas, such as the bottoms of impact craters, never receive direct sunlight over an entire lunar precession cycle. These so-called permanently shadowed regions (PSRs) exhibit temperatures low enough to trap and retain volatiles for billions of years (Vasavada et al., 1999). Due to improvements in engineering and technology, the PSRs are now considered potential target locations to prospect for and mine water ice-enriched volatiles.

The hypothesis that the Moon's poles contained water ice was confirmed in 1999 and 2009 when Lunar Prospector (Binder, 1998) and Lunar Reconnaissance Orbiter (Chin et al., 2007) detected significant decreases in the neutron flux over the lunar poles due to an increase in hydrogen (Feldman et al., 1998; Hubbard et al., 2002). Additionally, using a variety of remote sensing methods, multiple research groups have established that water ice is indeed present in the Moon's polar regions (Nozette et al., 1994,1996;

Feldman et al., 1998; Spudis et al., 2010, 2013; Colaprete et al., 2010; Mitrofanov et al., 2010; Gladstone et al., 2012; Lucey et al., 2014; Hayne et al., 2015, 2020; Li et al., 2018; Fisher et al., 2017; Yang et al., 2019) and that the thermal conditions within PSRs are sufficient to retain the water ice along other organic and inorganic volatiles species likely delivered from asteroids and comets, interstellar dust particles, the continuous solar wind hydrogen, or from the Moon's interior (Schorghofer & Taylor, 2007; Zhang & Paige, 2009; Anand, 2010; Paige et al., 2010; Bockelée-Morvan and Biver, 2017; Williams et al., 2019) for extended time-periods.

Ground truth obtained during the Lunar Crater Observation and Sensing Satellite (LCROSS) mission confirmed observations made from orbit when a spent Centaur rocket stage impacted the floor of Cabeus crater, a shadowed location representative of the Moon's PSRs (Colaprete et al., 2010; Schultz et al., 2010). The impact produced a plume of debris, dust, and vapor, which was analyzed by instruments onboard the LCROSS shepherding spacecraft (Gladstone et al., 2010), confirming the presence of water ice in significant amounts (5.6 ± 2.6% by mass) along with other frozen volatiles such as hydrogen sulfide, carbon dioxide, ammonia, methane, and carbon dioxide (Colaprete et al., 2010).

It remains unclear whether the composition of the frozen volatiles or the amount of water ice detected in the LCROSS plume is representative of all locations on the Moon with suitable temperatures to trap volatiles. If so, locations enriched in volatiles can be developed into mine sites, where ices would theoretically be extracted and processed to produce O_2 and H_2O for life support, liquid H_2 and O_2 for fuel and propellant, NH_3 for fertilizer, and other chemicals for mineral processing of the Moon's regolith to produce

metals. However, their lateral and horizontal distribution, nature, and composition are still relatively unknown (National Research Council, 2007).

The Moon's potential as a reservoir of water ice prompted scientists and engineers to design innovative mining techniques specifically designed for lunar operations. However, due to the different environmental constraints imposed by the lunar environment (e.g., low gravity, vacuum, dust), conventional mining techniques used on Earth must be significantly modified for lunar ice mining (Toklu and Järvstråt, 2003). For example, due to launch costs, lunar mining technologies must have low mass (Ruess et al., 2008), but common excavation techniques used on Earth depend on the effect of gravitational acceleration, which turns mass into force to cut, scoop, and move soil (Bernold, 1991).

Rather than relying on terrestrial mining techniques, engineers are adapting approaches from non-traditional terrestrial industries to develop new mining methods for use on the Moon. For example, drawing from Earth's environmental remediation industry, the Colorado School of Mines is developing a mining concept known as thermal desorption, which applies heat directly by concentrating sunlight onto a portion of the Moon's surface using an optical system (Sowers & Dreyer, 2019). Additionally, heat is applied to the near subsurface using conducting rods, converting the surface and subsurface ice to vapor, which is collected in a capture tent covering the surface (Sowers & Dreyer, 2019). The vaporized ice is then vented into a storage container known as a "cold finger" and hauled to a facility for further processing (Sowers & Dreyer, 2019).

The University of Central Florida is developing a low-energy mechanical separation technique called Aqua Factorem, which will separate the ice by exploiting

differences in density, magnetic susceptibility, and microwave susceptibility relative to the other minerals on the Moon (Metzger, 2021). Alternatively, TransAstra–an aerospace startup–has invented a concept known as Radiant Gas Dynamic Mining. Using radio, microwave, and infrared radiation, their technology can target ice with a depth-controlled heating profile (Sercel et al., 2021).

As lunar mining technology continues to mature, it is paramount that we identify locations on the Moon that are the most conducive for establishing successful water ice mine sites. In this paper, we present a Lunar Mining Map Tool that identifies the most suitable locations to prospect for water ice and for establishing a base for operations. We demonstrate the potential use of the tool by assessing the mining potential of the Artemis III candidate landing regions.

The Lunar Mining Map Tool can also serve as a spatial planning tool for implementing a contract system for managing future lunar mining activities. Additionally, the design of the tool facilitates the implementation of Area-Based Management Tools to regulate actors from mining in specified areas, promote equitable access, and monitor the effects of mining activities on the lunar environment.

4.2 Mining Map of the Lunar South Pole Resource System

The Lunar Mining Map Tool divides an area on the Moon into a grid of ~1 km x 1 km blocks. To identify which blocks are suitable for mining and for establishing bases for operations, the Lunar Mining Map Tool classifies each block according to its potential to harbor water ice (average maximum summer temperature), navigability (average slope), access to power (average percent illumination), and communications with Earth (average percent Earth visibility) (Figure 4.1).

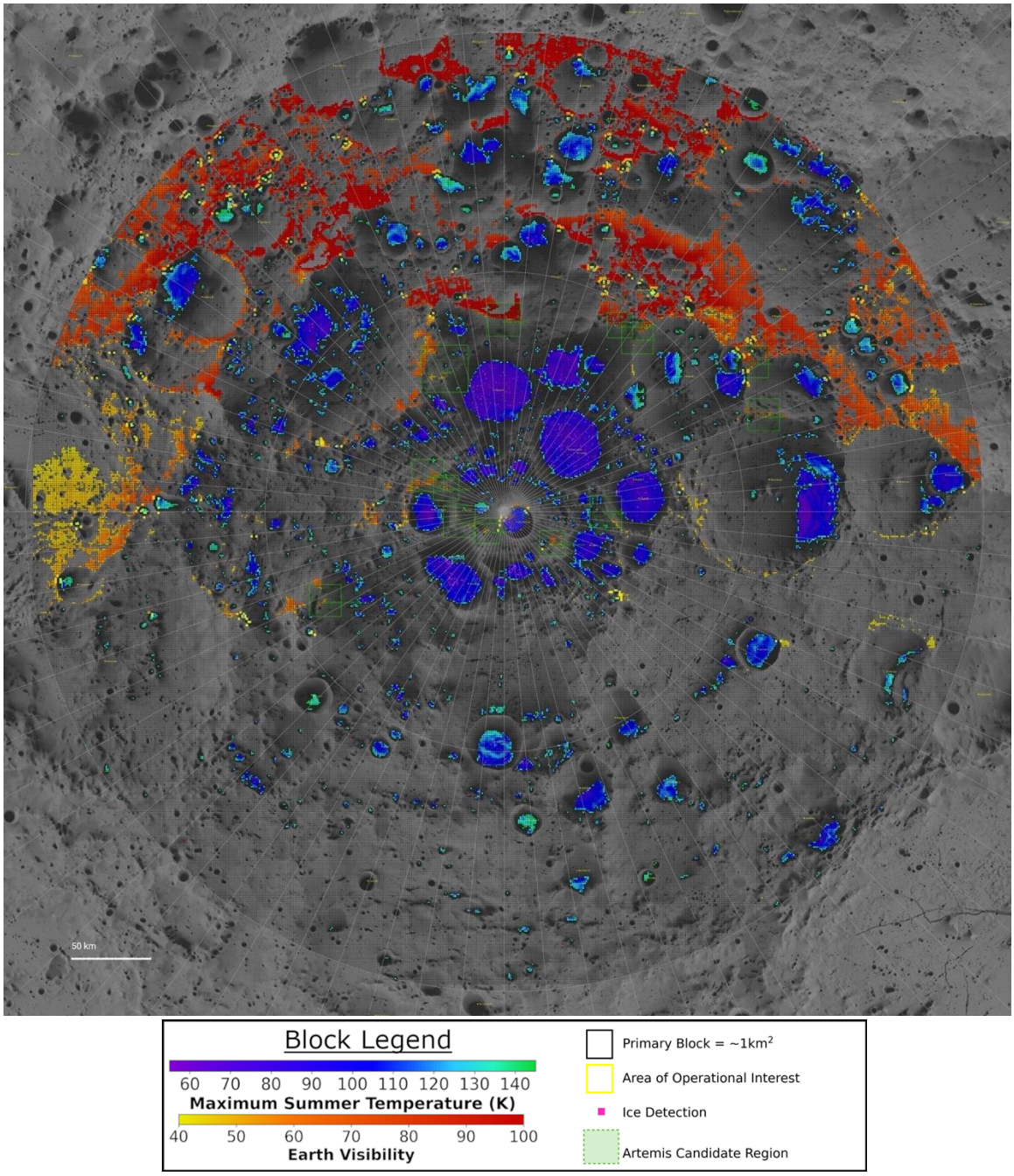

Figure 4.1 – Mining map of the Lunar South Pole from 80-90ºS overlaid on an illumination basemap derived from Mazarico et al., 2011. The Lunar Mining Map Tool divides the South Pole into a grid containing 288,142 blocks ~1 km x 1 km in size. Each block is classified according to its suitability for mining and for establishing bases for operations. A block is classified as suitable for mining if it exhibits an average maximum summer temperature suitable to trap water ice and terrain with average slopes navigable by rovers. A block is classified as potentially suitable for establishing a base for operations if it exhibits sufficient average illumination conditions to generate solar-electric power, Earth visibility to establish Earth-Moon communications and terrain with

slopes navigable by rovers. Suitable mining blocks are colored according to their average maximum summer temperature, and blocks suitable for operations are colored according to their average percent Earth visibility. Operations blocks and suitable mining blocks within ~3 km are bordered in yellow. Blocks without colors are deemed unsuitable for a mining operation.

4.2 Blocks Suitable for Mining

Preliminary prospecting of the lunar surface began in the late 1950s with Lunar Orbiter 1. As technology advanced, our knowledge of the available raw materials on the Moon that could be processed into functional commodities and consumables has dramatically increased. Based on ~382kg of samples returned during the Apollo era, remotely-sensed data returned from both orbiters and landers, and the compositions of lunar meteorites, numerous raw materials on the Moon have been identified for use in-situ, including:

- Water ice (targeted for H_2O),
- Other frozen volatiles delivered by comets (e.g., CO_2, CO, H_2CO Ca, Hg, Mg, H_2S, NH_3, SO_2, C_2H_4, CH_3OH, HCOOH, CH_4, OH, and Na)
- Plagioclase-rich highlands regolith (minerals containing Si, Al, and Ca)
- Ilmenite-rich mare regolith, (minerals containing Ti, Fe, Mg and O)
- KREEP basalts (minerals containing targeted for K, P, and rare earth elements)
- Pyroclastic deposits (volcanic glass beads containing $FeTiO_3$ for O_2, and surficial volatile elements such as S, Zn, Ge, Gn, Ir, Ag, Au, and F)
- Immature regolith deposits (a proxy for low concentrations of agglutinate and higher concentrations of monomineralic fragments such as plagioclase and olivine)
- Mature regolith deposits (a proxy for higher concentrations of solar wind implanted volatiles such as He^3 and H).

In this paper, we focus on water ice since it is being considered for use in the near term to produce rocket propellant, oxygen, drinking water, and for in-situ mineral processing. To determine the areas on the Lunar South Pole that are most suitable for mining, we first classify each block according to its potential to trap water ice. Surface temperatures are the key factor that determines the location of lunar ice deposits, their composition, and how long they will survive because as surface temperature increases, the evaporation rate of water ice into a vacuum increases (Vasavada et al., 1999). However, temperatures within permanently shadowed regions near the poles are low enough for water ice to be stable at the surface and subsurface for periods extending beyond the age of the Solar System (Paige et al., 1992).

We incorporate temperature data derived from ten years of Diviner observations aboard the Lunar Reconnaissance Orbiter, which was used to generate a seasonal bolometric brightness temperature map of the Moon's surface from 80ºS to 90ºS (Williams et al., 2019). Diviner provides calibrated radiance measurements in seven infrared channels between 7.55 and 400μm at a spatial resolution of ~240m/pixel, which are used to fit an equivalent blackbody to estimate surface temperature (Paige et al., 2010). The temperature value for each mining block is an average of multiple Diviner pixels within each block. We elected to use the average maximum summer temperature rather than the annual average temperature to eliminate the effects of drastic temperature variations ($\gtrsim$100K) that the poles experience between the summer and winter seasons (Williams et al., 2019).

Blocks in the Lunar South Pole Resource System are classified as Category I ($\leq$112K), Category II (112-145K), or Category III ($\geq$145K) (Table 1). Category I blocks

are considered the most suitable for surface mining if their average maximum temperatures in the summer are at or below the sublimation point of crystalline H_2O in a vacuum. The cutoff temperature is derived from Vasavada et al. (1999), who calculate sublimation rates for several relevant volatile species, reporting that at ~112K, water ice should be stable at the Moon's surface over time scales of billions of years.

It is also possible for water ice to be present in the subsurface in areas with slightly warmer temperatures. For example, if water ice is covered by a regolith cover, it would be protected from peak surface temperatures and surface loss processes, which could limit the loss rate by diffusion through the regolith cover (Killen et al., 1997). Thus, assuming the annual average surface temperature is approximately equal to the upper meter of the subsurface temperature (Hayne et al., 2015; Landis et al., 2022), we classify blocks with average maximum summer temperatures between 112-145K as Category II blocks. Category II blocks are considered suitable for near subsurface mining (<1-meter depth) targets because ice beneath approximately one meter of porous regolith can survive average annual temperatures of ~145K for more than a billion years (Schorghofer, 2008; Hayne et al., 2015). Thus, frozen volatiles may remain trapped beneath the surface of mining blocks at or below these temperatures. We elected to use the average maximum temperature rather than the average annual temperature to narrow down the most prospective regions for subsurface mining.

Blocks in Category III exhibit average temperatures >145K and are not considered suitable locations for mining since their average maximum summer temperatures are too high for water ice to be stable. Of the 288,142 blocks in Lunar Mining Map Tool, ~4% are classified as Category I and ~3% as Category II (Table 1). In

total, 20,243 blocks exhibit temperatures suitable for water ice to be present for surface and subsurface mining.

Each mining block was further classified based on its navigability. The navigability of each mining block was determined by integrating data from a slope map into the Lunar Mining Map Tool. The Mars Space Flight Facility at ASU produced the map product from resampled, interpolated altimetry data acquired by the Lunar Orbiter Laser Altimeter (LOLA) instrument (Smith et al., 2010 a,b) aboard the Lunar Reconnaissance Orbiter. The slope map is at a resolution of 1,024 ppd, which translates to ~30 m/pixel.

The Lunar Roving Vehicle was designed to carry two astronauts and a science payload at 13 km/h on a smooth, level surface and at reduced velocities on slopes of up to 25º (Basilevsky et al., 2019). The vehicle operated well on slopes between 20-23º in favorable circumstances, with the maximum slope-climbing capacity of the Lunar Roving Vehicle wheel ranging between 18-23º (Costes et al., 1972). The Endurance and INSPIRE rover concepts are designed to traverse terrain with slope angles of up to +/- 20º. However, because the nominal traverse distances and mission durations were much greater than the Apollo missions, the maximum slope of the traverse was limited to slopes of ≤15º to enable longer and safer travel (Keane et al., 2022). Using these parameters, we further classified each suitable mining block into three categories:

I: navigable (average slope ≤15º),

II: difficult to navigate (average slope 15-23º), and

III: not navigable (average slope ≥23º).

We elected to use ≤15º as our most "navigable" cutoff value because mining activities (i.e., prospecting, exploration, hauling, etc.) will likely contain lengthy and numerous traverses. Thus, similar to the requirements of Keane et al. (2022), we wanted to identify less undulating mining routes to be time and energy efficient. Our "difficult to navigate" cutoff value was determined by using the maximum slope value where the Lunar Roving Vehicle operated well in "favorable circumstances."

In total, 19,699 blocks with suitable temperatures to trap water ice exhibit average slope angles falling in Categories I and II. ~97% of the blocks in Categories I and II are considered navigable, with ~11% classified as difficult to navigate (Table 4.1), suggesting that if technological advances permit rovers to operate in blocks with harsh temperature conditions, much of that landscape is navigable.

Table 4.1 - Distribution of suitable mining blocks in the Lunar Mining Map Tool as a function of average maximum temperature in the summer (Williams et al., 2019) and average slope (Smith et al., 2010 a, b). Thirty-nine blocks were removed from the analysis since they did not contain temperature data, all of which are located at ~80º latitude.

Temperature (K)	≤112	112-145	≥145	
Category	I	II	III	
	Surface mining	Subsurface mining	Not suitable for mining	Block Totals
	Number of Blocks			
	11,722	8,521	267,860	288,103
Slope				
Navigable (≤15°)	10,695	6,725	252,987	270,407
Difficult to navigate (15°-23°)	890	1,389	13,108	15,387
Not navigable (≥23°)	137	407	1,765	2,309

Slope angles and maximum temperatures represent the average value of the pixels within each block, with the number of pixels within each block varying slightly (Table

S1) depending on location. Classifying a mining block based on its average temperature value could overlook small-scale areas with suitable mining temperatures if they are adjacent to areas with higher temperatures. In total, 11,722 blocks in the Lunar South Pole Mining Map exhibit average maximum temperatures in the summer less than or equal to the 112K threshold, which is 10% less than the total cold trap area (~13,000 km^2) poleward of 80ºS reported by Williams et al. (2019).

Recent research has identified an additional ~2,500 km^2 of cold trap area at spatial scales <100 m and ~700 km^2 of cold traps <1 m, with the most numerous cold traps at the centimeter scale (Hayne et al., 2021). Due to averaging multiple data points within a 1 km^2 block, the Lunar Mining Map Tool certainly overlooks small cold traps in blocks with higher average temperatures. However, because the volume of small cold traps would account for a small amount of the total cold-trapping volume (Hayne et al., 2021), it is unlikely that a mine site would be established in these locations.

Similarly, an average slope value may overlook topographic challenges that might impede the accessibility of ice deposits. Nonetheless, the average summer maximum temperature and slope angle values for the 1 km^2 blocks help narrow down which mining blocks are more suitable for establishing a mine site relative to others.

4.4 Blocks Suitable for Constructing Bases for Operations

4.4.1 Classification Scheme and Rationale

A block is classified as *potentially* suitable for establishing a base for operations if it exhibits an average slope of ≤23º, an average illumination of ≥40% of a lunation cycle, and average visibility with Earth of ≥40% of a lunation cycle. In total, 22,173 Lunar

Mining Map Tool blocks satisfy these criteria. To identify the blocks in the Lunar Mining Map Tool that are potentially suitable for establishing bases for operations, 120 m/pixel by 120 m/pixel illumination and Earth visibility data (Mazarico et al., 2011) and slope data produced from the Lunar Reconnaissance Orbiter's Lunar Orbiter Laser Altimeter (Smith et al., 2010a,b) were incorporated. The Earth visibility data and illumination data are averages derived from six-hour increments over the course of an entire lunation cycle and four lunation cycles, respectively, with the average values representing the percentage of timesteps where a pixel was either illuminated or Earth's disc was visible. For example, if we had five time steps where any part of the pixel was illuminated (by any fraction of the solar disk), and five where the Sun not visible, we would report 50% illumination.

The map's illumination and Earth visibility values represent the average of the pixels within each block, which allows us to search for large areas that may be suitable for establishing operations bases to support an industrial-scale mining venture. For example, if a block exhibits an illumination value of 20%, the Sun is visible within that 1 km^2 area for an average of 20% of the 18.6-year lunation cycle. Because each location at the Moon's poles will have a unique pattern of alternation between light and darkness over time (Vanoutryve et al 2010), it might be preferable to assess illumination at shorter time periods. However, a full lunar processional cycle covers all seasonal and orbital illumination effects, allowing the Mining Map to narrow down regions where a long-term industrial scale base could be established.

Earth-Moon communication is essential for remote command and control of mining activities, returning prospecting and mining data, and providing feedback

information on the status of mining assets to those supporting lunar mining activities from Earth. If lunar mining is established before a network of orbiting relay stations exists, first-generation mine sites will need to construct ground-based communications stations with a direct line-of-sight with Earth to enable robotic systems to receive mining operations commands and downlink data at all times. Because the Moon is tidally locked with the Earth, certain areas in blocks from -80°N to -90°N will exhibit a continuous line-of-sight communication between the Earth and the Moon. However, the Earth follows an "extended-eight shape" over the course of a lunar month when viewed from the poles, ranging between ±6.5° in elevation, and in a confined, narrow azimuth band of ~8° (Vanoutryve et al 2010). This would make the Earth disappear under the local horizon for blocks close to the pole for long periods. Moreover, communications stations must be strategically placed to ensure that topographic obstructions do not obscure Earth from view.

Because smooth terrain is critical for navigation and construction, the best operations blocks are those with gentle slopes. The average slope cutoff value of ≤23º is based on the same navigability classification scheme described for the Lunar Mining Map Tool's mining blocks. Blocks with average slope angles ≤15º will be easy to navigate (Keane et al., 2022), are suitable for landing (De Rosa et al., 2012), and require moderate site preparation, while blocks with average slope angles between 15º and 23º will be difficult to navigate. Many operations blocks will likely contain terrain that is navigable but too undulating for cost-effective construction and assembly of operations stations without significant site preparation such as leveling, spreading, piling, grading, and compacting (Connolly and Shoots, 1994; Boles and Connolly, 1996; Reuss et al., 2010).

Based on the slope tolerance of the Human Landing System (NASA, 2021) and a surface preparation requirement for a lunar habitat in Howard (2021), we also identified the operations blocks with average slope angles of ≤5º, for these blocks will have preexisting terrain suitable for constructing bases for operations. Limiting site preparation activities is paramount for cost-effective, responsible, and safe lunar mining because such activities could loft dangerous quantities of abrasive dust into the lunar exosphere. Significant amounts of suspended dust could pose many hazards to mining activities, including false instrument readings, visual obscuration, dust coatings and contamination of mining systems (e.g., optical surfaces, solar arrays), thermal control problems, seal failures in processing systems, communications issues, mechanical jamming and wear, and human health risks (Zelenyi et al., 2021; Cain, 2010). Furthermore, limiting dust suspension helps reduce anthropogenic activities' effects on the lunar environment.

Finally, in addition to requiring communication with Earth and navigable terrain, first-generation lunar water ice mining sites will also require a significant amount of power to operate (National Research Council, 2001; Girish and Aranya, 2012; Kornuta et al., 2018). We assume that future lunar mining operations will largely or exclusively rely on solar power since it is the only energy supply that can be produced in situ in the near term (Gläser et al., 2018). The Moon is a good place to harvest solar energy because the lack of an atmosphere allows more of the sun's incident energy to be converted to power than on Earth. For example, current state-of-the-art solar cells can offer up to >32% efficiency (Azur Space, 2020) vs. the ~15-20% efficiency of most commercial solar panels on Earth. We also focused on solar-powered mining activities because of its high specific power, or power-to-mass ratio. For example, a lunar surface photovoltaic power

system exhibits a power-to-mass ratio of 130 W/kg, a factor of 26 times higher than space-rated nuclear fission reactors (Colozza, 2020).

The most recurring argument against solar power on the Moon is the exceptionally long lunar nights. Typical surfaces at the Moon's equator are illuminated for half of a lunar month and in darkness for the other half (Bryant, 2009), implying that energy storage solutions are critical for powering a lunar base at these locations. However, unlike the equatorial regions, no specific statement about the duration of illumination periods can be made about the polar regions (Gläser et. al., 2018). Illumination at the poles is based on the geographic location, the slight seasons caused by the Moon's small rotational obliquity (1.54°), local topography, height above the ground, and on the lunar processional cycle (Vanoutryve et al 2010; Gläser et. al., 2018). These characteristics create illumination conditions at the Moon's poles that differ considerably from the lower latitudes. In fact, at the poles, each area will have its own unique pattern between light and darkness (Bussey et al., 2010; Vanoutryve et al 2010). For example, some blocks centered on the floors of impact craters will exhibit no direct sunlight. In contrast, blocks containing areas with topographic highs, such as crater rims and mountains, can exhibit periods of extended illumination for a majority of a lunation cycle (Bussey et al., 1999,2003; Noda et al., 2008; Bryant, 2009; Speyerer and Robinson, 2013). The Lunar Mining Map Tool blocks containing these locations are most suitable for constructing solar farms and energy storage systems to supply power to mine sites.

The Lunar Mining Map Tool's illumination cutoff value of ≥40% is based on an engineering framework for a company that would provide services for the sampling, excavation, and storage of lunar regolith from the Moon's polar regions (Coto et al.,

2021). In Coto et al. (2021), their plan of work requires a fleet of four RASSOR excavators and a CubeRover developed by Astrobotic whose batteries would be recharged using energy produced from a solar panel equipped to a lander. The framework offers solar production estimates and the mass and power requirements for vertical solar arrays ranging in size from 5–30 m^2 and battery banks for an area with 40% illumination (Coto et al., 2021). Assuming a solar flux of 1361 W/m^2, a solar panel efficiency of 25%, 360º solar array tracking, and 40% illumination (~270 solar hours over 28 days), the maximum peak power for a 15 m^2 vertical solar array is ~2 kW, with a 28-day production of 551 kWh and an annual production of 7,140 kWh (Coto et al., 2021).

While the cutoff value stems from a relatively small surface operation, the total power demand for lunar mining activities will vary depending on the number of systems, usage time, and efficiency of the energy storage system (Palos et al., 2020; Kaczmarzyk & Musial, 2021). For example, Colozza (2020) estimated that an oxygen production facility and base camp with six people would require ~28 kW and ~26 kW of power, respectively (Colozza, 2020). Khan et al. (2006) concluded that ~80 kW of power was required for a lunar base, with an additional ~42kW for mining purposes. However, industrial-scale mine sites and downstream manufacturing facilities will likely require >1 MW of electrical power (Waldron, 1990; Landis et al., 1990), demonstrating that mine sites must be close to large areas that are sufficiently illuminated for long periods of time to construct multiple photovoltaic systems. Therefore, we searched for $1km^2$ areas with ≥40% illumination. At these locations, photovoltaic systems can be mounted on tall towers (Fincannon, 2008; Ruppert et al., 2022) to circumvent topographic obstacles and further improve illumination conditions (Mazarico et al., 2010; Gläser et al., 2018).

4.4.2 Operations Blocks Results

As shown in Figure 4.2a, 90% of the operations blocks are classified as navigable and 10% as difficult to navigate. Approximately 46% of the operations blocks exhibit relatively flat terrain (average slope angles ≤5º), making these areas most suitable for constructing solar farms, communications stations, and lunar bases. The shape of the Earth visibility data of the operations blocks is skewed left (Figure 4.2b). The median average percent Earth visibility for the operations blocks over the lunar precession cycle is ~76%, equating to ~124,000 hours of Earth visibility over one 18.6-year cycle. However, the cadence is important, meaning that lunar operations stations will need near-continuous communications with Earth. Without these characteristics, orbiting communications stations will be needed. 25% of the operations blocks exhibit surfaces with an average percent visibility with Earth for >95% of the 18.6-year lunar precession cycle, 15% for >99% of the cycle, and 10% for >99.9% of the cycle. It is these blocks that are most suitable for establishing ground communication stations. For the rest of the blocks, the Earth will be obscured for some time, making continuous direct communication impossible. To circumvent this issue, an integrated network of communications stations could be established to ensure that the Earth would be in view at any given time. However, mining equipment would still have to be in view of the communications station.

The spread of the illumination data for the operations blocks is quite narrow, ranging from 40–52.2%. Approximately 12% of the blocks exhibit an average illumination six percentage points above the 40% cutoff value (Figure 4.2c). This is

because the blocks at the high end of the distribution contain very small areas with relatively high illumination.

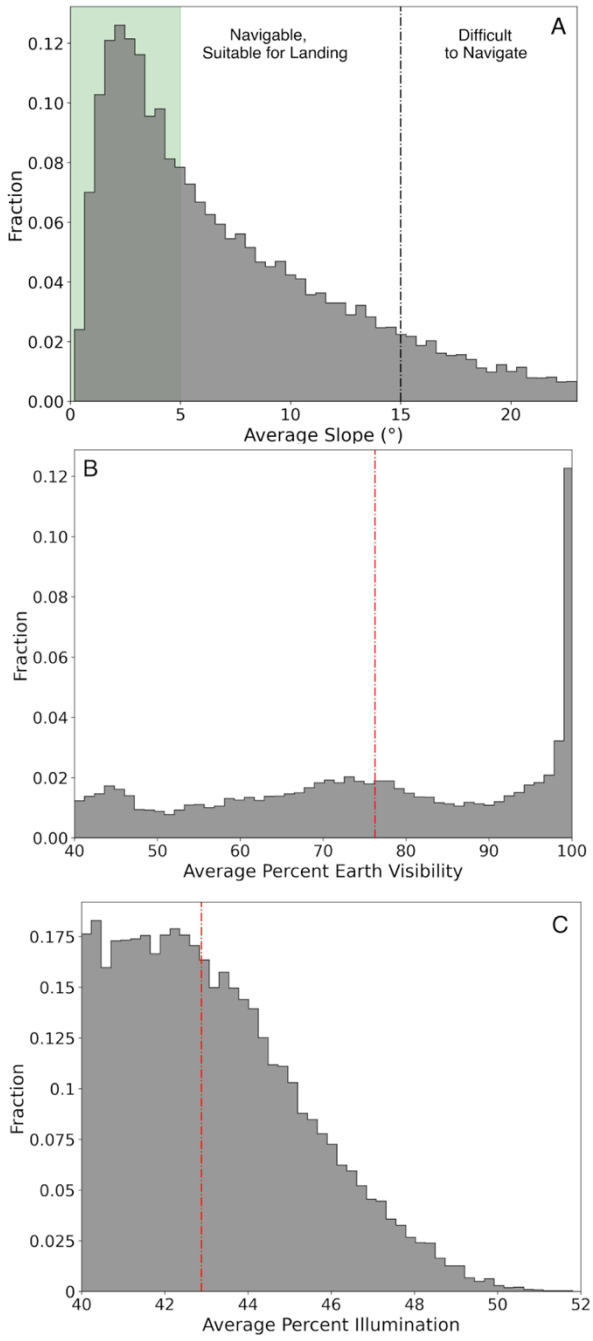

Figure 4.2 – Distributions of the (a) average slope, (b) average percent Earth visibility over a lunar precession cycle, and (c) and average percent illumination over a lunar precession cycle for the 22,173 potentially suitable operations blocks identified in the Lunar Mining Map Tool. Blocks to the left of the dashed vertical line in (a) are

considered navigable, while those to the right are considered difficult to navigate, and the area shaded in green (average slope angle of ≤5º) represents the blocks most suitable for the construction of operations stations since little site preparation would be required. The vertical red lines in (b) and (c) correspond to the median value for each distribution.

However, they get averaged into the larger block area, so the averages fall within this range. Nonetheless, suppose multiple photovoltaic systems are equipped on high towers in these blocks. In that case, some could be used to power mining operations during sunlit periods, while others could be used to charge batteries for use during periods of darkness.

Geographic location strongly influences the distribution of operations blocks. Because the Moon is tidally locked, ~94% (n=20,747) of the operations blocks reside on the Lunar near side between 270ºE and 90ºE longitude (Figure 4.3b). An effect called libration, caused by the Moon's elliptical orbit and axial tilt relative to Earth's, makes the face of the Moon toward the Earth rotate slightly from east to west over its period. This effect extends the longitudes of operations blocks slightly further around each limb of the Moon. About one week after perigee and apogee, up to ~8º of additional longitude on the Eastern and Western far side is viewable from certain areas on Earth (McClure, 2022). Even accounting for the Moon's libration, ~2% (n=756) of the operable blocks are found on the lunar far side. However, only three exhibit Earth visibility conditions above the median. The block's center coordinates are -80.92ºS, 172.36ºE, -82.29ºS, 254.15ºE, and -80.43ºS, 224.12ºE. The frequency of operations blocks decreases significantly at higher latitudes because of Earth visibility (Figure 4.3a). ~97% (n=21,579) of the operations blocks are located between 80ºS-86ºS and ~3% from 86ºS-90ºS (n=594), accounting for ~2.7% of the operations blocks and <0.3% of the total blocks in the Lunar Mining Map Tool. Furthermore, only five blocks located between 86ºS-90ºS exhibit average Earth visibility above the median value. This demonstrates that future mine sites dependent on

ground-based Earth-Moon communications are best positioned on the lunar near side and at lower latitudes (~80º-86ºS).

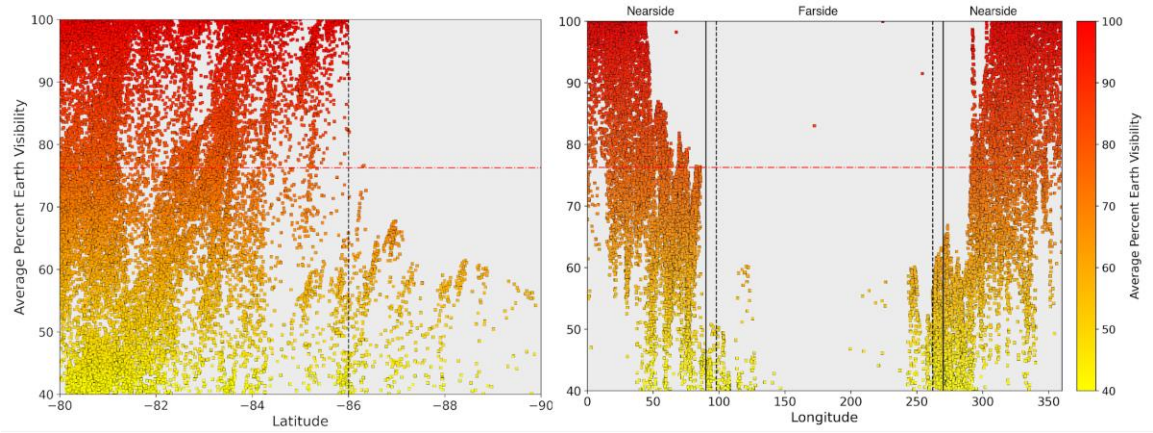

Figure 4.3 – The distribution of blocks suitable for operations as a function of geographic location and Earth visibility as an average percent of an entire lunation cycle (color bar). The dashed vertical line in the left plot at -86º latitude marks the most rapid decline of operations blocks with rising southern latitude. The solid vertical lines on the right divide the plot into the Lunar near side and far side and the dashed vertical lines show the additional 8º longitude visible to Earth because of libration. The red dashed-dotted line represents the operations blocks' median Earth visibility value (~76%).

Compared to the Earth visibility data, there does not appear to be as strong of a correlation between the geographic location of the operations blocks and their illumination conditions (Figure 4.4). The ratio of operations blocks above and below the median illumination value is split 50:50 between 80ºS-86ºS and 43:57 for those within 4º of the pole, demonstrating that further away from the pole, the average illumination conditions of operations blocks improve slightly. However, while only three operations blocks on the lunar far side exhibit average Earth visibility conditions above the median, high topography affords 48% (n=216) of the far side operations blocks with illumination conditions above the median, with only 33 located within 4º of the pole. This demonstrates that if mining operations are to be conducted near the pole and on the far side, power could be supplied using nearby operations stations constructed in operations

blocks. However, orbiting communications satellites or an interconnected network of ground communications stations would likely be required to receive commands from and transmit data to Earth.

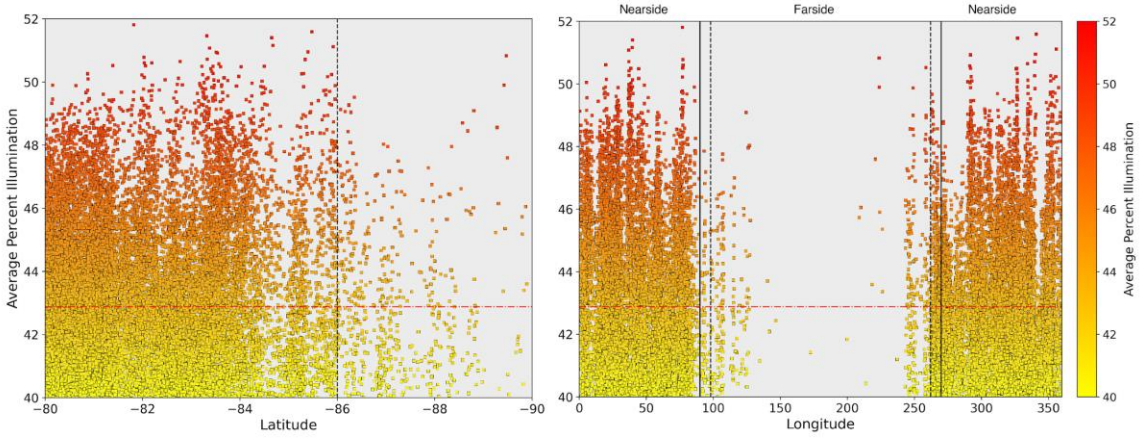

Figure 4.4 – Displaying the distribution of blocks suitable for operations as a function of average percent illumination (color bar) and geographic location. The dashed vertical line in the left plot at 86ºS latitude marks the most rapid decline of operations blocks with rising southern latitude. The solid vertical lines on the right divide the plot into the Lunar near side and far side, and the dashed vertical lines show the additional 8º longitude visible to Earth because of libration. The horizontal red dashed-dotted line represents the median illumination value (~43%).

4.4.3 The Best Blocks for a Lunar Base to Support Mining Activities

The blocks that would require the least site preparation, and therefore best for operations, have an average percent Earth visibility over an entire lunation cycle that is above the median (~76%), illumination conditions above the median (~43%), and average slope angles ≤5º. In total, 2,419 blocks satisfy these criteria (Figure 4.5). All of the blocks are located between 80ºS-86ºS, and all, but one are located on the near side.

Lemelin et al. (2014) ranks candidate landing site areas based on their proximity to PSRs, with the closest sites being the most favorable. Thus, all operations blocks <3 km from a mining block were identified. The justification is that mining operations

stations will be constructed adjacent to a mining block rather than in the block itself, for the mining areas themselves exhibit harsh temperature conditions and little to no illumination and line-of-sight with Earth. Constructing an operations station outside a mining block is also beneficial because it limits damage to the resource itself and reduces the human footprint on the lunar surface.

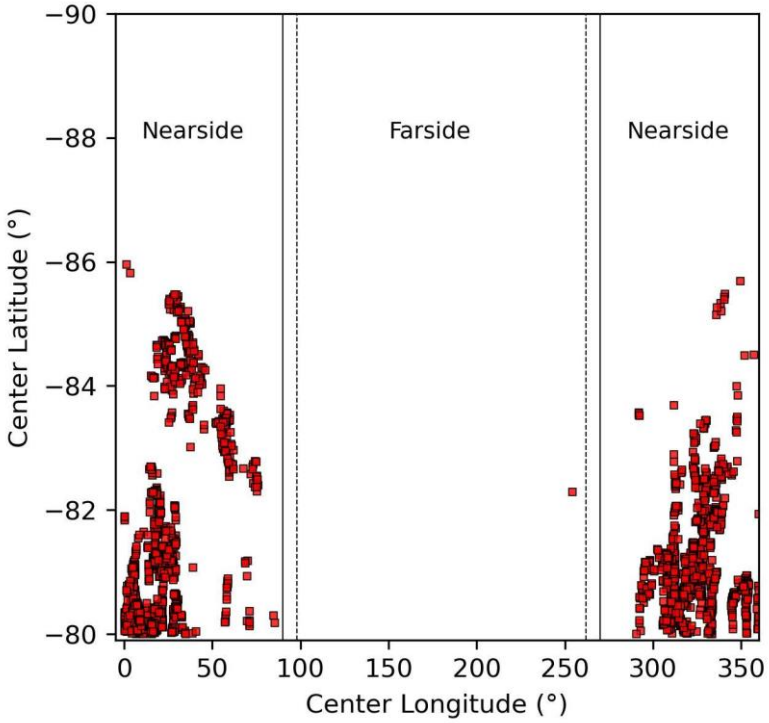

Figure 4.5 – Locations of the best operations blocks at the Lunar South pole. The best blocks for establishing a base for operations were those with an average percent illumination over an entire lunation cycle above the median (~43%), an average percent Earth visibility over an entire lunation cycle (~76%) above the median, and if the block's preexisting terrain requires little site preparation (average slope angle ≤5º). The solid vertical lines divide the plot into the Lunar near side and far side, and the dashed vertical lines show the additional 8º longitude visible to Earth because of libration.

Additionally, establishing a base close to a mining block will improve the efficiency of the mining operation by reducing the distances required to haul the water ice to a processing plant and ensuring that the processing plant will have a continuous feedstock, which limits processing downtime. For example, if prospecting reveals that

suitable mining blocks contain amounts of water ice sufficient to warrant a mine site, robotic mining equipment could excavate water-rich regolith and transport it to a beneficiation unit, in a nearby operations block, capable of sizing and physically separating the volatiles (resource) and removing unwanted minerals (gangue) from the ore stream. This step reduces gangue mass transported by haulers, increases ore grade of the feedstock concentrate, and improves H_2O recovery rates during downstream processing (Cilliers et al., 2020). After beneficiation, haulers would transport the water ice concentrate in the solid phase to an operations station comprised of a solar-powered processing plant and power station. The processing plant would process the concentrate to extract volatiles, purify the volatiles to isolate the water ice and remove contaminants, and finally separate the water ice to produce LOH and LOX to produce rocket propellant. The haulers could also transport batteries to and from the operations station to supply power to the mining assets.

In total, 295 (~1.3%) of the operations blocks are within 3 km of a mining block. Moreover, despite the significant number of suitable mining blocks identified using the Lunar Mining Map Tool, only 200 (~1% of the mining blocks) are within 3 km of an operations block (Figure 4.6). We consider these blocks to be the most likely locations for first-generation mining activities. About 8% (n=18) of the suitable mining blocks are classified as Category I, with the remaining 92% classified as Category II, suggesting that if volatiles are present in sufficient quantities to warrant a mine site, both surface and subsurface operations are required. ~77% (n=155) of the mining blocks adjacent to an operations block exhibit favorable traverse conditions for humans and rovers ($\leq 15^{o}$ average slope), and ~90% (n=181) are navigable by the Endurance and Inspire rover

concepts (≤20º average slope), demonstrating that very few mining blocks exhibit terrain that would be difficult to navigate for mining (Figure 4.6). The mining and operations blocks in close proximity are bordered yellow in Figure 4.1.

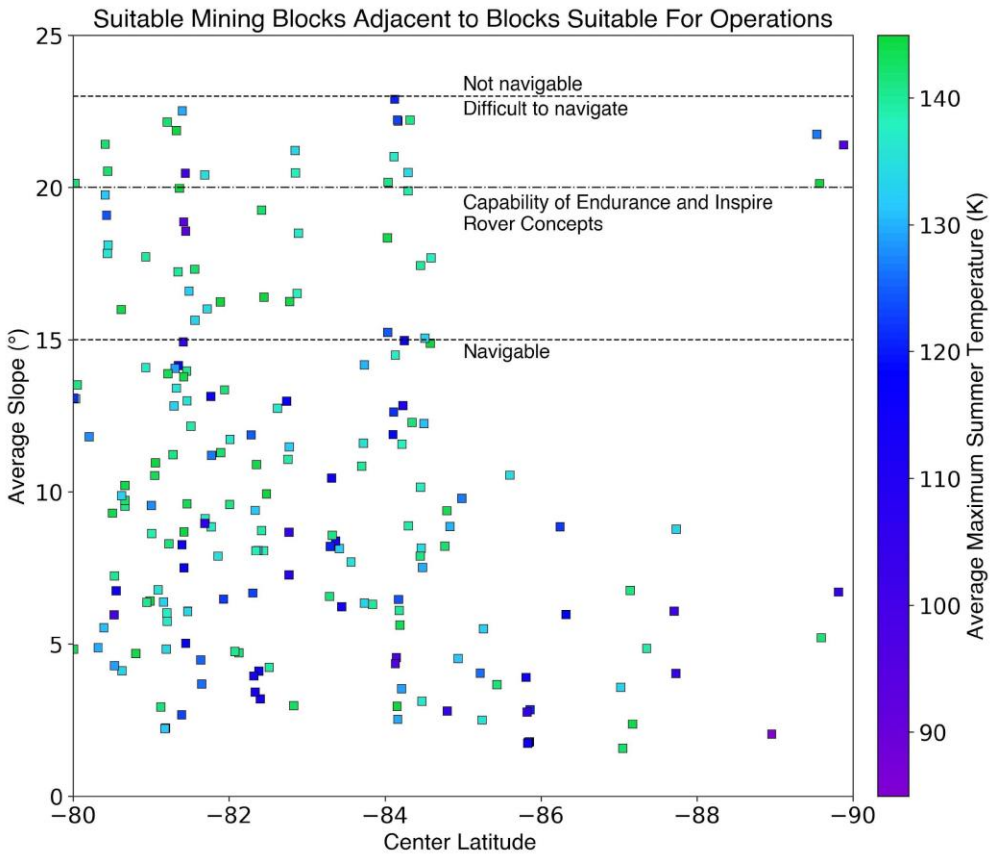

Figure 4.6 – Scatter plot displaying the locations of suitable mining blocks within 3 km of an operations block as a function of the average slope angle and maximum summer temperature. The dashed lines divide the blocks into their navigability categories. The dashed-dotted line represents the capability of the Endurance and Inspire rover concepts described in the 2023 Planetary Science Decadal Survey (Keane et al., 2022). The blocks are colored according to their average maximum temperature in the summer and correspond to the same colors used in the map in Figure 1. Category I mining blocks exhibit average maximum summer temperatures that are cold enough (≤112K) for water ice to be stable at the surface.

The Artemis missions focus on initial prospecting for water ice within 4º of the pole. However, the Lunar Mining Map Tool demonstrates that this might be misguided. Only 16 mining blocks within close proximity to an operations block are found at these

latitudes. Moreover, ~94% of the operations blocks in close proximity to mining blocks are located from 80ºS to 86ºS latitude, and none of the operations blocks within 4º of the pole satisfy the 'best operations block' criteria (Figure 4.7).

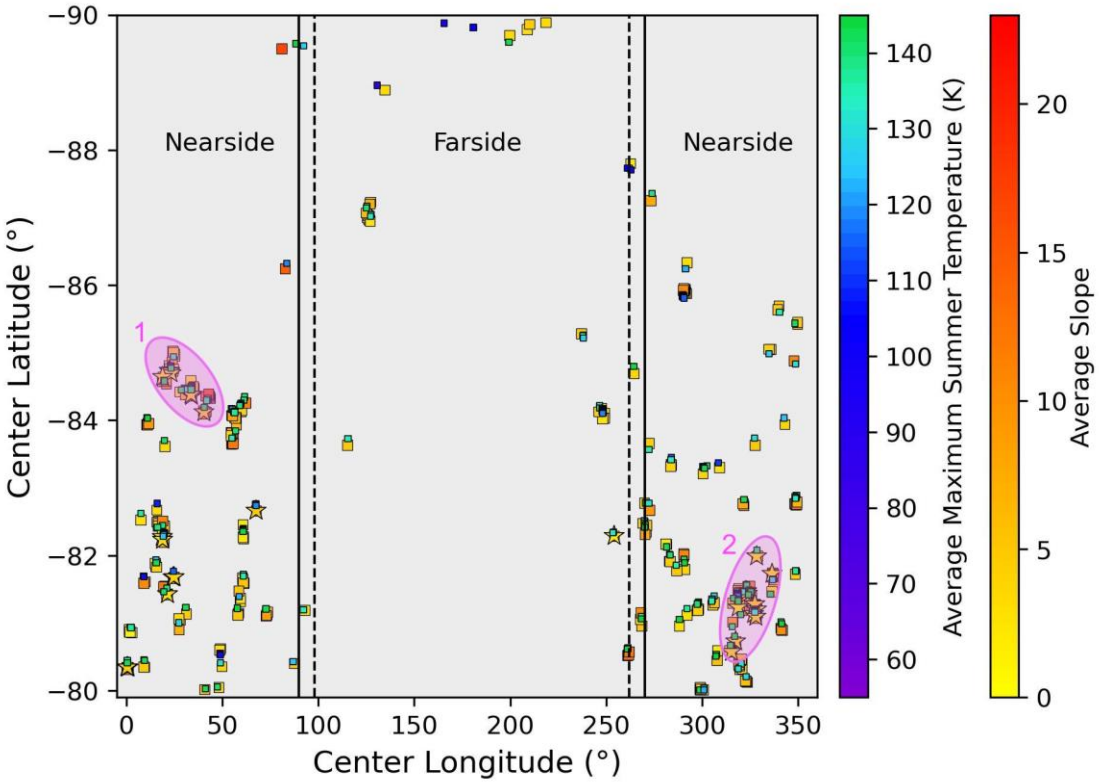

Figure 4.7 – Locations of suitable mining blocks (small squares) within 3km of an operations block (big squares). Suitable mining blocks are colored according to their average maximum temperature in the summer and operations blocks are colored according to their average slope. The "best operations blocks" (Figure 4.5) are labeled on the plot as gold stars. The pink ovals indicate two regions with high concentrations of mining blocks and best operations blocks within 3km of one another. The solid vertical lines divide the plot into the Lunar near side and far side, and the dashed vertical lines incorporate the additional 8º longitude visible to Earth because of libration.

A large majority of mining blocks within 3 km of an operations block are within close proximity to just one operations block. Such locations may not be suitable for industrial-scale water ice mining because the area for development is small. However, Figure 4.7 reveals two locations overlooked by Artemis III due to their distance from the

South Pole, with high concentrations of mining blocks and best operations blocks. Mining blocks at these locations should be considered for initial prospecting because if water ice exists in economic quantities, the numerous operations and mining blocks will enable the development of large-scale industrial mining operations. After a qualitative investigation of the two regions using the Lunar Mining Map Tool, we deemed Region 2 (Figure 4.8) most suitable for mining. The area contains large contiguous areas suitable for operations, along with numerous clusters of mining blocks. Thirty-one mining blocks and forty-six operations blocks are in close proximity, with 22% (n=10) classified as a "best operations block." The area with the highest concentration of mining blocks is associated with a PSR northwest of the crater Cabeus A. Seven operations blocks (one best operation block) are located within 3km of the mining block cluster, all of which could be used to establish operations bases to support mining activities within the PSR (Figure 4.8).

The scarcity of "best operations blocks" could trigger future land disputes. For example, the first mining companies with the necessary technological capabilities could grab the land with the best operations and mining conditions, similar to the pioneering investors mining the deep seabed (Zalik, 2018). Thus, spatial limitations should be imposed to regulate the amount of initial land actors can utilize so that future spacefaring nations can also participate in lunar water ice mining activities. We also recommend that area-based regulations be implemented to prohibit mining activities within operations blocks <3 km of a suitable mining block since the operations blocks are requisite to other sectors' operations, such as power generation, resource processing, and communications. Certain activities (e.g., excavation, launches) might also need to be prohibited in between

mining and operations blocks in close proximity, for such blocks will need to be reserved as corridors to deliver the extracted ice from the mining blocks to the operations base for processing. Without restrictions, activities within these blocks could also loft dust into the Moon's exosphere, which would complicate supplying power to mining assets and inhibit the use of optical communication systems between the mining assets and the operations base.

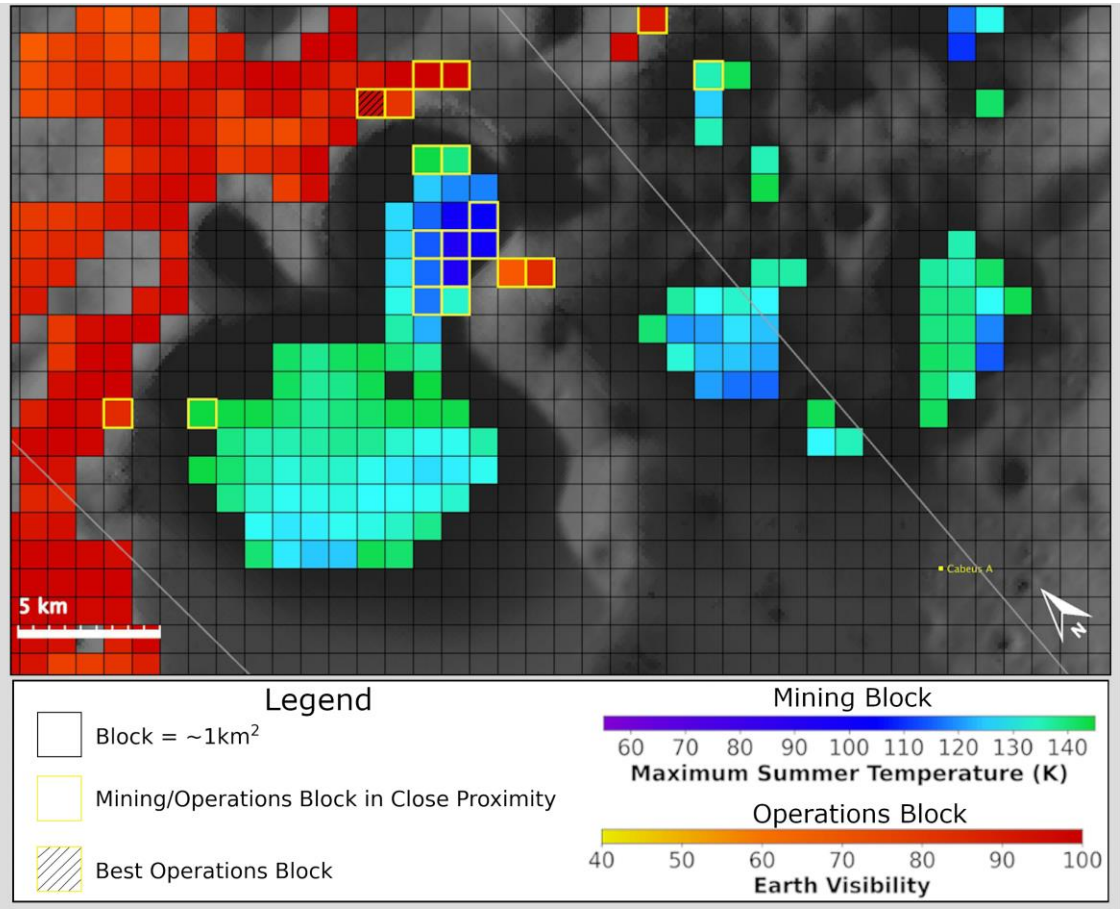

Figure 4.8 – Lower latitude region of the Lunar Mining Map Tool near crater Cabeus A that, based off the classification scheme, is suitable for establishing a large-scale industrial mining operation. The image is overlaid on an illumination base map (Mazarico et al., 2011) centered at 81.585°S, 318.643°E. Mining blocks are colored according to their average maximum temperature in the summer, while operations blocks are colored according to their Earth visibility as an average percent over an entire lunar precession cycle. Mining and operations blocks in close proximity are bordered in

yellow. The block most suitable for establishing a base for operations is indicated with black diagonal lines.

4.5 Discussion: The Mining Potential of Artemis III Candidate Landing Sites

A primary goal of Artemis III is to take the first steps toward establishing a sustained human presence on the Moon. Doing so will also enable addressing primary science objectives, including understanding planetary processes, interpreting the impact history of the Earth-Moon system, understanding the character and origin of lunar polar volatiles, untangling the record of the ancient sun and our astronautical environment, and conducting experimental science in the lunar environment (NASA, 2020). The missions will deploy precursor robotic payloads such as VIPER (Colaprete, 2021) to prospect for resources and characterize the navigability of local terrain. Additionally, a Lunar Terrain Vehicle will be delivered to transport astronauts around the selected landing site, followed by a habitable mobility platform to enable long-duration trips away from the Artemis Base Camp and a surface habitat to enable short-term stays to conduct more detailed exploration (NASA, 2020).

In August 2022, NASA announced thirteen candidate regions for the Artemis III lunar landing (NASA, 2022). The regions are located within six degrees of the lunar South Pole and were selected based on launch window availability, landing system capabilities, the terrain's slope, communications with Earth, and illumination conditions (NASA, 2022). Each region must also be near a permanently shadowed region where astronauts and rovers will collect samples of volatile-rich regolith to determine the form, composition, and lateral and vertical distribution of water ice (Kumari et al., 2022). Information gathered during the Artemis campaigns will also help determine whether a landing site is suitable for mining.

We used the Lunar Mining Map Tool to determine which Artemis III candidate regions are best suited for prospecting and establishing a water ice mine site large enough for commercial exploitation. Thus, while the Artemis missions are focused on the near-term, we attempted to determine whether one of these sites is most suitable for a longstanding industrialized-scale mine site. From the blocks defined in this work, 151 mining blocks and 579 suitable operations blocks lie within the boundary of an Artemis III candidate landing region (Figure 4.9). The two sites with the highest concentration of suitable mining blocks are Faustini Rim A and Nobile Rim 2 (Table 4.2). Faustini Rim A contains 69 mining blocks, with 48% (n=33) classified as Category I and 52% (n=36) as Category II. Nobile Rim A contains 39 mining blocks, with 64% (n=24) classified as Category I and 36% (n=15) as Category II.

Each identified block was subsequently divided into twenty-five 200 m x 200 m subblocks and classified according to the scheme described in Section 4.2. Summary statistics for the subblocks are listed in Tables 4.2 and 4.3. Subdividing the blocks identifies more precise locations within each block with suitable conditions for mining and establishing bases for operations while also eliminating unsuitable block areas resulting from averaging data within the larger primary blocks. Seventeen percent of the mining subblocks in Faustini Rim A either exhibited average maximum summer temperatures too high to retain water ice or terrain with slopes too steep to navigate. Sixty-three percent (n=1,088) of the remaining subblocks are classified as Category I and twenty percent (n=339) as Category II, amounting to about eighty-three percent of the original suitable mining block area and fourteen percent of the entire candidate region's square area. Sixty-one percent (n=591) of the mining subblocks in Nobile Rim 2 are

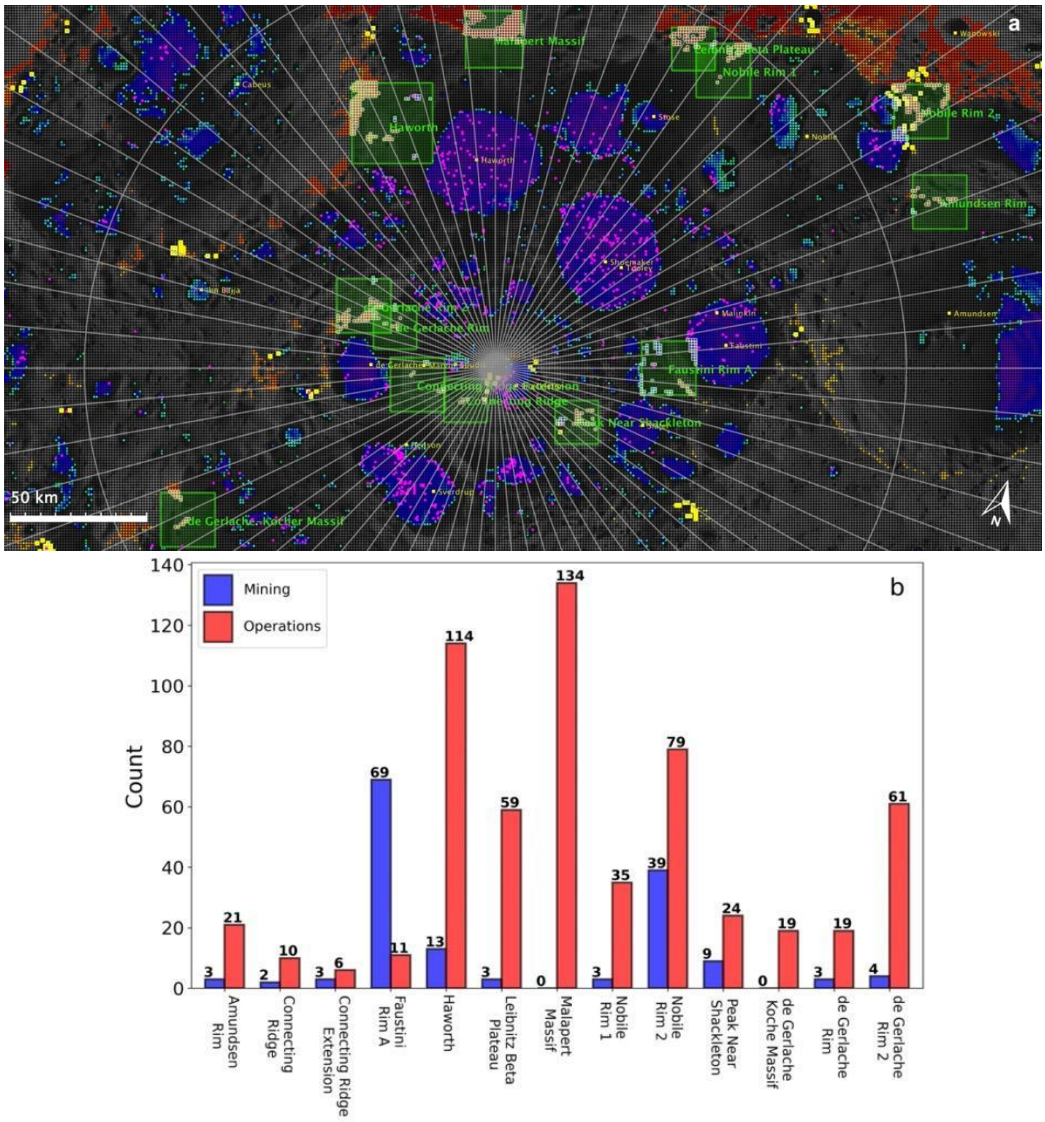

Figure 4.9 – (a) Utilizing the Lunar Mining Map Tool to assess the mining potential of Artemis III candidate landing regions. The map is centered at (-88.856°N, 17.072°E) The base map is a stereographic projection of the average percent illumination of the Lunar South Pole at a resolution of 512 pixels per degree. The illumination data was calculated by Mazarico et al. (2011) over four lunar node precession cycle simulations from 1970-2044. The candidate landing regions for the Artemis III mission are displayed using green boxes. Suitable mining blocks and blocks suitable for establishing bases for operations within the Artemis regions are bordered in white. Suitable mining blocks and operations blocks in close proximity are bordered in yellow. (b) Bar chart displaying the distribution of mining and operations blocks within the candidate landing regions.

classified as suitable for surface mining and thirty-one percent (n=298) for subsurface mining, which sums to about ninety-two percent of the original mining block area and nine percent of the entire candidate regions area.

Table 4.2 – Summary statistics of the suitable mining blocks within the Artemis III candidate landing regions.

ARTEMIS III Candidate Region for Landing	Area (km^2)	Mining Block Total within Area A	Mining Subblock Totals*		% of Region
	A	B	C	D	E=[0.04*(C+D)/A]*100
			Surface Mining (≤112K)	Subsurface Mining (112K-145K)	
Peak Near Shackleton	256.2	9	138 (61%)	44 (20%)	2.8
Faustini Rim A	400.1	69	1,088 (63%)	339 (20%)	14.3
Connecting Ridge	256.2	2	16 (32%)	16 (32%)	0.5
Connecting Ridge Extension	400.3	3	0	52 (69%)	0.5
Nobile Rim 1	399.1	3	45 (69%)	17 (26%)	0.6
Nobile Rim 2	398.1	39	591 (61%)	298 (31%)	8.9
Leibnitz Beta Plateau	255.4	3	55 (65%)	25 (29%)	1.3
Amundsen Rim	398.3	3	0	73 (97%)	0.7
Malapert Massif	440.3	0	0	0	0
Haworth	887.4	13	118 (36%)	139 (43%)	1.2
de Gerlache Rim	256.2	3	0	60 (80%)	0.9
de Gerlache Rim 2	400.2	4	0	75 (75%)	0.7
de Gerlache-Kocher Massif	399.3	0	0	0	0
**Subblocks with average slope angles too steep to navigate (≤23°) were excluded.*					

The remaining Artemis III candidate regions contain very few or no mining blocks (Table 4.2). This is expected given that the criteria used to identify the sites (e.g., access to sunlight, communication with Earth, mild temperature conditions, gentle slopes) were meant to accommodate a safe landing (NASA, 2022) and conflict with the criteria used to identify suitable mining blocks (low average maximum summer temperatures). While there are likely small areas suitable for prospecting in the other 11 candidate regions, the analysis focused on Faustini Rim A and Nobile Rim 2.

Table 4.3 – Summary statistics of the blocks suitable for establishing bases for operations within the Artemis III candidate landing regions

ARTEMIS III Candidate Region for Landing	Area (km^2)	Operations Block Total within Area A	Operations Subblock Totals				% of Region
	A	B	C	D	E	F	H=[(0.04*F)/A]*100
			≥40% Illumination	≥40% Earth visibility	Slope ≤23°	All criteria met	
Peak Near Shackleton	256.2	24	433 (72%)	534 (89%)	600 (100%)	420 (70%)	6.6
Faustini Rim A	400.1	11	208 (76%)	258 (94%)	275 (100%)	225 (82%)	2.2
Connecting Ridge*	256.2	10	107 (67%)	140 (87.5%)	157 (98%)	175 (70%)	2.7
Connecting Ridge Extension*	400.3	6	178 (74%)	226 (94%)	240 (100%)	102 (68%)	1.0
Nobile Rim 1*	399.1	35	691 (83%)	807 (97%)	836 (100%)	687 (79%)	6.9
Nobile Rim 2	398.1	79	1,721 (87%)	1,910 (97%)	1,975 (100%)	1,724 (87%)	17.3
Leibnitz Beta Plateau*	255.4	59	1,344 (89%)	1,493 (99%)	1,514 (100%)	1,361 (92%)	21.3
Amundsen Rim	398.3	21	382 (73%)	513 (98%)	525 (100%)	402 (77%)	4.0
Malapert Massif	440.3	134	3,132 (94%)	3,322 (99%)	3,200 (96%)	3,039 (91%)	27.6
Haworth	887.4	114	2,596 (91%)	2,782 (98%)	2,850 (100%)	2,629 (92%)	11.8
de Gerlache Rim*	256.2	19	338 (81%)	399 (96%)	415 (100%)	348 (73%)	5.4
de Gerlache Rim 2*	400.2	61	1,057 (84%)	1,233 (98%)	1,260 (100%)	1,089 (71%)	10.9
de Gerlache-Kocher Massif	399.3	19	387 (81%)	436 (92%)	475 (100%)	387 (81%)	3.9

**Contains overlapping area with another candidate landing region. Operations blocks within overlapping areas were considered in the analysis for each respective candidate region.*

4.5.1 Faustini Rim A

Faustini Rim A (Figure 4.10) includes pre-Nectarian basin terrain in the South and a pre-Nectarian crater unit, Faustini Crater, in the North (Fortezzo et al., 2020). We identified nine clusters of mining subblocks in the candidate region (Figure 4.10b). Eight are located in the cratered terrain south of Faustini Crater, and one (Cluster 1) is within Faustini Crater in the Northwestern portion of the site. Cluster 1 is the largest in the site

and is associated with the large concentration of mining blocks located on the floor of Faustini Crater.

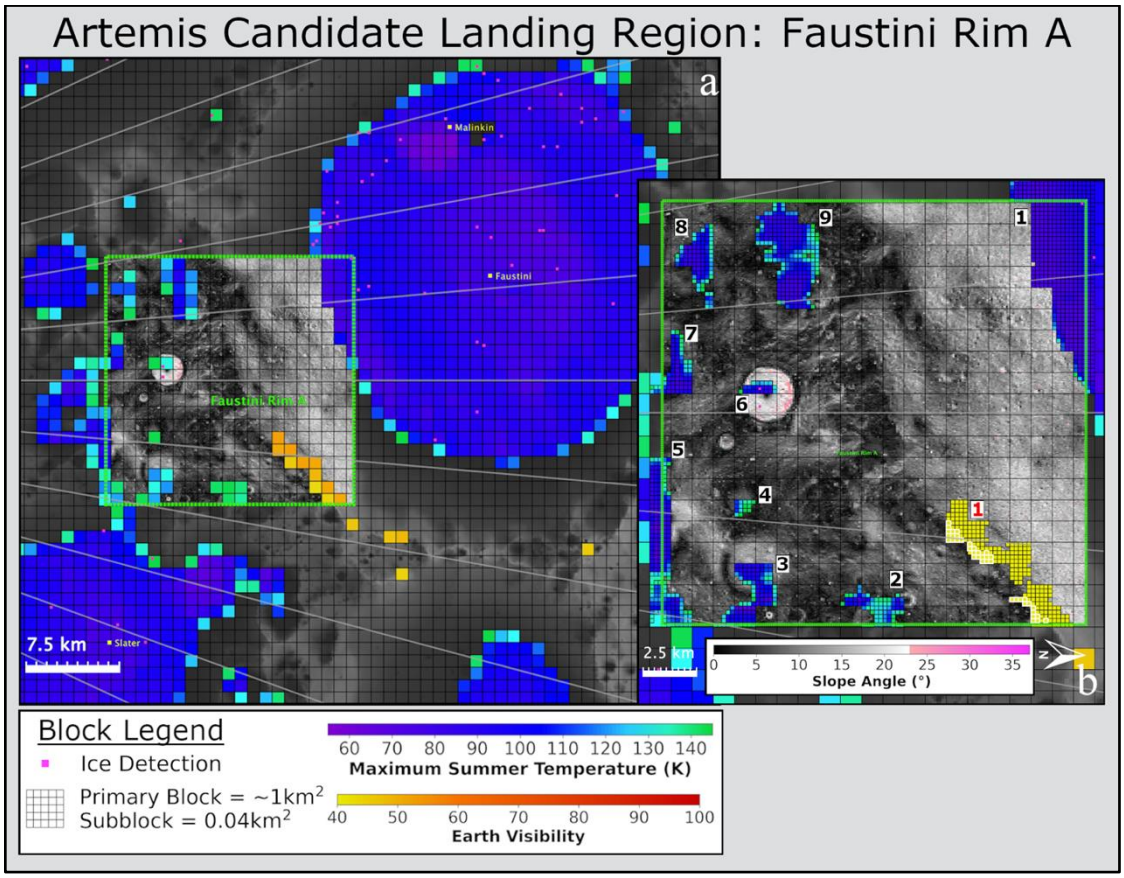

Figure 4.10 – (a) Regional view of the Faustini Rim A Artemis III candidate landing region, revealing the abundance of suitable mining blocks and the paucity of operations blocks outside the candidate region. The site is considered suitable for initial prospecting due to the number of mining clusters. The image is centered at -87.894°N, 91.249°E. The base map is a composite consisting of a global morphology mosaic (Speyerer et al., 2011) depicts the average percent illumination over four lunar precession cycles (Mazarico et al., 2011), which is overlaid by the Lunar Mining Map Tool. (b) Local view of the Faustini Rim A candidate region centered at -87.894°N, 91.249°E. The base layer is a slope map at 5 m/pixel from Barker et al. (2021). Black terrain is easy to navigate, white is difficult to navigate, and pink is too steep for navigation. Suitable mining blocks and subblocks are colored based on their average maximum summer temperature. Operations blocks and subblocks are colored according to their average percent Earth visibility. The best locations for establishing a base for operations are bordered in white, which exhibit an average percent illumination above the median and terrain with an average slope of ≤5º, which would limit the amount of site preparation required to construct an operations base. Each subblock is 200 m x 200 m in size. Subblocks are divided into contiguous clusters, with mining clusters numbered in black and operations clusters in red.

Nearly all the mining subblocks are in permanent shadow and are classified as Category I, suggesting that water ice can be present at the surfaces within these blocks. Unless technological advancement permits rovers and humans to operate in PSRs for extended periods, it is unlikely Cluster 1 will be the initial target for prospecting. Moreover, pathways from a landing site outside Faustini Crater to its crater floor would require traversing terrain with steep slope angles, complicating accessibility. Most of the subblocks in Cluster 1 are located on the crater's wall, which also exhibits steep slopes that complicate deploying prospecting and mining instruments. Additionally, the mining subblocks are far from the only cluster of operations subblocks (Figure 4.10b), adding additional complexity to supplying power, warming critical systems, and protecting the instrument from low temperatures in periods of extended shadow.

The remaining eight mining clusters are located on heavily-cratered highlands terrain comprised of erosionally-degraded impact-related structures and ejecta material (Fortezzo et al., 2020). Identified craters >1 km in diameter are at different stages of degradation and exhibit a range of diameters, depths, and rim wall slope angles. Prospecting in mining subblocks containing a diversity of craters will enable obtaining the necessary information for future mining activities such as the geotechnical characteristics and accessibility of cold traps, the composition, form, and vertical extent of polar volatiles, the relationships between crater age and the spatial and vertical distribution of water ice (Deutsch et al., 2020), and the role of impact gardening on the removal, preservation, and redistribution of volatiles (Hurley et al., 2012; Crider & Vondrak, 2003).

If technological capabilities enable water ice to be transported from great distances, large concentrations of suitable mining blocks occur outside the candidate region within Faustini Crater to the north and Slater Crater to the east. The mining blocks are dispersed in numerous unnamed PSRs to the south (Figure 4.10a). Surface-exposed water ice detections using near-infrared reflectance data acquired by the Moon Mineralogy Mapper instrument on the Chandrayaan-1 spacecraft (Li et al., 2018) are also found in several mining blocks in craters Faustini and Slater just outside the region.

The main limitation of Faustini Rim A is the small number of operations subblocks and their distances from suitable mining subblocks. While ~36% of the operations subblocks exhibit average illumination values above the median value of all the operations blocks in the Lunar Mining Map Tool (Figure 4.2b), they are all constrained to the northeastern portion of the site and are >3km from the nearest mining cluster. Additionally, their Earth visibility conditions over the course of a precession cycle are below the median of the entire distribution of operations blocks. This suggests that while these blocks are the best locations in Faustini Rim A for establishing a base for operations, the site is less optimal than other Artemis sites for establishing a mine site requiring large areas to construct solar farms and ground-based communications stations with Earth. Nonetheless, we highlight the best locations in Faustini Rim A for establishing bases for operations (n=39), which are bordered in white in Figure 4.10b. The best locations were defined as the subblocks exhibiting an average percent illumination above the median (~43%) and terrain flat enough (average slope angle of ≤5°) to limit the need for significant site preparation.

Using the Lunar Reconnaissance Orbiter Camera Quickmap software, we identified a nominal traverse in Faustini Rim A to prospect for water ice. The terrain exhibits slope angles of ≤15º to accommodate both human (NASA, 2021) and robotic (Keane et al., 2022) exploration and was limited to a maximum distance of 13.25 km based on the notional traverse distance of VIPER (Colaprete, 2021). The traverse begins with a southeastward descent from Operations Cluster 1 to Mining Cluster 2, where the rover would survey eight Category I mining subblocks and fourteen Category II mining subblocks to estimate the form, composition, and abundance of volatiles. The traverse could look similar to the example shown by Coto et al. (2021, Fig. 14). The traverse path mainly comprises slopes of ≤10º throughout the distance traveled, though some locations reach ~15º when the pathway intersects a crater. Because mining blocks exhibit low Earth visibility, the traverse returns to Operations Cluster 1 to transmit data to Earth, preventing prospecting in other clusters. Due to limited lighting conditions, the rover would need to be powered and warmed by a radioisotope thermoelectric generator and rechargeable batteries to survive mining conditions.

If an appreciable amount of water ice was detected during the limited traverse, a follow-up exploration campaign using a rover with long-range capabilities such as Endurance or INSPIRE (Keane et al., 2022) could be implemented to survey all eight mining clusters outside of Faustini Crater. This would enable complete coverage of all mining blocks in the candidate region, enabling a more robust assessment of volatiles in mining block areas in and around Faustini Rim A, which is necessary before establishing a mine site.

4.5.2 Nobile Rim 2

The Nobile Rim 2 candidate landing region is strategically positioned near the rim of Nobile Crater to include appropriate environmental conditions for landing (i.e., the central portion of the site) while also remaining near a PSR to explore for water ice (i.e., the south/southeastern portion of the site). The region surrounding the Nobile Rim 2 site contains numerous operations blocks to its west and a concentration of suitable mining blocks associated with Nobile Crater to the south and southeast (Figure 4.11a). The site is centered on pre-Nectarian crater terrain, with the most eastern area of the site located on a Nectarian crater unit with subdued terrain and material from a primary impact event (Fortezzo et al., 2020). The south and southeastern parts of the site contain a portion of Nobile Crater's discontinuous, subdued rim, rim crest remnants, and the rim and wall of an overlapping lesser crater. Additionally, the southern portion of the site contains two patches of permanently shadowed areas where ice has been detected (Li et al., 2018).

A total of 121 operations subblocks in the site are classified as best areas for constructing an operations base (Figure 4.11b). Twelve of these "best operations blocks" are located in Operations Clusters 2 and 3 on the rim of Nobile Crater, while the rest are found in Operations Cluster 5 in the northwestern area of the site. Nobile Rim 2 contains four clusters of mining subblocks (Figure 4.11b). Mining Cluster 10 is located to the east of a lesser crater overlying the rim of Nobile Crater rim in the southeastern portion of the site. The cluster is associated with a more significant concentration of mining blocks within Nobile Crater and contains slopes navigable by humans and rovers. Blocks on the northern exterior of Cluster 10 exhibit subsurface mining conditions, while the interior blocks exhibit temperatures suitable for surface mining. Blocks located in the most

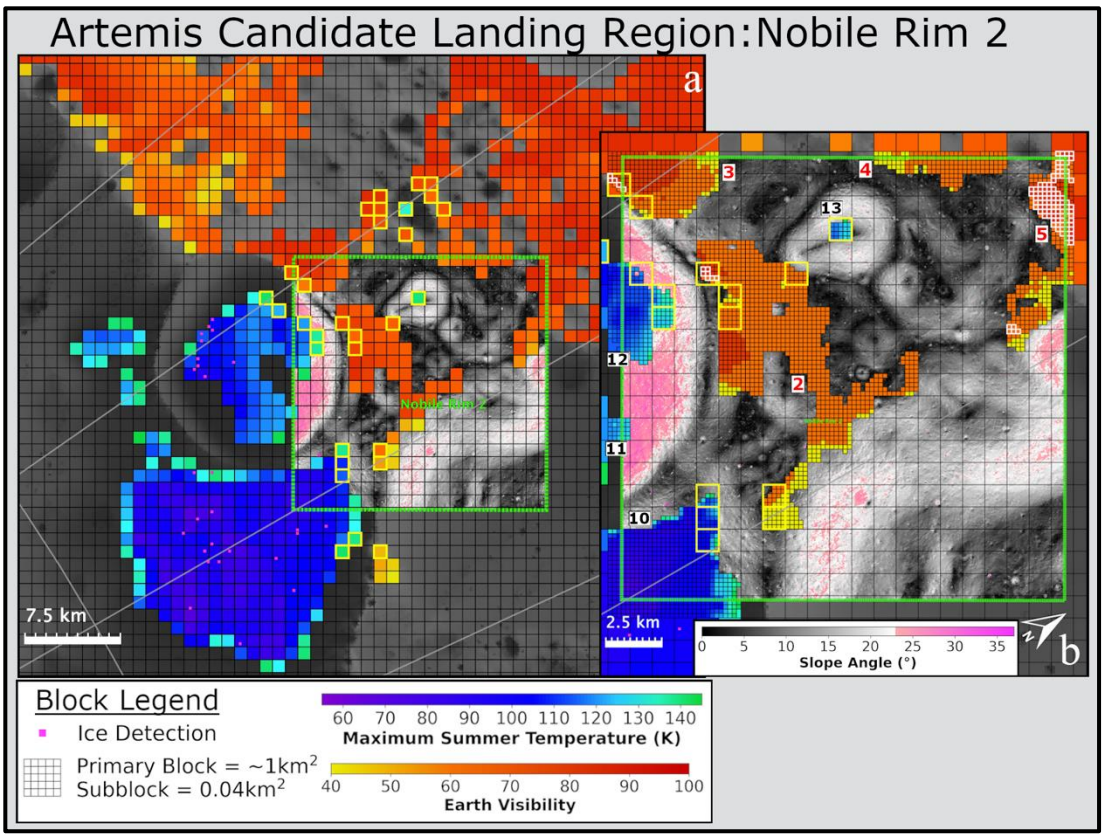

Figure 4.11 – (a) Regional view of the Nobile Rim 2 candidate landing region. Numerous suitable operations blocks are located in the northern and western portions of the region. The closest concentration of suitable mining blocks are found just south of the Nobile Rim 2 site. The image is centered at -84.061°N, 57.697°E. The base map is a composite consisting of a global morphology mosaic (Speyerer et al., 2011) depicts the average percent illumination over four lunar precession cycles (Mazarico et al., 2011), which is overlaid by the Lunar Mining Map Tool. (b) Local view of the Nobile Rim 2 candidate region centered at -83.973°N, 59.135°E. The base layer is a slope map at 5 m/pixel from Barker et al. (2021). Black terrain is easy to navigate, white is difficult to navigate, and pink is too steep for navigation. Suitable mining blocks and subblocks are colored based on their average maximum summer temperature. Operations blocks and subblocks are colored according to their average percent Earth visibility over four lunar precession cycles. Operations and mining blocks in close proximity (<3 km) are bordered in yellow. The best locations for establishing a base for operations are bordered in white, which exhibit an average percent illumination and Earth visibility over four procession cycles above the median and terrain with an average slope of ≤5º, which would limit the amount of site preparation required to construct an operations base. Each subblock is 200 m x 200 m in size. Subblocks are divided into contiguous clusters, with mining clusters numbered in black and operations clusters in red.

eastern portion of Operations Cluster 2 are best for establishing a base for operations to support a mine site in Mining Cluster 10 due to their close proximity. However, none of these blocks are considered the best in the region as a result of their suboptimal Earth visibility values (all blocks fall below the median).

Mining Clusters 11 and 12 are located inside the lesser crater overlying the rim of Nobile Crater in the southern portion of the site. However, these clusters are inaccessible for prospecting due to the crater wall's steep slopes. Cluster 13 is a small cluster of subsurface mining blocks located in a bowl-shaped crater to the north of the rim of Nobile Crater. We identified a prospecting traverse for an Endurance or Inspire-like rover ($\leq 20^{o}$) that is less than the traverse distance of VIPER (~13.14km; Colaprete, 2021) from the best operations blocks in Operations Cluster 2 into Mining Cluster 13. The traverse path navigates within Operations Cluster 2 until it reaches the crater containing Mining Cluster 13. Once in the crater, the traverse would enable a rover to characterize six mining subblocks for water ice.

Due to its size, navigable terrain, proximity to operations subblocks, and its relation to a larger concentration of mining blocks, Cluster 10 is considered the best location for mining in the Nobile Rim 2 candidate region. Therefore, we recommend a prospecting campaign that surveys Cluster 10 for water ice and other volatiles. The results from Cluster 10 could be used to develop a geological model to extrapolate how much volatiles are present within the larger concentration of mining blocks in Nobile Crater. If prospecting reveals that blocks in Cluster 10 contain water ice, a mine site could then be established, where water ice enriched regolith would be excavated (Just et al., 2020) and transported to nearby operations subblocks such as those in Cluster 2. We

believe that water ice mining should refrain from beneficiation in-situ to avoid dumping the waste stream and contaminating the PSR, which might impede future mining activities. After being hauled to Cluster 2, the feedstock would undergo a series of beneficiation steps (Rasera et al., 2020; Trigwell et al., 2013; Shaw et al., 2021) to create a volatile-rich concentrate. The concentrate would then be processed by thermally treating the regolith to volatilize the ices. The multi-component gas can then be separated using a cold trap/cold finger. After purification, the water can finally be split to produce LOH and LOX for rocket propellant. Rather than disposing of the regolith fragments, the "tailings" could used as a feedstock for sintering or to produce oxygen and metals. Moreover, the byproduct volatiles separated during the purification step can be stored, for they will have many use cases on the lunar surface. While the best operations blocks in the Nobile Rim 2 site for processing are located >3 km from Cluster 10, we identified multiple navigable traverses from the beneficiation station to the processing plant within Operations Cluster 2, which exhibits suitable Earth visibility, illumination, and navigable terrain.

4.5.3 Malapert Massif

The "Malapert Massif" candidate region (Figure 4.12a) was delineated as an Artemis III candidate region for landing because Mons Malapert (Malapert Mountain), a mountain within the massif, has long been considered for a lander/outpost site and to establish a permanent lunar base (Busey et al., 1999; Sharpe & Schrunk, 2003). The ~30 x 50 km mountain is located at 86° south latitude and 0° longitude, with its summit standing ~5 km above the 1,838 km datum (Basilevsky et al., 2019). Because of the high elevation of the summit region of Malapert Mountain, the entire disk of the Earth is

always above the horizon at the summit, permitting Earth-facing locations with continuous line-of-sight communications (Sharpe & Schrunk, 2003). Additionally, locations near and at the summit experience long periods of continuous illumination (Krujiff, 2000). For example, Bussey et al. (1999, 2010) identified areas on Malapert Mountain that are illuminated for >70% of the year and seasonal illumination conditions as high as 95%. Thus, locations in the Malapert Massif site with slopes permissible for installing space infrastructure and navigable by rovers and humans are also most suitable for solar-electric power generation (Lowman et al., 2008). However, the mountain has local slopes ranging from 20–30°, making climbing difficult for current technologies.

The northern portion of the Malapert Massif candidate region contains a pre-Nectarian Basin Massif unit interpreted as uplifted bedrock during the formation of the South-Pole Aitken Basin (Basilevsky et al., 2019), while the Southern portion is a pre-Nectarian Basin unit interpreted as erosionally degraded impact-related structures and ejecta materials (Fortezzo et al., 2020). The morphology of the summit area has been analyzed previously and contains numerous craters from meters to hundreds of meters in diameter and a paucity of rock boulders (Basilevsky et al., 2019).

The percentage of the candidate region's square area classified as suitable for operations is the highest of all the Artemis III candidate regions (Table 4.3). Additionally, it contains the highest number of operations subblocks (n=3,039), with 95% (n=2,889) exhibiting an average percent Earth visibility over the course of a precession cycle above the median and ~62% (n=1,890) with average percent illumination above the median. Approximately 43% of the subblocks are difficult for rovers to navigate (average slope between 15º-23º), 57% are navigable by humans and rovers (≤15º), and ~12% exhibit

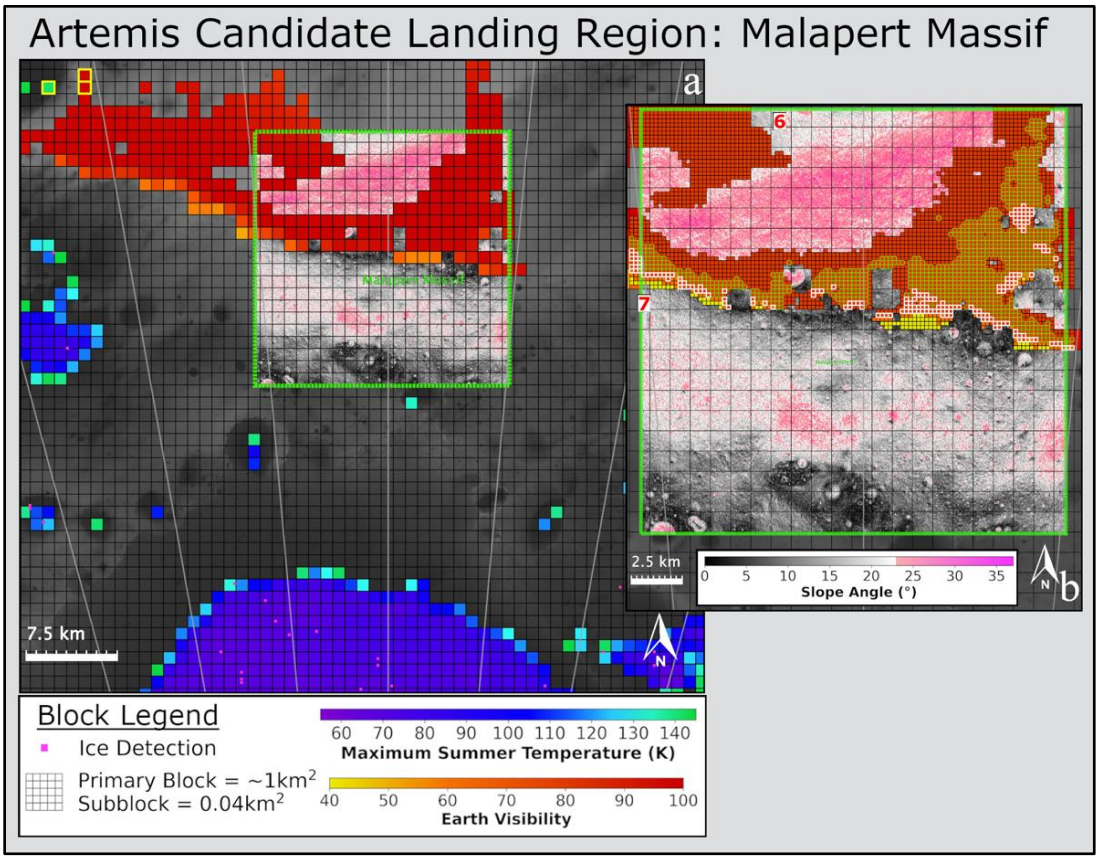

Figure 4.12 – (a) Regional view of the Malapert Massif candidate landing region centered at -86.314°N, 358.878°E. The base map is a composite consisting of a global morphology mosaic (Speyerer et al., 2011) depicts the average percent illumination over four lunar precession cycles (Mazarico et al., 2011), which is overlaid by the Lunar Mining Map Tool.. Numerous operations blocks are located within and outside the site to the northwest. The closest concentrations of mining blocks are found in Haworth crater to the south. Suitable mining blocks are colored based on their average maximum summer temperature, and operations blocks are colored according to their average Earth visibility. Operations blocks and suitable mining blocks in close proximity are bordered in yellow. (b) Local view of the Malapert Massif candidate region centered at -86.236°N, 0.148°E. The base layer is a slope map at 5 m/pixel from Barker et al. (2021), colored according to its average slope. Black terrain is easy to navigate, white is difficult to navigate, and pink is too steep for navigation. The candidate landing region does not contain a suitable mining block, suggesting that the site may not be suitable for prospecting and establishing a long-term mine site. Suitable mining blocks are colored based on their average maximum summer temperature. Operations blocks and subblocks are colored according to their average percent Earth visibility over four lunar precession cycles. The best locations for constructing an operations base are bordered in white, which exhibit an average percent illumination and Earth visibility over the course of four precession cycles above the median and terrain with an average slope of ≤5º, which would limit the amount of site preparation required to construct a base for operations. Each subblock is 200 m x 200 m in size. The operations clusters are numbered in red. Subblocks bordered green could be used as a highway between the best operations subblocks.

terrain flat enough to establish a base with little site preparation (≤5º). About 6% (n=175) of the operations subblocks meet the "best operations block" criteria described above and are generally located in the center of the candidate region in Operations Cluster 7 (Figure 4.12b). It is at these locations where we believe operations stations should be established.

A lunar operations base will likely include a communications station, photovoltaic arrays, a regenerable fuel cell power plant, pressurized habitat, a landing pad, mineral and chemical processing plants, and a propellant refueling depot (Sherwood, 2018). To construct these elements in the "best operations blocks" at Malapart Massif using local materials, the feedstock should be sourced from within the site due to the steep slopes of the mountain, increasing the dependency of the site on supplies delivered by rockets from Earth. While navigable routes identified by Basilevsky et al. (2019) from the summit to the base of the mountain could be used to conduct scientific operations and access mining blocks to extract water ice, the closest cluster of mining blocks to an operation block within the site is >15 km away, and the traverse would likely be much longer to avoid steep slopes. Moreover, the volatile enriched regolith would have first to be hauled to a beneficiation plant at the base of the mountain to reduce the gangue mass. The treated concentrate would then have to be transported from the mine site to the Malapert operations base over steep and undulating terrain, which is less economical relative to other locations such as Nobile Rim 2.

While Malapert Massif is likely not the most suitable Artemis III candidate region for prospecting and establishing a water ice mine site, it could be used to construct concentrating solar thermal and photovoltaic power plants to generate and deliver power

to mining blocks with less optimal illumination conditions. On Earth, concentrated solar thermal energy is a relatively new technology for electricity production and heating (Pfhal et al., 2017). Moving mirrors called heliostats (Stoica et al., 2014) reflect the sun's energy to a receiver (e.g., "solar tower plant"), which absorbs the radiation and supplies thermal energy via a fluid (e.g., molten salt), which can also act as a heat storage medium to supply thermal energy on demand (Pfhal et al., 2017). At the Malapert site, heliostats could be equipped on tall towers, such as the Deployable Interlocking Actuated Band for Linear Operations (DIABLO; Honeybee Robotics, 2022) and the Multifunctional Expandable Lunar Lightweight, Tall Tower (MELTT; Amy et al., 2020), to reflect sunlight to a solar tower plant stationed near a mining block, where it can deliver electrical power to mining equipment or store as thermal energy for use in periods of darkness. While molten salts are used to store energy reflected by the Heliostats, regolith is being considered to store energy on the Moon (Colozza, 1991; Lu et al., 2016).

A power station on Malapert Massif could also be used to concentrate, convert, and direct power to other locations on the Moon via a method known as power beaming. Power beaming is the point-to-point transfer of electrical (i.e., optical, millimeter wave, and microwave) energy across free space by a directed electromagnetic beam (i.e., laser) to a photovoltaics receiver where it is difficult to generate (Rodenbeck et al., 2021). The technique is advantageous for the Moon since electromagnetic energy will not have to travel through any atmosphere. While optical and millimeter wave beams are best suited to deliver power to small sites and mobile platforms, microwave beams excel for high-power, long-distance applications (Rodenbeck et al., 2021). Assets and infrastructure close to the power station would require optical or millimeter wave receivers, while those

far from the site would require microwave receivers (Rodenbeck et al., 2021). Via power beaming, the towers could also be used to power mining assets equipped with solar arrays operating in permanent shadow, to other systems stationed in operations blocks with suboptimal illumination conditions, or redirect solar energy directly on the surface of a mining block with surficial water ice to be collected by mining assets equipped with a capture tent and cold trap (Sowers & Dreyer, 2019).

Thirty-eight percent of the operations subblocks in the Malapert Massif candidate with average percent illumination and Earth visibility above the median are navigable by rovers. Using the Lunar Mining Map Tool, we delineate a nearly continuous traverse path using these subblocks to connect all of the best operations subblocks in Operations Cluster 7 to one another (Figure 4.12b). Humans and rovers would use the subblocks as a highway to access operations systems (i.e., solar farms, power storage stations, heliostats, communications stations, landing pads, habitats, etc.) located across the Malapert site. To mitigate traffic from suspending dust, pathways would be developed by sintering or melting regolith in situ (Taylor and Meek, 2005; Fateri et al., 2013; Imhof et al., 2017; Farries et al., 2021).

While the Malapert Massif site is suitable for establishing a base for operations, it is limited by its distance from mining blocks for in situ resource utilization and inaccessibility to other parts of the lunar surface, deemed essential for scientific and operational activities. The region's closest concentrations of mining blocks are located in Haworth Crater to the south and an unnamed area to the east associated with three large permanently shadowed areas. However, both are far from the candidate region relative to other Artemis III sites. Furthermore, there are no mining blocks within the site since the

temperatures are too warm to trap water ice and the few isolated mining blocks close to the site are difficult to access by humans and rovers due to steep terrain.

4.5 Concluding Remarks

We developed a Lunar Mining Map Tool that identifies the locations suitable for water ice mining and for establishing bases for operations. The tool divides the Lunar South Pole from 80°S-90°S latitude into a grid of 288,142 blocks ~1km^2 in area and classifies each block according to its average percent Earth visibility and illumination over the course of four lunar precession cycles, average slope, and maximum summer temperature.

The tool identifies 19,699 blocks suitable for mining and 22,173 blocks suitable for establishing bases for operations, demonstrating that ~15% of the Lunar South Pole is suitable for mining or for other activities that would be required to support a mine site. About 59% of the identified mining blocks exhibit average maximum summer temperatures suitable for water ice to be stable at the surface, while 41% exhibit average maximum summer temperatures low enough for water ice to be stable within the upper meter of the surface, demonstrating that a combination of surface and subsurface technologies will need to be deployed for future mine sites. About 99% of the blocks with suitable temperature conditions to retain volatiles exhibit terrain navigable by rovers (≤23º), and ~88% are navigable by humans (≤15º).

Most operations blocks (~94%) are located between -80ºN and -86ºN latitude and 290ºE and 50ºE longitude, while the best locations for mining are less dependent on geographic location, and more dependent on surface morphology (i.e., the floors of impact craters). To determine the blocks with the best operations conditions, we

identified the blocks with an average percent illumination and Earth visibility above the median values that exhibit terrain flat enough to limit the need for significant site preparation activities. The best blocks are all located between -80ºN and -86ºN latitude, and all but one are located on the lunar near side. While prospecting can be conducted using robotic assets powered by radioisotope thermoelectric generators, mine sites will likely require solar power. Thus, the proximity of an operations station to a mine site is paramount for sustainable operations. In total, only 29 of the best operations blocks are located within 3 km of a mining block. The scarcity of such blocks could lead to disputes.

The scarcity of suitable operations blocks within close proximity to mining blocks also demonstrates that site preparation equipment, innovative power supply and delivery systems, and orbital communications will likely be required to make more blocks functional to support a mine site. This will be necessary to create more operable locations at the Lunar South Pole as the number of actors increases. Doing so may reduce the onset of disputes that could arise if prime operations locations are limited.

The Lunar Mining Map Tool was also used to assess the mining potential of the Artemis III candidate landing regions. Faustini Rim A was determined suitable for prospecting, but the operations blocks were far from seven of the eight mining block clusters. Moreover, the operations blocks are less optimal for establishing communication stations than other candidate regions such as Malapert Massif. Due to its optimal operations blocks, the high number of mining blocks, and access to a larger concentration of suitable mining blocks in Nobile Crater, Nobile Rim 2 is considered the most suitable Artemis III candidate region for establishing a mine. Malapert Massif is the best site for establishing a base for operations, particularly for generating power. However, the site

did not contain any mining blocks, and the surrounding region has only a limited number of mining blocks, which are inaccessible due to the steep slopes of Malapert.

The utility of the Lunar Mining Map Tool will only increase as we obtain more information about the Lunar South Pole. For example, as more robust orbital remote sensing and initial prospecting data are collected, the map can estimate the number of mining blocks required for companies to sustain a mining operation and the number of operations blocks needed to establish a mine site. Additionally, the Lunar Mining Map grid can support the coordination and monitoring of mining activities, the development of mining regulations, and the implementation and enforcement of mining contracts and environmental policies, which we will showcase in future work.

References

Amy, C., Bégin, M.-A., Browder, B., Chan, M., Dawson, C., do Vale Pereira, P., Hank, T.J., Hinterman, E., Lordos, G., Martell, B., Miller, A., O'Neill, C., Padia, V.J., Stamler, N., Todd, J., Wang, N., Newman, D.J., de Weck, O.L., & Hoffman, J.A. (2020). Autonomously Deployable Tower Infrastructure for Exploration and Communication in Lunar Permanently Shadowed Regions. *ASCEND 2020*, p.4019.

Anand, M. (2010). Lunar water: A brief review. *Earth, Moon, and Planets,* 107, 65–73.

Arnold, J.R. (1979). Ice in the lunar polar regions. *Journal of Geophysical Research*, 84(B10), 5659-5668.

Azur Solar Power GmbH. (2020). SPACE Solar Cells. https://www.azurspace.com/index.php/en/products/products-space/space-solar-cells [Accessed January 28, 2023].

Barker, M.K., Mazarico, E., Neumann, G.A., Smith, D.E., Zuber, M.T., & Head, J.W. (2021). Improved LOLA Elevation Maps for South Pole Landing Sites: Error Estimates and Their Impact on Illumination Conditions. *Planetary & Space Science*, 203(1)105119, 1-16.

Basilevsky, A., Krasilnikov, S.S., Ivanov, M.A., Malenkov, M.I., Michael, G.G., Liu, T., Head, J.W., Scott, D.R., & Lark, L. (2019). *Solar System Research,* 53(5), 383–398.

Bernold, L. (1991). Experimental studies on mechanics of lunar excavation. *Journal of Aerospace Engineering*, 4(1), 9–22. ASCE, NY.

Binder, A.B. (1998). Lunar Prospector: A Review. *Science*, 281(5382), 1475-1476.

Bockelée-Morvan, D., & Biver, N. (2017). The composition of cometary ices. *Phil. Trans. R. Soc. A,* 375(2016252), 1-11.

Boles, W., & Connolly, J. (1996). Lunar Excavating Research. *Proceedings of SPACE 96* (Pp. 699–705).

Bryant, S. (2009). Lunar Pole Illumination and Communications Maps Computed from GSSR Elevation Data. *IEEEAC*, Big Sky, MT, USA. Pp. 1-19.

Bussey, D.B.J., Lucey, P.G., Robinson, M.S., Steutel, D., Robinson, M.S., Spudis, P.D., & Edwards, K.D. (2003). Permanent Shadow in simple craters near the poles. *Geophysical Research Letters,* 30(6), 1–4.

Bussey, D.B.J., McGovern, J.A., Spudis, P.D., Neish, C.D., Noda, H., Ishihara, Y., & Sørensen, S.-A. (2010). Illumination conditions of the south pole of the Moon derived using Kaguya topography. *Icarus,* 208, 558–564.

Bussey, D.B.J., Spudis, P.D., & Robinson, M.S. (1999). Illumination conditions at the lunar south pole. *Geophysical Research Letters,* 26, 1187–1190.

Cain, J.R. (2010). Lunar dust: The Hazard and Astronaut Exposure Risks. *Earth, Moon, and Planets,* 107, 107–125.

Chin, G., Brylow, S., Foote, M., Garvin, J., Kasper, J.., Keller, J., Litvak, M., Mitrofanov, I., Paige, D., Raney, K., Robinson, M., Sanin, A., Smith, D., Spence, H., Spudis, P., Stern, S.A., & Zuber, M. (2007). Lunar Reconnaissance Orbiter Overview: The Instrument Suite and Mission. *Space Science Reviews,* 129, 319–419.

Cilliers, J.J., Rasera, J.N., & Hadler, K. (2020). Estimating the scale of Space Resource Utilisation (SRU) operations satisfy lunar oxygen demand. *Planetary and Space Science,* 180(104749), 1-8.

Colaprete, A. (2021). Volatiles Investigating Polar Exploration Rover (VIPER). NASA. https://ntrs.nasa.gov/api/citations/20210015009/downloads/20210015009%20-%20Colaprete-VIPER%20PIP%20final.pdf.

Colaprete, A., Schultz, P., Heldmann, J., Wooden, D., Shirley, M., Ennico, K., Hermalyn, B., Marshall, W., Ricco, A., Elphic, R.C., Goldstein, D., Summy, D., Bart, G.D., Asphaug, E., Korycansky, D., Landis, D., & Sollitt, L. (2010). Detection of water in the LCROSS ejecta plume. *Science*, 330(6003), 463.

Colozza, A.J. (1990). Analysis of Lunar Regolith Thermal Energy Storage. NASA/CR 189073. (Pp. 1-9).

Colozza, A.J. (2020). Small Lunar Base Camp and In Situ Resource Utilization Oxygen Production Facility Power System Comparison; NASA/CR 2020-2200368. (pp. 98). Available Online. https://ntrs.nasa.gov/api/citations/20200001622/downloads/20200001622.pdf [accessed January 28, 2023].

Connolly, J., & Shoots, D. (1994). Transferring Construction Technology to the Moon and Back. *Proceedings of SPACE 94.* ASCE, NY. Pp. 1086–1096.

Costes, N.C., Farmer, J.E., & George, E.B. (1972). Mobility Performance of the Lunar Roving Vehicle: Terrestrial Studies – Apollo 15 Results. NASA TR R-401. (Pp.86).

Coto, M.E., Pazar, C.C., McKeown, B., & Shanley, C. (2021). Lunar Regolith Sample Excavation Company: A Space Resource Business Plan. *ASCEND 2021*, (Pp. 45).

Crider, D.H., & Vondrak, R.R. (2003). Space weathering effects on lunar cold trap deposits. *Journal of Geophysical Research.* 108(E7), 1-11.

Deutsch, A.N., Head, J.W., & Neumann, G.A. (2020). Analyzing the ages of south polar craters on the Moon: Implications for the sources and evolution of surface water ice. *Icarus,* 336(15), 1-10.

De Rosa, D., Bussey, B., Cahill, J.T., Lutz, T., Crawford, I.A., Hackwill, T., van Gasselt, S., Neukum, G., Witte, L., McGovern, A., Grindrod, P.M., & Carpenter, J.D. (2012). Characterisation of potential landing sites for the European Space Agency's Lunar Lander project. *Planetary and Space Sciences,* 74(1), 224–246.

Farries, K., Visintin, P., Smith, S.T., & van Eyk, P. (2021). Sintered or melted regolith for lunar construction: state-of-the-art review and future research directions. *Construction and Building Materials,* 296, 1–31.

Fateri, M., Meurisse, A., Sperl, M., Urbina, D., Madakashira, H.K., Govindaraj, S., Gancet, J., Imhof, B., Hoheneder, W., Waclavicek, R., Preisinger, C., Podreka, E., Mohamed, M.P., & Weiss, P. (2019). *Journal of Aerospace Engineering,* 32(6), 04019101.

Feldman, W.C., Maurice, S., Binder, A.B., Barraclough, B.L., Elphic, R.C., & Lawrence, D.J. (1998). Fluxes of fast and Epithermal Neutrons from Lunar Prospector: Evidence for Water Ice at the Lunar Poles. *Science*, 281(5382), 1496-1500.

Fincannon, J. (2008). Lunar Polar Illumination for Power Analysis. *In: 6th International Energy Conversion Engineering Conference (IECEC), July 28-30, 2006,* p. 5631.

Fisher, E.A., Lucey, P.G., Lemelin, M., Greenhagen, B.T., Siegler, M.A., Mazarico, E., Aharonson, O., Williams, J.-P., Hayne, P.O., Neumann, G.A., Paige, D.A., Smith, D.E., & Zuber, M.T. (2017). Evidence for surface water ice in the lunar polar regions using reflectance measurements from the Lunar Orbiter Laser Altimeter and temperature measurements from the Diviner Lunar Radiometer Experiment. *Icarus,* 292, 74–85.

Fortezzo, C.M., Spudis, P.D., & Harrel, S.L. (2020). Release of the Digitial Unified Global Geologic Map of the Moon at 1:5,000,000-scale. *Lunar and Planetary Science Conference 2020. No. 2326.*

Girish, T.E., & Aranya, S. (2012). Photovoltaic power generation on the moon: problems and prospects. *In: Moon*. Springer, Berlin, Heidelberg. (pp. 367-376).

Gladstone, G.R., Hurley, D.M., Retherford, K.D., Feldman, P.D., Pryor, W.R., Chaufray, J.Y., Versteeg, M., Greathouse, T.K., Steffl, A.J., Throop, H., Parker, J.W., Kaufmann, D.E., Egan, A.F., Davis, M.W., Slater, D.C., Mukherjee, J., Miles, P.F., Hendrix, A.R., Colaprete, A., & Stern, A. (2010). LRO-LAMP Observations of the LCROSS Impact Plume. *Science,* 330(6003), 472–476.

Gläser, P., Oberst, J., Neumann, G.A., Mazarico, E., Speyerer, E.J., & Robinson, M.S. (2018). Illumination conditions at the lunar poles: Implications for future exploration. *Planetary and Space Science,* 162, 170–178.

Hayne, P.O., Aharonson, O., & Schörghofer, N. (2021). Micro cold traps on the Moon. *Nature Astronomy,* 5, 169-175.

Hayne, P.O., Hendrix, A., Sefton-Nash, E., Siegler, M.A., Lucet, P.G., Retherford, K.D., Williams, J.-P., Greenhagen, B.T., & Paige, D.A. (2015). Evidence for exposed water ice in the Moon's south polar regions from Lunar Reconnaissance Orbiter ultraviolet albedo and temperature measurements. *Icarus,* 255(15), 58–69.

Hodges Jr., R.R. (1981). Migration of Volatiles on the Lunar Surface. *Lunar and Planetary Science Conference,* 12, 451-453.

Honeybee Robotics. (2022). Honeybee and mPower Technology selected as Lunar Power Grid Provider (Artemis Exploration) Retrieved from Honeybee Robotics' database. https://www.honeybeerobotics.com/?attachment_id=wyqnfueosxc.

Howard, R.L. (2021). A Common Habitat Basecamp for Moon and Mars Surface Operations. *ASCEND 2021,* 4065, 1-15.

Hubbard, G.S., Feldman, W., Cox, S.A., Smith, M.A., & Chu-Thielbar, L. (2002). LUNAR PROSPECTOR: FIRST RESULTS AND LESSONS LEARNED. *Acta Astronautica,* 50(1), 39–47.

Hurley, D.M., Lawrence, D.J., Bussey, B.J., Vondrak, R.R., Elphic, R.C., & Gladstone, G.R. (2012). Two-dimensional distribution of volatiles in the lunar regolith from space weathering simulations. *Geophysical Research Letters,* 39(L09203), 1-6.

Imhof, B., Urbina, D., Weiss, P., Sperl, M., Hoheneder, W., Waclavicek, R., Madakashira, H.K., Salini, J., Govindaraj, S., Gancet, J., Mohamed, M.P., Gobert, T., Fateri, M., Meurisse, A., Lopez, O., & Preisinger, C. (2017). Advancing Solar Sintering for Building a Base on the Moon. *69th IAC, Adelaide, Australia,* pp.1-17.

Just, G.H., Smith, K., Joy, K.H., & Roy, M.J. (2020). Parametric review of existing regolith excavation techniques for lunar *In Situ* Resource Utilisation (ISRU) and recommendations for future excavation experiments. *Planetary and Space Science,* 180(104746), 1-12.

Kacmarzyk, M., & Musial, M. (2021). Parametric Study of Lunar Base Power Systems. *Energies,* 14(4), 1-31.

Keane, J.T., Tikoo, S.M., & Elliott, J. (2022). Endurance: Lunar South Pole-Aitken Basin Traverse and Sample Return Rover. Mission Concept Study Report for the 2023–2032 Planetary Science and Astrobiology Decadal Survey. (pp. 296).

Khan, Z., Vranis, A., Zavorico, A., Fried, S., Manners, B. (2006). Power system Concepts for the Lunar Outpost: A Review of the Power Generation, Energy Storage, Power Management, and Distribution (PMAD) System Required and Potential Technologies for Development of the Lunar Outpost. *AIP Conference Proceedings,* 813, 1083–1092.

Killen, R.M., Benkhoff, J., & Morgan, T.H. (1997). Mercury's polar caps and the generation of an OH exosphere. *Icarus,* 125, 195–211.

Kornuta, D., Abbud-Madrid, A., Atkinson, J., Barr, J., Barnhard, G., Bienhoff, D., Blair, B., Clark, V., Cyrus, J., deWitt, B., Dreyer, C., Finger, B., Goff, J., Ho, K. Kelsey, L., Keravala, J., Kutter, B., Metzger, P., Montgomery, L., Morrison, P., Neal, C., Otto, E., Roesler, G., Schier, J., Seifert, B., Sowers, G., Spudis, P., Sundahl, M., Zacny, K., & Zhu, G. (2019). Commercial lunar propellant architecture: A collaborative study of lunar propellant production. *Reviews in Human Space Exploration,* 129(100026), 1-77.

Krujiff, M. (2000). The Peaks of Eternal Light on the Lunar South Pole: How they were found and what they look like. *In: Exploration and Utilisation of the Moon,* 462:333-336.

Kumari, N., Bretzfelder, J.M., Ganesh, I., Lang, A., & Kring, D.A. (2022). Surface Conditions and Resource Accessibility at Potential Artemis Landing Sites 007 and 011. *The Planetary Science Journal,* 3(224):1-23.

Landis, G.A., Bailey, S.G., Brinker, D.J., & Flood, D.J. (1990). Photovoltaic Power for a Lunar Base. *Acta Astronautica,* 22, 197–203.

Landis, M.E., Hayne, P.O., Williams, J.-P., Greenhagen, B.T., & Paige, D.A. (2022). Predicted Surface Volatile and Subsurface Water Ice Thermal Stability Zones at the Lunar Poles from Diviner Data. *53rd Lunar and Planetary Science Conference,* Ab# 1651.

Lemelin, M., Li, S., Mazarico, E., Siegler, M.A., Kring, D.A., & Paige, D.A. (2021). Framework for Coordinated Efforts in the Exploration of Volatiles in the South Polar Region of the Moon. *The Planetary Science Journal,* 2(103), 1-17.

Lemelin, M., Blair, D.M., Roberts, C.E., Runyon, K.D., Nowka, D., & Kring, D.A. (2014). High-priority lunar landing sites for in situ and sample return studies of polar volatiles. *Planetary and Space Science,* 101, 149–161.

Li, S., Lucey, P.G., Milliken, R.E., Hayne, P.O., Fisher, E., Williams, J.-P., Hurley, D.M., & Elphic, R.C. (2018). Direct evidence of surface exposed water ice in the lunar polar regions. *Earth, Atmospheric, and Planetary Sciences,* 115(36), 8907–8912.

Lowman Jr., P.D., Sharpe, B.L. and D.G. Shrunk. (2008). Moonbase Mons Malapert? Making the Case. Aerospace America, 46(10), 38-43.

Lu, X., Ma, R., Wang, C., & Yao, W. (2016). Performance analysis of a lunar based solar thermal power system with regolith thermal storage. *Energy,* 107, 227-233.

Lucey, P.G., Neumann, G.A., Riner, M.A., Mazarico, E., Smith, D.E., Zuber, M.T., Paige, D.A., Bussey, D.B., Cahill, J.T., McGovern, A., Isaacson, P., Corley, L.M., Torrence, M.H., Melosh, H.J., Head, J.W., & Song, E. (2014). The global albedo of the Moon at 1064 nm from LOLA. *JGR Planets,* 199(7), 1665–1679.

Mazarico, E., Neumann, G.A., Smith, D.E., Zuber, M.T., & Torrence, M.H. (2011). Illumination conditions of the lunar polar regions using LOLA topography. *Icarus*, 211, 1066–1081.

McClure, B. (2022, January 6). Lunar libration: January 7 moon maximum for 2022. *EarthSky*. https://earthsky.org/astronomy-essentials/lunar-libration-see-more-than-50-of-moon/.

Metzger, P. (2021). System for Extracting Water from Lunar Regolith and Associated Method. U.S. Patent No. US 2021/0404338 A1.

Mitrofaov, I.G., Sanin, A.B., Boynton, W.V., Chin, G., Garvin, J.B., Golovin, D., Evans, L.G., Harshman, K., Kozyrev, A.S., Litvak, M. L., Malakhov, A., Mazarizo, E., McClanahan, T., Milikh, G., Mokrousov, M., Nandikotkur, G., Neumann, G.A., Nuzhdin, I., Sagdeev, R., Shevchenko, V., Shvetsov, V., Smith, D.E., Starr, R., Tretyakov, V.I., Trombka, J., Varenikov, A., Vostruhkin, A., & Zuber, M.T. (2010). Hydrogen Mapping of the Lunar South Pole Using the LRO Neutron Detector Experiment LEND. *Science,* 330(6003), 483–486.

NASA. (2021). Sustained Phase Human Landing System (HLS) Program System Requirements Document, HLS-RQMT-006. https://govtribe.com/file/government-file/hls-rqmt-006-sustained-phase-dot-pdf.

NASA. (2022, August 19). NASA Identifies Candidate Regions for Landing Next Americans on Moon. https://www.nasa.gov/press-release/nasa-identifies-candidate-regions-for-landing-next-americans-on-moon.

NASA. (2020). NASA's Plan for Sustained Lunar Exploration and Development. (p.13). https://www.nasa.gov/sites/default/files/atoms/files/a_sustained_lunar_presence_nspc_report4220final.pdf.

National Research Council. (2001). Laying the Foundation for Space Solar Power: An Assessment of NASA's Space Solar Power Investment Strategy. Washington, D.C.: The National Academies Press. (Pp.94). https://doi.org/10.17226/10202.

National Research Council. (2007). The scientific context for exploration of the Moon. Washington, DC: The National Academies Press. (pp.120). https://doi.org/10.17226/11954.

Noda, H., Araki, H., Goossens, S., Ishihara, Y., Matsumoto, K., Tazawa, S., Kawano, N. and S. Sasaki, S. (2008). Illumination conditions at the lunar polar regions by Kaguya (SELENE) laser altimeter. *Geophysical Research Letters,* 35(L24203), 1-5.

Nozette, S., Lichtenberg, C.L., Spudis, P., Bonner, R., Ort, W., Malaret, E., Robinson, M., & Shoemaker, E.M. (1996). The Clementine Bistatic Radar Experiment. *Science*, 274(5292), 1495-1498.

Nozette, S., Rustan, P., Pleasance, L.P., Kordas, J.F., Leis, I.T., Park, H.S., Priest, R.E., Horan, D.M., Regeon, P., Lichtenberg, C.L., Shoemaker, E.M., Eliason, E.M., McEwen, A.S., Robinson, M.S., Spudis, P.D., Action, C.H., Buratti, B.J., Duxbury, T.C., Baker, D.N., Jakosky, B.M., Blamont, J.E., Corson, M.P., Resnick, J.H., Rollins, C.J., Davies, M.E., Lucey, P.G., Malaret, E., Massie, M.A., Pieters, C.M., Reisse, R.A., Smith, D.E., Soernson, T.C., Vorder Breugge, R.W., & Zuber, M.T. (1994). The Clementine Mission to the Moon: Scientific Overview. *Science*, 266(5192), 1835–1839.

Paige, D.A., Siegler, M.A., Zhang, J.A., Hayne, P.O., Foote, E.J., Bennett, K.A., Vasavada, A.R., Greenhagen, B.T., Schofield, J.T., McClesse, D.J., Foote, M.C., Dejong, E., Bills, B.G., Hartford, W., Murray, B.C., Allen, CC., Snook, K., Soderblom, L.A., Calcutt, S., Taylor, F.W., Bowles, N.E., Bandfield, J.L., Elphic, R., Ghent, R., Glotch, T.D., Wyatt, M.B., Lucey, P.G. (2010). Diviner Lunar Radiometer Observations of Cold Traps in the Moon's South Polar Region. *Science*, 330(6003), 479-482.

Paige, D.A., Wood, S.A., & Vasavada, A.R. (1992). The Thermal Stability of Water Ice at the Poles of Mercury. *Science*, 258(5082), 643-646.

Palos, M.F., Serra, P., Fereres, S., Stephenson, K., & González-Cinca, R. (2020). Lunar ISRU energy storage and electricity generation. *Acta Astronautica*, 170, 412-420.

Pfahl, A., Coventry, J., Röger, M., Wolderstetter, F., Vásquez-Arango, J.P., Gross, F., Arjomandi, M., Schwarzbözl, P., Geiger, M., & Lidke, P. (2017). Progress in heliostat development. *Solar Energy*, 152, 3-37.

Rasera, J.N., Cilliers, J.J., Lamamy, J., & Hadler, K. (2020). The beneficiation of lunar regolith for space resouruce utilization: A review. *Planetary and Space Science*, 186(104879), 1-15.

Reuss, F., Braun, B., Zacny, K., & Pinni, M. (2010). Lunar Base Site Preparation. (Ed.) Haym Benaroya. *In: Lunar Settlement.* CRC Press. p. 433-450.

Robinson, M.S., et. al. (2010). Lunar Reconnaissance Orbiter Camera (LROC) Instrument Overview. *Space Science Reviews*, 150, 81–124.

Rodenbeck, C.T., Jaffe, P.I., Strassner II, B.H., Hausgen, P.E., McSpadden, J.O., Kazemi, H., Shinohara, N., Tierney, B.B., & DePuma, C.B. (2021). Microwave and Millimeter Wave Power Beaming. *IEEE Journal of Microwaves,* 1(1), 229–259.

Ruppert, S., Ross, A., Vlassak, J.J., & Elvis, M. (2021). Tall Towers on the Moon. arXiv preprint arXiv:2103.00612. p. 1-12.

Schorghofer, N. (2008). The lifetime of ice on main belt asteroids. *The Astrophysical Journal,* 682, 697–705.

Schorghofer, N., & Taylor, G.J. (2007). Subsurface migration of H_2O at lunar cold traps. *Journal of Geophysical Research*, 112(E02010), 1-11.

Schultz, P.H., Hermalyn, B., Colaprete, A., Ennico, K., Shirley, M., & Marshall, W.S. (2010). The LCROSS Cratering Experiment. *Science*, 330, 468-472.

Sercel, J.C., Longman, A., & Small, J. (2021). Systems and Methods for Radiant Gas Dynamic Mining of Permafrost for Propellant Extraction. U.S. Patent No. 11,143,026 B2.

Sharpe, B.L., & Schrunk, D.G. (2003). Malapert Mountain: Gateway to the Moon. *Advances in Space Research,* 31(11), 2467–2472.

Shaw, M.G., Humbert, M.S., Brooks, G.A., Rhamdhani, A., Duffy, A.R., & Pownceby, M.I. (2021). Mineral Processing and Metal Extraction on the Lunar Surface – Challenges and Opportunities. *Mineral Processing and Extractive Metallurgy Review*. 43(7), 865–891.

Sherwood, B. (2018). Principles of a Practical Moon Base. *69th International Astronautical Congress.* IAC-18.A3.1.6.x46496. (p.1–13).

Smith, D.E., Zuber, M.T., Neumann, G.A., Lemoine, F.G., Mazarico, E., Torrence, M.H., McGarry, J.F., Rowlands, D.D., Head, J.W., Duxbury, T.H., Aharonson, O., Lucey, P.G., Robinson, M.S., Barnouin, O.S., Cavanaugh, J.F., Sun, X., Liiva, P., Mao, D.-D., Smith, J.C., & Bartels, A.E. (2010a). Initial observations from the Lunar Orbiter Laser Altimeter (LOLA). *Geophysical Research Letters*, 37(18), 37(L18204):1-6.

Smith, D.E., Zuber, M.T., Jackson, G.B., Cavanaugh, J.F., Neumann, G.A., Riris, H., Sun, X., Zellar, R.S., Coltharp, C., Connelly, J., Katz, R.B., Kleyner, I., Liiva, P., Matuszeski, A., Mazarico, E.M., McGarry, J.F., Novo-Gradac, A.-M., Ott, M.N., Peters, C., Ramos-Izquierdo, L.A., Ramsey, L., Rowlands, D.D., Schmidt, S., Scott III, V.S., Shaw, G.B., Smith, J.C., Swinski, J.-P., & Torrence, M.H. (2010b). The lunar orbiter laser altimeter investigation on the lunar reconnaissance orbiter mission. *Space Science Reviews*, 150(1-4), 209-241.

Sowers, G., & Dreyer, C.B. (2019). Ice Mining in Lunar Permanently Shadowed Regions. *New Space*, 7(4), 235-244.

Speyerer, E.J., & Robinson, M.S. (2013). Persistently illuminated regions at the lunar poles: Ideal sites for future exploration. *Icarus*, 222(1), 122-136.

Speyerer, E.J., Robinson, M.S., Denevi, B.C., & the LROC Science Team. (2011). Lunar Reconnaissance Orbiter Camera Global Morphological Map of the Moon. *42nd Lunar and Planetary Science Conference, No. 2387.*

Spudis, P.D., Bussey, D.B.J., Baloga, S.M., Butler, B.J., Carl, D., Carter, L.M., Chakraborty, M., Elphic, R.C., Gillis-Davis, J.J., Goswami, J.N., Heggy, E., Hillyard, M., Jensen, R., Kirk, R.L., LaVallee, D., McKerracher, P., Neish, C.D., Nozette,S., Nylund, S., Palsetia, M., Patterson, W., Robinson, M.S., Raney, R.K., Schulze, R.C., Sequeira, H., Skura, J., Thompson, T.W., Thomson, B.J., Ustinov, E.A., & Winters, H.L. (2010). Initial results for the north pole of the Moon from Mini-SAR, Chandrayaan-1 mission. *Geophysical Research Letters*, 37(L06204), 1-6.

Spudis, P.D., Bussey, D.B.J., Baloga, S.M., Cahill, J.T.S., Glaze, L.S., Patterson, G.W., Raney, R.K., Thompson, T.W., Thomson, B.J., & Ustinov, E.A. (2013). Evidence for water ice on the Moon: results for anomalous polar craters from the LRO Mini-RF imaging radar. *J. Geophysical Research,* 118(10), 2016–2029.

Stoica, A., Ingham, M., Tamppari, L., Mitchell, K., & Quadrelli, M. (2014). TransFormers for Extreme Environments. NIAC Phase 1 Final Report. (pp.72). https://www.nasa.gov/sites/default/files/files/Stoica_2013_PhI_Transformers.pdf.

Taylor, L.A., & Meek, T.T. (2005). Microwave sintering of lunar soil: properties, theory, and practice. *Journal of Aerospace Engineering*, 18(3), 188–196.

Toklu, Y., & Järvstråt, N. (2003). Design and construction of a self sustainable lunar colony with in-situ resource utilization. *CE: The Vision for the Future Generation in Research and Applications,* pp. 623–628.

Trigwell, S., Captain, J., Weis, K., & Quinn, J. (2012). Electrostatic beneficiation of lunar regolith: applications in in situ resource utilization. *Journal of Aerospace Engineering,* 26, 30-36.

Vanoutryve, B., De Rosa, D., Fisackerly, R., Houdou, B., Carpenter, J., Philippe, C., Pradier, A., Jojaghaian, A., Espinasse, S., & Gardini, B. (2010). An analysis of illumination and communication conditions near lunar south pole based on Kaguya data. *Proceedings of International Planetary Probe Workshop, Barcelona.* (pp. 1-7).

Vasavada, A. R., Paige, D. A., & Wood, S. E. (1999). Near-Surface Temperatures on Mercury and the Moon and the Stability of Polar Ice Deposits. *Icarus,* 141(2), 179-193.

Waldron, R.D. (1990). Lunar Base Power Requirements. *In: Engineering, Construction, and Operations in Space II, ASCE,* 1288–1297.

Watson, K., Murray, B.C., & Brown, H. (1961a). On the possible presence of ice on the Moon. *Journal of Geophysical Research,* 66(5):1598–1600.

Watson, K., Murray, B.C., & Brown, H. (1961b). The behavior of volatiles on the lunar surface. *Journal of Geophysical Research,* 66(9), 3033–3045.

Williams, J.-P., Greenhagen, B.T., Paige, D.A., Schörghofer, D., Sefton-Nash, E., Hayne, P.O., Lucey, P.G., Siegler, M.A., Aye, K.M. (2019). Seasonal Polar Temperatures on the Moon. *JGR Planets,* 124(10):2502-2521.

Yang, F., Xu, Y., Chan, K.L., Zhang, X., Hu, G., & Li, Y. (2019). Study of Chang'E-2 microwave radiometer data in the lunar polar region. *Advances in Astronomy,* 3940837.

Zalik, A. (2018). Mining the seabed, enclosing the Area: ocean grabbing, proprietary knowledge and the geopolitics of the extractive frontier beyond national jurisdiction. *International Social Science Journal,* 68(229-230), 343–359.

Zelenyi, L.M., Zakharov, A.V., Kuznetsov, I.A., & Shekhovtsova, A.V. (2021). Moondust As a Risk Factor in Lunar Exploration. *Herald of the Russian Academy of Sciences,* 91, 637–646.

Zhang, J.A., & Paige, D.A. (2009). Cold-trapped organic compounds at the poles of the Moon and Mercury: Implications for origins. *Geophysical Research Letters,* 36(L16203), 1-5.

CHAPTER 5

AN AREA-BASED MANAGEMENT APPROACH FOR GOVERNING LUNAR WATER ICE MINING ACTIVITIES

5.1 Introduction

Since its inception in 1959, the United Nations Committee on the Peaceful Uses of Outer Space sponsored nation states to develop a substantive set of binding international laws to govern space activities (The Outer Space Treaty, 1967; The Rescue Agreement, 1968; The Liability Convention, 1968; The Liability Convention, 1972; The Registration Convention, 1975; The Moon Agreement, 1979). The Outer Space Treaty (1967) provided overarching principles that were met with little resistance, including that space should be used for only peaceful purposes, that no actor can be excluded from the use and exploration of the space environment, that States retain sovereignty over their assets, and that space and celestial bodies are not subject to national appropriation. As of 2023, the Outer Space Treaty has 112 ratifications and 23 signatories, including all major spacefaring nations.

While the Outer Space Treaty is considered the most significant treaty in international space law, it did not provide any detailed procedures to govern specific activities regarding the use of resources located on planetary bodies such as the Moon, Mars, and asteroids. However, by means of Article II (Outer Space Treaty, 1967), the treaty excludes nations from making exclusive claims to the Moon and its resources through discovery, access, and use (O'Brien, 2021). The lack of regulation surrounding the development of space resources led developing nations to believe that technologically advanced countries would lead a commercial space race that would exacerbate wealth

disparities already present in the international community (Reynolds, 1995). Thus, in 1979, the Moon Agreement was formulated, which to this day remains the only intergovernmental legal instrument to address the exploration, use, and exploitation of the Moon and its natural resources.

Only 18 States have ratified the Moon Agreement, none of which are spacefaring. This lack of support stems mainly from how developed states interpret the common heritage principle (The Moon Agreement, 1979, Art. 11(5)). The principle was the first codification of a property rights regime that transcends national sovereignty and designates certain international areas (i.e., the Moon, the deep seabed), due to their economic and scientific value, to be managed by all States rather than owned by one or the few with the near-term capacity to exploit them (Joyner, 1986; Tronchetti, 2010).

While there is no universal definition of the common heritage principle, most interpretations agree that the Moon cannot be appropriated, its common-pool resources must be universally managed, that there must be some form of benefit sharing, that activities must be peaceful, and that it should be preserved for future generations (Heim, 1990; Shackelford, 2009). Developing countries interpreted common heritage to mean that the Moon is common property requiring management by a singular group possessing exclusive rights to exploit its resources and distribute profits equally to all nations (Buxton, 2004). Such an idea was highly contested and was considered a substantial disincentive for pioneering nations to ratify the Moon Agreement and invest in the development of the Moon because nations that do not contribute financially can still reap the benefits of exploitation activities of another nation (Reynolds, 1995; Buxton, 2004). Industrialized nations interpret the common heritage principle as a means to ensure that

any nation can exploit resources on the Moon so long as no single nation claims exclusive jurisdiction to the area from which those resources are recovered (Schwind, 1986). In other words, heritage lies in the free access to the Moon's resources, not the profits (Buxton, 2004).

Article 11(5) of the Moon Agreement provides that States Parties begin establishing an international regime, "…including appropriate procedures, to govern the exploitation of the natural resources of the moon as such exploitation is about to become feasible." The main purposes of the regime were the orderly and safe development of the moon's natural resources, rational management of those resources, and the expansion of opportunities in the use of those resources (The Moon Agreement, 1979, Art. 11(7a-c)). In addition, the regime was to support the equitable sharing by all States Parties in the benefits derived from those resources, with special consideration for the interests and needs of developing countries and the efforts of the pioneering countries which have contributed to the exploration of the Moon (The Moon Agreement, 1979, Article 11(7d)). At the time of its ratification, space resources technologies had yet to be developed. Though, the Moon Agreement mandates that once it was in force for more than five years, States Parties can request to convene a conference to consider whether an international regime should be established, "…taking into account in particular any relevant technological advancements" (The Moon Agreement, Art. 18).

It is difficult to determine when lunar mining activities will become technically and financially feasible. Yet over the past few decades, there has been an increase in both the opportunity and willingness to prospect, explore, and exploit the Moon's resources. The increased opportunity is reflected in the upsurge of space launches (Federal Aviation

Administration, 2022) and the improvement in the technological readiness of critical capabilities required to transform raw materials on the Moon's surface into consumables, products, and commodities for use in-situ (i.e., prospecting, excavation, beneficiation, extraction, purification, and additive manufacturing) (Lomax et al., 2020; Schlüter & Cowley, 2020; Rasera et al., 2020; Meurisse & Carpenter, 2020; Schlüter et al., 2021; Rohde et al., 2022; Shaw et al., 2021). An increased willingness is reflected in the growth and expansion of the commercial private space sector, international cooperation through the development and signing of the Artemis Accords (NASA, 2020), and preliminary steps toward a regulatory environment through domestic legislation (Exec. Order No. 13914, 2020; U.S. Commercial Space Launch Competitiveness Act, 2015; Law of 15 December 2020 on Space Activities; Space Resources Act, 2021; Federal Law No. 12 of 2019 on the Regulation of the Space Sector).

The "building blocks" for an international governance framework on the utilization of space resources developed by the Hague International Space Resources Working Group (universiteitleiden.nl, 2019) have been discussed at the international stage (United Nations Committee on the Peaceful Uses of Outer Space, 2020). However, it was only recently when the United Nations approved a working group to discuss the development of an international regime to govern space resources activities (United Nations Committee on the Peaceful Uses of Outer Space, 2022). During its 2022 session, the Legal Committee of the United Nations Committee on the Peaceful Uses of Outer Space mandated the new working group to address unresolved issues related to space resources, including:

- Collecting relevant information on activities in the exploration, exploitation, and use of space resources, including scientific and technological developments and current practices, considering their innovative and evolving nature;
- Studying existing legal frameworks for such activities;
- Assessing the benefits of further development of a framework for such activities, including by way of additional international governance instruments;
- Developing a set of initial recommended principles for [space resources] activities;
- Identifying areas for future work […], which may include developing potential rules and/or norms, for activities in the exploration, exploitation and utilization of space resources, including with respect to related activities and benefit sharing.

Despite indications that the development of lunar mineral resources is on the horizon, the Moon Agreement has yet to be revisited, no supranational governing authority has been established, and no instruments for managing and regulating lunar mining activities have been proposed. This paper advocates for governing lunar mining activities using a contract-based licensing system similar to the International Seabed Authority (ISA) and the Beeby Proposal (Raclin, 1986; Paxson III, 1993). The system issues temporary, but exclusive rights over allotted areas of the lunar surface, and suggests area-based management tools to promote the development of lunar resources, ensure equitable access, and safeguard the lunar environment.

A contractual system requires a governing authority to develop, implement, and oversee compliance of regulations and best mining practices in specified areas on the Moon requiring higher protections or restrictions on human activity. Because no international regime currently exists to implement such instruments, we propose an

international management regime analogous to the ISA–the Lunar Resource Management Authority (LRMA)–which would be responsible for administering the development, operationalization, and compliance of the legal regime over lunar mining activities. The institution and recommended regulations satisfy many requirements set forth in Moon Agreement and some of the unresolved space resource issues identified by the Legal Committee of the United Nations Committee on the Peaceful Uses of Outer Space, while also attempting to circumvent reservations made in the past by industrialized nations. The area-based contract system would be successful because it provides a predictable and stable framework that will be required to encourage the development of space resources while also granting the LRMA the capacity to develop and enforce area-based regulations to protect the lunar environment and promote equitable access.

We review how mineral resources are managed in terrestrial Areas Beyond National Jurisdiction (ABNJ) to identify potential best practices and applicable regulations for a future lunar governance regime. We focus on the "the seabed and the ocean floor and subsoil thereof, beyond the limits of national jurisdiction" (United Nations General Assembly, 1970) as the primary case study, for it is the only ABNJ with an existing intergovernmental institution and regulatory framework responsible for regulating mining activities. The case study reviews the structure, authority, and responsibilities of the ISA and the regulations found in its 'Mining Code.' Based on the case study, we propose a governance structure, a notification system for prospecting, a contract system for issuing mining rights to conduct exploration activities, guidelines and best practices for operators to conduct their mining activities, and area-based regulations to safeguard the lunar environment and promote equitable access.

We also propose that the LRMA implement a spatial planning tool, such as the Lunar Mining Map Tool introduced in Chapter 4, to administer the contract system and area-based management regulations. The Lunar Mining Map Tool is used throughout this paper to demonstrate how a spatial planning tool can facilitate responsible management of future lunar mining activities. The tool establishes the boundaries of a water-ice resource system at the Lunar South Pole where operators can apply for licenses to conduct mining activities. Similar to the oil and gas and mineral extraction industries, the tool also implements a "block system," which, among other things, streamlines the licensing process, simplifies implementing area-based regulations, facilitates compliance and enforcement, and supports a transparent management process.

5.2 Similarities Between the Deep Seabed and Lunar Surface

The deep seabed and the lunar surface share many commonalities that permit utilizing the ISA and its Mining Code as a blueprint for managing lunar mining activities. First, the deep seabed and the Moon are both ABNJs, making their resources the common heritage of mankind. Because no nation has exclusive control over resources in these areas, they are non-excludable, meaning that any person, nation, company, etc. can access and use them (Ostrom, 2010). Moreover, some resources in these locations (i.e., seabed minerals, lunar water ice) are finite and subtractable, meaning that when they are extracted and used by an entity that there are less for others to use (Ostrom, 2010). This classifies such resources as common-pool resources. If a common-pool resource is highly valued, ungoverned appropriation can cause negative externalities to others (Ostrom,

2002). Without an effective and enduring governance regime, the "tragedy of the commons" can occur, where users act in their own self-interest rather than the collective benefit of others, causing depletion of the resource over time (Hardin, 1968).

Next, both the Moon and the deep seabed contain numerous resources of economic interest. The three primary resources of commercial interest located on the seabed are cobalt-rich ferromanganese crusts, which are found at seamounts mainly in the Pacific Ocean, seafloor massive sulfides at hydrothermal vents, and polymetallic manganese nodules located on the abyssal plains (Hein et al., 2013).

Polymetallic nodules are the most sought-after seabed resource. The resources are potato-shaped metal-rich concretions that form on the surface of Earth's deep-sea abyssal plains at water depths of approximately 3,000 to 6,500 m (Hein et al., 2013). The nodules are found near the seabed surface, with some partially buried and others completely buried, making them relatively accessible for extraction, and are located in complex topography consisting of submarine canyons, oceanic trenches and ridges, hydrothermal vents, and seamounts, necessitating the development of unique prospecting, exploration, and exploitation technologies tailored to the deep-sea environment (Hein et al., 2013; Kang & Liu, 2021; Miller et al., 2018). While the nodules are disseminated throughout the high seas, the Clarion-Clipperton Zone is the area of greatest economic interest due to elevated nodules abundances and their high nickel, copper, and rare-earth element concentrations (Hein et al., 2013). Interest in seabed mining in the Clarion-Clipperton Zone is reflected in the numerous exploration contracts granted by the ISA (International Seabed Authority, 2023a) and that the Convention defined as a priority the adoption of

rules, regulations, and procedures for the exploration and exploitation of polymetallic nodules (UNCLOS, 1982, Art. 162(2)(o)(ii)).

Similar to the deep seabed, numerous lunar resources located at the surface/near subsurface have also been identified for future use in-situ. The primary lunar resource requiring management in the near term is water ice. Yet paradoxically, our knowledge about the resource is limited. Before the Apollo era, researchers predicted that the Moon captured water ice in cold traps delivered from asteroids and comets (Watson et al., 1961; Arnold, 1979). Since then, substantial quantities of water ice have been estimated to be present in areas near the Moon's poles that are shielded from sunlight (i.e., Permanently Shadowed Regions; Kerr, 1998; Pieters et al., 2009; Spudis et al., 2010,2013; Gladstone et al., 2012; Li et al., 2018; Fisher et al., 2017; Hayne et al., 2015,2021; Feldman et al., 1998,2001; Nozette et al., 1994,1996; Zhang & Paige, 2009).

Yet, unlike the seabed's polymetallic nodules, the form, quantity, composition, and vertical and spatial extent of lunar water ice remain uncertain. Thus far, the only ground truth evidence for water ice came from the Lunar Crater Observation Sensing Satellite mission, which measured $5.6 \pm 2.9\%$ H_2O by mass in a plume derived from a Centaur upper state impacting a permanently shadowed region (Gladstone et al., 2010; Colaprete et al., 2010, 2012). Lunar water ice could come in the form of blocky ice deposits, adsorbed molecules, pore-filling ice, ice grains mixed with regolith, or hydrated minerals (Spudis et al., 2013; Hurley et al., 2016; Kornuta et al., 2018) and their distribution–similar to seabed nodules–is likely heterogeneous both laterally and vertically. Though, recent models suggest that impact gardening over time could lead to increased homogeneity (Cannon & Britt, 2020). The expected patchiness of lunar water

ice implies that future exploration licenses will need to be large enough for an operator to identify areas with quantities viable to sustain a mining operation. Yet, until we characterize the resource, it will be difficult to develop the necessary infrastructure for their development.

In addition, access to resources within both ABNJs is difficult due to their harsh and unique environmental conditions. Such conditions prevent using conventional "high-heritage" mining equipment designed for Earth's surface and require developing novel technologies and processes tailored to those environments. Additionally, human access is severely restricted in both locations, necessitating automation, robotics, and uncrewed equipment. Finally, the deep seabed is also analogous to the lunar surface because the vast majority of both environments remain unexplored. Only a fraction of the Earth's oceans has been systematically explored by humans, and an even smaller amount when focusing on seabed environments (Miller et al., 2018). As for the Moon's available resources, our knowledge is limited to samples returned on the Apollo and Luna missions, meteorites, and from orbital mapping by satellites. Moreover, the Moon's polar regions–which contain the primary resource for near-term mining (water ice)–have never been investigated in situ.

5.3 Areas Beyond National Jurisdiction

Specific locations such as the high seas, the deep seabed, Antarctica, Earth orbit, and outer space are classified as Areas Beyond National Jurisdiction (ABNJ), where no nation can exercise sovereignty. Consequently, no nation-state, organization, or institution assumes full management responsibility for the numerous activities conducted

in ABNJ or over their resources. In maritime ABNJ, the sheer amount of space and the diverse range of human activities (e.g., fishing, biodiversity conservation, oil and gas exploration and production, scientific research, bioprospecting, global trade and maritime shipping, seabed mining of mineral resources, submarine cable installation) (Merrie et al., 2014; UNEP-WCMC, 2019) warrants a sectoral approach for management, where individual governing bodies are responsible for managing specific activities. Sectoral management divides responsibilities in the high seas into a fragmented "patchwork" of international bodies and treaties that govern resources and human activities (Ortuño-Crespo et al., 2020). For example, the 1982 United Nations Law of the Sea Convention and its implementing agreements codified general legal frameworks specifically for managing mining activities on the seabed beyond national jurisdiction (Figure 5.1).

ABNJs are considered the last frontiers of exploitation (Merrie et al., 2014) and contain a wealth of untapped resources. The resources of the deep seabed, legally known as "The Area," were deemed the "common heritage of mankind" by the UN General Assembly in 1970, a principle codified into law in the 1982 Law of the Sea Convention (i.e., the Convention) (Art. 136). While no claim or exercise of sovereign rights over resources in an ABNJ is recognized, the recovery of mineral resources is considered legal. Because resources in ABNJ are only accessible in the near term to nations with the necessary technological capabilities, they have the potential to be unevenly distributed, which could cause global economic imbalances and increase the propensity of disputes. Thus, some degree of international management is required for countries to conduct their activities fairly and responsibly.

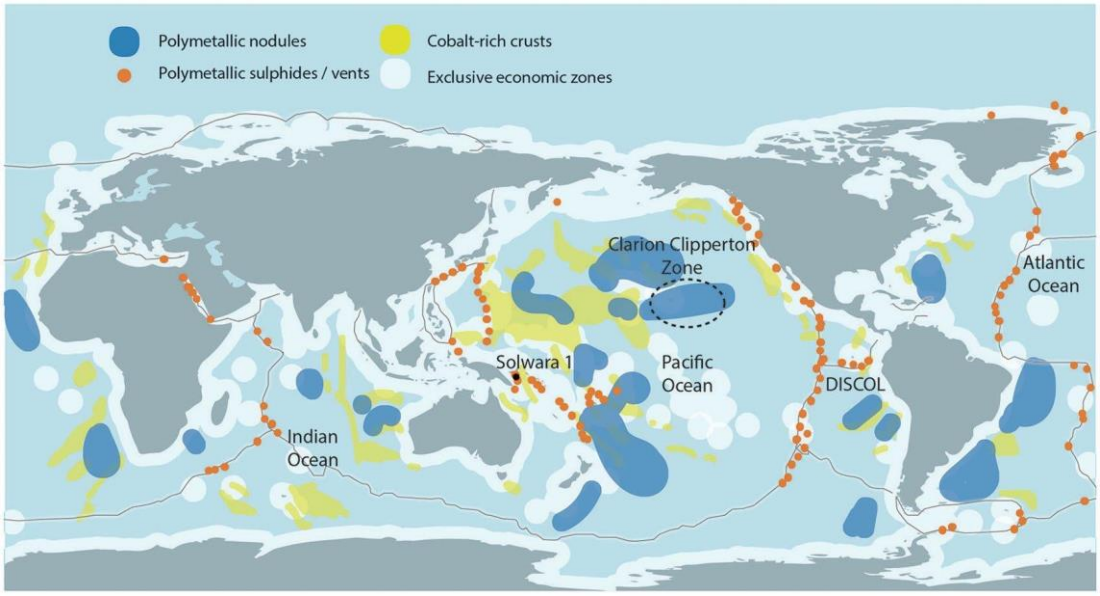

Figure 5.1 – Global map of the Earth. Areas in white represent the Exclusive Economic Zones of nation states, where sovereign states are granted exclusive rights regarding the exploration and use of resources. Exclusive economic zones extend up to 200 nautical miles from the coast of a nation-state. The light blue area represents ocean ABNJ. The areas in yellow, dark blue, and orange represent seabed mineral resources currently being targeted for exploitation, most of which reside in ABNJ. While numerous exploration licenses have been granted to contractors, no exploitation license has yet to be granted. Image reproduced from Miller et al. (2018). Licensed for use under Creative Commons: https://creativecommons.org/licenses/by/4.0/.

5.4 The International Seabed Authority: Regime Overview

The ISA is an autonomous intergovernmental organization through which States Parties to the Law of the Seas Convention (1982) regulate, organize, control, and in principle, carry out seabed mining activities. All States Parties to the Convention are a member of the ISA However, states not party to the Law of the Seas Convention are not subject to the ISA's regulations and recommendations outlined in their Mining Code.

The ISA's jurisdiction extends to The Area, which is spatially constrained by the outer limits of nations' exclusive economic zones, a jurisdictional boundary recognized under international law that extends 200 nautical miles from a state's coastline

(UNCLOS, 1982, Art. 1, para. 1(1); Part VI, Art. 7). The boundary dividing the exclusive economic zones and the Area is part of a larger "zoning framework" that governs anthropogenic activities in Earth's oceans according to the distance from sovereign land.

Seabed mining activities in The Area are governed by provisions in Part XI and Annex III of the Law of the Sea Convention, as amended by the 1994 Agreement (United Nations General Assembly, 1994), which are interpreted and applied together as a single instrument. Part XI of the Convention provides the legal framework for governing seabed mining activities, Annex III contains the "Basic Conditions of Prospecting, Exploration, and Exploitation" for resources in the Area, and the 1994 Agreement updates Part XI of the Convention with the introduction of significant changes to the regime based on a series of negotiations between developing and industrialized Nation States during from 1973–1982 (Lodge, 2002; Jaeckel, 2017).

The ISA is mandated to encourage the development of seabed resources, protect and conserve the marine environment and its natural resources as it will be affected by seabed mining activities, and ensure equitable access and sharing of economic benefits between seabed miners and the rest of the international community (Madueira et al., 2016). To encourage the development of resources, the ISA developed a contract-based system that issues licenses to allotted areas of the seabed to regulate the development of mineral resources in the Area. Activities conducted within these areas (i.e., prospecting, exploration, and exploitation) are subject to specific regulations, rules, and procedures, and each mineral resource found in the Area is subject to its own set of regulations. The suite of regulations constitutes the ISA's 'Mining Code' (ISBA/25/C/WP.1), which will be discussed in detail later in this paper. Additionally, the ISA's Mining Code contains

Area-Based Management measures such as environmental management plans (ISBA/18/C/22; ISBA/17/LTC/7) to safeguard the marine environment and promote equitable access.

The need for a Mining Code arose because investors in seabed mining activities could not exercise exclusive rights over previously prospected regions in The Area, and there were no agreed-upon norms, rules, or guidelines for how operators should conduct their mining activities. Without a Mining Code, the locations where seabed prospectors contributed significant amounts of investment and characterize the seabed environment and its resources would otherwise be subject to the freedom of the high seas, making them accessible to any actor exercising the same freedoms without any norms, rules, and guidelines (Nandan, 2006), jeopardizing the economic security and investment of operators. Currently, the Moon does not contain any zones or boundaries recognized under international law, meaning that the Moon is entirely a sovereign-free zone similar to the deep seabed.

Some resources located far from the centers of governmental authority are managed entirely by appropriators (Ostrom, 2002). However, it is extremely rare to find a resource system governed entirely by participants without rules established by some institutional authority (Ostrom et al., 1994; Ostrom, 2002). Similar to deep-sea mining, it is likely that an intergovernmental regime for managing lunar mining activities will emerge because precedent established through international space law that States are responsible for their space activities, whether carried out by governmental or non-governmental entities (Outer Space Treaty 1967, Art. VI). While lunar mining activities are expected to be conducted by both States and private entities, a launching State–

defined as a State "which launches or procures the launching of a space object" and a State "whose territory or facility a space object is launched" (The Liability Convention, 1972, Art. I)–is currently liable for damages caused by space objects in space if the damage is due to its fault or the fault of persons for whom it is responsible (The Liability Convention, 1972, Art. IIII).

To ensure that States have knowledge and oversight over space activities, States are also responsible for registering the objects belonging to the State itself or private companies (Jakhu et al., 2018). Similar to the registration of vessels to their flag State operating in the high seas (UNCLOS, 1982, Art. 91–94), the registration of space objects effectively allocates jurisdiction and control to the launching State operating in the sovereign-free environment of outer space (Outer Space Treaty, Article VIII). Because space objects include any tangible human-made material or physical object or device, irrespective of its size, composition, and shape launched from Earth (Schmidt-Tedd & Soucek, 2020), States are ultimately liable under Article VI of the Outer Space Treaty (1967) for damages caused by all future space resources activities, even those developed and operated by private companies.

The current responsibilities of States over space objects and the reliance of private companies on their respective States suggest it would be surprising to see a shift away from international and national governance to an approach governed entirely by those conducting mining activities (self-governance). Thus, we utilize the International Seabed Authority as a blueprint for a future regime for managing lunar mining activities.

5.4.1 Structure Principal Organs, and Responsibilities of the ISA

To facilitate comprehension of our proposal for managing lunar water ice mining activities, a high-level overview of the ISA's structure is provided below. For details on the evolution, structure, processes, functions, responsibilities, and negotiations leading to the development of the ISA, see these references (Hayashi, 1989; Kirsch & Fraser, 1989; Wolfrum, 1995; Lodge, 2002, 2011; Harrison, 2013; Antrim, 2005; Jaeckel, 2015, 2016, 2017; Nandan et al., 2002; Nandan, 2006; Lévy, 2014; Wood, 1999, 2007; Egede et al., 2019).

The ISA's structure comprises three main organs (e.g., the Assembly, Council, and Secretariat) and three subsidiary organs (e.g., the Finance Committee, Legal and Technical Commission, and Economic Planning Commission). Additionally, the ISA has a commercial arm known as the Enterprise.

The Assembly serves as the plenary body where each State Party to the Convention is represented and is the supreme policymaking organ of the ISA to which the other principal organs are accountable (UNCLOS, 1982, Art. 160). In addition, the Assembly acts as a forum for all States Parties, governs by consensus rule processes, establishes the general policies and standards of the ISA, and has the power to establish general policies to implement the provisions of the Convention.

The ISA's Council is the executive organ of the ISA and comprises 36 state-members. The structure of the Council is derived from a complex formula outlined in the 1994 Agreement that reflects the interests of producers and consumers most interested in seabed mining while also ensuring geographical, economic, and social representation (UN Doc A/RES/48/263, p. 16). The Council supervises and coordinates implementing the provisions of the seabed mining regime, draws up the terms of contracts, reviews and

approves contract plans of work submitted by operators to explore and exploit the seabed adopts, applies the rules, regulations, and procedures in the Mining Code, and establishes environmental and other standards for operators (UNCLOS, 1982, Art. 162). The regulations adopted and applied by the Council are based on the recommendations from the Legal and Technical Commission (UNCLOS, 1982, Art. 165). The Secretariat carries out the day-to-day administrative tasks for the other two main organs (UNCLOS, 1982, Art. 166). It is headed by the Secretary-General–the chief administrative officer of the ISA– whose responsibilities are to provide information, advice, and assistance to States and international organizations to understand better the Convention and its implementation (UNCLOS, 1982, Art. 166).

The three subsidiary organs–The Finance Committee, The Legal and Technical Commission, and the Economic and Planning Commission–contain elected members with term limits that provide recommendations to the ISA's main organs in specialized matters relating to budgetary concerns, legal questions, environmental assessments, and trends and factors affecting the supply, demand, and information of seabed minerals.

The Enterprise is unique, for it is both an independent organ of an international organization and an industrial and commercial corporation conceived to engage in seabed mining (UNCLOS, 1982, Art. 170). The Enterprise was developed to operationalize the common heritage principle and ensure that humanity as a whole and especially developing States can participate in deep seabed mining in ABNJ. Once it begins operations, the Enterprise will have the capacity to engage in seabed mining activities in the Area (UNCLOS 1982, Article 153(a)), including the exploration and recovery of minerals from the seabed, beneficiation and mineral separation, waste disposal,

transportation, processing and refinement, and marketing of recovered minerals (UNCLOS 1982, 170(1)). It would also own all the minerals and processed materials that it produced and would also be able to sell its products on a non-discriminatory basis (UNCLOS. 1982, Annex IV, Art. 12 (4-5)).

5.5. The Lunar Resource Management Authority

In the near term, the Moon will require an intergovernmental institution to responsibly and equitably supervise the development of its resources. Based on the ISA's structure, we propose the establishment of the Lunar Resource Management Authority (LRMA), an intergovernmental regime operating under the auspices of the United Nations, whose primary responsibilities are to administer and regulate mining activities on the Moon. The LRMA's primary obligations are to (i) encourage the sustainable development of lunar resources, (ii) safeguard the lunar environment as it may be affected by mining activities, and (iii) ensure responsible and equitable use of and economic benefits to lunar mineral resources.

The LRMA's initial activities should include the following:

- Developing and overseeing compliance with a Lunar Mining Code containing rules, regulations, and best practices related to prospecting, exploration, and exploitation on the Moon,
- Receiving, reviewing, and approving plans of work in the form of applications for licenses for conducting mining activities,

- Developing and implementing area-based policies to eliminate or substantially reduce effects of mining activities on the lunar environment, promote sustainability, and ensure equitable access to the lunar surface and its resources,
- Provide best practices, recommendations, and guidelines for operators to comply with the rules, regulations, and procedures developed by the LRMA, and
- Maintaining a public registry containing information on all mining activities.

The Hague Space Resources Governance Working Group, comprised of government, industry, academia, civil society, and research centers, has already developed Building Blocks for the Development of an International Framework on Space Resources Activities. During the design of the LRMA, numerous principles already outlined in the Hague's Building Blocks should be incorporated, including: consistency with current international law, adaptive management, the attribution of priority rights to promoting the sustainable use of space resources and sustainable technologies, preventing disputes, promoting peaceful, orderly and safe mining activities, considering the needs of all countries regardless of their degree of development and scientific development, science, and the contributions of pioneer investors, and providing legal certainty and predictability for operators (de O Bittencourt Neto et al., 2020).

Similar to the ISA's structure, we propose that the LRMA be comprised of an Assembly, Council, Secretariat, and Legal and Technical Commission. Though contentious, we also argue for a Lunar Mining Consortium based off the ISA's Enterprise.

5.5.1 A Lunar Assembly and Secretariat

A state-centric lunar governance regime responsible for managing mining activities requires a plenary body similar to ensure universal participation when developing and administering the mining regulations, rules, and procedures on the Moon. The regime's development and operation must have universal representation, not just input from the spacefaring nations. Thus, similar to the ISA, the LRMA should contain a Lunar Assembly that serves as a forum for spacefaring and non-space-faring nations to provide input on the rules, regulations, and procedures surrounding lunar mining activities.

A centralized supranational structure governing lunar mining activities affords nation-states the primary responsibility to influence how mining on the Moon will be managed. However, private industry, non-profits, intergovernmental organizations, non-governmental organizations, and individuals (e.g., scientific experts) can be granted consultative or observer status to participate in the regime's development.

In addition to the Assembly, the LRMA will need a Secretariat similar to the ISA to carry out its day-to-day administrative tasks, including preparing and releasing reports, research findings, and policy suggestions to the other organs of the LRMA, producing publications, analytical studies, and disseminating information on the LRMAs activities and the status of lunar mining activities as a whole to the public, organizing workshops where rules, regulations, and policies can be reviewed, to maintaining the registry, and ensuring that operators are compliant with the regulations set forth in their contracts.

5.5.2 A Lunar Council

The Lunar Council would be the executive organ of the LRMA. It's primary responsibility would be to establish the procedures, best practices, and regulations in the Lunar Mining Code along with area-based regulations related to environmental protection, sustainability, and equal access. Additionally, the Lunar Council be responsible for approving the applications submitted by operators for exploration and exploitation licenses, which would grant them priority rights. While the Lunar Assembly is the supreme organ, the Lunar Council provides a balance of power within the LRMA.

The composition of limited membership organs in intergovernmental organizations must ensure equitable geographic participation and representation of special interests (Wolfrum, 1995). Thus, the Lunar Council could be structured by reserving seats for members in chambers comprising groups that reflect the entire international community, including (a) spacefaring nations (i.e., United States, Europe, China, Russia, India), (b) emerging or prospective spacefaring nations defined by certain milestones such as those listed by the European Space Policy Institute (2021), and for (c) non-spacefaring nations. Additional seats could be reserved for those who have made the most significant investments in developing the necessary infrastructure for delivering mining assets to the Moon, those who made the most significant investments in lunar mining technologies, for members who will likely be the largest exporters and importers of materials that will be produced and used on the Moon that would otherwise have been delivered from Earth (i.e., rocket propellant, water, construction materials), or other special interest groups that are more social in nature such as indigenous groups with alternative positions about the development of the Moon's resources. Each of these

groups would compose a chamber, and a rotation system would be utilized to ensure that more nation-states can participate in the legal process (UNCLOS, 1982, Art. 161).

Similar to the ISA, the LRMA's Council could operate with a non-uniform voting system, meaning that voting procedures would exist for different categories of decisions (Wolfrum, 1995). For example, consensus can be the main principle for adopting and applying rules, regulations, and procedures implementing the LRMA's Mining Code. Yet for questions of procedure, only a simple majority is required. In addition, the ISA uses its chamber voting system on substantive matters which could also be implemented by the LRMA. In this system, decisions cannot be opposed by a majority in any of the chambers (UNCLOS, 1982, Art. 161, Sect. 3). In addition to the three different voting systems, the ISA also used an "automatic approval system" for exploration contracts that fulfill certain requirements (Wolfrum, 1995). For example, if the ISA's Legal and Technical Commission recommends approval of an exploration contract, the Council must approve it within 60 days unless disapproved by a two-thirds majority (International Seabed Authority, 2015).

5.5.3 A Lunar Legal and Technical Commission

A technical arm of the LRMA's Council will be required to effectively exercise its functions on all legal and technical matters related to the exploration and exploitation of lunar resources. This will require a Legal and Technical Commission comprised of elected experts in the fields relevant to lunar mining, including, among others: law, conservation, terrestrial and space mining, economic geology, mineralogy, petrology, mineral processing, space resources, planetary science, solar physics, geochemistry,

geophysics, economics, urban planning, social science, and cosmochemistry. Alternatively, the Commission could be comprised of experts from different industries along the value chain of space resources (Luxembourg Space Agency, 2018; Lamboray, 2019), including transportation, prospecting, site planning and excavation, resource extraction and processing, product synthesis and manufacturing, construction, supporting operations (e.g., power, communications, maintenance, and recycling).

When selecting the members of The Lunar Legal and Technical Commission, "due account" must be taken to ensure that its members reflect an equitable geographical representation, special interests, and those with varying degrees of economic and technical development (The International Seabed Authority, 2023b). Because the Lunar Legal and Technical Commission would inform decisions made by the LRMA's Council, the scientific community is afforded participatory power to influence how lunar resources will be managed and developed.

Similar to the ISA's Commission, The Lunar Legal and Technical Commission functions would be to formulate and update the rules, regulations, and procedures relating to prospecting, exploration, and exploitation, review applications for exploration and exploitation licenses, defining the Moon's resource systems where mining can be conducted and where their rules apply, develop environmental regulations and best practices for mining activities to safeguard the lunar environment, assess the effects of mining on the lunar environment vis-à-vis annual reports submitted by operators, and prepare environmental assessments on the effects of mining on the lunar environment based on annual reports submitted by operators.

A phased/evolutionary approach should be adopted by the LRMA, meaning that institutions should only be developed when needed. Thus, when the exploitation phase of mining begins, the LRMA should also create an Economic Commission to review and track the supply and demand of lunar resources and how their extraction affects the lunar space economy.

5.5.4 The Lunar Mining Consortium

To promote equal access to and equitable sharing of the Moon's resources, we recommend that the LRMA develop the Lunar Mining Consortium similar to the ISA's Enterprise. This organ would act as the commercial arm of the LRMA and would be limited to conducting mining activities in Reserved Areas (See Section 5.8.4) The Lunar Mining Consortium operationalizes the common heritage principle in Article 11 of the Moon Treaty, allowing for all humanity to benefit from the Moon's natural resources rather than just those with the technological capabilities.

Initially, the ISA was conceived by developing states to carry out seabed mining activities on behalf of the *entire* international community vis-à-vis the Enterprise, where the Enterprise would enjoy a monopoly on resource extraction in seabed areas beyond national jurisdiction and distribute its profits among member states (Sparenberg, 2019). To become operational, the Enterprise was to be financed by significant assistance from member states, voluntary contributions, and interest-free loans (Jaeckel, 2017; UNCLOS, 1982, Art. 171). The assumption was that seabed mining would be so profitable that the pioneering investors in seabed mining would be able to make substantial contributions to support the Enterprise (Glasby, 2002). Once it began operations, the Enterprise was

envisioned to then become self-financing. The Law of the Sea Convention (1982) also mandated private and State Enterprises to transfer mining technologies to the Enterprise and developing countries based on "fair and reasonable commercial terms and conditions" to the Enterprise over the period of 10-20 years (Glasby, 2002), distribute profits through a system of compensation (UNCLOS, 1982, Art. 151), and be subject to production limits (Law of the Sea Convention, 1982, Art. 151).

The competitive advantages of these provisions to industrialized states such as the United States were considered so onerous that several industrialized countries refused to sign the Law of the Seas Convention (Glasby, 2000). After years of negotiations, the 1994 Agreement was adopted, which amended the contentious provisions related to the Enterprise, including eliminating the transfer of technology, reducing the benefit-sharing elements and economic assistance by developed nations, and cutting production policies (Jaeckel, 2017). Under the principles of cost-effectiveness and the evolutionary approach, the 1994 Agreement also shifted control of the Enterprise to the Secretariat until the first exploitation contract of another entity is approved or if an application is received by the Council for a joint venture operation with the Enterprise (Lévy, 2014; Egede et al., 2019). Moreover, the 1994 Agreement eliminated the requirement of Member States to fund the Enterprise (1994 Agreement, Annex, Sec. 2).

Proposals led by industrialized states ultimately reformed the nature of the seabed regime into a dual system of access. Known as the "parallel system," private companies and State enterprises would operate alongside or enter into a joint venture with the Enterprise (Bailey, 1983). The process required operators applying for an exploration license to submit a plan of work containing mineral and environmental data to define two

sites of equal economic value capable of allowing two mining operations (UNCLOS, 1982, Annex III; 1994 Agreement, Sect. 1(10). The ISA would then issue an exploration license for one area to the operator and withhold the other as a Reserved Area for the Enterprise or a developing state. The system promotes equal access to and benefit sharing of seabed resources in the Area to developing states by lowering the costs and efforts associated with prospecting (Nandan, 2002).

The ISA's Enterprise is the only example of an intergovernmental institution attempting to institutionalize equal access to resources in ABNJ. While the initial vision of the Enterprise may be too contentious for lunar mining, the parallel system should be considered as a potential approach to afford non-spacefaring nations the capacity to conduct lunar mining activities alongside spacefaring nations. Without such an institution, it may be impossible for developing states without the technological capabilities to reap the benefits of the Moon's resources. In the past, the Enterprise was considered a threat to industrialized states because operators would be in direct competition with an internationally funded mining venture. However, it seems necessary to consider developing such an organ so that all of humanity can benefit from lunar water ice mining activities.

The Lunar Mining Consortium would reserve a portion of its profits to be self-financing and distribute the remaining to all members of the LRMA. Production limits, and economic assistance should not be imposed on commercial companies operating alongside the Consortium. Yet, some form of assistance is going to be required to foster the initial development of the Consortium. Thus, we propose that the LRMA not mandate, but recommend members to transfer technology to the Lunar Mining

Consortium for developing countries to utilize to participate in lunar water ice mining activities. Similar to the ISA, operators from spacefaring nations who are granted a contract to conduct mining activities must also host a training program for personnel of the Lunar Mining Consortium and emerging/non-spacefaring nations (ISBA/18/A/11, Reg. 29). This affords developing states to develop the expertise needed to participate in lunar mining activities.

5.6 The ISA's Mining Code as an Analog for Regulating Lunar Mining Activities

The development of seabed mineral resources was hindered by two major factors: (1) the absence of a mechanism to obtain long-term exclusive rights to explore and exploit a specified area of the seabed and (2) a process by which a title could be acquired to conduct such activities (Antrim, 2005). To resolve these issues, the ISA established an area-based suite of rules and regulations to manage seabed mining activities.

The regulations–colloquially known as the Mining Code–are unique to each seabed resource (i.e., polymetallic nodules, polymetallic sulfides, ferromanganese crusts) but are similar in their format, scope, and content (Lodge et al., 2014). Therefore, it was recommended that the regulations should be as close as possible. However, slight adjustments would be required to reflect the different nature of the resources (Polymetallic Nodules: ISBA/6A/18, ISBA/19/A/9, ISBA/19/A/12, ISBA/19/C17, ISBA/20/A/9; Polymetallic Sulfides: ISBA/16/A/12/Rev.1, ISBA/19/A/12 and ISBA/20/A/10; Cobalt-Rich Crusts: ISBA/18/A/11 and ISBA/19/A/12). Alongside the regulations, the Mining Code contains recommendations and best practices to guide prospecting, exploration, and exploitation activities relevant to lunar mining. States

Parties, State enterprises, or private corporations that possess the nationality of states parties or are effectively controlled by them or their nationals can conduct mining activities. (UNCLOS, 1982, Art. 153(2)(b)). Additionally, the Enterprise can carry out mining operations on behalf of the international community (UNCLOS 1982, Art. 153(2)(a); 1994 Agreement, Annex section 2).

5.6.1 Seabed Prospecting Regulations

During prospecting, the mineral deposit of interest is sampled to estimate the lateral and vertical extent of the ore, metals grade, and physical properties. Large-scale, high-level surveys are conducted to produce coarse-resolution data products that characterize the nature of the deposit (i.e., regional setting, geological setting, physicochemical characteristics, potential hazards, and other physical conditions) in a relatively short time period (Madureira et al., 2016). Once a suitable setting is identified, the prospecting campaign's area narrows to produce higher-resolution data, and exploration activities can begin. For example, the initial prospecting area in the Clarion Clipperton Fracture Zone by the Pioneer Investor Interoceanmetal was 550,000 km^2, a factor of ~1.83 times larger than its approved exploration contract area (Abramowski, 2014). Thus, large swaths of seabed area are surveyed before applying for a seabed exploration license.

Part II of each regulation in the ISA's Mining Code pertains to prospecting. First, an operator must notify the ISA of its intention to engage in prospecting, though neither spatial nor temporal limits are imposed on such activities. After the notification is submitted, it is reviewed for approval by the ISA, who records the information in a

register (ISBA/18/A/11, Reg. 4(1-3)). There are no spatial or temporal restrictions on prospecting activities except in areas where an exploration contract has been approved or if the prospecting location falls within a restricted area such as an Area of Particular Environmental Interest. This means that prospecting activities may be conducted simultaneously by more than one actor in a given block (ISBA/18/A/11, Reg. 2(6); ISBA/19/C/17, Reg. 2(6); ISBA/16/A/12/Rev.1, Reg 2(6)). However, prospectors must exercise "due regard" to the rights, duties and freedoms of other states conducting activities in the Area (Law of the Seas Convention, 1982, Art. 87(2)).

Seabed prospectors do not receive any exclusive rights with respect to the prospecting location or the resources identified within the notification area. However, a prospector may recover a "reasonable quantity" of minerals necessary for testing, which cannot be used for commercial use (ISBA/18/A/11, Reg. 2(5); ISBA/19/C/17, Reg. 2(5); ISBA/16/A/12/Rev.1, Reg 2(5)). Additionally, all actors conducting prospecting activities within the Area must take necessary measures and implement best environmental practices (i.e., monitoring the effects of prospecting on the marine) to minimize adverse environmental impacts to the marine environment arising from prospecting as well as to minimize or eliminate conflicts or interference with existing or planned scientific research activities (ISBA/18/A/11, Reg. 5; ISBA/19/C/17, Reg. 5; ISBA/16/A/12/Rev.1, Reg 5).

5.6.2 Seabed Exploration Regulations

Exclusivity is one of the main differences that differentiate the prospecting and exploration activities. After prospecting, contractors apply for a license for exclusive but

temporary rights to conduct exploration activities in a particular area of the deep seabed beyond national jurisdiction. The application is in the form of a contract plan of work, which constitutes the law governing the parties (ISBA/18/A/11, Annex II-III). Once the contract has been approved, and the license has been issued, the ISA must ensure that no other entity can operate within the approved contract area for the same or other resources that might interfere with the operator's operations (ISBA/19/C/17, Reg. 24).

The boundaries of a seabed exploration contract are defined using blocks, with each seabed resource having a specified block size. Limits are imposed on the number of blocks that can be requested for each resource, with the maximum total area allocated to a seabed operator by the International Seabed Authority varying as a function of deposit type (ISBA/19/C/17, Reg.25; ISBA/16/A/12/Rev. 1, Reg. 12; ISBA/18/A/11, Reg. 12).

A contract area's morphology can be mapped to a reasonable resolution (>150 meters) within 30-50 days of dedicated ship time (Madureira et al., 2016). However, to define a mine, data collection becomes more time-consuming. Thus, the ISA grants exploration license for a period of fifteen years, with the possibility of a five-year extension (ISBA/19/C/WP.1, Reg 26; ISBA/18/A/11., Reg 28; ISBA/19/C/17, Reg. 26). However, exploration is viewed as a preparatory phase for future exploitation and is not meant to be extended indefinitely (Le Gurun, 2014). After fifteen years, the operator is expected to apply for a license for exploitation or renounce its rights to the area under contract (ISBA/19/C/17, Reg. 26). The ISA also requires the collection of environmental baseline data and to develop monitoring programs to assess the effects of exploration activities to the marine environment. Therefore, the fifteen-year exploration contract period was considered enough time for a seabed miner to characterize its contract area

while also complying with its commitments to collect environmental baseline data and implement monitoring programs.

Part III of the regulations in the ISA's Mining Code addresses applications for approval of contract plans of work for exploration. Part IV addresses, among other things, the exploration contract itself, the operator's rights, the contract area's size, relinquishment, contract durations, training programs, periodic reviews, termination of sponsorship, and the responsibilities and liabilities of the operator during exploration. Part V focuses on the protection and preservation of the marine environment. Additional regulations notable for a future mining regime on the Moon include those surrounding confidentiality (Part VI), settlement of disputes (VIII), resources other than those explicitly listed in the regulations (Part IX), and periodic reviews of the regulations (Part X) (ISBA/19/A/9; ISBA/16/A/12/Rev.1; ISBA/18/A/11).

Regulations can be amended, which aligns with the adaptive management principle (UNCLOS, 1982, Art. 165). However, new amendments would only apply to new contracts to ensure that existing operators enjoy security of tenure (UNCLOS, 1982, Art. 153). To date, the ISA has approved 31 contracts for exploration, effectively enclosing an Area Beyond National Jurisdiction under temporary jurisdiction (Zalik, 2018; Lambach, 2021). Nineteen are for exploration of polymetallic nodules in the Clarion-Clipperton Zone (Figure 5.2), seven for polymetallic sulfides found at mid-ocean ridges, and five are for cobalt-rich crusts.

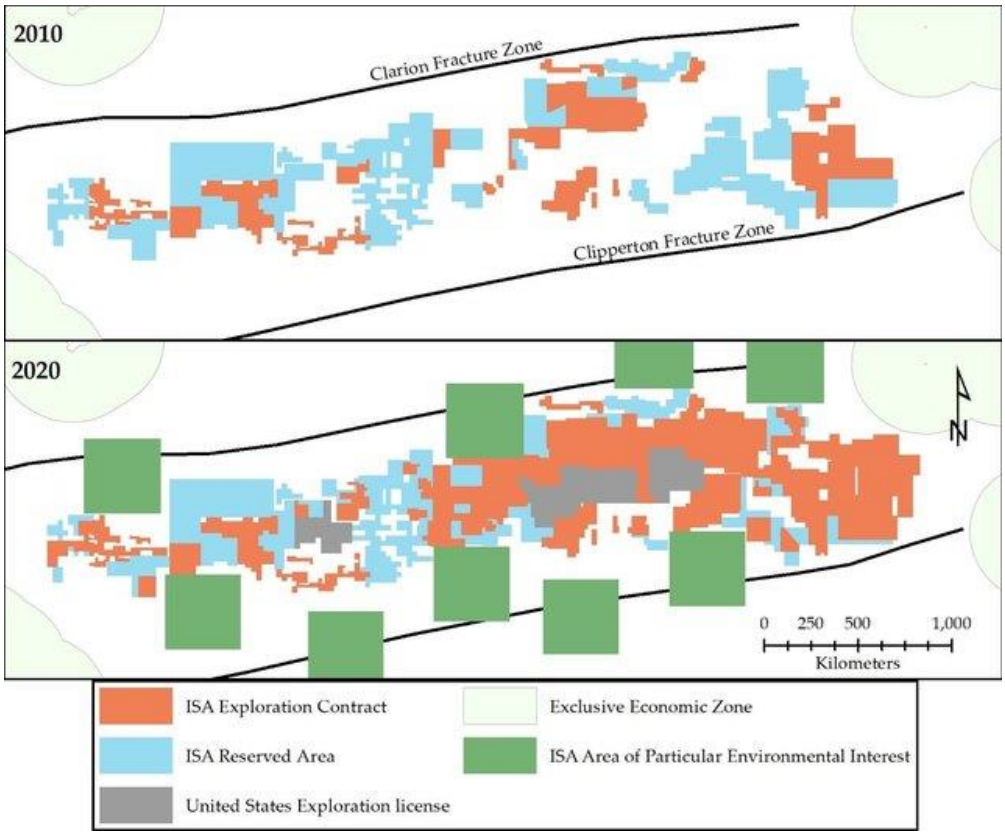

Figure 5.2 – Map of the Clarion-Clipperton Fracture Zone in the Western Pacific, depicting the areas licensed to contractors to conduct exploration activities and the implementation of Areas of Particular Environmental Interest from 2010 to 2020. The map displays exploration contract areas issued by the ISA to seabed mining companies (orange), Reserved Areas (blue), unilateral claims made by the United States (gray), and Areas of Particular Environmental Interest (green). Image reproduced from Parianos et al. (2021). Licensed for use under Creative Commons: https://creativecommons.org/licenses/by/4.0/.

5.6.3 Management of the Seabed Beyond National Jurisdiction

Area-Based Planning is one way for sectors operating in ABNJ to spatially plan their activities (UNEP-WCMC, 2019). The process involves identifying and agreeing on spatially-explicit measures to manage human activities to meet specific objectives or achieve a set of goals (UNEP-WCMC and Seascape Consultants Ltd., 2019). Area-Based Management Tools operationalize the planning process and implement context-specific measures over specified areas (Molenaar, 2013). Such tools are conventionally used in

marine spatial planning and have been applied in many contexts, including conservation and environmental protection, managing access to and safeguarding the sustainable use of resources, and to provide a public good (e.g., to increase navigational safety) (Roberts et al., 2010; Singh & Araujo, 2023; Lambach, 2021). Area-Based Management Tools regulate the distribution, timing, and intensity of activities in numerous sectors on Earth, such as fishing, shipping and navigation, mining, conservation, and cultural and natural heritage sites (Gissi et al., 2022). Each activity requires a designated authority or governance regime to implement and oversee compliance with rules, regulations, measures, and procedures.

Like any form of human development, seabed mining activities will impact the surrounding environment. For example, in the case of deep-sea mining for polymetallic nodules, mining vehicles operating on the seafloor will disturb the sediment and its organisms, noise and light pollution from mining equipment and support vessels will impact biological communities. In addition, sediment plumes created during extraction and the discharge of tailings in the water column will spread over extensive areas (Jones et al., 2020). Thus, a challenge facing the ISA is to find ways to promote the development of seabed mineral resources while also sustaining the ecosystems surrounding them (Wedding et al., 2015).

To fulfill their legal obligation to protect and preserve the marine environment, the ISA specified in their Mining Code that preservation reference zones be delineated prior to the exploitation phase. In these areas, mining is prohibited to ensure representative and stable biota of the seabed and to assess if mining activities change the biodiversity of the marine environment (ISBA/19/C/17, Reg. 33(6); ISBA/18/A/11, Reg.

33(6); ISBA/16/A/12/Rev.1, Reg. 33(6)). In 2012, the ISA adopted an environmental management plan for the Clarion-Clipperton Fracture Zone, which developed and implemented "Areas of Particular Environmental Interest," an Area-Based Management Tool to protect the marine environment (ISBA/18/C/22).

Areas of Particular Environmental Interest are a configured network of "no-mining zones" strategically positioned across the Clarion-Clipperton Zone to protect a representative subset of ecosystems in the region (Figure 5.2). The strategic aims of the areas are to ensure environmentally responsible seabed mining, apply internationally accepted conservation management tools to maintain biodiversity and ecosystem structure, sustainably manage the Clarion-Clipperton Zone as a whole system, protect and conserve natural resources, and reduce the impact on the biota of the marine environment (ISBA/17/LTC/7, Section V).

To meet the management objectives, the Clarion-Clipperton Zone was divided into nine subregions (Wedding et al., 2013), and the no-mining zones were strategically placed in a stratified pattern to protect the full range of habitats and biodiversity across the zone. The zones were designed to protect ~30–50% of the Clarion-Clipperton Zone from mining. In addition, each zone needed to be large enough to maintain minimum viable population sizes for species and to capture the full range of habitat variability and biodiversity within each subregion (Smith et al., 2008). The ISA also stressed the use of adaptive management, meaning that the sizes, locations, and numbers of the no-mining zones should be modifiable based on improved knowledge about the location of the mining activity, the biota, and impacts from mining (ISBA/17/LTC, Section D).

Each Area-Based Management Tool comprises a system of rights, measures, and procedures and can be designed to be: (1) internationally, regionally, nationally, or independently managed, (2) static or dynamic in space and time, (3) completely or partially prohibitive, (4) feature specific or applicable to entire regions, and 5) sector-specific, multi-sectoral, or cross-sectoral. Thus, Area-Based Management Tools can be implemented anywhere, are designed to be flexible as new information becomes available, scaled accordingly based on the activity being managed, and governed using adaptive management as activities and priorities change over time. Due to the flexibility of their applications and adaptability across sectors, area-based management tools should be considered for managing and regulating mining activities on the Lunar surface. Utilizing the Lunar Mining Map Tool proposed in Chapter 5, we advocate for an area-based management approach for issuing exploration licenses over allotted areas of the lunar surface and for implementing policies to regulate mining activities, safeguard the lunar environment, and promote equitable access.

5.7 Managing Lunar Mining Activities Using the Lunar Mining Map Tool

To facilitate fulfilling its primary management responsibilities, we propose that the LRMA utilize the Lunar Mining Map Tool introduced in Chapter 4. The map divides a given area on the lunar surface into a grid of blocks/cells ~1km x 1km in size (Figure 5.3). Because the Lunar Mining Map Tool was developed using a stereographic projection, the size of grid blocks varies slightly since distortion of area and distance increases away from the center of projection. However, the average block size is 0.999 km^2, and there is only ~1.5% difference between the smallest (0.987 km^2) and largest

(1.002 km^2) grid block. We opted to prioritize the grid's shape since the use of straight lines is a fundamental principle in the design of terrestrial area-based management tools used in areas beyond national (Wedding et al., 2013; Sladek-Nowlis & Friedlander, 2004).

In the oil and gas and seabed mining industries, exploration licenses are allocated to an operator using a block system (Daintith and Gault, 1977; Peters and Manu, 2013; Peters & Kumar, 2013). Similarly, the Lunar Mining Map Tool's blocks/cells standardize how areas on the surface of the Moon can be issued to operators to conduct mining activities. Dividing the Moon using the block system effectively promotes functional territorialization (Lambach, 2021), where lunar spaces are parceled into temporal territories that are administered and controlled by the LRMA. The Lunar Mining Map Tool affords the following advantages for a future governance regime:

(1) Identifies locations suitable for mining and for establishing bases for operations:

Water-ice mine sites will likely require large square areas with specific environmental conditions to support the operation. For example, lunar water ice will only be present at lunar surfaces exhibiting temperatures of <112K (Vasavada et al., 1999) and in the upper meter of the lunar surface if the average temperature is <145K (Landis et al., 2022). These areas must also exhibit terrain with slopes that are navigable by mining equipment. Additionally, areas near a mine site must have the appropriate illumination and Earth visibility conditions to establish solar-electric power and communications stations and terrain flat enough to eliminate the need for significant site preparation for

construction. The Lunar Mining Map Tool has already been used to identify areas with suitable mining conditions and for establishing bases for operations (Chapter 4).

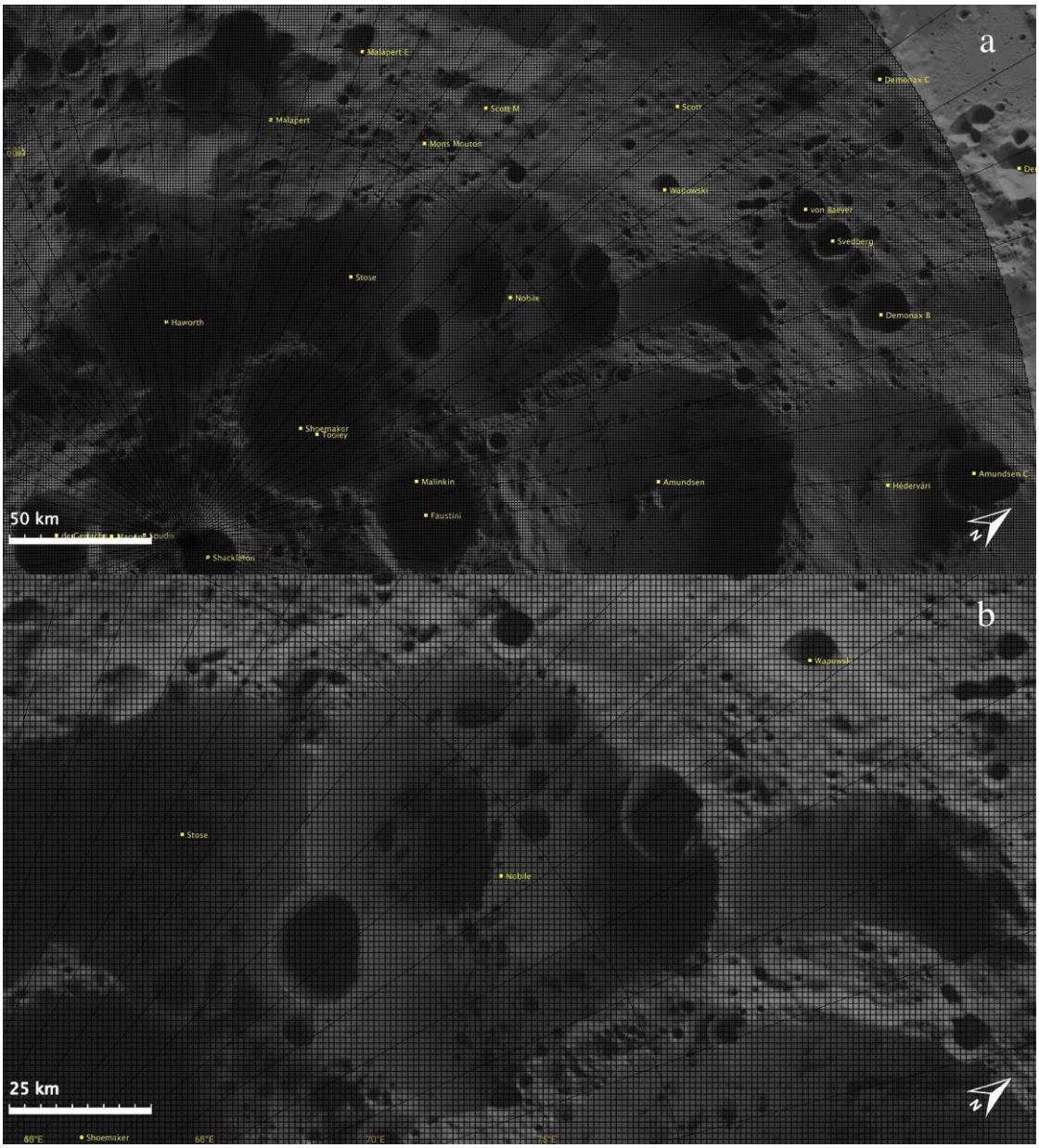

Figure 5.3 – (a) Zoomed out and (b) zoomed in views of the Lunar South Pole divided into blocks using the Lunar Mining Map Tool. The images are stereographic projections of the centered at -85.129ºN, 53.103ºE at a resolution of 512 pixels-per-degree, with the Lunar Mining Map Tool overlaid on a composite base map consisting of a global morphology mosaic (Robinson et al., 2010; Speyerer et al., 2011) and a map of the average percent illumination over an entire precession cycle (Mazarico et al., 2011). The Lunar Mining Map Tool incorporates a "block system" to divide the south pole from 80ºS poleward into a grid, where each block is ~1 km^2 in size. Doing so simultaneously

defines the boundary of the Lunar South Pole Resource System, where the Lunar Resource Management Authority can exercise its jurisdiction.

(2) Establishes the boundary of a resource system:

A common-pooled resource (i.e., lunar resource) is a natural or man-made system that is sufficiently large to make it costly to exclude potential beneficiaries from its use (Ostrom, 2015). Resource units are what is appropriated by those conducting activities in a defined resource system. Terrestrial examples include fishing grounds, groundwater basins, parking garages, lakes, and oceans (Ostrom, 1990). Defining the boundaries of a resource system is essential to establish where a governance regime's rules apply, what resources are being governed, and delineate who has the right to conduct activities in that area (Weeden & Chow, 2012). Otherwise, no one knows what is being managed (Ostrom, 1999).

In this case, the Lunar Mining Map Tool defines the land area from 80ºS to 90ºS latitude as the Lunar South Pole Resource System and contains 288,142 blocks available for use by lunar operators to conduct mining activities and establish bases for operations to support ISRU. While the Moon's regolith contains multiple components that could be considered a resource unit, the initial resource units requiring management in the Lunar South Pole Resource System are water-enriched frozen volatiles, which are the prime targets on the Moon to produce O_2 and H_2O for life support, liquid H2 for fuel, and liquid O_2 as an oxidizing agent to combine with H_2 to make rocket propellant.

(3) Enables rapid recognition of rights, compliance, and enforcement of rules, regulations, and procedures:

The use of straight-line boundaries is a fundamental principle in the design of mining claims in the United States (MyLandMatters.com, 2000) and marine protected areas implemented in Areas Beyond National Jurisdiction (Wedding et al., 2013; Sladek-Nowlis & Friedlander, 2004). Thus, the Lunar Mining Map's grid incorporates a block system with uniform and straight-line boundaries. The blocks are simple and easily recognizable, which facilitates compliance. Moreover, the block system enables a governing authority to easily delineate areas where specific regulations to be enforced, providing security to the entities conducting mining activities within the Lunar South Pole Resource System. Depending on the objective, regulations can be applied to a cluster of blocks, multiple blocks, a single block, or subblocks.

(4) Supports the recommended contract system:

In most licensing regimes, the licensing authority establishes a grid, and the prospective operator can apply for a specified number of predetermined blocks (ISBA/7/C/2). This "self-selecting" block system is used by terrestrial (Land Matters, 2014) and seabed mining companies (Mucha et al., 2013, Fig. 1) and is a common feature in offshore oil and gas licensing regimes (Dam, 1965; Salter & Ford, 2000; Ghandi & Lin, 2014). Thus, the Lunar Mining Map Tool's grid is our attempt at streamlining and standardizing how operators will notify where they will conduct prospecting activities and apply for exploration licenses for water ice on the Moon.

The governing entity can also use the Lunar Mining Map Tool's blocks to catalog and monitor where operations are being conducted in the system, take inventory of the blocks with active and inactive assets, guarantee to operators through the use of contracts

that multiple applicants are not applying to conduct mining activities in the same areas, and ensure that rights afforded to operators are secure.

(5) Can be used as a space registry's graphic interface:

Similar to the ISA's proposed register for exploitation activities (ISBA/25/C/WP.1) and the United Nations Register of Space Objects Launched into Outer Space, we recommend that the LRMA manage a registry of all objects delivered to the Lunar Surface, including all prospecting, exploration, and production equipment. The Lunar Mining Map Tool's block system simplifies this responsibility. For example, mining equipment's operational status, productivity, hazard potential, and environmental impacts could be "geo-cataloged" according to the blocks in the Lunar Mining Map Tool. All blocks under contract can also be easily managed and visualized, promoting transparency, safety, cooperation, and compliance within the system.

5.8. The Lunar Resource Management Authority's Mining Code

A necessary aspect of the ISA Mining Code is that it provides working that define the scope of the regulations, differentiate the activities being regulated, and define the environment where activities are being conducted that will be subject to said regulations (ISBA/18/A/11, Reg. 1(3a,b,c,e); ISBA/19/C/17, Reg. 1(3a,b,c,e); ISBA/16/A/12/Rev.1, Reg 1(3a,b,c,e). A future governance regime for managing lunar mining must also develop definitions for each mining activity to identify the minerals being managed, differentiate which rules, regulations, and procedures pertain to each activity, and clearly define where on the Moon regulations are to be enforced.

The terrestrial mining sector defines mineral resources as concentrations or occurrences of materials of intrinsic economic interest in or on the Earth's crust in such form, quality, and quantity that there are reasonable prospects for eventual economic extraction. The Colorado School of Mines defines space resources as "any material element or intangible property outside of Earth that has potential value because of its utilization" (Dr. Angel Abbud-Madrid, personal communication, 2022). Japan defines space resources as water, minerals, and other natural resources that exist in outer space, including on the moon and other celestial bodies (Space Resources Act, 2021). In the context of these regulations, lunar resources are defined as:

- ***Lunar Resource:*** Any extractable and recoverable naturally occurring abiotic material of intrinsic economic interest located on the lunar surface, subsurface, or exosphere.

This definition includes all components in the lunar regolith (i.e., rock and mineral fragments, brecciated material, impact and volcanic glass, native metal, solar-wind implanted volatiles, frozen volatiles) and megaregolith, bedrock, and dust suspended in the lunar exosphere. This definition excludes other "resources" relevant to mining, such as solar energy, areas of persistent sunlight and in permanent shadow, radio quiet zones, frequencies, lava tubes, vacuum, gravity, ideal landing and roving locations, orbits, etc. Each of these resources would require a separate suite of regulations in the Lunar Mining Code.

The ISA also provides definitions for each mineral resource of economic interest and each activity pertaining to each activity. Using the definitions provided by the ISA as

a blueprint, we provide working definitions of the different mining activities to be regulated by the LRMA for water ice:

- ***Prospecting:*** The searching for lunar resources in-situ in the Lunar South Pole Resource System, including the estimation of the deposit composition, size, and distribution, and their economic values.
- ***Exploration:*** The searching for lunar resources in-situ in the Lunar South Pole Resource System *with exclusive rights*, the analysis of such deposits, the use and testing of recovery systems and equipment, processing facilities, and transportation systems, and the carrying out of studies of the environmental, technical, economic, commercial and other appropriate factors that must be considered prior to exploitation.
- ***Exploitation:*** The recovery for commercial purposes of lunar resources in-situ in the Lunar South Pole Resource System *with exclusive rights* and the extraction of minerals therefrom, the construction and operation of mining equipment, the construction and use of processing plants and transportation systems, the production and marketing of water-ice and other byproduct volatiles, minerals, and metals, as well as the decommissioning and closure of mining operations.

5.8.1 A Notification System to Prospect for Lunar Water Ice

The first phase in lunar resource development is orbital prospecting. The second will be in-situ prospecting. Like seabed mining, lunar water ice prospecting campaigns will identify the locations where ice is present in economic quantities. Prospecting regulations should remain as limited as possible to attract investment and safeguard the universal freedom to conduct scientific research in ABNJ, which aligns with the OST's

freedom of scientific investigation (Outer Space Treaty, 1967, Art. I). However, rules and norms should be established for safe and orderly prospecting, equitable access, and to safeguard the lunar environment. Based on the ISA's Mining Code, we propose the following regulations and freedoms to manage prospecting activities (Table 5.1):

Table 5.1 – Proposed Regulations and Freedoms on Prospecting for Water Ice in the Lunar South Pole Resource System

Proposed Regulations and Freedoms on Prospecting for Water Ice in the Lunar South Pole Resource System

1. Operators do not receive exclusive rights over an area on the Moon during prospecting but can recover a "reasonable" quantity of its resources necessary for testing and initial characterization of the deposit and deposit environment.

2. No spatial or temporal limits are imposed on prospecting activities.

3. Multiple actors can conduct prospecting activities within the same block but must exercise due regard to the rights, duties, and freedoms of other States' activities on the lunar surface.

4. Samples and data acquired during prospecting can be deemed proprietary to the operator.

5. An operator (State, private company, joint venture, or the Lunar Mining Consortium) must notify the Lunar Resource Management Authority of its intention to engage in prospecting. Each notification shall be in the form of a contract between the applicant and the LRMA and contain the following:

   (a) Information concerning the applicant, including:
   - The applicant's name and nationality/nationalities; if the applicant is a juridical person (i.e., State, a private company, or the Lunar Enterprise), identify its place of registration and principal place of business.
   - Address and contact information of the instrument operator(s) on the campaign,
   - If the application contains a partnership or a consortium of entities, each member must submit the relevant information in 7(i-ii) for each party.
   - A certificate of sponsorship issued by a State of which it is a national or by which or whose nationals effectively controls the operation.

   (b) Information concerning delivery of the prospecting payload, including:
   - The proposed date, time, and location of landing and deployment of the payload

   (c) A general description of the proposed prospecting activities, including:
   - The coordinates (in the form of mining blocks/cells prescribed by the LRMA) of the broad area where prospecting will be conducted,
   - The start date and approximate duration of the prospecting campaign,
   - A general description of the equipment and methods expected to be used during prospecting, along with other relevant information about the characteristics of the technology, excluding proprietary information.

6. Operators shall take necessary measures to prevent, minimize, and limit effects on the lunar environment through the application of the precautionary approach and best environmental practices, including:
   (a) The collection of environmental baseline data;
   (b) The development and implementation of monitoring programs;
   (c) The submission of annual reports detailing the effects of exploration activities on the lunar environment and the strategies to reduce such impacts.

7. Each notification shall provide written undertakings that the operator will:
   (a) Cooperate, comply, and accept as enforceable the rules, regulations, and procedures adopted by the Lunar Resource Management Authority;
   (b) Adopt the precautionary approach and best environmental practices in the design and use of instrumentation and the design and planning of its operations, take necessary measures to prevent, minimize, and limit the effects of their activities on the lunar environment, develop and implement monitoring programs, collect environmental baseline data, and submit annual reports detailing the effects of prospecting on the lunar environment and their strategies to reduce such impacts;
   (c) Refrain from conducting activities in Lunar Preservation Areas, Impact Reference Zones, and areas already under contract;
   (d) Release non-proprietary data collected during prospecting to the public to enable equitable and open access to scientific data and encourage sustainable development of lunar surface operations;
   (e)The operator must act in "due regard" of other actors conducting operations in the Lunar South Pole Resource System and is liable for any damages to other assets and the lunar environment;
   (f) The operator will release non-proprietary prospecting and environmental data to the public to enable equitable use and sustainable development of lunar surface operations;

8. All information submitted by the operator will be cataloged in a Lunar Mining Register managed by the Lunar Resource Management Authority. All information submitted by the Contractor will be public in support of transparency except voluntarily disclosed confidential information. The Lunar Mining Register will also manage a Mining Map Tool to aid in the spatial planning of mining activities on the lunar surface.

9. These regulations are to be interpreted and applied together with The Outer Space Treaty, The Rescue Agreement, The Liability Convention, The Registration Convention, and The Moon Agreement.

Regulations 1 and 2 in Table 5.1 align with Article I of the Outer Space Treaty, which maintains that the exploration and use of the Moon shall be the province of all [hu]mankind, that there shall be free access by all States to all areas of the Moon, and that there shall be freedom of scientific exploration (Article I). Regulation 3 supports the due regard principle in Article IX of the Outer Space Treaty.

Regulation 4 departs from the ISA's prospecting regulations, which prohibits the recovery of minerals for commercial use. Based on a recent precedent, where NASA vowed to purchase the rights of future moon samples recovered from private companies (Wall, 2020), our recommendation supports the commercial use of samples and data derived during prospecting to promote the development of a nascent lunar economy. However, future policy-makers should consider that if the prospecting phase becomes commercialized and regulations are limited, the pioneering companies derived from spacefaring nations will be the only actors capable of reaping the benefits of prospecting which could lead to monopolization. While it should be the responsibility of a future regime to support the development of space resources, some form of regulations on the commercial use of samples recovered during prospecting and its data is likely required to ensure equitable use of the lunar surface. The commercialization of prospecting data and samples also begs the question as to whether spatial and temporal regulations should be imposed on prospecting activities since the data and material recovered can be commercialized and potentially monopolized by pioneering prospectors. However, because only a "reasonable" quantity of material can be recovered during prospecting (Regulation 1), temporal and spatial limits are not obligatory at this stage of development.

Our proposal requires an operator to notify the LRMA of its intention to engage in prospecting activities in the form of an application contract plan of work (Regulation 5). Within the notification, the prospector will provide written undertakings that she will abide by the rules set forth by the LRMA (Regulation 7). This provides a streamlined and standardized procedure to help manage lunar resource development. Information required

in the notification facilitates the LRMA's obligation to develop a comprehensive register (Regulation 8) of all space objects and activities conducted on the lunar surface.

Similar to the ISA's Mining Code (ISBA/19/C/17, Reg. 5; ISBA/16/A/12/Rev.1; Reg. 5; ISBA/18/A/11, Reg.5), we recommend lunar prospectors minimize or eliminate adverse environmental impacts resulting from their prospecting activities (Regulation 6). Under Regulation 6, operators must employ the precautionary approach in their mission planning and instrument development. Regulatory oversight typically comes after the public recognizes the adverse impacts of human activity on the environment. (Kramer, 2020). The precautionary approach is a widely accepted principle central to achieving sustainable development that aims to ensure adequate environmental protection by taking early action in response to potential environmental threats, even in the context of scientific uncertainty (1992 Rio Declaration; Jaeckel, 2017).

It remains uncertain whether lunar prospecting activities will cause severe irreversible damage to the lunar environment. However, rather than adopting regulations after irreversible environmental damages have been observed on the Moon, Regulation 6 requires prospectors to collect environmental baseline data and implement monitoring programs a priori in anticipation that some adverse environmental effects will likely emerge from lunar mining activities.

Annual reports will be paramount for lunar resource management, for they serve as a form of self-compliance and provide information to future prospectors on reducing the effects of their mining activities on the lunar environment. Thus, we recommend that prospectors be required to submit annual reports to the LRMA. The reports describe the status of the prospecting campaign, report on the effects of prospecting on the lunar

environment, and their plans to reduce such impacts. If such effects can be identified during the prospecting phase, they can be addressed and reduced prior to the exploration phase.

While restricting actors from conducting prospecting activities in certain areas arguably violates the Outer Space Treaty, we seek to develop a new regime that promotes the responsible development of lunar mineral resources while safeguarding the lunar environment. If operators were allowed to conduct prospecting activities within an area already under contract, the LRMA could not guarantee that an operator's investments are secure. Without that security, actors will likely not invest in lunar resource development. Furthermore, if prospecting is allowed in Lunar Preservation Areas (see Section 5.8.8), the area would no longer be undisturbed by human activities. Thus, some restriction is necessary to achieve development, sustainability, and equal access goals within the Lunar South Pole Resource System.

Under the management of the LRMA, the process for initiating a prospecting campaign could go as follows. First, the prospector submits a notification of intent to engage in prospecting containing the information in Regulation 5, including the blocks where they will conduct their activities. The LRMA would review the notification to ensure that the operator provided all the necessary information and that her contract is compliant with the regulations established by the LRMA. Once approved, the LRMA will catalog the blocks listed in the notification in a register and delineate them in the Lunar Mining Map (Figure 5.4). Doing so supports a level of transparency underlined in the Artemis Accords (Section 4) that will enable actors on the surface of the Moon to act with "due regard to the corresponding interests" of other actors (Outer Space Treaty,

1967, Art. IX). Moreover, the provision of prospecting areas by the LRMA could reduce the propensity of disputes related to liability and compliance (Outer Space Treaty, 1967, Art. VI-VII), prevent harmful interference of future actors' activities on existing mining activities (The Artemis Accords, Section 11), as well as provide geographical information to other commercial actors seeking to provide other services (i.e., power, communications, launch services), promoting international cooperation (Outer Space Treaty, 1967, Art. XI).

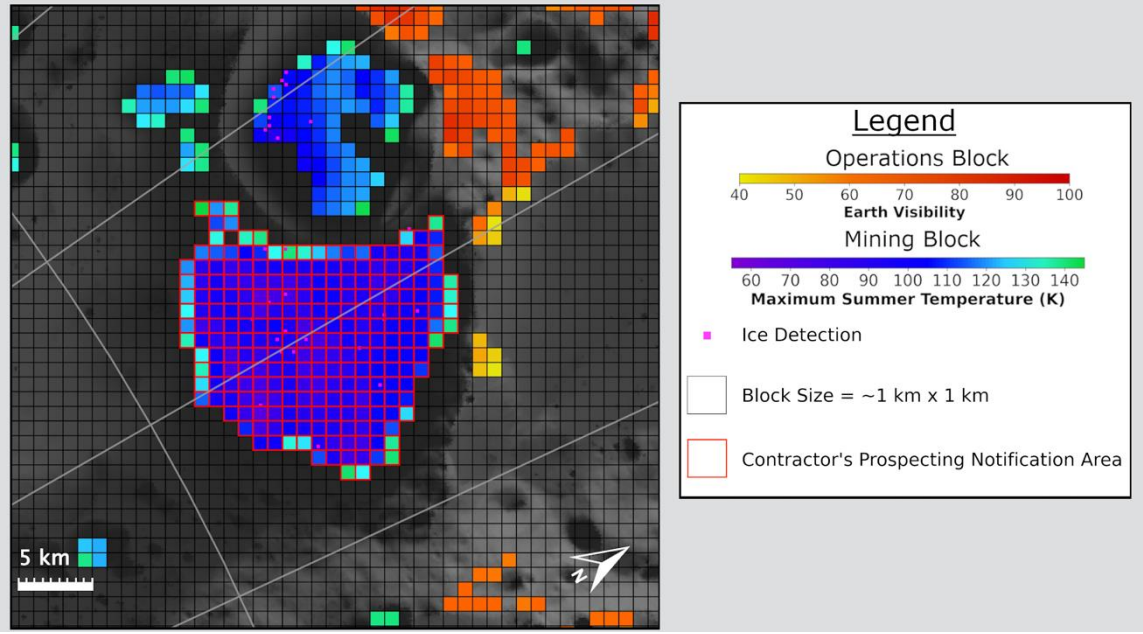

Figure 5.4 – Depiction of an operator's prospecting notification using the Lunar Mining Map Tool. In the notification to the LRMA, a prospector would provide the index number and center coordinates of the blocks where they intend to conduct prospecting activities. The LRMA would catalog the blocks and the prospector's information submitted in their notification in a mining register. The Lunar Mining Map Tool blocks selected for our hypothetical prospecting notification are bordered in red and are derived from a set of blocks classified as suitable for mining (Chapter 4). The image is centered at -84.52ºN, 59.962ºE with a resolution of 2,048 ppd. The Lunar Mining Map Tool is overlaid on a composite base map comprised of a global morphology mosaic (Speyerer et al., 2011) illumination data (Mazarico et al., 2011).

5.8.2 Lunar Water Ice Exploration Contracts

Inspired by the ISA's Mining Code, the licensing system proposed by Tronchetti (2008), the Beeby Proposal (Raclin, 1986), and the Hague International Space Resources Working Group's Building Blocks, we advocate for an area-based contract system where the LRMA issues out licenses to operators to conduct exploration activities within the Lunar South Pole Resource System. A license grants an operator temporary but exclusive rights over an allotted area of the lunar surface to explore or exploit the Moon for water ice. Exploration licenses can only be issued within a resource system defined by the LRMA (e.g., the Lunar South Pole from 80ºS-90ºS), and an operator can only conduct exploration activities within the approved area under the contract.

The main argument for a contract (license) system is to transform the Moon from a 'first come, first served' open access regime into a regime that can be responsibly and predictably managed and protect the effort and investment of operators (de O. Bittencourt Neto et al., 2020). A contract system is advantageous for the development of lunar resources because contracts fill regulatory gaps in regimes with thin regulatory structures, supplement or create conditions or constraints on activities, can establish adequate revenue sharing, and require accountability and responsibility for both anticipated and unanticipated environmental and social impacts of mining (Ochoa, 2021). In addition, contracts offer mutability, flexibility, and nimbleness relative to statute-based governance approaches, making them better equipped to create an enforceable regime that incorporates novel concepts (Ochoa, 2021) that will inevitably be required to govern mining on the Moon.

The proposed system requires an applicant to submit a contract for approval to the LRMA containing a plan of work to conduct exploration activities for mineral resources

in the Lunar South Pole Resource System. Once the Lunar Council approves the application based on recommendations made by the Lunar Legal and Technical Commission, the operator receives a license that grants exclusive but temporary rights to conduct exploration activities within the areas under contract, and property rights to the mineral resources extracted from the contract area. The contract also provides security of tenure, meaning that the contract cannot be suspended or amended unless the operator violates the terms of the contract. (ISBA/19/C/17, Annex IV, Sect. 2). Similar to the ISA (ISBA/19/C/17, Annex IV, Sect. 22), the rights and obligations of the Contractor under the contract plan of work may be transferred in whole or in part with the consent of the LRMA. Our proposed regulations on exploration for mineral resources in the Lunar South Pole are listed in Table 5.2.

Table 5.2 – Proposed Regulations and Freedoms on Exploration Activities for Water Ice in the Lunar South Pole Resource System

Proposed Regulations and Freedoms on Exploration Activities for Water Ice in the Lunar South Pole Resource System
1. An approved exploration contract grants a license to conduct exploration activities to the blocks under contract
2. The LRMA will ensure that no other entity operates in the contract area in a manner that might interfere with the operator's exploration activities.
3. Spatial and temporal limits are imposed on exploration contracts (Table 5.3)
4. Material and data obtained during the exploration can be deemed proprietary and sold for profit.
5. Operators shall take necessary measures to prevent, minimize, and limit effects on the lunar environment vis-à-vis the same measures as set forth in Table 1, Regulation 6. In addition, operator's conducting exploration activities must establish Impact Reference Zones (Table 5.6)
6. Each application must contain the same information required in the application to conduct prospecting activities (Table 5.1, Reg. 5-6). In addition, the operator must provide information related to the exploration area, including:
The boundaries of the exploration area:

(a) The applicant must attach a list of the center coordinates of each block in the Lunar South Pole Resource System where they wish to conduct exploration activities,
(b) Information on the resource units being targeted during the exploration campaign and their intended use cases.
(c) A map and prospecting data on the physical and geological characteristics of the exploration area and data showing the abundance, grade, and elemental contents of water-,

Information related to the exploration plans, including:
(d) A general description and schedule of the exploration mission for the first five years of exploration, including the date of commencement, timeline, and schedule of the proposed exploration activities and critical requirements,
(e) A schedule of anticipated yearly expenditures for the first five years of exploration
(f) A general description of the equipment and methods expected to be used during exploration, along with other relevant information about the characteristics of each technology, excluding proprietary information.

7. Information related to measures that will be taken to safeguard the lunar environment:
(a) A preliminary impact assessment of the potential effects of the applicant's exploration activities on the lunar environment based on prospecting data
(b) A proposal for a monitoring program and environmental baseline studies that will be employed using the Impact Reference Zones defined by the operator that will enable the assessment of the potential effects of the proposed exploration activities on the lunar environment.
(c) Prospecting data that could be used to establish an environmental baseline prior to exploration.

8. Each application must contain information related to the financial and technical capabilities of the operator, including:
(a) Sufficient information to enable the Lunar Council to determine whether the applicant is financially and technically capable of carrying out its exploration plans.
(b) A general description of the applicant's previous experience, knowledge, skills, technical qualifications, and expertise relevant to its mining activities.

9. The operator shall provide in their application the same written undertakings provided in (Table 5.1, Reg. 7).

10. Excluding any proprietary information, all information submitted by the operator will be cataloged in a Lunar Mining Register managed by the Lunar Resource Management Authority. The information will be made public in support of transparency except voluntarily disclosed confidential information.

5.8.3 Spatial and Temporal Regulations on Exploration Contracts

Because the exploration phase is meant to be a preparatory step prior to exploitation, lunar exploration contracts should only be as sufficiently large and last as long and as needed for an operator to adequately characterize their exploration area and

define which blocks will be used for a mine site. In addition, appropriation of the lunar surface is prohibited under international law (Outer Space Treaty 1967, Art. II) and sustainable mining practices emphasize extracting only what is presently needed without compromising the ability of future generations to meet future needs (World Commission on Environment and Development, 1987). Thus, we propose spatial and temporal constraints on lunar exploration contracts.

Such constraints should be imposed to prevent the monopolization of a particular area by a single operator (ISBA/7/C/2). Without this regulation, the first spacefaring nations with the knowledge and technological capabilities to conduct exploration activities could apply for an excessive number of blocks with high abundances of water ice that are unnecessary for their activities as a way to control resources and block future companies from conducting mining activities. Imposing temporal and spatial constraints on lunar exploration contracts would also inhibit the possibility of "lunar land grabbing" akin to what has been observed on Earth (Zalik, 2015,2018; Margulis et al., 2013).

To estimate the maximum number of mining blocks for a lunar water ice exploration contract, we use a conservative estimate of 0.5 wt% and an upper bound of 5.6 wt% based on (Colaprete et al., 2010) for the amount of water ice present in the lunar regolith's upper meter. Using densities of ~920 kg/m^3 (Gertsch et al., 2006) and 1,655 kg/m^3 (Mitchell et al., 1974; Carrier et al., 1991) for water ice and bulk lunar regolith, respectively, we estimate that the upper meter of one mining block could contain ~$9.0x10^3$–$9.7x10^4$ m^3 and ~8.2x106–$8.9x10^7$ kg of ice, assuming that the ice is evenly disseminated in the upper meter. However, water ice deposits will likely be patchy and heterogeneously distributed.

While the demand for lunar water ice is uncertain, Kornuta et al. (2019) identified a near-term annual demand of 2.45×10^6 kg processed lunar water per year. Using our assumptions above, a lunar operator could fulfill this demand for ~3–40 years from one mining block. In all likelihood, volatile deposits within each mining block will be unevenly distributed due to the extraordinary topographic and illumination conditions at the lunar poles. Nonetheless, our calculations provide an initial estimate of how much water ice one mining block could supply.

Although it is difficult to determine how much land will be required for a mine site, we recommend that the initial number of mining blocks per exploration contract be limited to 60. Using our high-level estimations, 30 km^2 of suitable mining area would sustain a mining operation for ~90-1,200 years based on the demand put forth by Kornuta et al. (2019). To allow an operator to identify 30 km^2 that they would want to develop as a mine site, they are granted 60 blocks. The 50% of unused licensed area must be relinquished back to the Lunar South Pole Resource System (Section 5.8.7) to prevent lunar land grabbing and promote equitable access to the Moon's resources.

We turn to the Lunar Polar Volatiles Explorer (LPVE) Mission Concept study (Shearer and Tahu, 2010) to establish a preliminary exploration contract duration. The LPVE mission incorporates a rover concept powered by an Advanced Stirling Radioisotope Generator that is capable of traversing 174 km and acquiring 460 total samples in approximately one year (Shearer and Tahu, 2010). The primary science objectives of the mission are analogous to the likely requirements of future mining operators to define a suitable mine site, including determining (1) the form, species, and chemical composition of the volatile compounds at the lunar poles and (2) the

vertical/lateral distribution of volatiles in the lunar polar regolith (Shearer and Tahu, 2010). Assuming an operational scenario where an LPVE-like rover traverses the blocks in their exploration contract in the manner shown in Figure 5.5, a lunar operator could adequately explore ~5-6 mining blocks in their contract per year. A 60-block contract area could be characterized in ~11 years, excluding transit and downtime due to unfavorable environmental conditions such as periods without access to power.

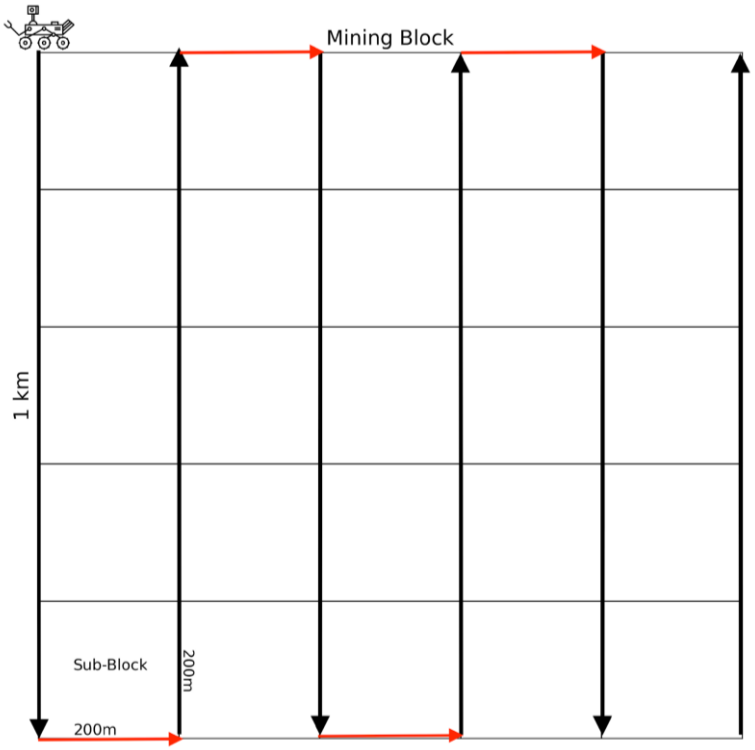

Figure 5.5 – Example traverse and sampling scenario for one mining block in a lunar exploration contract. The rover would traverse 1 km down track (black arrows) and 200 m across track (red arrows) in an evenly spaced manner, sampling every 200 m. Prospecting in this manner would require the rover to traverse ~31 km and would provide 36 samples for each block.

Because all aspects of the ISRU value chain are likely to improve significantly over the coming decades, it is reasonable to assume that a lunar operator could adequately characterize a 60-block exploration contract in 30 years to a reasonable level

of geologic confidence to establish a mine site. Therefore, we recommend the following spatial and temporal regulations for lunar exploration contracts in Table 5.3.

Table 5.3 - Spatial and Temporal Constraints for Mining Blocks in Lunar Exploration Contracts

Spatial and Temporal Constraints for Mining Blocks in Lunar Exploration Contracts
1. An exploration contract shall be approved for no more than 30 years. Upon the contract's expiration, the operator can apply for an exploitation contract or renounce their rights to the area covered in their work plan.
2. The area granted to the operator shall be comprised of not more than 60 mining blocks (60 km^2), prior to relinquishment.
3. The mining blocks covered in the exploration contract must be arranged in clusters. (i) Each cluster of blocks must contain at least 2 contiguous blocks. (ii) Two blocks that touch at any point are considered to be contiguous. (iii) Clusters need not be contiguous, but shall be within a proximate distance and confined within a geographical area of 20 kilometers by 20 kilometers, where the longest side does not exceed 20 kilometers in length.

In addition to spatial and temporal constraints, the ISA required the blocks in exploration contract areas be arranged in clusters (ISBA/18/A/11, Annex II, Sect. 19). The ISA has not reported why this measure was imposed on seabed operators. However, we believe this is meant to constrain the sprawl of a seabed miner's activities, reducing the likelihood of an incident with another contractor and constraining the effects on the marine environment. Thus, we also propose requiring an applicant to arrange blocks in their exploration contract in clusters close in proximity.

5.8.4 Lunar Reserved Areas and Joint Venture Arrangements

The ISA established the parallel system to ensure equitable access to and benefit sharing of the seabed for developing states (UNCLOS, 1982, Art. 153, Annex III Art. 8-

9). The system was originally developed to lower the threshold for an interested developing state to actively participate in mining and be involved in collective natural resource management (Jaeckel et al., 2016). To obtain an exploration contract, a seabed contractor must include data and information for two sites of estimated equal economic value within their exploration contract capable of allowing two mining operations (UNCLOS, 1982, Annex III Article 8; 1994 Agreement, Annex Section 1(10)). If two sites can be identified, the ISA grants an exploration license for one of the sites to the operator, while the second becomes a Reserved Area, which is held in a site bank by the ISA. The advantage of Reserved Areas for developing countries is that they can apply for exploration and exploitation countries without taking on the costs and efforts associated with locating a potential mine site (Jaeckel et al., 2016). As of 2019, Reserved Areas have been allocated to six operators from developing countries.

While the regulations for polymetallic nodules require applicants to contribute a Reserved Area, companies wishing to explore and exploit polymetallic sulfides or cobalt-rich crusts are offered a choice between contributing a Reserved Area or offering equity interest in a joint-venture arrangement with the Enterprise (ISBA/18/A/11, Reg. 16–19; ISBA/16/A/12/Rev.1, Reg. 16–19). If the contractor chooses the latter, they must share between 20-50% of its profits obtained during the exploitation phase. The rationale behind this measure is that prospecting for polymetallic sulfides and cobalt-rich crusts is technologically much more difficult than polymetallic nodules, making it difficult to envision a situation where an operator would be financially willing to conduct the exploration work necessary to establish two mine sites (Jaeckel, 2020, 2022; ISBA/7/C/2).

To promote equitable access and the sharing of the benefits of lunar resources, we recommend that the LRMA require an operator to either (1) contribute a Reserved Area or (2) enter into an interest/joint venture agreement with the Lunar Mining Consortium. If an operator elects to contribute a Reserved Area, its maximum allotted contract area doubles from 60 to 120 blocks. As a tradeoff for allowing the first lunar mining companies to choose their exploration contract areas on a first-come-first-served basis, they must divide the contract area into two equal areas with sufficient extractable resources to develop two mine sites. One area will be designated as a Reserved Area for use by a developing country or non-spacefaring nation, and the other will be granted to the company. The company would have to provide sufficient prospecting data from the LRMA verifying the division of the contract area. Such data affords the Legal and Technical Commission to make a scientifically sound recommendation to the Lunar Council granting one site to the applicant and the other as a Reserved Area.

If an operator elects to offer an equity interest in a joint venture arrangement, the Lunar Mining Consortium will receive a share of the profits from the operator's future mining activities. However, the applicant would be limited to an initial contract area of 60 blocks. Our recommended exploration contract requirements for contributing a Reserved Area or entering into a joint venture arrangement with the Lunar Mining Consortium are listed in Table 5.4.

Table 5.4 - Exploration Contract Requirements for Reserved Areas and Joint Venture Arrangements in Lunar Exploration Contracts.

Exploration Contract Requirements: Reserved Areas and Joint Venture Arrangement in Lunar Exploration Contracts
Lunar Reserved Area
(1) If a lunar operator elects to contribute a Reserved Area, the number of blocks granted to the applicant is limited to a maximum of 120 blocks.

(2) The operator must divide its exploration contract into two equal areas with sufficient estimated commercial value to allow two mining operations using the block system provided by the LRMA or using subblocks that are equal in size. A Lunar Reserved Area does not need to be a single continuous area, but the mining blocks must be arranged in "clusters" and be reasonably close in proximity.

(3) The application must contain sufficient information and data available to the applicant for the Lunar Resource Management Authority to designate a Reserved Area, including:
(a) A list of subblock coordinates and associated map dividing the total area into two parts of equal estimated commercial value;
(b) Data on the location, survey, and evaluation of volatiles in each subblock, including a description of the prospecting technologies and techniques utilized by the applicant to characterize the deposit,
(c) A map of the geological and physical characteristics, such as mineralogy, temperature, illumination conditions, local topography, and radiation levels.
(d) A map showing remotely sensed and in-situ data used to determine the lateral and vertical extent of water ice.
(e) Average compositional information about the polar volatiles, including contaminant species
(f) A calculation and statistical analysis utilizing the data submitted proving that both areas contain recoverable water ice deposits of equal estimated commercial value.

(4) The Lunar Resource Management Authority will determine which area will be granted to the operator and which will be designed as a Reserved Area.

(5) Data associated with the operator's exploration area will not be disclosed to the public.

Joint Venture Arrangement
(1) If an applicant elects to enter into a joint arrangement, The Lunar Mining Consortium shall obtain a percentage of the equity from the applicant's future exploitation activities. The equity arrangement shall be negotiated between the two parties.

Figure 5.6 displays a hypothetical scenario of the exploration contract application process and how the Lunar Mining Map Tool could be used to administer such a process. Suppose that after conducting prospecting activities within their notification area (Figure 5.6a), the operator submits an application to the LRMA and elects to contribute a Reserved Area. They would be granted an exploration license to explore 120 mining blocks (Figure 5.6b). Next, the operator would indicate the center coordinates of the

blocks that divide the initial contract into two parts of equal estimated commercial value (Figure 5.6c) according to the requirements in Table 5.4. Upon review, the LRMA would grant the applicant an exploration license over one part and designate the other as a Reserved Area (Figure 5.6d).

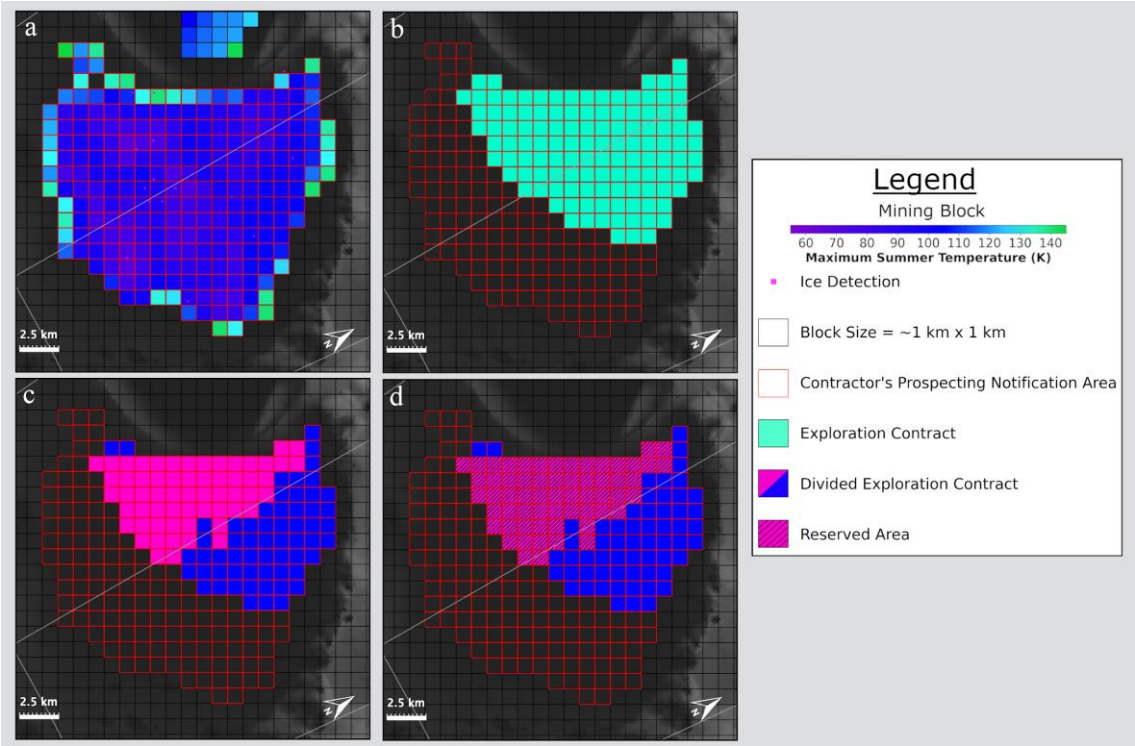

Figure 5.6 – Depiction of how the Lunar Mining Map Tool supports the recommended contract system for issuing exploration licenses to operators. Each Plate (a–d) displays the Lunar Mining Map Tool overlaid on a composite base map consisting of a global morphology mosaic (Speyerer et al., 2011) and average percent illumination data (Mazarico et al., 2011). Plate (a) displays suitable mining blocks identified in Chapter 5, which are colored according to their average maximum temperature in the summer, ice detections reported by Li et al. (2018), and the blocks of a hypothetical operator's prospecting area outlined in red. Plate (b) displays a hypothetical exploration contract reported by an applicant to the LRMA. The center coordinates of each block would be submitted to the LRMA in the applicant's contract. Plate (c) shows the division of the hypothetical exploration contract into two areas of equal estimated commercial value (pink and blue blocks). Plate (d) displays the 60-block contract area issued by the LRMA to the applicant (blue) and the Reserved Area (pink with diagonal black lines) to be used by a developing state/future spacefaring nation.

In this theoretical example, the exploration contract was divided into two parts using temperature and slope data. However, multiple variables will need to be incorporated to divide a contract area into two areas of equal estimated value, including the locations, resource estimates, grade or quality, extent and variability and other geological characteristics of the water ice, number of byproducts, proximity to areas with suitable illumination conditions, visibility with Earth, proximity to processing plants, etc. This will likely result in two contracts broken up into multiple clusters rather than two mostly contiguous areas.

5.8.5 A Relinquishment Procedure for Lunar Exploration Contracts

In the oil and gas industry, private companies granted exploration contracts are frequently obligated to surrender a self-selected portion of their exploration license in a scheduled manner (Daintith and Gault, 1977). Similarly, a seabed mining contractor is legally obligated by the ISA to progressively relinquish portions of its original exploration contract area (ISBA/25/LTC/8). The relinquished blocks revert back to the Area and can be used in future seabed mining contracts. The relinquishment procedure allows for "first movers" investing significant amounts of capital in seabed mining to explore an adequate number of blocks to identify a suitable exploitation site, while also preventing them from "grabbing" large swaths of unused that could otherwise be utilized by future miners.

The ISA designed the relinquishment protocol to be flexible, with the size, area, and schedule of relinquishment depending on the resource under contract. For example, to explore for cobalt-rich ferromanganese crusts, an operator is granted a maximum of

150 blocks 20 km^2 in size. By the end of the eighth year of its contract, at least one third of the original allocated contract area must be relinquished and two thirds by the end of the tenth year or when the company applies for exploitation rights (ISBA/18/A/11, annex).

The ISA recommends that relinquishment be carried out by subdividing the primary blocks under contract into cells using the equal area principle (ISBA/25/LTC/8). Using the ISA's recommendations, the China Ocean Mineral Resources Research and Development Association began its relinquishment process by subdividing its primary blocks into approximately equal-sized subblocks (Figure 5.7). To determine which portions of their contract area to relinquish and the order of their relinquishment, a suite of evaluation parameters were used to evaluate and classify each subblock into "non-resource areas," "unclear areas," and "orebodies" (Yang et al., 2022). The criteria was then used in a scheduled, step-by-step method to define which subblocks to reserve and relinquish back to the Area (Figure 5.7). The contractor must provide the ISA with a list and map of the relinquished areas. Entire blocks or individual subblocks can be relinquished.

To prevent "lunar land grabbing" and operationalize the common heritage principle, we propose that the LRMA implement a similar area-based relinquishment procedure for lunar exploration contracts according to the requirements in Table 5.5.

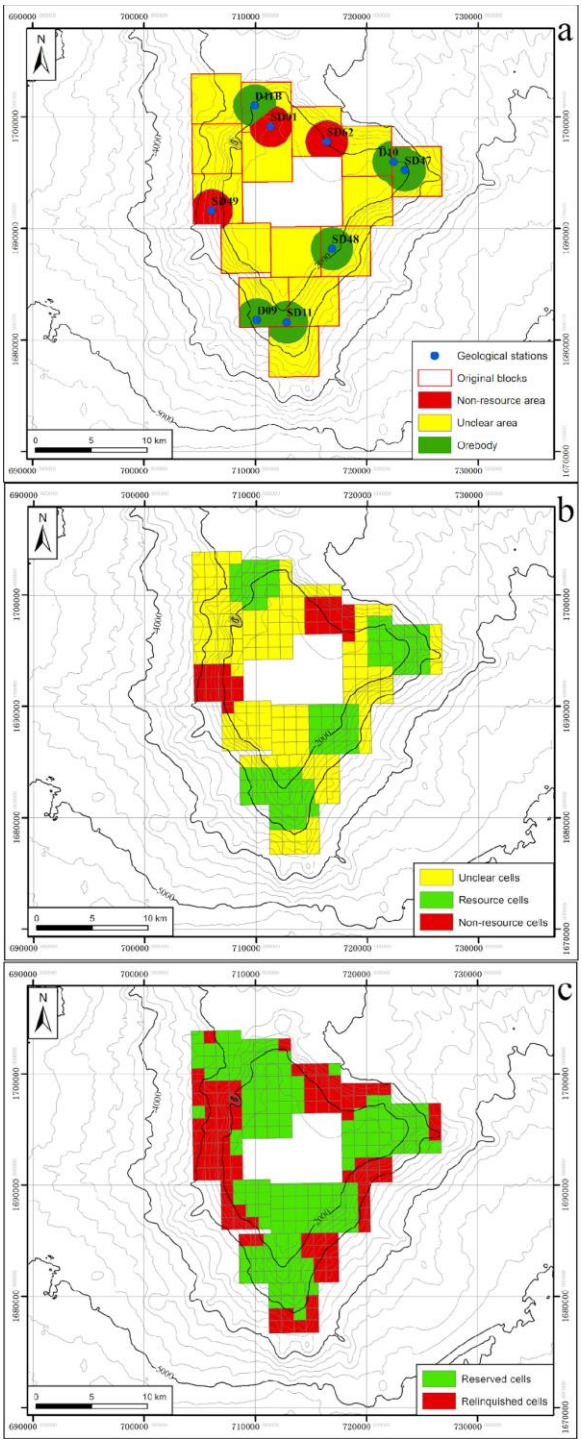

Figure 5.7 – (a) A portion of China Ocean Mineral Resources Research and Development Association's exploration contract for cobalt-rich ferromanganese crusts. The cobalt-rich crusts are located on guyots east of the Mariana Trench. Each primary block is ~20 $km^{2,}$ and the colors represent whether the block area is an orebody, a non-resource area, or an unclear area. (b) Example of how the contract area was divided into subblocks and classified according to their mining potential. The classification scheme

determined which blocks to relinquish and the order of their relinquishment. (c) Depiction of the blocks reserved by COMRA for further exploration and eventual exploitation and those relinquished back to the Area. Images reproduced from Yang et al. (2022).

Table 5.5 – Requirements for the Relinquishment of Unused Blocks in Lunar Water Ice Exploration Contracts

Requirements for the Relinquishment of Unused Areas in Lunar Exploration Contracts
1. To relinquish portions of its exploration contract back to the Lunar South Pole Resource System, the operator must divide its blocks using the equal area principle.
2. The operator must relinquish parts of its original contract area according to the following schedule: (i) Phase 1: By the end of the tenth year, the operator must relinquish 25% of the original contract area back to the Lunar South Pole Resource System. (ii) Phase 2: By the end of the twentieth year, the operator must relinquish at least 50% of its original contract area. (iii) Phase 3: By the end of the thirtieth year, the operator shall apply for a plan of work for exploitation from the remaining 50% of its original exploration contract area. An operator has the preference and priority before other applicants to submit a plan of work in the same blocks within the remaining contract area for an exploitation license to establish a mine site.
3. Relinquished areas revert back to the Lunar South Pole Resource System. Once relinquished, the blocks are available for use by another operator.

Building on our hypothetical exploration contract displayed in Figure 5.6, suppose that the LRMA granted an exploration license to a mining company for the 60 blocks in Figure 5.8a. The proposed relinquishment process would require an operator to progressively relinquish 50% of its original contract area, leaving 30 blocks (or the equivalent square area of subblocks) to establish a mine site. For simplicity, the operator would subdivide each primary block in her exploration contract using the equal area principle (Figure 5.8b).

By the end of the tenth year of the contract, the operator must relinquish 25% of its original contract area back to the Lunar South Pole Resource System (Figure 5.8c), and by the end of the twentieth year, it must relinquish at least 50% of its original

contract area (Figure 5.8d). By the end of the thirtieth year, the operator will have relinquished its required number of blocks back to the Lunar South Pole Resource System, and the exploration contract expires. The operator would provide the coordinates of the relinquished blocks to the LRMA, who will then catalog and display them in the Lunar Mining Map Tool, promoting transparency in the development of lunar resources. Similar to seabed mining contractors, if the lunar operator chooses, she will have priority rights to apply for an exploitation contract from its remaining contract area (ISBA/18/A/11, Reg. 26), so long as their activities do not have serious harmful effects to the lunar environment or prevent other operations from being conducted within other approved contract areas.

In our hypothetical example, we relinquished areas based on average temperature (a proxy for resource potential), average slope (a proxy for navigability), and distance from the best operations blocks (a proxy for accessibility) identified by Hubbard et al. (*in preparation*). In reality, each mining operator will need to establish their own evaluation parameters using extensive data acquired during prospecting and exploration.

If the LRMA adopts the principle of adaptive management, the relinquishment requirements can be updated once our knowledge of lunar water ice and mining technologies improves. For example, upon improved knowledge of how much water ice is available in the Lunar South Pole Resource System and how much time is required to characterize a mining block adequately, the regulations in Table 5.5 can be updated accordingly. Moreover, once we can determine the amount of mining blocks that will be required to sustain a mine site, the number of blocks in an exploration contract (Table

5.3) can be updated accordingly. Such a responsibility would fall under the purview of the scientific and technical experts on the Lunar Legal and Technical Commission.

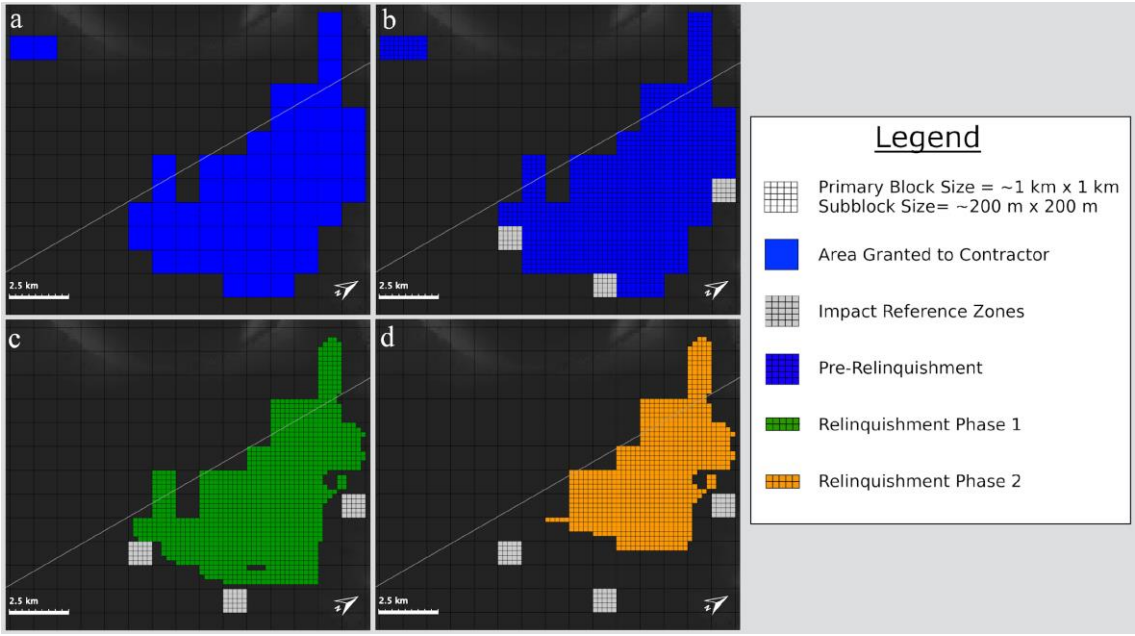

Figure 5.8 – A theoretical example of how operators can use the Lunar Mining Map's block system to relinquish portions of their exploration contracts back to the Lunar South Pole Resource System. The process begins when a mining company is granted a license to conduct exploration activities (a). Under our recommendations, an operator shall only be allowed a maximum of 30 blocks (30 km^2) to establish a mine site, which would be able to sustain a mining operation based on our assumptions and the demand put forth by Kornuta et al. (2019). Rather than limiting an operator to 30 blocks, the operator is granted 60 blocks to adequately explore and identify suitable mining locations. However, to prevent lunar land grabbing and support equitable access, she must relinquish 25% (15 km^2) by the end of the tenth year of the contract and 50% (30 km^2) by the end of the twentieth year. This leaves ten years to conduct further exploration activities in the remaining blocks to identify a mine site. In this example, the primary blocks (n=60) are subdivided into 25 subblocks (n=1500) using the equal area principle. After ten years, 375 of the 1,125 subblocks would be relinquished (c) and after twenty years, 750 would be relinquished (d). Impact Reference Zones can also be easily delineated using the Lunar Mining Map tool (gray subblocks).

5.8.6 Lunar Impact Reference Zones

To conserve the marine environment, the ISA recommended contractors implement Impact Reference Zones (ISBA/16/A/12/Rev.1, Reg. 33). Impact Reference

Zones are spatial management tools that operators would define in their exploration claim area to monitor the impacts of their activities on the marine environment. While the guidelines for the establishment of such zones have yet to be released by the ISA, Jones et al. (2020) synthesize why they are paramount for safeguarding the marine environment:

- They characterize and quantify mining impacts on the marine environment;
- They separate mining impacts from natural environmental change;
- They evaluate the efficacy of environmental management/mitigation measures, which helps build a knowledge base and inform future adaptive management strategies;
- They help clarify the amount of precaution needed during seabed mining operations;
- They ensure that mining activities comply with the ISA's environmental objectives.

While the environmental effects of our current activities on the Moon are relatively insignificant, future mining and operations activities (i.e., excavation, mineral processing drilling, road building, infrastructure development) will alter the surfaces of landscapes and thermal environment, suspend dust, contribute to frequency interference, and potentially release gases into the lunar exosphere (Vondrak, 1992; Budden, 2019). To effectively eliminate or reduce these effects, previous scholars have argued for international standards for extraterrestrial environmental assessment processes (Kramer, 2014). Kramer (2020) and Dallas et al. (2021) have already introduced frameworks for extraterrestrial environmental assessments.

Similar to the ISA (ISBA/18/A/11, Reg. 34), we recommend that the LRMA require operators to designate Impact Reference Zones in their exploration contract areas where mining is prohibited. We propose that the Impact Reference Zones be

implemented in a subset of blocks to collect environmental baseline data and implement a monitoring program in their claim area. Thus, the Impact Reference Zones are de facto lunar conservation areas stationed within an operator's exploration contract. Data collected in Impact Reference Zones would be compared to data collected from blocks where mining activities are conducted to assess exploration activities' effects on the lunar environment. A monitoring program is beneficial because it allows an operator to identify the activities that have no potential to cause harm to the lunar environment. Such information could establish norms of behavior for future operators to implement when designing their mining equipment and exploration campaigns.

We also recommend that the LRMA require operators to submit annual reports containing the results of their monitoring programs within their Impact Reference Zones. The annual reports would entail both environmental assessments and impact statements of their mining activities in their contract area as well as results of the efficacy of their monitoring programs and what measures will be taken (if needed) to moderate adverse effects on the lunar environment. The report would be submitted to the Lunar Legal and Technical Commission, who would then conduct an analysis on the effects of mining activities in the Lunar South Pole Resource System. The report would be disseminated by the Secretariat.

Based on the discussion above, we recommend the following requirements for Impact Reference Zones in Lunar Exploration Contracts (Table 5.6). The size of seabed Impact Reference Zones designed needed to be sufficiently large and sufficiently separated to contain a representative subset of organisms sufficient for statistical assessments of ecosystem integrity. A lunar criterium must also be formulated to

determine the size and separation of Lunar Impact Reference Zones. To start, we recommend that Impact Reference Zones cover ~5% of an operator's contract area.

Table 5.6 – Requirements for Impact Reference Zones in Lunar Water Ice Exploration Contracts

Requirements for Impact Reference Zones in Lunar Exploration Contracts
1. The operator shall designate ~5% of its original exploration contract area as Impact Reference Zones prior to relinquishment.
2. All mining activities are prohibited in Impact Reference Zones.
3. Impact Reference Zones shall be defined in the form of subblocks using the grid provided by the LRMA or using subblocks designated by the contractor using the equal area principle. (a) Impact Reference Zones can fall in relinquished areas. (b) Impact Reference Zones must be established prior to the first phase of relinquishment. (c) The designated blocks should be designed to include some occurrence of the target resource in order for the Impact Reference Zone to be similar to an area where mining activities are being conducted. (d) Impact Reference Zones shall represent the geologic and environmental settings of the operator's claim area.
4. The operator shall develop and implement a monitoring program within their Impact Reference Zones to collect environmental baseline data and assess the effects of exploration activities on the lunar environment.
5. The operator shall submit in their annual report data obtained in their Impact Reference Zones and information on the measures taken to prevent, reduce, and control the effects of their exploration activities on the lunar environment.

We designate hypothetical Impact Reference Zones in Figure 5.8. The advantage of using the Lunar Mining Map Tool block system is that it simplifies how operators can delineate to the LRMA and the public where they will implement environmental management plans. Additionally, the tool can be used in tandem with the annual reports to support environmentally sound spatial planning in the Lunar South Pole Resource System. For example, suppose a developing state applies for an exploration contract using the Reserved Area in Figure 5.6c. Because an operator's Impact Reference Zones

will be made public in annual reports and in the Lunar Mining Map registry, the applicant will be able to strategically position the Impact Reference Zones in their claim area to enable regional environmental management.

The orientation of Impact Reference Zones is up to the operator. However, it is advantageous to arrange them in clusters close in proximity to facilitate monitoring. Impact Reference Zones should also be designed to be highly flexible. For example, their size, percent of total contract area, and configuration strategy may need to be altered as we learn more about the effects of human activities on the lunar environment. Furthermore, it might be that over time, operator's will prove that their mining activities do not adversely affect the lunar environment. If so, the LRMA might provide the option for operators to decommission their activities in impact reference areas. The benefit of governing under the principle of adaptive management is that the LRMA would be alter the requirements of Impact Reference Areas quickly.

5.8.7 Lunar Exploitation Activities: Adopting an Evolutionary Approach

A fundamental principle guiding the development of the ISA and its Mining Code is that they are established using the evolutionary or "phased" approach (A/RES/48/263). The approach has an institutional dimension relating to the establishment and functions of the organs and a substantive dimension concerning the progressive development and implementation of its Mining Code (Le Gurun, 2014). Similar to the ISA, we believe that the LRMA will need to employ the evolutionary approach to establish its organs and Mining Code. While we provide high-level recommendations for which principal organs

are needed for managing lunar mining activities, the ISA required ten years to establish its principal and subsidiary organs (Le Gurun, 2014).

The ISA's initial substantive tasks have been to formulate the rules, regulations, and procedures for prospecting and exploration activities, develop recommendations and standards to guide operators in fulfilling their contractual obligations, processing exploration contracts, and promoting marine scientific research to evaluate the environment impacts of activities in the Area. Because polymetallic nodules were the primary seabed resource of interest (UNCLOS Article 162(2)), the development of prospecting and exploration regulations for this resource were prioritized (ISBA/19/A/9). We recommend LRMA also implement the evolutionary approach as an operational principle for developing its Mining Code. Once the LRMA is established, and its functions are determined, the first substantive task is to develop the procedures for approving lunar water ice prospecting and exploration contracts and associated regulations and environmental management measures.

Draft regulations on the exploitation phase of mineral resources in the Area were not published until twenty-five years after the establishment of the ISA and twenty years after the adoption of the first prospecting and exploration regulations (ISBA/25/C/WP.1). In other words, the ISA's Mining Code was not completed all at once but progressively developed following the pace of development of seabed mineral resources. Due to the many unknowns surrounding the lunar environment and its resources, we recommend that the LRMA refrain from drafting regulations on exploitation until its prospecting and exploration rules, regulations, and procedures prove successful. While the Law of the Sea Convention (1982) set out the initial legal framework for the deep seabed mining regime,

numerous details were left out to be decided later in parallel with advances in scientific research (Harrison, 2013). Before developing exploitation regulations, lunar operators will first need to determine whether water ice is even present in minable quantities via prospecting. Additionally, operators will need to determine during the exploration phase whether lunar mining is technologically achievable, whether such activities are economically feasible, and whether they can conduct operations without damaging the lunar environment. Furthermore, the LRMA will need to prove that its existing Mining Code will guarantee that operators' rights are secure, that its measures and recommendations adequately safeguard the lunar environment, and that they can assure that the Moon remains accessible to all nations.

5.8.8 Lunar Preservation Areas

The idea that certain surfaces on celestial bodies should be protected from human activities is not new (Hardgrove, 1986; Race, 2011). The Committee on Space Research (2020) has developed planetary protection standards to prevent forward contamination in areas significant to our understanding about the origin of life in our Solar System or in areas with conditions where terrestrial organisms could survive and replicate (i.e., special regions). Cockell and Horneck (2004, 2006) introduce the idea of a Planetary Park System, which would limit access to scientifically interesting regions, allowing them to be adequately studied and appreciated. In summary, Cockell and Horneck argue that a 'wilderness policy' for other planets is necessary because: (1) it creates a complete and healthy concept of culture and civilization in space, (2) pristine land has intrinsic value and should be left in appreciation of this value, (3) extraterrestrial land should be

protected for future generations, and because (4) the land may contain things that are beneficial at some time in the future.

Matthews and McMahon (2018) proposed the term "exogeoconservation," which extends geoconservation principles and activities to celestial bodies to identify geological and geomorphic features with scientific, historic, aesthetic, ecological or cultural value. The valuable features that warrant conservation and protection are termed 'exogeosites' (Matthews and McMahon, 2018). Additionally, drawing from Buddhist cultural values and environmental ethics, Capper (2022) argues to protect the Moon from mining by establishing multipurpose nature reserves.

Based on the normative shift in marine spatial planning toward the use of area-based management tools to manage activities in areas beyond national jurisdiction (Merrie et al., 2014), we recommend the LRMA develop an area-based measure to delineate "Lunar Preservation Areas" where mining activities in the Lunar South Pole Resource System are prohibited. Lunar Preservation Areas are inspired by Areas of Particular Environmental Interest described in Section 6.3 and proposals introduced by Matthews & McMahon (2018) and Capper (2022).

Similar to the ISA, whose aims are to encourage the development of seabed resources and safeguard the marine environment, the LRMA will be responsible for ensuring that Lunar Preservation Areas capture a full range and representative number of lunar features that exhibit important, unusual, extraordinary, or exceptional scientific without also impeding the development of the Moon's resources and the lunar economy. The primary objective of Lunar Preservation Areas is to conserve portions of the lunar environment from being distributed by human activity. Here, we focus on developing

Lunar Preservation Areas for PSRs and cold traps at the poles, for these features will contain water ice.

A portion of PSRs should be delineated as Lunar Preservation Areas because of the scientific value of the volatiles presumed to be present within such areas. A white paper submitted to The Decadal Survey in Planetary Science and Astrobiology 2023-2032 (Prem et al., 2020) identifies multiple reasons why conserving portions of volatile-rich areas in the Lunar South Pole Resource System is warranted:

- They will help us understand the Moon's primordial water content, which is critical in understanding the formation and early evolution of the Earth-Moon system and inner Solar System. In addition, the volatile history of the lunar interior is recorded in polar volatiles, which may preserve traces of ancient volcanic degassing.
- PSRs near the poles hold a unique record of the delivery of water to the inner solar system over the past several billion years and the processes that have shaped our local space environment.
- They will help us understand the processes that control global surface hydration on the Moon, which is critical for understanding hydration on other airless bodies and thereby the origin and distribution of water in our Solar System.
- PSRs will serve as natural laboratories to study abiotic/prebiotic chemistry.
- PSRs will contain information on the origin and evolution of the lunar exosphere, which will help us understand how airless bodies and their atmospheres evolve over time.

Additionally, Prem et al. (2020) provide a list of unknowns about lunar volatiles that will be difficult to address if mining activities alter the volatiles deposits themselves

as well as their environments, including (1) the distribution and physical form of polar volatiles, (2) whether the water present at the poles was derived from impacts, volcanic degassing, the solar wind and micrometeoroid bombardment, or a combination, (3) whether surface and sub-surface volatile deposits are connected or independent, (4) how volatiles on airless bodies are preserved, altered, destroyed, and distributed, and if the Moon is in a state of volatile accumulation, loss, or balance, (5) if/how volatiles migrate across the lunar surface, and (6) whether volatiles preserve traces of past lunar atmospheres, which is critical to understanding planetary atmospheric evolution. Additionally, polar volatiles will provide insight on the role of comets and meteorites in delivering pre-biotic organic materials to Earth and our Solar System (Pierzzo and Chyba, 1999; Chyba and Sagan, 1992).

In addition to the science objectives, representative PSR and cold trap areas in the Lunar South Pole Resource System should remain preserved for when technology and instrumentation advances. This argument aligns with the rationale for why samples delivered to Earth during the Apollo era were preserved for decades. A suite of universally accepted design principles will need to be developed to define the size, number, and locations of Lunar Preservation Areas. Based on the applied principles for designing the ISA's Areas of Particular Environmental Interest and Planetary National Parks, we provide a list of potential design principles for Lunar Preservation Areas in Table 5.7.

Table 5.7 - Design Principles for Lunar Preservation Areas in the Lunar South Pole Resource System.

Design Principles for Lunar Preservation Areas in the Lunar South Pole Resource System

(1) A pre-defined percentage of the Lunar South Pole Resource System must be delineated as Lunar Preservation Areas to preserve the lunar environment and conserve certain areas for scientific analysis by future generations.

(2) The boundaries of Lunar Preservation Areas must be clearly defined using straight lines;

(3) The design of Lunar Preservations Areas must be flexible, allowing for their numbers, locations, and sizes to be modified based on improved knowledge of the lunar environment and the impacts of mining activities;

(4) Lunar Preservation Areas should be designed as a configured network to conserve and preserve a full range and representative number of lunar features and be implemented prior to the onset of exploration and exploitation activities.

(5) Lunar Preservation Areas should be strategically placed to ensure that the development of lunar resources is not inhibited and so that the economic viability of the Moon is not depreciated, and

(6) Access to Lunar Preservation Areas should be limited to predefined routes.

(7) To define a Lunar Preservation Area, a formal request would be submitted to the Lunar Council, which would approve the request upon the recommendation of the Lunar Legal and Technical Commission. The request would require the attachment of:

(a) A list of the center coordinates of the blocks in the Lunar Mining Map Tool's grid to be classified as a Lunar Preservation Area
-Primary blocks can be subdivided into subblocks using the equal area principle to delineate specific areas or features within a block.
(c) A description of why human activities should be restricted in the blocks attached,
(d) A statement defining the science questions that could be addressed using the Preservation Areas in the future,
(e) A description of how lunar mining activities in the defined Area could negatively impact addressing one or more high-priority science goals.

(8) The locations of Lunar Preservation Areas will be made available in a public register and depicted in the Lunar Mining Map Tool.

Before mining activities, scientists will need to determine which and how much PSR area should be preserved. To avoid resource depletion, Elvis & Milligan (2019) argue that while economic growth remains exponential, humans should be limited to one-eighth of the exploitable materials in the Solar System, with the remainder seven-eighths being left as "space wilderness." The Lunar Mining Map Tool identified 19,699 blocks suitable for mining in the Lunar South Pole Resource system (Chapter 4). If we apply the

"one-eighth principle" for determining how many mining blocks should be delineated as Lunar Preservation areas, ~2,462 mining blocks remain eligible for development. This would significantly reduce the number of suitable mining areas for applicants seeking a license to conduct exploration activities, which may impede the development of the lunar mining industry and discourage investment.

To determine which PSR and cold trap areas should be delineated as Lunar Preservation Areas, a methodology should be developed to identify a representative set of PSRs and cold traps that exhibit a range of environmental conditions (i.e., minimum, maximum, and average temperatures, illumination), geographic locations, compositions, sizes, ages, and geomorphologic characteristics. However, this would be difficult without extensive in-situ prospecting, which would likely disturb the very areas requiring protection. Thus, high-resolution orbital remote sensing campaigns will likely be required if Lunar Preservation Areas are to be delineated before mining activities begin.

A simple alternative would be to require Lunar Preservation Areas be equal to the number of blocks licensed to operators and, if possible, require the areas to be within the same geologic unit or feature where mining activities are being conducted. The benefit of this regulation is that as the number of exploration contracts increases, the same area would be conserved. While the alternative regulation conserves less area than the one-eighth principle, such a measure aligns with the ISA's Areas of Particular Environmental Interest, which has proven successful since more seabed area has been preserved as exploration contracts continue to increase. As an example, we delineate a cluster of 120 suitable mining blocks west of our hypothetical exploration contract in Nobile crater in Figure 5.9.

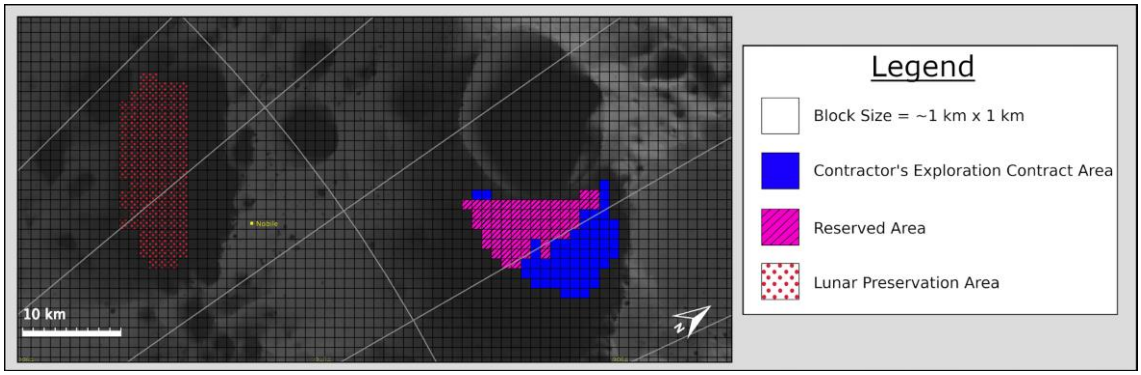

Figure 5.9 – Delineation of Lunar Preservation Areas using the Lunar Mining Map Tool, where mining would be prohibited. The Lunar Mining Map Tool is overlaid on a composite base map consisting of a global morphology mosaic (Speyerer et al., 2011) and average percent illumination data (Mazarico et al., 2011). The image is centered at -84.875ºN, 55.021ºE at a resolution of 1,024 ppd. The size of the Lunar Preservation Area equals the number of blocks comprising the hypothetical exploration contract issued by the LRMA and the Reserved Area where mining activities will be conducted by a future operator. In an attempt to preserve an area similar to the blocks being developed, the Lunar Preservation Area was delineated within the same crater as the proposed activities. The straight lines of the Lunar Mining Map Grid standardize implementing Lunar Preservation Areas where mining activities are prohibited. It also makes it simple for operators to comply with the LRMAs environmental regulations.

PSRs are not the only features on the Moon with extraordinary scientific value. Additional lunar features that should be considered as Lunar Preservation Areas include lunar swirls, irregular mare patches, dark mantle deposits, non-mare silicic volcanism, paleo regolith, peaks of eternal light, outcrops representing the diversity of lunar rocks and radio-quiet zones.

5.9 Concluding Remarks

This paper has advocated for the development of an intergovernmental institution–The Lunar Resource Management Authority–whose primary responsibilities are to foster the responsible development of lunar resources, safeguard the lunar environment, and ensure equitable use of and economic benefits to lunar mineral resources. While a multilateral agreement such as the Artemis Accords provides a

framework that could be used to formulate a regime to manage lunar mining activities, lessons from negotiations during the development of the seabed mining regime have shown that without a universally recognized management system, complications will emerge.

During the development of the Laws of the Sea, several industrialized countries perceived that many of the policies contained in Part XI of the Law of the Seas Convention related to deep-sea mining catered to the interests of developing states, which led to a stalemate in the adoption of the Convention and threatened the economic security of seabed mining companies who had already made significant investments. To protect the investments made by initial prospectors, several industrialized states adopted national laws empowering their governments to issue nationality licenses to explore and recover deep seabed minerals (Nandan et al., 2002). They also entered into a reciprocal arrangement where each participating state agreed to respect one other's exploration claims. This "mini-treaty" ultimately led to the emergence of dual regimes and the potential of overlapping claims, threatening the credibility International Seabed Authority and preventing the development of a universally recognized set of rules to mine the seabed. (Hayashi, 1989; Sparenberg, 2019).

The international community must formulate a regime with universal participation to ensure a legitimate and enduring regime. If states opt for multilateral agreements over a single regime, states could enter into different agreements with opposing norms and practices and issue exploration licenses over the same areas on the Moon. This would increase the propensity for disputes, create confusion over rights, and threaten resource development (Broadus & Hoagland III, 1984).

To fulfill its management responsibilities, we proposed that the LRMA develop a Lunar Mining Code comprised of area-based regulations to manage prospecting and exploration activities for water ice in the Lunar South Pole Resource System. We recommended that the LRMA exercise limited authority over prospecting activities, requiring operators to adhere to a notification process to notify where they will conduct their prospecting activities. To conduct exploration activities, operators would be required to submit an application in the form of a contract detailing where and how they will conduct their exploration activities. Upon approval by the LRMA, the operator would be issued an exploration license that grants them temporary but exclusive rights to explore water ice in allotted areas of the Lunar South Pole Resource System. To facilitate administering both recommendations, the LRMA should use a spatial planning tool such as the Lunar Mining Map Tool introduced in Chapter 4.

We also proposed a suite of principles and best practices to guide the behavior of future mining operators, including spatial and temporal constraints on exploration contracts, the incorporation of Reserved Areas to promote equitable access, a relinquishment procedure to promote sustainability and prevent monopolization, the use Impact Reference Zones to assess the effects of mining activities on the lunar environment, and Lunar Preservation Areas to conserve the lunar environment for future generations and scientific purposes. To simplify development, compliance, transparency, and enforcement, each measure and regulation could also be implemented using the Lunar Mining Map Tool's block system.

Finally, we also recommend the LRMA incorporate the evolutionary approach by focusing its efforts on developing a Mining Code for water ice, for it will likely be the

first resource to be developed in the near term to produce rocket propellant, H_2O for life support, and as a reagent in the processing of regolith and development of construction materials (i.e., concrete). However, many other resources can be recovered from the Moon's regolith, which will all require their own suite of regulations, including: other frozen volatiles delivered by comets (target for CO_2, CO, H_2CO Ca, Hg, Mg, H_2S, NH_3, SO_2, C_2H_4, CH_3OH, HCOOH, CH_4, OH, and Na) (Bockelée-Morvan & Biver, 2017; Colaprete et al., 2010), (2) plagioclase-rich highlands soil (target for O_2, Si, Al, and Ca), (3) ilmenite-rich mare soil, (target for O_2, Ti, Cr, Fe, and Mg) (McKay & Williams, 1979; Heiken & Vaniman, 1990; Gibson & Knudsen, 1985), (4) KREEP basalt fragments (target for K, P, Th, U, Zr, and rare earth elements), (5) pyroclastic deposits (target for H_2O, S, F, and Cl), (6) immature regolith deposits (a proxy for low concentrations of agglutinate and higher concentrations of monomineralic fragments), (7) mature regolith deposits (a proxy for higher concentrations of solar wind implanted volatiles such as He^3 and H) (Fegley & Swindle, 1993), and (8) iron-nickel metal (target for Ni, Fe, and noble metals) (Duke et al., 2006).

Other areas on the Moon containing appreciable amounts of other resources units could also be defined as a resource system using the Lunar Mining Map Tool. For example, a resource system could be defined for a dark mantle deposit, which contains water-enriched resource units (pyroclastic materials) (Milliken & Li, 2017) that could be targeted in the future to produce H_2O. Just as the ISA developed regulations for the different resources of the seabed, the pyroclastics would warrant their own Mining Code and best practices for responsible, equitable, and sustainable management.

References

Abramowski, T. (2014). Activities of the IOM within the scope of geological exploration for polymetallic nodule resources. *Workshop on Polymetallic Nodule Resources Classification*. October 13–17, 2014, Goa, India.

Agreement relating to the Implementation of Part XI of the United Nations Convention on the Law of the Sea. 10 December 1982, A/RES/48/263, Annex.

Antrim, C.L. (2005). Mineral Resources of Stateless Space: Lessons From the Deep Seabed. *Journal of International Affairs*, 59(1), 55-80.

Arnold, J.R. (1979). Ice in the lunar polar regions. *Journal of Geophysical Research*, 84(B10), 5659-5668.

Bailey, J.S. (1983). The Future of the Exploitation of the Resources of the Deep Seabed and Subsoil. *Law & Contemp. Probs*, 46(2), 70-76.

Bockelée-Morvan, D., & Biver, N. (2017). The composition of cometary ices. *Phil. Trans. R. Soc. A*, 375(2016252), 1-11.

Broadus, J.M., & Hoagland III, P. (1984). Conflict Resolution in the Assignment of Area Entitlements for Seabed Mining. Conflict Resolution, *San Diego Law Review*, 21(3), 541-576.

Budden, J. (2019). Defending the lunar landscape. *Phys. World*, 32(7), 21.

Buxton, C.R. (2004). Property in Outer Space: The Common Heritage of Mankind Principle Vs. the "First in Line, First in Right" Rule of Property Law. *Journal of Air and Law Commerce*, 69(4), 689-708.

Cannon, K.M., & Britt, D.T. (2020). A geologic model for lunar ice deposits at mining scales. *Icarus*, 347(113778), 1-11.

Capper, D. (2022). What Should We Do With Our Moon?: Ethics and Policy for Establishing International Multiuse Lunar Land Reserves. *Space Policy*, 59(101462), 1-10.

Carrier III, W.D., Olhoeft, G.R., & Mendell, W. (1991). Physical Properties of the Lunar Surface. In: Heiken, G.H., Vaniman, D.T. and B.M. French (Eds.) *Lunar Sourcebook*. pp. 475-594.

Chyba, C.F., & Sagan, C. (1992). Endogenous production, exogenous delivery and impact-shock synthesis of organic molecules: an inventory for the origins of life. *Nature*, 355, 125–132.

Colaprete, A., Elphic, R.C., Heldmann, J., & Ennico, K. (2012). An Overview of the Lunar Crater Observation and Sensing Satellite (LCROSS). *Space Science Reviews*, 167, 3–22.

Colaprete, A., Schultz, P., Heldmann, J., Wooden, D., Shirley, M., Ennico, K., Hermalyn, B., Marshall, W., Ricco, A., Elphic, R.C., Goldstein, D., Summy, D., Bart, G.D., Asphaug, E., Korycansky, D., Landis, D., & Sollitt, L. (2010). Detection of water in the LCROSS ejecta plume. *Science*, 330(6003), 463.

Cockell, C., & Horneck, G. (2004). A Planetary Park system for Mars. *Space Policy*, 20, 291–295.

Cockell, C., & Horneck, G. (2006). Planetary Parks-formulating a wilderness policy for planetary bodies. *Space Policy*, 22(4), 256–261.

Committee on Space Research. (2021). COSPAR Policy on Planetary Protection. *Space Research Today*, 211, 12-25.

Daintith, T., & Gault, I. (1977). Pacta Sunt Servanda and the Licensing and Taxation of North Sea Oil Production. *Cambrian Law Review*, 8, 27–44.

Dallas, J.A., Raval, S., Saydam, S., & Dempster, A.G. (2021). An Environmental Impact Assessment Framework for Space Resource Extraction. *Space Policy*, 57(101441), 1-12.

Dam, K.W. (1965). Oil and Gas Licensing and the North Sea. *The Journal of Law & Economics*, 8, 51–75.

de O. Bittencourt Neto, O., Hoffmann, M., Masson-Zwaan, T., & Stefoundi, D. (2020). Building Blocks for the Development of an International Framework for the Governance of Space Resources Activities: A Commentary. (pp. 167). Eleven.

Duke, M.B., Gaddis, L.R., Taylor, G.J., & Schmitt, H.H. (2006). Development of the Moon. *Reviews in Mineralogy and Geochemistry*, 60(1), 597–655.

Egede, E., Pal, M., & Charles, E. (2019). A Study Related to Issues on the Operationalization of the Enterprise. Legal, Technical and Financial Implications for the International Seabed Authority and for States Parties to the United Nations Convention on the Law of the Sea. Technical Report 1/2019. Pp. 1-50.

Elvis, M., & Milligan, T. (2019). How much of the Solar System should we leave as wilderness? *Acta Astronautica*, 162, 574–580.

European Space Policy Institute. (2021). Emerging Spacefaring Nations – Full Report. European Space Policy Institute (Eds). Pp 127. https://www.espi.or.at/wp-content/uploads/2022/06/ESPI-Report-79-Emerging-Spacefaring-Nations-Full-Report.pdf

Exec. Order. No. 13,914, 85 FR 20381. (2020). https://www.federalregister.gov/documents/2020/04/10/2020-07800/encouraging-international-support-for-the-recovery-and-use-of-space-resources

Federal Aviation Administration. (2022). Commercial Space Data. https://www.faa.gov/data_research/commercial_space_data/, Accessed: March 3, 2023.

Fegley, B., & Swindle, T.D. (1993). Lunar volatiles: implications for lunar resource utilization. In J. Lewis, M.S. Matthews & M.L. Guerrieri (Eds.), *Resources of Near-Earth Space*, 367–426.

Feldman, W.C., Maurice, S., Binder, A.B., Barraclough, B.L., Elphic, R.C., & Lawrence, D.J. (1998). Fluxes of fast and Epithermal Neutrons from Lunar Prospector: Evidence for Water Ice at the Lunar Poles. *Science*, 281(5382), 1496-1500.

Feldman, W.C., Maurice, S., Lawrence, D.J., Little, R.C., Lawson, S.L., Gasnault, O., Wiens, R.C., Barraclough, B.L., Elphic, R.C., Prettyman, T.H., Steinberg, J.T., & Binder, A.B., (2001). Evidence for water ice near the lunar poles. *J. Geophys. Res. Planets*, 106, 23231–23251.

Fisher, E.A., Lucey, P.G., Lemelin, M., Greenhagen, B.T., Siegler, M.A., Mazarico, E., Aharonson, O., Williams, J.-P., Hayne, P.O., Neumann, G.A., Paige, D.A., Smith, D.E., & Zuber, M.T. (2017). Evidence for surface water ice in the lunar polar regions using reflectance measurements from the Lunar Orbiter Laser Altimeter and temperature measurements from the Diviner Lunar Radiometer Experiment. *Icarus*, 292. 74–85.

Gertsch, L., Gustafson, R., & Gertsch, R. (2006). Effect of Water Ice Content on Excavatability of Lunar Regolith. *AIP Conference Proceedings*, 813, 1093-1100.

Ghandi, A., &, Lin, C.-Y. (2014). Oil and gas service contracts around the world: A review. *Energy Strategy Rewards*, 3, 63–71.

Gibson, M.A., & Knudsen, C.W. (1985). Lunar oxygen production from ilmenite. In: W.W. Mendell (Ed.), *Lunar bases and space activities of the 21st century*. pp.543-550.

Gissi, E., Maes, F., Kyriazi, Z., Ruiz-Frau, A., Santos, C. F., Neumann, B., Quintela, A., Alves, F. L., Borg, S., Chen, W., da Luz Fernandes, M., Hadjimichael, M., Manea, E.,

Marques, M., Platjouw, F. M., Portman, M. E., Sousa, L. P., Bolognini, L., Flannery, W., Grati, F., & Unger, S. (2022). Contributions of marine area-based management tools to the UN sustainable development goals. *Journal of Cleaner Production*, 330, 129910. https://doi.org/10.1016/j.jclepro.2021.129910.

Gladstone, G.R., Hurley, D.M., Retherford, K.D., Feldman, P.D., Pryor, W.R., Chaufray, J.Y., Versteeg, M., Greathouse, T.K., Steffl, A.J., Throop, H., Parker, J.W., Kaufmann, D.E., Egan, A.F., Davis, M.W., Slater, D.C., Mukherjee, J., Miles, P.F., Hendrix, A.R., Colaprete, A., & Stern, A. (2010). LRO-LAMP Observations of the LCROSS Impact Plume. *Science*, 330(6003), 472–476.

Gladstone, G.R., Retherford, K.D., Egan, A.F., Kaufmann, D.E., Miles, P.F., Parker, J.W.,Horvath, D., Rojas, P.M., Versteeg, M.H., Davis, M.W., Greathouse, T.K., Slater, D.C., Mukherjee, J., Steffl, A.J., Feldman, P.D., Hurley, D.M., Pryor, W.R., Hendrix, A.R.,Mazarico, E., & Stern, S.A. (2012). Far-ultraviolet reflectance properties of the Moon's permanently shadowed regions. *J. Geophys. Res. Planets*, 117(E00H04), 1-13.

Glasby, G.P. (2000). Lessons Learned from Deep-Sea Mining. *Science*, 289(5479), 551-553.

Glasby, G.P. (2002). Deep Seabed Mining: Past Failures and Future Prospects. *Marine Georesources and Geotechnology*, 20, 161–176.

Hardgrove, E.C. (1986). Beyond Space Earth: Environmental Ethics and the Solar System. Sierra Club Books. p.336.

Hardin, G. (1968). The Tragedy of the Commons. *Science*, 162, 1243–1248.

Harrison, J. (2013). Making the Law of the Sea: A Study in the Development of International Law. Cambridge: Cambridge University Press. pp. 321.

Hayaski, M. (1989). Registration of the First Group of Pioneer Investors by the Preparatory Commission for the International Sea-Bed Authority and for the International Tribunal for the Law of the Sea. *Ocean Development and International Law*, 20(1), 1-34.

Hayne, P.O., Aharonson, O., & Schörghofer, N. (2021). Micro cold traps on the Moon. *Nature Astronomy*, 5, 169-175.

Hayne, P.O., Hendrix, A., Sefton-Nash, E., Siegler, M.A., Lucet, P.G., Retherford, K.D., Williams, J.-P., Greenhagen, B.T., & Paige, D.A. (2015). Evidence for exposed water ice in the Moon's south polar regions from Lunar Reconnaissance Orbiter ultraviolet albedo and temperature measurements. *Icarus*, 255(15), 58–69.

Heim, B.E. (1990). Exploring the Las Frontiers for Mineral Resources: A Comparison of International Law Regarding the Deep Seabed, Outer Space, and Antarctica. *Vanderbilt Journal of Transnational Law*, 23, 819-849.

Heiken, G.H., & Vaniman, D.T. (1990). Characterization of Lunar Ilmenite Resources. *Proceedings of the 20th Lunar and Planetary Science Conference*, pp. 239-247.

Hein, J.R., Mizeli, K., Koschinsky, A., & Conrad, T.A. (2013). Deep-ocean mineral deposits as a source of critical metals for high- and green-technology applications: Comparison with land-based resources. *Ore Geology Reviews*, 51, 1–14.

Hurley, D., Colaprete, A., Elphic, R., Farrell, W., Hayne, P., Heldmann, J., Hibbits, C., Livengood, T., Lucey, P., Klaus, K, Kring, D.A., Patterson, W., & Sherwood, B. (2016). Lunar Polar Volatiles: Assessment of Existing Observations for Exploration. NASA Goddard Space Flight Center. (pp.11). https://www.lpi.usra.edu/science/kring/lunar_exploration/LunarPolarVolatiles.pdf

International Seabed Authority. (2015). Consolidated Regulations and Recommendations on Prospecting and Exploration. Revised Edition. Pp. 264.

International Seabed Authority. (2023a). Exploration Contracts. https://www.isa.org.jm/exploration-contracts/

International Seabed Authority. (2023b). The Legal and Technical Commission. https://www.isa.org.jm/organs/the-legal-and-technical-commission/.

International Seabed Authority. (2000). Decision of the Assembly Relating to the Regulations on Prospecting and Exploration for Polymetallic Nodules in the Area, ISBA/6/A/18.

International Seabed Authority. (2001). Considerations relating to the regulations for prospecting and exploration for hydrothermal polymetallic sulphides and cobalt-rich ferromanganese crusts, ISBA/7/C/2.

International Seabed Authority. (2012a). Decision of the Council relating to an environmental management plan for the Clarion-Clipperton Zone, ISBA/18/C/22.

International Seabed Authority. (2012b). Regulations on Prospecting and Exploration for Cobalt-rich Ferromanganese Crusts in the Area, ISBA/18/A/11.

International Seabed Authority. (2010). Regulations on Prospecting and exploration for polymetallic sulphides in the Area, ISBA/16/A/12/Rev.1.

International Seabed Authority. (2013). Regulations on Prospecting and Exploration for Polymetallic Nodules in the Area, ISBA/19/C/17.

International Seabed Authority. (2019). Draft Regulations on Exploitation of Mineral Resources in the Area, ISBA/25/C/WP.1.

International Seabed Authority. (2019b). Recommendations for the guidance of contractors on the relinquishment of areas under exploration contracts for polymetallic sulphides or cobalt-rich ferromangense crusts, ISBA/25/LTC/8.

International Seabed Authority. (2011). Environmental Management Plan for the Clarion-Clippterton Zone, ISBA/17/LTC/7.

Jaeckel, A. (2020). Benefitting from the Common Heritage of Mankind: From Expectation to Reality. *The International Journal of Marine and Coastal Law*, 35:660–681.

Jaeckel, A. (2022). Benefitting from the Common Heritage of Mankind: From Expectation to Reality. Valuing the Deep Sea for the Benefit of Humankind. *Renewable Resource Journal*, 37(3), 11-22.

Jaeckel, A. (2015). The International Seabed Authority and Marine Environmental Protection: A Case Study in Implementing the Precautionary Principle. Doctoral thesis (pp. 293). UNSW Australia.

Jaeckel, A. (2017). The International Seabed Authority and the Precautionary Principle: Balancing Deep Seabed Mineral Mining and Marine Environmental Protection. *Publications on Ocean Development*. 83:1-382. Brill.

Jaeckel, A., Ardron, J. A., & Gjerde, K. M. (2016). Sharing benefits of the common heritage of mankind – Is the deep seabed mining regime ready? *Marine Policy*, 70, 198-204. https://doi.org/10.1016/j.marpol.2016.03.009

Jaeckel, A. (2016). Deep seabed mining and adaptive management: The procedural challenges for the International Seabed Authority. *Marine Policy*, 70, 205–211.

Jakhu, R.S., Jasani, B., & McDowell, J.C. (2018). Critical issues related to registration of space objects and transparency of space activities. *Acta Astronautica*, 143, 406-420.

Japan. (2021). Space Resources Act. Act No. 83 of 2021. https://kanpou.npb.go.jp/old/20210623/20210623g00141/20210623g001410004f.html

Jones, D.O., Ardron, J.A., Colaço, A., & Durden, J.M. (2020). Environmental considerations for impact and preservation reference zones for deep-sea polymetallic nodule mining. *Marine Policy*, 118(103312), 1-9.

Jones, D.O., Kaiser, S., Sweetman, A.K., Smith, C.R., Menot, L., Vink, A., Trueblood, D., Greinert, J., Billet, D.S., Arbizu, P.M., Radziejewska, T., Singh, R., Ingole, B., Stratmann, T., Simon-Lledó, E., Durden, J.M, &, Clark, M.R. (2017). Biological responses to disturbance from simulated dee-sea polymetallic nodule mining. *PLoS ONE*, 12(2), e0171750.

Joyner, C. (1986). Legal Implications of the Concept of the Common Heritage of Mankind. *International & Comparative Law Quarterly*, 35(1), 190-199.

Kang, Y., & Liu, S. (2021). The Development History and Latest Progress of Deep-Sea Polymetallic Nodule Mining Technology. *Minerals*, 11(1132), 1-17.

Kerr, R.A. (1998). Cheapest mission finds moon's frozen water. *Science*, 270(5357), 1628.

Kirsch, P., & Fraser, D. (1989). The Law of the Sea Preparatory Commission after Six Years: Review and Prospects. *Canadian Yearbook of International Law*, 26, 119-154.

Kornuta, D., Abbud-Madrid, A., Atkinson, J., Barr, J., Barnhard, G., Bienhoff, D., Blair, B., Clark, V., Cyrus, J., deWitt, B., Dreyer, C., Finger, B., Goff, J., Ho, K. Kelsey, L., Keravala, J., Kutter, B., Metzger, P., Montgomery, L., Morrison, P., Neal, C., Otto, E., Roesler, G., Schier, J., Seifert, B., Sowers, G., Spudis, P., Sundahl, M., Zacny, K., & Zhu, G. (2019). Commercial lunar propellant architecture: A collaborative study of lunar propellant production. *Reviews in Human Space Exploration*, 129(100026), 1-77.

Kramer, W.R. (2014). Extraterrestrial environmental impact assessments – A foreseeable prerequisite for wise decisions regarding outer space exploration, research and development. *Space Policy*, 30, 215–222.

Kramer, W.R. (2020). A Framework for Extraterrestrial Environmental Assessment. *Space Policy*, 52(101385), 1-6.

Lambach, D. (2021). The functional territorialization of the high seas. *Marine Policy*, 130, 104579.

Lamboray, B. (2019). Luxembourg's SpaceResources.lu Initiative: The Space Resources Value Chain and the Role of Robotics and Autonomous Systems. *CZ-LUX Robotic Day, March 13, 2019, Luxembourg*.

Land Matters. (2014). http://www.mylandmatters.org/Maps/Mining.html. Accessed 28 April 2022.

Le Gurun, G. (2014). Some Reflections on the Evolutionary Approach to the Establishment of the International Seabed Authority. In M. Lodge & M. Nordquist, Peaceful Order in the World's Oceans. pp. 249-264. Brill Nijhoff.

Lévy, J.-P. (2014). International Seabed Authority: 20 Years. Pp. 150. International Seabed Authority.

Li, S., Lucey, P.G., Milliken, R.E., Hayne, P.O., Fisher, E., Williams, J.-P., Hurley, D.M., & Elphic, R.C. (2018). Direct evidence of surface exposed water-ice in the lunar polar regions. *Earth, Atmospheric, and Planetary Sciences*, 115(36), 8907–8912.

Lodge, M.W. (2011). Current Legal Developments: International Seabed Authority. *The International Journal of Marine and Coastal Law*, 26(3), 463-480.

Lodge, M.W. (2002). International Seabed Authority's Regulations on Prospecting and Exploration for Polymetallic Nodules in the Area. Journal of Energy & Natural Resources Law, 20(3), 270-295.

Lodge, M., Johnson, D., Le Gurun, G., Wengler, M., Weaver, P., & Gunn, V. (2014). Seabed mining: International Seabed Authority environmental management plan for the Clarion–Clipperton Zone. A partnership approach. *Marine Policy*, 49, 66–72.

Lomax, B.A., Conti, M., Khan, N., Bennett, N.S., Ganin, A.Y., & Synes, M.D. (2020). Proving the viability of an electrochemical process for the simultaneous extraction of oxygen and production of metal alloys from lunar regolith. Planetary and Space *Science*, 180, 104748.

Luxembourg Space Agency. (2018). Opportunities for Space Resources Utilization. Future Markets & Value Chains: Study Summary. (pp.16). https://space-agency.public.lu/dam-assets/publications/2018/Study-Summary-of-the-Space-Resources-Value-Chain-Study.pdf.

Madureira, P., Brekke, H., Cherkashov, G., & Rovere, M. (2016). Exploration of polymetallic nodules in the Area: Reporting practices, data management and transparency. *Marine Policy*, 70, 101–107.

Margulis, M.E., McKeon, N. Borras Jr., S.M. (2013). Land Grabbing and Global Governance: Critical Perspectives. *Globalizations*, 10(1), 1–23.

Matthews, J.J., & McMahon, S. (2018). Exogeoconservation: Protecting geological heritage on celestial bodies. *Acta Astronautica*, 149, 55–60.

Mazarico, E., Neumann, G.A., Smith, D.E., Zuber, M.T., & Torrence, M.H. (2011). Illumination conditions of the lunar polar regions using LOLA topography. *Icarus*, 211, 1066–1081.

McKay, D.S., & Williams, R.J. (1979). A geologic assessment of potential lunar ores. Space Resources and Space Settlements, NASA SP–428, 243–255.

Merrie, A., Dunn, D.C., Metian, M., Boustany, A.M., Takei, Y., Elferink, A.O., Ota, Y., Christensen, V., Halpin, P.N., & Österblom, H. (2014). An ocean of surprises – Trends in human use, unexpected dynamics and governance challenges in areas beyond national jurisdiction. *Global Environmental Change*, 27, 19–31.

Meurisse, A., & Carpenter, J. (2020). Past, present and future rationale for space resource utilization. *Planetary and Space Science*. 182(104853), 1-13.

Miller, K.A., Thompson, K.F., Johnston, P., & Santillo, D. (2018). An Overview of Seabed Mining Including the Current State of Development, Environmental Impacts, and Knowledge Gaps. *Frontiers in Marine Science*, 4, 1-24.

Milliken, R., & Li, S. (2017). Remote detection of indigenous water in lunar pyroclastic deposits. *Nature Geoscience*, 10, 461-465.

Mitchell, J.K., Houston, W.N., Carrier III, W.D., & Costes, N.D. (1974). Apollo Soil Mechanics Experiment S-200. https://www.lpi.usra.edu/lunar/documents/NASA%20CR-134306.pdf

Molenaar, E.J. (2013). Area-based management tools. In Intersessional Workshops on the Conservation and Sustainable Use of Marine Biodiversity Beyond Areas of National Jurisdiction (Oceans and the Law of the Sea division, 2013). https://go.nature.com/3m5jylf.

Mucha, J., Wasilewska-Blaszczyk, M., Kotlinski, R.A, & Maciąg, L. (2013). Variability and accuracy of polymetallic nodules abundances estimations in the IOM area-statistical and geostatistical approach. In *Tenth ISOPE Ocean Mining and Gas Hydrates Symposium*, *Szczecin, Poland, September 22-26, 2013*. Pp.27-31.

Nandan, S.N., Lodge, M.W., & Rosenne, S. (2002). The development of the regime for deep seabed mining. International Seabed Authority. pp. 1-73.

Nandan, S.N. (2006). Administering the Mineral Resources of the Deep Seabed. Chapter 5. In: Freestone, D., Barnes, D.M. (Eds.), *The Law of the Sea. Progress and Prospects*, pp 75-92. Oxford.

National Aeronautics and Space Administration. (2020). The Artemis Accords: Principles for cooperation in the civil exploration and use of the Moon, Mars, comets and

asteroids for peaceful purposes. https://www.nasa.gov/specials/artemis-accords/img/Artemis-Accords-signed-13Oct2020.pdf

Nozette, S., Lichtenberg, C.L., Spudis, P., Bonner, R., Ort, W., Malaret, E., Robinson, M., & Shoemaker, E.M. (1996). The Clementine Bistatic Radar Experiment. *Science*, 274(5292), 1495-1498.

Nozette, S., Rustan, P., Pleasance, L.P., Kordas, J.F., Leis, I.T., Park, H.S., Priest, R.E., Horan, D.M., Regeon, P., Lichtenberg, C.L., Shoemaker, E.M., Eliason, E.M., McEwen, A.S., Robinson, M.S., Spudis, P.D., Action, C.H., Buratti, B.J., Duxbury, T.C., Baker, D.N., Jakosky, B.M., Blamont, J.E., Corson, M.P., Resnick, J.H., Rollins, C.J., Davies, M.E., Lucey, P.G., Malaret, E., Massie, M.A., Pieters, C.M., Reisse, R.A., Smith, D.E., Soernson, T.C., Vorder Breugge, R.W., & Zuber, M.T. (1994). The Clementine Mission to the Moon: Scientific Overview. *Science*, 266(5192), 1835–1839.

O'Brien, D. (2021). Is outer space a de jure common-pool resource. The Space Review. Accessed: March 3, 2023. https://www.thespacereview.com/article/4270/1

Ochoa, C. (2021). Contracts on the Seabed. *Yale Journal of International Law*, 46(1), 103-154.

Official newspaper of the Grand Duchy of Luxembourg. (2017). Law of July 20, 2017 on the exploration and use of space resources. https://legilux.public.lu/eli/etat/leg/loi/2017/07/20/a674/jo

Official newspaper of the Grand Duchy of Luxembourg. (2020). Law of December 15, 2020 on space activities. https://legilux.public.lu/eli/etat/leg/loi/2020/12/15/a1086/jo

Ortuño Crespo, G., Mossops, J., Dunn, D., Gjerde, K., Hazen, E., Reygondeau, G., Warner, R., Tittensor, D., & Halpin, P. (2020). Beyond static spatial management: Scientific and legal considerations of dynamic in the high seas. *Marine Policy*, 122(104012), 1-7.

Ostrom, E. (2002). Common-Pool Resources and Institutions: Toward a Revised Theory. In B. Gardner & G. Rausser, (Eds.), *Handbook of agricultural economics*, 2:1315–1339. Elsevier.

Ostrom, E. (1999). Design Principles and Threats to Sustainable Organizations that Manage Commons. Workshop in Political Theory and Policy Analysis, W99–6. Center for the Study of Institutions, Population and Environmental Change.

Ostrom, E. (1990). Governing the Commons: The Evolution of Institutions for Collective Action. Cambridge University Press.

Ostrom, E., Gardner, R., & Walker, J. (1994). Rules, Games, and Common-Pool Resources. University of Michigan Press.

Ostrom, E. (2010). Beyond Markets and States: Polycentric Governance of Complex Economic Systems. *American Economic Review*, 100(3), 641-672.

Parianos, J., Lipton, I., & Nimmo, M. (2021) Aspects of Estimation and Reporting of Mineral Resources of Seabed Polymetallic Nodules: A Contemporaneous Case Study. *Minerals*, 11(200), 1-33.

Paxson III, E.W. (1993). Sharing the Benefits of Outer Space Exploration.: Space Law and Economic Development. *Michigan Journal of International Law*, 14(3), 487-517.

Peters, M., & Kumar, M. (2013). Unique UK's licensing policy favours the state than the industry: Contradicting conventional wisdom. *Hungarian journal of legal studies*, 54(2), 200-204

Pierazzo, E., & Chyba, C.F. (1999). Amino acid survival in large cometary impacts. *Meteoritics & Planetary Science*. 34, 909–918.

Pieters, C.M., Goswami, J.N., Clark, R.N., Annadurai, M., Boardman, J., Buratti, B., Combe, J.-P., Dyar, M.D., Green, R., Head, J.W., Hibbits, C., Hicks, M., Isaacson, P., Klima, R., Kramer, G., Kumar, S., Livo, E., Lundeen, S., Malaret, E., McCord, T., Mustard, J., Nettles, J., Petro, N., Runyon, C., Staid, M., Sunshine, J., Taylor, L.A., Tompkins, S., & Varanasi, P. (2009). Character and Spatial Distribution of OH/H_2O on the Surface of the Moon Seen by M^3 on Chandrayaan-1. Science, 326(5952), 568-572.

Prem, P., Keresturi, A., Deutsch, A.N., Hibbitts, C.A., Schmidt, C.A., Grava, C., Honniball, C.I., Hardgrove, C.J., Pieters, C.M., Goldstein, D.B., Barker, D.C., Needham, D.H., Hurley, D.M., Mazarico, E., Dominguez, G., Patterson, G.W., Kramer, G.Y., Brisset, J., Gillis-Davis, J.J., Mitchell, J.L., Szalay, J.R., Halekas, J.S., Keane, J.T., Head, J.W.,…& Farrell, W.M. (2020). *Lunar Volatiles and Solar System Science*, 1-7 https://arxiv.org/pdf/2012.06317.pdf.

Race, M.S. (2011). Policies for scientific exploration and environmental protection: Comparison of the Antarctic and outer space treaties. *Science diplomacy: Antarctica, science, and the governance of international spaces*, Pp. 143-152.

Raclin, G.C. (1986). From Ice to Ether: The Adoption of a Regime to Govern Resource Exploitation in Outer Space. *Northwestern Journal of International Law & Business*, 7, 727-761.

Rasera, J.N., Cilliers, J.J, Lamamy, J.A., & Hadler, K. (2020). The beneficiation of lunar regolith for space resource utilization: A review. *Planetary and Space Science*, 186(104879),1-15.

Reynolds, G.H. (1995). The Moon Treaty: prospects for the future. *Space Policy*, 11(2), 115–120.

Rio Declaration on Environment and Development. (1992). 31 ILM 874.

Roberts, J., Chircop, A. and S. Prior. (2010). Area-based management on the high seas: possible application of the IMO's particularly sensitive sea area concept. *International Journal of Marine and Coastal Law*, 25, 483–522.

Salter, E., & Ford, J. (2000). Environmental Pollution Challenges and Associated Planning and Management Issues Facing Offshore Oil and Gas Field Development in the UK. *Journal of Environmental Planning and Management*, 43(2), 253–276.

Schlüter, L., & Cowley, A. (2020). Review of techniques for In-Situ oxygen extraction on the Moon. *Planetary and Space Science*, 181(104753), 1-17.

Schlüter, L., Cowley, A., Pennec, Y., & Roux, M. (2021). Gas purification for oxygen extraction from lunar regolith. *Acta Astronautica*, 179, 371-381.

Schmidt-Tedd, B, & Soucek, A. (2020). Registration of Space Objects. In: *Oxford Research Encyclopedia of Planetary Science.* https://doi.org/10.1093/acrefore/9780190647926.013.95.

Schwind, M. (1986). Open Stars: An Examination of the United States Push to Privatize International Telecommunications Satellites. *Suffolk Transnational Law Journal*, 10, 87.

Sebenius, J.L. (1984). Negotiating the Law of the Sea Cambridge: Harvard University Press.

Shackelford, S.J. (2009). The Tragedy of the Common Heritage of Mankind. *Stanford Environmental Law Journal*, 28(1), 109-169.

Shearer, C., & Tahu, G. (2010). Lunar Pole Volatiles Explorer (LPVE). NASA Mission Concept Study. (Pp. 50). https://nap.nationalacademies.org/resource/13117/App%20G%2006_Lunar_Polar_Volatiles_Explorer.pdf

Sherwood, B. (2018). Principles of a Practical Moon Base. *69th International Astronautical Congress.* IAC-18.A3.1.6.x46496. (p.1–13).

Singh, P.A., & Araujo, F.C.B. (2023). The Past, Present and Future of Ocean Governance: Snapshots from Fisheries, Area-Based Management Tools and International Seabed Mineral Resources. In M. Bavinck, M. Hadjimichael, & A.-K. Hornidge (Eds.), *Ocean Governance*. Springer. (pp.113–135). https://doi.org/10.1007/978-3-031-20740-2.

Sladek-Nowlis, J., & Friedlander, A. (2004). Design and Designation of Marine Reserves. In: J. Sobel & C. Dahlgren (Eds.), *Marine Reserves: A Guide to Science, Design and Use*. Washington DC: Island Press. pp. 128-163.

Smith, C.R., Gaines, S., Friedlander, A.., Morgan, C., Thurnherr, A., Mincks, S., Watling, L., Rogers, A., Clark, M., Baco-Taylor, A., Bernardino, A., De Leo, F., Dutriuex, P., Riser, A., Kittinger, J., Padilla-Gamino, J., Prescott, R., & Srsen, P. (2008). Preservation Reference Areas for Nodule Mining in the Clarion-Clipperton Zone: Raitionale and Recommendations to the International Seabed Authority. In *Workshop to Design Marine Protected Areas for Seamounts and the Abyssal Nodule Province in Pacific High Seas*, October 23-26, 2007, University of Hawaii at Manoa.

Sparenberg, O. (2019). A historical perspective on deep-sea mining for manganese nodules, 1965–2019. *The Extractive Industries and Society*, 6:842–854.

Speyerer, E.J., Robinson, M.S., Denevi, B.C., & the LROC , Team. (2011). Lunar Reconnaissance Orbiter Camera Global Morphological Map of the Moon. *42nd Lunar and Planetary Science Conference, No. 2387*.

Spudis, P.D., Bussey, D.B.J., Baloga, S.M., Butler, B.J., Carl, D., Carter, L.M., Chakraborty, M., Elphic, R.C., Gillis-Davis, J.J., Goswami, J.N., Heggy, E., Hillyard, M., Jensen, R., Kirk, R.L., LaVallee, D., McKerracher, P., Neish, C.D., Nozette,S., Nylund, S., Palsetia, M., Patterson, W., Robinson, M.S., Raney, R.K., Schulze, R.C., Sequeira, H., Skura, J., Thompson, T.W., Thomson, B.J., Ustinov, E.A., & Winters, H.L. (2010). Initial results for the north pole of the Moon from Mini-SAR, Chandrayaan-1 mission. *Geophysical Research Letters*, 37(L06204), 1-6.

Spudis, P.D., Bussey, D.B.J., Baloga, S.M., Cahill, J.T.S., Glaze, L.S., Patterson, G.W., Raney, R.K., Thompson, T.W., Thomson, B.J., Ustinov, E.A., (2013). Evidence for water-ice on the Moon: results for anomalous polar craters from the LRO Mini-RF imaging radar. *Journal of Geophysical Research*, 118(10), 2016–2029. https://doi.org/10.1002/jgre.20156.

The Hague International Space Resources Working Group. (2019). Building Blocks for the Development of an International Framework on Space Resources Activities. https://www.universiteitleiden.nl/binaries/content/assets/rechtsgeleerdheid/instituut-voor-publiekrecht/lucht--en-ruimterecht/space-resources/hisrgwg_building-blocks-for-space-resource-activities.pdf.

Tronchetti, F. 2008. *The Korean Journal of Air & Space Law and Policy*, 23(1), 131–168.

Tronchetii, F. (2010). Commercial Exploitation of Natural Resources of the Moon and Other Celestial Bodies: What Role for the Moon Agreement? In: *Proceedings of the International Institute of Space Law*, 53, 614–624.

UNEP-WCMC (2019). A Marine Spatial Planning Framework for Areas Beyond National Jurisdiction. Technical document produced as part of the GEF ABNJ Deep Seas Project. Cambridge (UK): UN Environment Programme World Conservation Monitoring Centre. (pp. 1-45.)

UNEP-WCMC and Seascape Consultants Ltd. (2019). Learning form experience: Case studies of Area-Based Planning in ABNJ. Technical document Produced as part of the GEF ABNJ Deep Seas Project. Cambridge (UK):UN Environment World Conservation Monitoring Centre. (pp. 1-88).

United Arab Emirates. (2019). Federal Law No. (12) of 2019 on the Regulation of the Space Sector. https://www.moj.gov.ae/assets/2020/Federal%20Law%20No%2012%20of%202019%20on%20THE%20REGULATION%20OF%20THE%20SPACE%20SECTOR.pdf.aspx

United Nations Agreement Governing the Activities of States on the Moon and Other Celestial Bodies. (1979). 1363 UNTS 3.

United Nations Agreement on the Rescue of Astronauts, the Return of Astronauts and the Return of Objects Launched into Outer Space. (1968). 672 UNTS 119.

United Nations Committee on the Peaceful Uses of Outer Space. (2020). Building blocks for the development of an international framework on space resources activities, A/AC.105/C.2/L.315. https://documents-dds-ny.un.org/doc/UNDOC/LTD/V20/008/95/PDF/V2000895.pdf?OpenElement

United Nations Committee on the Peaceful Uses of Outer Space. (2022). Report of the Legal Subcommittee on its sixtieth session held in Vienna from 31 May to 11 June 2021, A/AC.105/1260. https://documents-dds-ny.un.org/doc/UNDOC/GEN/V22/022/49/PDF/V2202249.pdf?OpenElement

United Nations Convention on International Liability for Damaged Caused by Space Objects. (1972). 961 UNTS 187.

UNCLOS, United Nations Convention on the Law of the Sea. (1982). 1833 UNTS 397. https://www.un.org/depts/los/convention_agreements/texts/unclos/unclos_e.pdf.

United Nations Convention on the Registration of Objects Launched into Outer Space. (1975). 1023 UNTS 15.

United Nations General Assembly, Committee on the Peaceful Uses of Outer Space. (2022). Report of the Legal Subcommittee on its sixty-first session, held in Vienna from 28 March to 8 April 2022, UN Doc A/AC.105/1260. https://www.unoosa.org/oosa/oosadoc/data/documents/2022/aac.105/aac.1051260_0.html

United Nations General Assembly. (1970). Declaration of Principles Governing the Sea-Bed and the Ocean Floor, and the Subsoil Thereof, beyond the Limits of National Jurisdiction, UN Doc A/RES/2749, http://www.un-documents.net/a25r2749.htm

United Nations General Assembly. (1994). Agreement Relating to the Implementation of Part XI of the United Nations Convention on the Law of the Sea of 10 December 1982, UN Doc A/RES/48/263. https://treaties.un.org/doc/source/docs/A_RES_48_263-E.pdf.

United Nations Treaty on Principles Governing the Activities of States in the Exploration and Use of Outer Space, Including the Moon and Other Celestial Bodies. (1967). 610 UNTS 205.

United States Commercial Space Launch Competitiveness Act, H.R. 2262, 114th Cong. (2015). https://www.congress.gov/bill/114th-congress/house-bill/2262/text

Vasavada, A.R., Paige, D.A., & Wood, S.E. (1999). Near-surface temperatures on Mercury and the Moon and the stability of polar ice deposits. *Icarus,* 141(2), 179–193.

Vondrak, R.R. (1992).. Lunar Base Activities and the Lunar Environment. *2nd Conference on Lunar Bases and Space Activities*, 337-345.

Wall, M. (2020, December 3). NASA will buy moon dirt from these 4 companies. Space.com. https://www.space.com/nasa-will-buy-moon-dirt-masten-ispace-lunar-outpost

Watson, K., Murray, B.C., and H. Brown. (1961). On the possible presence of ice on the Moon. *Journal of Geophysical Research*, 66(5), 1598–1600.

Weeden, B.C., & Chow, T. (2012). Taking a common-pool resources approach to space sustainability: A framework and potential policies. *Space Policy*, 28(3), 166-172.

Wolfrum, R. (1995). The Decision-Making Process According to Sec. 3 of the Annex to the Implementation Agreement: A model to be Followed for Other International Economic Organisations? *Heidelberg Journal of International Law*, 55, 310-328.

Wood, M.C. (1999). International Seabed Authority: The First Four Years. *Max Planck Yearbook of United Nations Online*, 3(1), 173-241.

Wood, M.C. (2007). The International Seabed Authority: Fifth to Twelfth Sessions (1999-2006). *Max Planck Yearbook of United Nations Law*, 11, 47-98

World Commission on Environment and Development. (1987). Report of the World Commission on Environment and Development: Our Common Future. https://sustainabledevelopment.un.org/content/documents/5987our-common-future.pdf

Wedding, L.M., Friedlander, A.M., Kittinger, J.N., Watling, L., Gaines, S. D., Bennett, M., Hardy, S.M., & Smith, C.R. (2013). From principles to practice: a spatial approach to systematic conservation planning in the deep sea. *Proc. R. Soc. B*, 280(20131684), 1-10.

Wedding, L.M., Reiter, S.M., Smith, C.R., Gjerde, K.M., Kittinger, J.N., Friedlander, A.M., Gaines, S.D., Clark, M.R., Thurnherr, A.M., Hardy, S.M., & Crowder, L.B. (2015). Managing mining of the deep seabed. *Science*, 349(6244), 144–145.

Weeden, B.C., & Chow, T. (2012). Taking a common-pool resources approach to space sustainability: A framework and potential policies. *Space Policy*, 28, 166–172.

Yang, K., Yao, H., Ma, W., Li, Y., & He, G. (2022). A step-by-step relinquishment method for cobalt-rich crusts: A case study on Caiqi Guyot, Pacific Ocean. *Marine Georesources & Geotechnology*, 40(9), 1139–1150.

Zalik, A. (2015). Trading on the offshore: territorialization and the ocean grab in the international seabed. In Ervine, K. & G. Fridel (Eds.). Beyond Fair Trade, pp.173–190. London, Palgrave Macmillan.

Zalik, A. (2018). Mining the seabed, enclosing the Area: ocean grabbing, proprietary knowledge and the geopolitics of the extractive frontier. *International Social Science Journal*, 68(6), 343-359.

Zhang, J.A., & Paige, D.A. (2009). Cold-trapped organic compounds at the poles of the Moon and Mercury: Implications for origins. *Geophysical Research Letters*, 36(L16203), 1-5.

CHAPTER 6

CONCLUSION

This dissertation contributes to our understanding on how TIR-emission spectroscopy can be used to prospect for magmatic sulfide ore deposits, where the best locations for mining and establishing bases for operations are on the Lunar South Pole, and how to govern mining activities in space.

Chapter 2 presents a new calibration and measurement technique (the Reference Temperature Method) for deriving the absolute emissivity of graybody materials in the mid-infrared. The technique demonstrated that pyrrhotite ($Fe_{1-x}S$)–the most common sulfide phase in magmatic ore deposits–is nearly spectrally featureless and exhibits systematically low emissivity from 5-40 microns, which would make them very difficult to detect using infrared spectroscopy. In addition, we discovered that pyrrhotite lacks a Christiansen Frequency in the mid-infrared and is highly reflective across the mid-infrared.

Without a Christiansen Frequency, it is incredibly challenging to accurately determine its true kinetic temperature. Thus, when using the conventional calibration routine used in space applications, which assumes unit emissivity somewhere in its emissivity spectrum to estimate temperature (Ruff et al., 1997), pyrrhotite "appears" much colder than its true kinetic temperature and, as a result, its emissivity spectrum exhibits a severe spectral slope from high to low wavenumbers. These errors were significantly constrained using our new Reference Temperature Method by replacing the incorrect temperature with the temperature of a reference sample with a known Christiansen Frequency. These results can be applied to martian remote sensing data to

prospect for sulfides. Rather than searching for diagnostic absorption features to explore sulfide deposits, our experiments suggest searching for anomalously cold areas and surfaces with severe spectral slopes.

In Chapter 2, we present the emissivity results of a 100% sulfide sample. In reality, extraterrestrial magmatic sulfide deposits will be accompanied by co-existing silicates. To further advance our understanding of whether sulfide mineralization could be detected on the surface of Mars using infrared spectroscopy, we conducted a series of experiments using physically constructed silicate/sulfide mixtures with variable amounts of sulfide. The results are described in Chapter 3. Our research demonstrates that the apparent brightness temperature decreases linearly as sulfide increases. However, this is a temperature error resulting from a graybody material in the mixture. This temperature error will contribute to a spectral slope from high to low wavenumbers on the resultant spectrum if left uncorrected. While complicating mineralogical interpretations, this demonstrates that magmatic rocks enriched in sulfide will appear colder than their surroundings and have a sloped emissivity spectrum if the data were calibrated using the calibration routine commonly used in remote sensing applications.

Next, we discovered that the magnitude of an absorption feature of a coexisting silicate mineral decreases linearly as the proportion of sulfide increases. While reductions in spectral contrast also occur as grain size decreases, a reduction in grain size also creates new transparency features in its emissivity spectrum. Therefore, the effects of a graybody component (e.g., sulfide) in a composite emissivity spectrum can be differentiated from grain size effects by inspecting the emissivity spectrum for transparency features. Thus, to prospect for sulfides on Mars using TIR-emission

spectroscopy, the results presented in Chapter 3 suggest looking for anomalously cold mafic/ultramafic terrain with an emissivity spectrum exhibiting a spectral slope from high to low wavenumbers and spectral features with reduced spectral contrast.

The next stage in this work is to explore remote sensing data of Mars collected by the Thermal Emission Spectrometer and the Thermal Emission Imaging System to search for exposed sulfide ore bodies. While spectrally featureless areas on Mars have already been identified by Osterloo et al. (2008,2010) and surfaces with spectral slopes attributed to be from graybody materials have been identified by Bandfield (2009), one should examine mafic/ultramafic terrain for anomalously cold apparent brightness temperatures. Additionally, the terrain's emissivity spectra should exhibit a severe spectral slope from high to low wavenumbers and the spectral signatures of the silicate minerals present should be severely reduced in contrast across the mid-infrared.

The best test of our experimental laboratory research would be to send an infrared spectrometer to Mars to explore the spectrally featureless materials already identified by Osterloo et al. (2010) and determine whether they are chlorides, sulfides, or some other mineral. If these deposits are indeed sulfides, they could be separated into metals and elemental sulfur using a process known as molten salt electrolysis (Liu et al., 2023). However, if they are indeed chlorides–as proposed by Osterloo et al. (2008, 2010)–they could be used as the electrolyte in molten salt electrolysis to produce O_2, S_2, and metal alloys from martian regolith. Such a mission would significantly advance our understanding of in-situ resource utilization.

Investigating graybody materials using mid-IR spectroscopy led me to hypothesize that the technique could be used as more than a prospecting tool. Molten-salt

electrolysis is a leading technology to produce oxygen on the Moon and Mars from regolith. The process involves the solid-state electrochemical reduction of regolith to produce O_2 and a byproduct alloy comprised of the cations found in the starting material (Lomax et al., 2020). Thus far, the molten-salt process is validated by measuring the rate of oxygen removal using a mass spectrometer and powder X-Ray Diffraction (Lomax et al., 2020). I hypothesize that thermal infrared emission spectroscopy could be used to validate the molten salt process in situ. The features in emissivity spectra are directly attributed to the vibrational modes of the cation-anion bonds in the mineral (Nash et al., 1993; Hamilton, 2010). However, when regolith is reduced during the molten salt process, the cation-anion bonds are destroyed. I hypothesize that the Christiansen Frequency and the spectral signatures of the components within the regolith would be eliminated. Similar to our results in Chapters 2 and 3, this would lead to inaccurate brightness temperature measurements and an emissivity spectrum with a steep slope from high to low wavenumbers. However, it would confirm that the reduction process was successful. In the future, I plan to test this hypothesis by measuring regolith simulants using a benchtop infrared spectrometer that was processed for different times using the molten salt process.

Suppose a molten salt electrolysis demonstration payload was sent to Mars along with an infrared spectrometer. In that case, the spectrometer could measure the regolith before and after processing to validate if the molten salt process met its engineering objectives. Moreover, the spectral results could be used with a mass spectrometer to determine how much oxygen was removed from the regolith feedstock and whether any constituents were not completely reduced.

In Chapter 4, we sought to identify the best locations at the Lunar South Pole for water ice mining and establishing bases for operations stations. To answer this question, we developed the Lunar Mining Map Tool. The tool utilizes a block system to divide the Lunar South Pole from 80ºS to 90ºS into a grid of blocks 1 km x 1 km in size. Each block was classified according to their average percent Earth visibility, illumination, slope, and maximum summer temperature. As a result, the tool identified 19,699 blocks suitable for mining, which are mainly located on the floors of shadowed impact craters, and 22,173 blocks suitable for establishing bases for operations, which were primarily located on the lunar nearside between -80ºN and -86ºN latitude.

We also defined the "best" blocks in the Lunar Mining Map Tool where the first operations stations should be established. Such blocks exhibited an average percent illumination and Earth visibility above the median values of the distribution of operations blocks and terrain flat enough to limit the need for significant site preparation. In total, 2,419 blocks fit this criterion, though only 29 were within 3 kilometers of a mining block. Finally, we used the Lunar Mining Map tool to assess the mining potential of the Artemis III candidate landing region. Faustini Rim A was deemed suitable for prospecting, Nobile Rim 2 for mining, and Malapert Massif for establishing bases for operations.

Whether it be myself or a future Ph.D. student, the work presented in Chapter 4 can be expanded on. For example, in addition to the parameters described above, blocks could also be classified according to their boulder abundance, for blocks containing a large number of boulders would be less suitable for mining or establishing bases for operations. Moreover, the Lunar Mining Map Tool classified each suitable mining block as a "Class 1" or "Class 2" block, where Class 1 blocks exhibit average maximum

summer temperatures low enough for water ice to remain thermally stable at the surface (Vasavada et al., 1999) and Class 2 exhibited average temperatures suitable to retain water ice within the upper meter of the surface (Landis et al., 2022). Yet, based on the LCROSS impact and spectroscopic evidence of comets, it is likely that there will be multiple contaminant species associated with the water ice being targeted for mining (Colaprete et al., 2010; Gladstone et al., 2010).

While techniques are being designed to purify lunar water ice (Holquist et al., 2020; Kornuta et al., 2018), certain blocks on the Moon may exhibit the appropriate minimum and maximum temperatures to act as a natural purification system. For example, blocks with a minimum and maximum surface temperatures of 80K and 120K, respectively, would be too warm to trap highly volatile contaminants found in meteorites and comets such as Ar, CO_2, SO_2, CH_4, NH_3, and H_2S and too cold for many hydrocarbons, organic compounds, Hg, and S to be stable (Zhang &Paige, 2009; Berezhnoy et al., 2012; Bockelée-Morvan & Biver, 2017). Thus, the Lunar Mining Map Tool could be refined to identify mining blocks with the purest water ice. Such blocks might be considered the most valuable since the ice would require the least downstream processing/purification. Blocks could also be identified with the appropriate minimum and maximum temperatures to selectively enrich certain blocks in volatile species requisite for other applications. Landis et al. (2022) have already developed maps tracking specific volatile species, which could be incorporated into the Lunar Mining Map.

Moreover, the Lunar Mining Map Tool could be enhanced by implementing additional map layers. For example, an additional layer that would prove useful is a map

that report the illumination conditions above the surface. This would allow for us to develop a modular map that can determine specific use cases for operations blocks. For example, blocks containing suitable illumination at the surface would be useful for specific operations such as landing, habitation, and surface operations, and those with the best illumination at five meters above the surface would be most appropriate for establishing photovoltaic systems.

Despite the resurgence of interest in the Moon and the utilization of its resources, a governance structure has yet to be proposed to manage lunar mining activities. This was the motivation of our work presented in Chapter 5. In Chapter 5, we propose an intergovernmental regime–the Lunar Resource Management Authority (LRMA)–whose primary responsibilities are to foster the responsible development of lunar resources, safeguard the lunar environment, and promote equitable access. Inspired by the only intergovernmental regime responsible for managing mining activities in Areas Beyond National Jurisdiction, the International Seabed Authority, we recommended that the LRMA develop a Lunar Mining Code containing a notification process that operators must comply with to conduct prospecting activities for water ice and a contract system that issues out temporary, but exclusive licenses to conduct exploration activities in allotted areas of the lunar surface to identify a water ice mine site. We also proposed a set of area-based management principles and best practices to guide the behavior of operators, including spatial and temporal constraints on exploration licenses, Reserved Areas, a relinquishment procedure, Impact Reference Zones, and Lunar Preservation Areas. Each measure and regulation would be implemented using the Lunar Mining Map

Tool's block system to simplify development, compliance, transparency, and enforcement.

In Chapter 4, we identified the blocks in the Lunar South Pole Resource System most suitable for establishing a base for operations. In my future work, I plan to expand the Lunar Mining Code described in Chapter 5 to include rules, regulations, procedures, and best practices to manage operations activities. For example, the proposed "contract system" in Chapter 5 can be adapted to issue temporary but exclusive licenses to companies who wish to conduct operations activities to support a mine site, including:

(1) excavation, beneficiation, and regolith transport,

(2) site planning and preparation (i.e., leveling, landing pads, roads, berms),

(3) infrastructure development and utilities operations (i.e., propellant storage depot, mineral and chemical processing plant, landing facility, power plant, communications station, habitat complex),

(4) environmental remediation/recycling.

Similar to the "block system" we recommended for issuing licenses to explore for water ice, an applicant would be required submit an application for approval by the LRMA for a license to conduct operations activities in a pre-determined number of "operations blocks" within the Lunar South Pole Resource System. Operations licenses will also require some form of temporal and spatial limitations and area-based environmental regulations, for it is illegal to appropriate areas of the Moon, regardless of the activities. In the water ice Mining Code, 120 blocks were proposed per exploration contract, which will likely change as we learn more about the abundance of water ice. The number of blocks per operations contract would likely be much smaller. Sherwood

(2018) describes a minimal reference base concept whose primary industry is the production of liquid oxygen for propellant. The site plan for the base, which included a regolith-shielded habitat complex, three reusable cryogenic landers, twenty-four photovoltaic arrays, two regenerable fuel cell modules, a lunar liquid oxygen storage depot, an open workyard, and a spaceport with paved landing pads and connecting roads, required ~0.18 km^2 of the lunar surface (Sherwood, 2018). If the minimal reference base were required to expand by a factor of ten to account for an industrial-scale water-ice mining venture, just two blocks in the Lunar South Pole Resource System would be required to conduct such operations activities. Nonetheless, such areas will still require governance to ensure that the Moon's environment is not adversely affected and that other operators' activities are not compromised.

For example, suppose an operator elects to apply to the LRMA for an operations license to conduct excavation activities to produce materials for construction. Such activities would likely suspend significant amounts of dust into the lunar exosphere, implying that the LRMA will need to develop a suite of best operations practices and area-based regulations to limit the effects of such activities on the lunar environment.

The recommended regulations, best practices, and governance structure proposed in Chapter 5 should be understood as a preliminary framework and are subject to change as technology advances and as we learn more about the Moon's available resources. However, a structure and suite of regulations must be developed before mining activities begin to establish a precedent. Though nascent, the Lunar Mining Map's block system we proposed in Chapter 5 provides a simple and standardized way to administer a prospecting notification process, an exploration and exploitation contract system, develop

best mining practices, and implement area-based environmental regulations. Moreover, the block system is beneficial because it allows an institution to delineate specific areas on the Moon where an operator is afforded rights. This will ensure companies that their investments are secure and increase their willingness to develop the Moon.

References:

Bandfield, J. (2009). Effects of surface roughness and graybody emissivity on martian thermal infrared spectra. *Icarus*, 202(2), 414–428

Berezhnoy, A.A., Kozlova, E.A., Sinitsyn, M.P., Shangaraev, A.A., & Shevchenko, V.V. (2012). Origin and stability of lunar polar volatiles. *Advances in Space Research*, 50(12), 1238–1646.

Bockelée-Morvan, D., & Biver, N. (2017). The composition of cometary ices. *Phil. Trans. R. Soc. A*, 375(2016252), 1-11.

Colaprete, A., Schultz, P., Heldmann, J., Wooden, D., Shirley, M., Ennico, K., Hermalyn, B., Marshall, W., Ricco, A., Elphic, R.C., Goldstein, D., Summy, D., Bart, G.D., Asphaug, E., Korycansky, D., Landis, D., & Sollitt, L. (2010). Detection of water in the LCROSS ejecta plume. *Science*, 330(6003), 463.

Gladstone, G.R., Hurley, D.M., Retherford, K.D., Feldman, P.D., Pryor, W.R., Chaufray, J.-Y., Versteeg, M., Greathouse, T.K., Stefl, A.J., Throop, H., Parker, J.W.M., Kaufman. D.E., Egan, A.F., Davis, M.W., Slater, D.C., Mukherjee, J., Miles, P.F., Hendrix, A.R., Colaprete, A., & Stern, S.A. (2010). LRO-LAMP Observations of the LCROSS Impact Plume. *Science*, 330(6003), 472-476.

Hamilton, V.E. (2010). Thermal infrared (vibrational) spectroscopy of Mg-Fe olivines: A review and applications to determining the composition of planetary surfaces. *Chemie der Erde*, 70, 7–33.

Holquist, J.B., Pasadilla, P., Bower, C., Cognata, T., Tewews,, & Kelsey, P. (2020). Analysis of a Cold Trap as a Purification Step for Lunar Water Processing. *International Conference on Environmental Systems.* Pp. 1-12. https://ttu-ir.tdl.org/handle/2346/86336.

Kornuta, D., Abbud-Madrid, A., Atkinson, J., Barr, J., Barnhard, G., Bienhoff, D., Blair, B., Clark, V., Cyrus, J., deWitt, B., Dreyer, C., Finger, B., Goff, J., Ho, K. Kelsey, L., Keravala, J., Kutter, B., Metzger, P., Montgomery, L., Morrison, P., Neal, C., Otto, E., Roesler, G., Schier, J., Seifert, B., Sowers, G., Spudis, P., Sundahl, M., Zacny, K., & Zhu, G. (2019). Commercial lunar propellant architecture: A collaborative study of lunar propellant production. *Reviews in Human Space Exploration*, 129(100026), 1-77.

Landis, M.E., Hayne, P.O., Williams, J.-P., Greenhagen, B.T., & Paige, D.A. (2022). Spatial Distribution and Thermal Diversity of Surface Volatile Cold Traps at the Lunar Poles, *The Planetary Science Journal.* 3(39), 1–13.

Lomax, B.E., Conti, M., Khan, N., Bennett, N.S., Ganin, A.Y., & Symes, M.D. (2020). Proving the viability of an electrochemical process for the simultaneous extraction of oxygen and production of metal alloys from lunar regolith. *Planetary and Space Science*, 180(104748), 1–10.

Nash, D.B., Salisbury, J.W., Conel, J.E., Lucey, P.G., & Christensen, P.R. (1993). Evaluation of Infrared Emission Spectroscopy for Mapping the Moon's Surface Composition From Lunar Orbit. *Journal of Geophysical Research*, 98(E12), 23535-23552.

Osterloo, M. M., Anderson, F. S., Hamilton, V. E., & Hynek, B. M. (2010). Geologic context of proposed chloride-bearing materials on Mars. *Journal of Geophysical Research*, 115(E10012), 1–29.

Osterloo, M. M., Hamilton, V. E., Bandfield, J. L., Glotch, T. D., Baldridge, A. M., Christensen, P. R., et al. (2008). Chloride-bearing materials in the southern highlands of Mars. *Science*, 319(5870), 1651–1654.

Ruff, S.W., Christensen, P.R., Barbera, P.W., & Anderson, D.L. (1997). Quantitative thermal emission spectroscopy of minerals: A laboratory technique for measurement and calibration. *Journal of Geophysical Research*, 102(B7), 14899–14913.

Sherwood, B. (2018). Principles of a Practical Moon Base. *69th International Astronautical Congress.* IAC-18.A3.1.6.x46496. (p.1–13).

Vasavada, A. R., Paige, D. A., & Wood, S. E. (1999). Near-Surface Temperatures on Mercury and the Moon and the Stability of Polar Ice Deposits. *Icarus*, 141(2), 179-193. https://doi.org/10.1006/icar.1999.6175.

Zhang, J.A., & Paige, D.A. (2009). Cold-trapped organic compounds at the poles of the Moon and Mercury: Implications for origins. *Geophysical Research Letters*, 36(L16203), 1-5.

REFERENCES

Abramowski, T. (2014). Activities of the IOM within the scope of geological exploration for polymetallic nodule resources. *Workshop on Polymetallic Nodule Resources Classification*. October 13–17, 2014, Goa, India.

Abrams, M. (2000). The Advanced Spaceborne Thermal Emission and Reflection Radiometer (ASTER): Data products for the high spatial resolution imager on NASA's terra platform. *International Journal of Remote Sensing*, 21(5), 847–859.

Agreement relating to the Implementation of Part XI of the United Nations Convention on the Law of the Sea. 10 December 1982, A/RES/48/263, Annex.

Altunaiji, E., Edwards, C. S., Smith, M. D., & Christensen, P. R. (2017). Scientific payload of the Emirates Mars mission: Emirates Mars infrared spectrometer (EMIRS) overview. In *6th international workshop on the Mars atmosphere: Modelling and observations* (pp. 17–20).

Amy, C., Bégin, M.-A., Browder, B., Chan, M., Dawson, C., do Vale Pereira, P., Hank, T.J., Hinterman, E., Lordos, G., Martell, B., Miller, A., O'Neill, C., Padia, V.J., Stamler, N., Todd, J., Wang, N., Newman, D.J., de Weck, O.L., & Hoffman, J.A. (2020). Autonomously Deployable Tower Infrastructure for Exploration and Communication in Lunar Permanently Shadowed Regions. *ASCEND 2020*, p.4019.

Anand, M. (2010). Lunar water: A brief review. *Earth, Moon, and Planets,* 107, 65–73.

Anand, M., Crawford, I.A., Balat-Pichelin, M., Abanades, S., van Westrenen, W., Péraudeau, G., Jaumann, R. and W. Sebolt. (2010) A brief review of chemical and mineralogical resources on the Moon and likely initial in situ resource utilization (ISRU) applications. *Planetary and Space Science*, 74, 42–48.

Antrim, C.L. (2005). Mineral Resources of Stateless Space: Lessons From the Deep Seabed. *Journal of International Affairs,* 59(1), 55-80.

Arndt, N., Lesher, C. M., & Czamanske, G. K. (2005). Mantle-derived magmas and magmatic Ni-Cu-(PGE) deposits. In *Economic geology*, (pp. 5–24). 100th anniversary, Retrieved from https://hal.archives-ouvertes.fr/hal-00016864

Arnold, J.R. (1979). Ice in the lunar polar regions. *Journal of Geophysical Research*, 84(B10), 5659-5668.

Ashley, J. W. (2011). Meteorites on Mars as planetary research tools with special considerations for Martian weathering processes. Doctoral dissertation, Arizona State University (p.343).

Averill, S. A. (2011). Viable indicator minerals in surficial sediments for two major deposit types: Ni-Cu-PGE and porphyry Cu. *Geochemistry: Exploration, Environment, Analysis*, 11(4), 279–291.

Azur Solar Power GmbH. (2020). SPACE Solar Cells. https://www.azurspace.com/index.php/en/products/products-space/space-solar-cells [Accessed January 28, 2023].

Badri, K., Altunaiji, E., Edwards, C. S., Smith, M. D., Christensen, P. R., Almheiri, S., et al. (2018). Scientific payload of the Emirates Mars mission: Emirates Mars Infrared Spectrometer (EMIRS). In *European Planetary Science Congress* (pp. 1–3). Retrieved from https://meetingorganizer.copernicus.org/EPSC2018/EPSC2018-1007.pdf

Bailey, J.S. (1983). The Future of the Exploitation of the Resources of the Deep Seabed and Subsoil. *Law & Contemp. Probs*, 46(2), 70-76.

Bandfield, J. (2002). Global mineral distributions on Mars. *Journal of Geophysical Research*, 107(E6), 1–20.

Bandfield, J. (2009). Effects of surface roughness and graybody emissivity on martian thermal infrared spectra. *Icarus*, 202(2), 414–428

Bandfield, J., & Edwards, C.S. Edwards. (2008). Derivation of martian surface slope characteristics from directional thermal infrared radiometry. *Icarus*, 193, 139–157.

Barker, M.K., Mazarico, E., Neumann, G.A., Smith, D.E., Zuber, M.T., & Head, J.W. (2021). Improved LOLA Elevation Maps for South Pole Landing Sites: Error Estimates and Their Impact on Illumination Conditions. *Planetary & Space Science*, 203(1)105119, 1-16.

Barnes, S. J. (2006). Komatiite-hosted nickel sulfide deposits: Geology, Geochemistry, and Genesis (Vol. 13, pp. 51–118). Society of Economic Geologists.

Barnes, S. J., & Fiorentini, M. I. (2012). Komatiite magmas and sulfide nickel deposits: A comparison of variability endowed Archean terranes. *Economic Geology*, 107(5), 755–780.

Barnes, S. J., & Lightfoot, P. C. (2005). Formation of magmatic nickel-sulfide ore deposits and processes affecting their copper and platinum-group element contents. In *Economic Geology*, 100th anniversary (pp. 179–213).

Barnes, S. J., Holwell, D. A., & Le Vaillant, M. (2017). Magmatic sulfide ore deposits. *Elements*, 13(2), 89–95.

Basilevsky, A., Krasilnikov, S.S., Ivanov, M.A., Malenkov, M.I., Michael, G.G., Liu, T., Head, J.W., Scott, D.R., & Lark, L. (2019). *Solar System Research*, 53(5), 383–398.

Baumgartner, R. J., Fiorentini, M. L., Baratoux, D., Micklethwaite, S., Sener, A. K., Lorand, J. P., & McCuaig, T. C. (2015). Magmatic controls on the Genesis of Ni–Cu±(PGE) sulphide mineralisation on Mars. *Ore Geology Reviews*, 65, 400–412.

Baumgartner, R.J., Baratoux, D., Gaillard, F., & Fiorentini, M.I. (2017). Numerical modeling of erosion and assimilation of sulfur-rich substrate by martian lava flows: Implications for the genesis of massive sulfide mineralization on Mars. *Icarus*, 296, 257–274.

Begemannm D., Dorschner, J., Henning, T., Mutschke, H., & Thamm, E. (1994). A Laboratory Approach to the Interstellar Sulfide Dust Problem. *The Astrophysical Journal*, 423. L71–L74.

Berezhnoy, A.A., Kozlova, E.A., Sinitsyn, M.P., Shangaraev, A.A., & Shevchenko, V.V. (2012). Origin and stability of lunar polar volatiles. *Advances in Space Research*, 50(12), 1238–1646.

Bernold, L. (1991). Experimental studies on mechanics of lunar excavation. *Journal of Aerospace Engineering*, 4(1), 9–22. ASCE, NY.

Bibring, J.-P., Langevin, Y., Gendrin, A., Gondet, B., Poulet, F., Berthé, M., Soufflot, A., Arvidson, R.., Mangold, N., Mustard, J., Drossart, P., & the OMEGA Team. (2005). Mars Surface Diversity as Revealed by the OMEGA/Mars Express Observations. *Science*, 307(5715), 1576–1581.

Binder, A.B. (1998). Lunar Prospector: A Review. *Science*, 281(5382), 1475-1476.

Blake, D., Vaniman, D., Achilles, C., Anderson, R., Bish, D., Bristow, T., Chen, C., Chipera, S., Crisp, J., Des Marais, D., Downs, R.T., Farmer, J., Feldman, S., Fonda, M., Gailhanou, M., Ma, H., Ming, D.W., Morris, R.V., Sarrazin, P., Stolper, E., Treiman, A., & Yen, A. (2012). Characterization and Calibration of the CheMin Mineralogical Instrument on Mars Science Laboratory. *Space Science Reviews*, 170, 341–399.

Blakely, R.J., & Zientek, M.L. (1985). Magnetic Anomalies Over A Mafic Intrusion: The Stillwater Network. Ed: Czamanske, G.K. and M.L. Zientek *In: The Stillwater Complex, Montana: Geology and Guide. Special Publication 92*. pp. 39-46.

Bockelée-Morvan, D., & Biver, N. (2017). The composition of cometary ices. *Phil. Trans. R. Soc. A*, 375(2016252), 1-11.

Boles, W., & Connolly, J. (1996). Lunar Excavating Research. *Proceedings of SPACE 96.* (Pp. 699–705).

Bramble, M. S., Milliken, R. E., & Patterson, W. R., III. (2021a). Thermal emission measurements of ordinary chondrite mineral analogs in a simulated asteroid environment: 1. *Constituent mineral phases*. *Icarus*, 369(114561), 1–22.

Bramble, M. S., Milliken, R. E., & Patterson, W. R., III. (2021b). Thermal emission measurements of ordinary chondrite mineral analogs in a simulated asteroid environment: 2. Representative mineral mixtures. *Icarus*, 369(114251), 1–24.

Bramble, M. S., Yang, Y., Patterson, W. R., Milliken, R. E., Mustard, J. F., & Donaldson Hanna, K. L. (2019). Radiometric calibration of thermal emission data from the asteroid and lunar environment chamber (ALEC). *Review of Scientific Instruments*, 90(093101), 1–20.

Breitenfeld, L. B., Rogers, A. D., Glotch, T. D., Hamilton, V. E., Christensen, P. R., Lauretta, D. S., et al. (2021). Machine learning mid-infrared spectral models for predicting modal mineralogy of CI/CM chondritic asteroids and Bennu. *Journal of Geophysical Research: Planets*, 126(12), e2021JE007035.

Breitenfeld, L. B., Rogers, A. D., Glotch, T. D., Kaplan, H. H., Hamilton, V. E., & Christensen, P. R. (2022). Mapping phyllosilicates on the asteroid Bennu using thermal emission spectra and machine learning model applications. *Geophysical Research Letters*, 49(20), e2022GL100815.

Broadus, J.M., & Hoagland III, P. (1984). Conflict Resolution in the Assignment of Area Entitlements for Seabed Mining. Conflict Resolution, *San Diego Law Review*, 21(3), 541-576.

Bryant, S. (2009). Lunar Pole Illumination and Communications Maps Computed from GSSR Elevation Data. *IEEEAC*, Big Sky, MT, USA. Pp. 1-19.

Budden, J. (2019). Defending the lunar landscape. *Phys. World*, 32(7), 21.

Burns, R. G. (1988). Gossans on Mars. In *The proceedings of the 18th Lunar and Planetary Science* (pp. 713–721).

Burns, R. G., & Fisher, D. S. (1990). Iron-sulfur mineralogy of Mars: Magmatic evolution and chemical weathering products. *Journal of Geophysical Research*, 95(B9), 14415–14421.

Burns, R.G., & Huggins, F.E. (1972). Cation determinative curves for MG–Fe–Mn olivines from vibrational spectra. *American Mineralogist*, 57, 967–985.

Bussey, D.B.J., Lucey, P.G., Robinson, M.S., Steutel, D., Robinson, M.S., Spudis, P.D., & Edwards, K.D. (2003). Permanent Shadow in simple craters near the poles. *Geophysical Research Letters,* 30(6), 1–4.

Bussey, D.B.J., McGovern, J.A., Spudis, P.D., Neish, C.D., Noda, H., Ishihara, Y., & Sørensen, S.-A. (2010). Illumination conditions of the south pole of the Moon derived using Kaguya topography. *Icarus,* 208, 558–564.

Bussey, D.B.J., Spudis, P.D., & Robinson, M.S. (1999). Illumination conditions at the lunar south pole. *Geophysical Research Letters,* 26, 1187–1190.

Buxton, C.R. (2004). Property in Outer Space: The Common Heritage of Mankind Principle Vs. the "First in Line, First in Right" Rule of Property Law. *Journal of Air and Law Commerce*, 69(4), 689-708.

Cabri, L. J., Rudashevsky, N. S., Rudashevsky, V. N., & Oberthür, T. (2008). Paper 14: Electric-pulse disaggregation (EPD), hydroseparation (Hs) and their use in combination for mineral processing and advanced characterization of ores. In *40th Annual Meeting of the Canadian Mineral Processors* (Vol. 14, pp. 211–235).

Cain, J.R. (2010). Lunar dust: The Hazard and Astronaut Exposure Risks. *Earth, Moon, and Planets,* 107, 107–125.

Campbell, I.H. & Naldrett. A.J. (1979). The influence of silicate: sulfide ratios on the geochemistry of magmatic sulfides. Economic Geology, 74(6), 1503–1506.

Cannon, K.M., & Britt, D.T. (2020). A geologic model for lunar ice deposits at mining scales. *Icarus*, 347(113778), 1-11.

Capper, D. (2022). What Should We Do With Our Moon?: Ethics and Policy for Establishing International Multiuse Lunar Land Reserves. *Space Policy*, 59(101462), 1-10.

Carrier III, W.D., Olhoeft, G.R., & Mendell, W. (1991). Physical Properties of the Lunar Surface. In: Heiken, G.H., Vaniman, D.T. and B.M. French (Eds.) *Lunar Sourcebook*. pp. 475-594.

Cawthorne, R. G. (2010). The platinum group element deposits of the bushveld complex in South Africa. *Platinum Metals Review*, 54(4), 205–215.

Chen, G., & Fray, D. (2020). Chapter 11 – Invention and fundamentals of the FFC Cambridge Process. *In: Extractive Metallurgy of Titanium*, 227-286.

Chen, G., Fray, D., & Farthing, T. (2000). Direct electrochemical reduction of titanium dioxide to titanium in molten calcium chloride. *Nature*, 407, 361–364.

Chin, G., Brylow, S., Foote, M., Garvin, J., Kasper, J.., Keller, J., Litvak, M., Mitrofanov, I., Paige, D., Raney, K., Robinson, M., Sanin, A., Smith, D., Spence, H., Spudis, P., Stern, S.A., & Zuber, M. (2007). Lunar Reconnaissance Orbiter Overview: The Instrument Suite and Mission. *Space Science Reviews*, 129, 319–419.

Christensen, P. R., & Harrison, S. T. (1993). Thermal infrared emission spectroscopy of natural surfaces: Application to desert varnish coatings on rocks. *Journal of Geophysical Research*, 98(B11), 19819–19834.

Christensen, P. R., Anderson, D. L., Chase, S. C., Clark, R. N., Kieffer, H. H., Malin, M. C., et al. (1992). Thermal emission spectrometer experiment: Mars observer mission. *Journal of Geophysical Research*, 97(E5), 7719–7734.

Christensen, P. R., Bandfield, J. L., Hamilton, V. E., Howard, D. A., Lane, M. D., Piatek, J. L., et al. (2000). A thermal emission spectral library of rock-forming minerals. *Journal of Geophysical Research*, 105(E4), 9735–9739.

Christensen, P. R., Bandfield, J. L., Hamilton, V. E., Ruff, S. W., Kieffer, H. H., Titus, T. N., et al. (2001). Mars Global surveyor thermal emission spectrometer experiment: Investigation description and surface science results. *Journal of Geophysical Research*, 106(E10), 23823–23871.

Christensen, P. R., Bandfield, J. L., Smith, M. D., Hamilton, V. E., & Clark, R. N. (2000). Identification of a basaltic component on the Martian surface from thermal emission spectrometer data. *Journal of Geophysical Research*, 105(E4), 9609–9621.

Christensen, P. R., Hamilton, V. E., Mehall, G. L., Pelham, D., O'Donnell, W., Anwar, S., et al. (2018). The OSIRIS-REx thermal emission spectrometer (OTES) instrument. *Space Science Reviews*, 214(87), 1–39.

Christensen, P. R., Jakosky, B. M., Kieffer, H. H., Malin, M. C., McSween, H. Y., Jr., Nealson, K., et al. (2004). The thermal emission imaging system for the Mars 2001 Odyssey mission. *Space Science Reviews*, 110(1/2), 85–130.

Christensen, P. R., McSween Jr, H. Y., Bandfield, J. L., Ruff, S. W., Rogers, A. D., Hamilton, V. E., et al. (2005). Evidence for magmatic evolution and diversity on Mars from infrared observations. *Nature*, 436(7050), 504–509.

Christensen, P. R., Mehall, G. L., Silverman, S. H., Anwar, S., Cannon, G., Gorelick, N., et al. (2003). Miniature thermal emission spectrometer for the Mars exploration rovers. *Journal of Geophysical Research*, 108(E12), 1–23.

Christensen, P. R., Wyatt, M. B., Glotch, T. D., Rogers, A. D., Anwar, S., Arvidson, R. E., et al. (2004). Mineralogy at Meridiani Planum from the Mini-TES experiment on the opportunity rover. *Science*, 306(5702), 1733–1739.

Christensen, P.R. (1986). The spatial distribution of rocks on Mars. *Icarus*, 68, 217–238.

Christensen, P.R., Bandfield, J.L., Hamilton, V.E., Ruff, S.W., Kieffer, H.H., Titus, T.N., Malin, M.C., Morris, R.V., Lane, M.D., Clark, R.L., Jakosky, B.M., Mellon, M.T., Pearl, J.C., Conrath, B.J., Smith, M.D., Clancy, R.T., Kuzmin, R.O., Roush, T., Mehall, G.L., Gorelick, N., Bender, K., Murray, Dason, S., Greene, E., Silverman, S., & Greenfield, M. (2001). Mars Global Surveyor Thermal Emission Spectrometer experiment: Investigation description and surface science results. Journal of Geophysical Research, 106(E10), 23823–23871.

Christensen, P.R., Morris, R.V., Lane, M.D., Bandfield, J.L., & Malin, M.C. (2001). Global mapping of Martian hematite mineral deposits: Remnants of water-driven processes on early Mars. *Journal of Geophysical Research,* 106(E10), 23,873–23,885.

Christensen, P.R., Wyatt, M.B., Glotch, T.D., Rogers, A.D., Anwar, S., Arvidson, R.E. … Wolff, M.J. (2004). Mineralogy at Meridiani Planum from the Mini-TES Experiment on the Opportunity Rover. Science, 306, 1733–1739.

Chyba, C.F., & Sagan, C. (1992). Endogenous production, exogenous delivery and impact-shock synthesis of organic molecules: an inventory for the origins of life. *Nature*, 355, 125–132.

Cilliers, J.J., Rasera, J.N., & Hadler, K. (2020). Estimating the scale of Space Resource Utilisation (SRU) operations satisfy lunar oxygen demand. *Planetary and Space Science,* 180(104749), 1-8.

Cockell, C., & Horneck, G. (2004). A Planetary Park system for Mars. *Space Policy*, 20, 291–295.

Cockell, C., & Horneck, G. (2006). Planetary Parks-formulating a wilderness policy for planetary bodies. *Space Policy*, 22(4), 256–261.

Colaprete, A. (2021). Volatiles Investigating Polar Exploration Rover (VIPER). NASA. https://ntrs.nasa.gov/api/citations/20210015009/downloads/20210015009%20-%20Colaprete-VIPER%20PIP%20final.pdf.

Colaprete, A., Andrews, D., Bluethmann, W., Elphic, R.C., Bussey, B., Trimble, J., Zacny, K. and J.E. Captain. (2019). An Overview of the Volatiles Investigating Polar Exploration Rover (VIPER) Mission. American Geophysical Meeting, Fall Meeting 2019, ab. #P34B-03.

Colaprete, A., Elphic, R.C., Heldmann, J., & Ennico, K. (2012). An Overview of the Lunar Crater Observation and Sensing Satellite (LCROSS). *Space Science Reviews*, 167, 3–22.

Colaprete, A., Schultz, P., Heldmann, J., Wooden, D., Shirley, M., Ennico, K., Hermalyn, B., Marshall, W., Ricco, A., Elphic, R.C., Goldstein, D., Summy, D., Bart, G.D., Asphaug, E., Korycansky, D., Landis, D., & Sollitt, L. (2010). Detection of water in the LCROSS ejecta plume. *Science*, 330(6003), 463.

Colozza, A.J. (1990). Analysis of Lunar Regolith Thermal Energy Storage. NASA/CR 189073. (Pp. 1-9).

Colozza, A.J. (2020). Small Lunar Base Camp and In Situ Resource Utilization Oxygen Production Facility Power System Comparison; NASA/CR 2020-2200368. (pp. 98). Available Online. https://ntrs.nasa.gov/api/citations/20200001622/downloads/20200001622.pdf [accessed January 28, 2023].

Colwell, J.E., & Jakosky, B.M. (2002). Effects of topography on thermal infrared spectra of planetary surfaces. *Space Sci. Rev*. 110, 85–130.

Committee on Space Research. (2021). COSPAR Policy on Planetary Protection. *Space Research Today*, 211, 12-25.

Conel, J.E. (1969). Infrared emissivities of silicates: experimental results and a cloudy atmosphere model of spectral emission from condensed particulate mediums. *Journal of Geophysical Research*, 74(6), 1614–1634.

Connolly, J., & Shoots, D. (1994). Transferring Construction Technology to the Moon and Back. *Proceedings of SPACE 94.* ASCE, NY. Pp. 1086–1096.

Costes, N.C., Farmer, J.E., & George, E.B. (1972). Mobility Performance of the Lunar Roving Vehicle: Terrestrial Studies – Apollo 15 Results. NASA TR R-401. (Pp.86).

Coto, M.E., Pazar, C.C., McKeown, B., & Shanley, C. (2021). Lunar Regolith Sample Excavation Company: A Space Resource Business Plan. *ASCEND 2021*, (Pp. 45).

Cousin, A., Sautter, V., Fabre, C., Dromart, G., Montagnac, G., Drounet, C. … & Wiens, R.C. (2022). SuperCam calibration targets on board the perseverance rover: Fabrication and quantitative characterization. Spectrochimica Acta Part B: *Atomic Spectroscopy*, 188(106341), 1–26.

Crider, D.H., & Vondrak, R.R. (2003). Space weathering effects on lunar cold trap deposits. *Journal of Geophysical Research.* 108(E7), 1-11.

Daintith, T., & Gault, I. (1977). Pacta Sunt Servanda and the Licensing and Taxation of North Sea Oil Production. *Cambrian Law Review*, 8:27–44.

Dallas, J.A., Raval, S., Saydam, S., & Dempster, A.G. (2021). An Environmental Impact Assessment Framework for Space Resource Extraction. *Space Policy*, 57(101441), 1-12.

Dam, K.W. (1965). Oil and Gas Licensing and the North Sea. *The Journal of Law & Economics*, 8, 51–75.

de O. Bittencourt Neto, O., Hoffmann, M., Masson-Zwaan, T., & Stefoundi, D. (2020). Building Blocks for the Development of an International Framework for the Governance of Space Resources Activities: A Commentary. (pp. 167). Eleven.

De Rosa, D., Bussey, B., Cahill, J.T., Lutz, T., Crawford, I.A., Hackwill, T., van Gasselt, S., Neukum, G., Witte, L., McGovern, A., Grindrod, P.M., & Carpenter, J.D. (2012). Characterisation of potential landing sites for the European Space Agency's Lunar Lander project. *Planetary and Space Sciences,* 74(1), 224–246.

Deutsch, A.N., Head, J.W., & Neumann, G.A. (2020). Analyzing the ages of south polar craters on the Moon: Implications for the sources and evolution of surface water ice. *Icarus,* 336(15), 1-10.

Ding, S., Dasgupta, R., & Tsuno, K. (2014). Sulfur concentration of martian basalts at sulfide saturation at high pressures and temperatures – Implications for deep sulfur cycle on Mars. *Geochimica et Cosmochimica Acta*, 131, 227–246.

Donaldson Hanna, K. L., Cheek, L. C., Pieters, C. M., Mustard, J. F., Greenhagen, B. T., Thomas, I. R., & Bowles, N. E. (2014). Global assessment of pure crystalline plagioclase across the Moon and implications for the evolution of the primary crust. *Journal of Geophysical Research: Planets*, 119(7), 1516–1545.

Donaldson Hanna, K. L., Wyatt, M. B., Thomas, I. R., Bowles, N. E., Greenhagen, B. T., Pieters, C. M., et al. (2012). Thermal infrared emissivity measurements under a simulated lunar environment: Application to the Diviner Lunar Radiometer Experiment. *Journal of Geophysical Research*, 117(E12), 1–15.

Donaldson Hanna, K.L., Cheek, L.C., Pieters, C.M., Mustard, J.F., Wyatt, M.B., & Greenhagen, B.T. (2012). Global indications of crystalline plagioclase across the lunar surface using M3 and Diviner data. *Proc. Lunar Planet. Sci. Conf.*, 43,1968.

Duke, M.B., Gaddis, L.R., Taylor, G.J., & Schmitt, H.H. (2006). Development of the Moon. *Reviews in Mineralogy and Geochemistry*, 60(1), 597–655.

Eastes, J. (1989). Spectral properties of halite-rich mineral mixtures: Implications for middle infrared remote sensing of highly saline environments. *Remote Sensing of Environment,* 27(3), 289–304.

Edwards, C. S., & Christensen, P. R. (2013). Microscopic emission and reflectance thermal infrared spectroscopy: Instrumentation for quantitative in situ mineralogy of complex planetary surfaces. *Applied Optics*, 52(11), 2200–2217.

Egede, E., Pal, M., & Charles, E. (2019). A Study Related to Issues on the Operationalization of the Enterprise. Legal, Technical and Financial Implications for the International Seabed Authority and for States Parties to the United Nations Convention on the Law of the Sea. Technical Report 1/2019. Pp. 1-50.

Ehlmann, B., & Edwards, C. (2014). Mineralogy of the Martian surface. *Annual Review of Earth and Planetary Sciences*, 42(1), 291–315.

Elvis, M., & Milligan, T. (2019). How much of the Solar System should we leave as wilderness? *Acta Astronautica*, 162, 574–580.

European Space Policy Institute. (2021). Emerging Spacefaring Nations – Full Report. European Space Policy Institute (Eds). Pp 127. https://www.espi.or.at/wp-content/uploads/2022/06/ESPI-Report-79-Emerging-Spacefaring-Nations-Full-Report.pdf

Exec. Order. No. 13,914, 85 FR 20381. (2020). https://www.federalregister.gov/documents/2020/04/10/2020-07800/encouraging-international-support-for-the-recovery-and-use-of-space-resources

Farries, K., Visintin, P., Smith, S.T., & van Eyk, P. (2021). Sintered or melted regolith for lunar construction: state-of-the-art review and future research directions. *Construction and Building Materials,* 296, 1–31.

Fateri, M., Meurisse, A., Sperl, M., Urbina, D., Madakashira, H.K., Govindaraj, S., Gancet, J., Imhof, B., Hoheneder, W., Waclavicek, R., Preisinger, C., Podreka, E., Mohamed, M.P., & Weiss, P. (2019). *Journal of Aerospace Engineering*, 32(6), 04019101.

Federal Aviation Administration. (2022). Commercial Space Data. https://www.faa.gov/data_research/commercial_space_data/, Accessed: March 3, 2023.

Feely, K.C., & Christensen, P.R. (1999). Quantitative compositional analysis using thermal emission spectroscopy: Application to igneous and metamorphic rocks. *Journal of Geophysical Research*, 10(E10), 24195–24210.

Fegley, B., & Swindle, T.D. (1993). Lunar volatiles: implications for lunar resource utilization. In J. Lewis, M.S. Matthews & M.L. Guerrieri (Eds.), *Resources of near-Earth space*, 367–426.

Feldman, W.C., Maurice, S., Binder, A.B., Barraclough, B.L., Elphic, R.C., & Lawrence, D.J. (1998). Fluxes of fast and Epithermal Neutrons from Lunar Prospector: Evidence for Water Ice at the Lunar Poles. *Science*, 281(5382), 1496-1500.

Feldman, W.C., Maurice, S., Lawrence, D.J., Little, R.C., Lawson, S.L., Gasnault, O., Wiens, R.C., Barraclough, B.L., Elphic, R.C., Prettyman, T.H., Steinberg, J.T., & Binder, A.B., (2001). Evidence for water ice near the lunar poles. *J. Geophys. Res. Planets*, 106, 23231–23251.

Feng, J., Rivard, B., Gallie, E.A., & Sanchez, A. (2006). Quantifying total sulfide content of cores and cut-rock surfaces using thermal infrared reflectance. *Geophysics*, 71(3), M1-M9.

Filiberto, J. (2008). Similarities between the shergottites and terrestrial ferropicrites. *Icarus*, 197(1), 52–59.

Fincannon, J. (2008). Lunar Polar Illumination for Power Analysis. *In: 6th International Energy Conversion Engineering Conference (IECEC), July 28-30, 2006*, p. 5631.

Fisher, E.A., Lucey, P.G., Lemelin, M., Greenhagen, B.T., Siegler, M.A., Mazarico, E., Aharonson, O., Williams, J.-P., Hayne, P.O., Neumann, G.A., Paige, D.A., Smith, D.E., & Zuber, M.T. (2017). Evidence for surface water ice in the lunar polar regions using reflectance measurements from the Lunar Orbiter Laser Altimeter and temperature measurements from the Diviner Lunar Radiometer Experiment. *Icarus*, 292, 74–85.

Fisher, E.A., Lucey, P.G., Lemelin, M., Greenhagen, B.T., Siegler, M.A., Mazarico, E., Aharonson, O., Williams, J.-P., Hayne, P.O., Neumann, G.A., Paige, D.A., Smith, D.E., & Zuber, M.T. (2017). Evidence for surface water ice in the lunar polar regions using reflectance measurements from the Lunar Orbiter Laser Altimeter and temperature measurements from the Diviner Lunar Radiometer Experiment. *Icarus*, 292, 74–85.

Fortezzo, C.M., Spudis, P.D., & Harrel, S.L. (2020). Release of the Digitial Unified Global Geologic Map of the Moon at 1:5,000,000-scale. *Lunar and Planetary Science Conference 2020. No. 2326.*

Fray, D.J., Farthing, T.W. and Z. Chen. (1999). Removal of oxygen from Metal Oxides and Solid Solutions by Electrolysis in a Fused Salt. WO/99/64638. Retrieved from: https://patentimages.storage.googleapis.com/02/ff/c2/090b10cc5e821e/WO1999064638A1.pdf

Gaillard, F., & Scaillet, B. (2009). The sulfur content of volcanic gases on Mars. *Earth and Planetary Science Letters*, 279(1–2), 34–43.

Gaillard, F., Michalski, J., Berger, G., McLennan, S. M., & Scaillet, B. (2013). Geochemical reservoirs and timing of sulfur cycling on Mars. *Space Science Reviews*, 174(1–4), 25–300.

Ge, X.L., Wang, X.D., & Seetharaman, S. (2009). Copper extraction from copper ore by electro-reduction in molten $CaCl_2$–NaCl. *Electrochimica Acta*, 54, 4397–4402.

Gellert, R., Rider, R., Brückner, J., Clark, B.C., Dreibus, G., Klingelhöfer, G., Lugmair, G., Ming, D.W., Wänke, H., Yen, A., Zipfwl, J., & Squyres, S.W. (2006). Alpha Particle X-Ray Spectrometer (APXS): Results from Gusev crater and calibration report. *Journal of Geophysical Research: Planets*, 111(E2), 1-32.

Gertsch, L., Gustafson, R., & Gertsch, R. (2006). Effect of Water Ice Content on Excavatability of Lunar Regolith. *AIP Conference Proceedings*, 813, 1093-1100

Ghandi, A., &, Lin, C.-Y. (2014). Oil and gas service contracts around the world: A review. *Energy Strategy Rewards*, 3, 63–71.

Gibson, M.A., & Knudsen, C.W. (1985). Lunar oxygen production from ilmenite. In: W.W. Mendell (Ed.), *Lunar bases and space activities of the 21st century*. pp. 543-550.

Gillespie, A. (1992). Spectral mixture analysis of multispectral thermal infrared images. *Remote Sensing of Environment.* 42(2), 137-145.

Gillespie, A. Land Surface Emissivity. (2014). In: *Encyclopedia of Remote Sensing.* Njoku, E.G., (Ed.). Springer New York: New York, NY, USA. (pp. 303-311).

Gillespie, A., Rokugawa, S., Matsunga, T., Cothern, J.S., Hook, J., & Kahle, A.B. (1998). A temperature and emissivity separation algorithm for Advanced Spaceborne Thermal Emission and Reflection Radiometer (ASTER) images. *IEEE Transactions on Geoscience and Remote Sensing*, 36(4), 1113-1126.

Girish, T.E., & Aranya, S. (2012). Photovoltaic power generation on the moon: problems and prospects. *In: Moon*. Springer, Berlin, Heidelberg. (pp. 367-376).

Gissi, E., Maes, F., Kyriazi, Z., Ruiz-Frau, A., Santos, C. F., Neumann, B., Quintela, A., Alves, F. L., Borg, S., Chen, W., da Luz Fernandes, M., Hadjimichael, M., Manea, E., Marques, M., Platjouw, F. M., Portman, M. E., Sousa, L. P., Bolognini, L., Flannery, W., Grati, F., & Unger, S. (2022). Contributions of marine area-based management

tools to the UN sustainable development goals. *Journal of Cleaner Production,* 330, 129910. https://doi.org/10.1016/j.jclepro.2021.129910

Gladstone, G.R., Hurley, D.M., Retherford, K.D., Feldman, P.D., Pryor, W.R., Chaufray, J.-Y., Versteeg, M., Greathouse, T.K., Stefl, A.J., Throop, H., Parker, J.W.M., Kaufman. D.E., Egan, A.F., Davis, M.W., Slater, D.C., Mukherjee, J., Miles, P.F., Hendrix, A.R., Colaprete, A., & Stern, S.A. (2010). LRO-LAMP Observations of the LCROSS Impact Plume. *Science,* 330(6003), 472-476.

Gladstone, G.R., Retherford, K.D., Egan, A.F., Kaufmann, D.E., Miles, P.F., Parker, J.W.,Horvath, D., Rojas, P.M., Versteeg, M.H., Davis, M.W., Greathouse, T.K., Slater, D.C., Mukherjee, J., Steffl, A.J., Feldman, P.D., Hurley, D.M., Pryor, W.R., Hendrix, A.R.,Mazarico, E., & Stern, S.A. (2012). Far-ultraviolet reflectance properties of the Moon's permanently shadowed regions. *J. Geophys. Res. Planets,* 117(E00H04), 1-13.

Glasby, G.P. (2000). Lessons Learned from Deep-Sea Mining. *Science,* 289(5479), 551-553.

Glasby, G.P. (2002). Deep Seabed Mining: Past Failures and Future Prospects. *Marine Georesources and Geotechnology,* 20, 161–176.

Gläser, P., Oberst, J., Neumann, G.A., Mazarico, E., Speyerer, E.J., & Robinson, M.S. (2018). Illumination conditions at the lunar poles: Implications for future exploration. *Planetary and Space Science,* 162, 170–178.

Glotch, T. D., & Christensen, P. R. (2005). Geologic and mineralogic mapping of Aram Chaos: Evidence for a water-rich history. *Journal of Geophysical Research,* 110(E9), E09006.

Glotch, T. D., Bandfield, J., Wolff, M., Arnold, J., & Che, C. (2016). Constraints on the composition and particle size of chloride salt-bearing deposits on Mars. *Journal of Geophysical Research: Planets,* 121(3), 454–471.

Glotch, T. D., Morris, R. V., Christensen, P. R., & Sharp, T. G. (2004). Effect of precursor mineralogy on the thermal infrared emission spectra of hematite: Application to Martian hematite mineralization. *Journal of Geophysical Research,* 109(E7), 0700311–E70118.

Godel, B., & Barnes, S.-J. (2008). Platinum-group elements in sulphide minerals and the whole rocks of the J-M Reef (Stillwater Complex): Implication for the formation of the reef. *Chemical Geology*, 248(3–4), 272–294.

Greeley, R. &, Schneid, B.D. (1991). Magma generation on Mars: amounts, rates, and comparisons with Earth, Moon, and Venus. *Science,* 254(5034), 996-998.

Greenhagen, B. T., Lucey, P. G., Wyatt, M. B., Glotch, T. D., Allen, C. C., Arnold, J. A., et al. (2010). Global silicate mineralogy of the Moon from the Diviner Lunar Radiometer. *Science*, 329(5998), 1507–1509.

Guo, Y.Y., Li, X.Y., Zhao, Z.Q., Qu, J.K., Ma, Q., Wang, D.H., & Yin, H.Y. (2022). The electrochemical reduction process of converting solid sulfides to liquid metals in molten salt: ZnS. *Journal of Electroanalytic Chemistry*, 922(116801), 1-8.

Haberle, C. W., Christensen, P. W., & Ruff, S. W. (2019). Interpreting the petrogenetic history of Martian volcanic rocks using thermal emission spectroscopy and thermodynamic calculations of phase equilibria. American Geophysical Union, Fall Meeting 2019, abs. #P33F-3494.

Hamilton, V. E. (2000). Thermal infrared emission spectroscopy of the pyroxene mineral series. *Journal of Geophysical Research*, 105(E4), 9701–9716.

Hamilton, V. E. (2003). Thermal infrared emission spectroscopy of titanium-enriched pyroxenes. *Journal of Geophysical Research*, 108(E8), 5095.

Hamilton, V. E. (2010). Thermal infrared (vibrational) spectroscopy of Mg-Fe olivines: A review and applications to determining the composition of planetary surfaces. *Chemie der Erde*, 70(1), 7–33.

Hamilton, V. E., & Christensen, P. R. (2005). Evidence for extensive, olivine-rich bedrock on Mars. *Geology*, 33(6), 433–436.

Hamilton, V. E., & Ruff, S. W. (2012). Distribution and characteristics of Adirondack-class basalt as observed by Mini-TES in Gusev crater, Mars and its possible volcanic source. *Icarus*, 218(2), 917–949.

Hamilton, V. E., Christensen, P. R., Kaplan, H. H., Haberle, C. W., Rogers, A. D., Glotch, T. D., et al. (2021). Evidence for limited compositional and particle size variation on asteroid (101955) Bennu from thermal infrared spectroscopy. *Astronomy and Astrophysics*, 650, A120.

Hamilton, V. E., Christensen, P. R., McSween, H. Y., Jr., & Bandfield, J. L. (2000). Searching for the source regions of Martian meteorites using MGS TES: Integrating Martian meteorites into the global distribution of igneous materials on Mars. *Meteoritics & Planetary Sciences*, 38(6), 871–885.

Hamilton, V. E., Haberle, C. W., & Mayerhofer, T. G. (2020). Effects of small crystallite size on the thermal infrared (vibrational) spectra of minerals. *American Mineralogist*, 105(11), 1756–1760.

Hamilton, V. E., Simon, A. A., Christensen, P. R., Reuter, D. C., Clark, B. E., Barucci, M. A., & OSIRIS-Rex Team. (2019). Evidence for widespread hydrated minerals on asteroid (101955) Bennu. *Nature Astronomy*, 3, 332–340.

Hamilton, V.E., & Christensen, P.R. (2000). Determining the modal mineralogy of mafic and ultramafic igneous rocks using thermal emission spectroscopy. *Journal of Geophysical Research*, 105(E40), 9717-9733.

Hardgrove, E.C. (1986). Beyond Space Earth: Environmental Ethics and the Solar System. Sierra Club Books. p.336.

Hardin, G. (1968). The Tragedy of the Commons. *Science*, 162, 1243–1248.

Harrison, J. (2013). Making the Law of the Sea: A Study in the Development of International Law. Cambridge: Cambridge University Press. pp. 321.

Haughton, D. R., Roeder, P. L., & Skinner, B. J. (1974). Solubility of sulfur in mafic magmas. *Economic Geology*, 69(4), 451–467.

Hayaski, M. (1989). Registration of the First Group of Pioneer Investors by the Preparatory Commission for the International Sea-Bed Authority and for the International Tribunal for the Law of the Sea. *Ocean Development and International Law*, 20(1), 1-34.

Hayne, P.O., Aharonson, O., & Schörghofer, N. (2021). Micro cold traps on the Moon. *Nature Astronomy*, 5, 169-175.

Hayne, P.O., Hendrix, A., Sefton-Nash, E., Siegler, M.A., Lucet, P.G., Retherford, K.D., Williams, J.-P., Greenhagen, B.T., & Paige, D.A. (2015). Evidence for exposed water ice in the Moon's south polar regions from Lunar Reconnaissance Orbiter ultraviolet albedo and temperature measurements. *Icarus*, 255(15), 58–69.

Hecker, C., van der Meijde, M., & van der Meer, F. D. (2010). Thermal infrared spectroscopy on feldspars–successes, limitations, and their implications for remote sensing. *Earth-Science Reviews*, 103(1–2), 60–70.

Heiken, G.H., & Vaniman, D.T. (1990). Characterization of Lunar Ilmenite Resources. *Proceedings of the 20th Lunar and Planetary Science Conference*, pp. 239-247.

Heim, B.E. (1990). Exploring the Las Frontiers for Mineral Resources: A Comparison of International Law Regarding the Deep Seabed, Outer Space, and Antarctica. *Vanderbilt Journal of Transnational Law*, 23, 819-849.

Hein, J.R., Mizeli, K., Koschinsky, A., & Conrad, T.A. (2013). Deep-ocean mineral deposits as a source of critical metals for high- and green-technology applications: Comparison with land-based resources. *Ore Geology Reviews,* 51, 1–14.

Hiesinger, H., & Helbert, J. (2010). The Mercury radiometer and thermal infrared spectrometer (MERTIS) for the BepiColombo mission. *Planetary and Space Science,* 58(1–2), 144–165.

Hiesinger, H., Helbert, J., Alemanno, G., Bauch, K. E., D'Amore, M., Maturilli, A., et al. (2020). Studying the composition and mineralogy of the hermean surface with the Mercury radiometer and thermal infrared spectrometer (MERTIS) for the BepiColombo mission: An update. *Space Science Reviews,* 216(110), 1–37.

Hodges Jr., R.R. (1981). Migration of Volatiles on the Lunar Surface. *Lunar and Planetary Science Conference,* 12, 451-453.

Holquist, J.B., Pasadilla, P., Bower, C., Cognata, T., Tewews., & Kelsey, P. (2020). Analysis of a Cold Trap as a Purification Step for Lunar Water Processing. *International Conference on Environmental Systems.* Pp. 1-12. https://ttu-ir.tdl.org/handle/2346/86336.

Honeybee Robotics. (2022). Honeybee and mPower Technology selected as Lunar Power Grid Provider (Artemis Exploration) Retrieved from Honeybee Robotics' database. https://www.honeybeerobotics.com/?attachment_id=wyqnfueosxc.

Hook, S.J., Gabell, A.R., Green, A.A., & Kealy, P.S. (1992). A comparison of techniques for extracting emissivity information from thermal infrared data for geologic studies. *Remote Sensing of Environment,* 42(2), 123–135.

Howard, R.L. (2021). A Common Habitat Basecamp for Moon and Mars Surface Operations. *ASCEND 2021,* 4065, 1-15.

Hubbard, G.S., Feldman, W., Cox, S.A., Smith, M.A., & Chu-Thielbar, L. (2002). LUNAR PROSPECTOR: FIRST RESULTS AND LESSONS LEARNED. *Acta Astronautica,* 50(1), 39–47.

Hubbard, K.M., Haberle, C.W., Elkins-Tanton, L.T., Christensen, P.R., & Semken, S. (2023). Thermal infrared Emission Spectroscopy of Graybody Minerals (Sulfide): Implications for Extraterrestrial Exploration for Magmatic Ore Deposits. *Earth and Space Science.* 10, 1-24. DOI: 10.1029/2022EA002641.

Hunt, G. R., & Vincent, R. K. (1968). The behavior of spectral features in the infrared emission from particulate surfaces of various grain sizes. *Journal of Geophysical Research,* 73(18), 6039–6046.

Hunt, G.R., & Vincent, R.K. (1968). The behavior of spectral features in the infrared emission from particulate surfaces of various grain sizes. *Journal of Geophysical Research,* 73(18), 6039-6046.

Hurley, D., Colaprete, A., Elphic, R., Farrell, W., Hayne, P., Heldmann, J., Hibbits, C., Livengood, T., Lucey, P., Klaus, K, Kring, D.A., Patterson, W., & Sherwood, B. (2016). Lunar Polar Volatiles: Assessment of Existing Observations for Exploration. NASA Goddard Space Flight Center. (pp.11). https://www.lpi.usra.edu/science/kring/lunar_exploration/LunarPolarVolatiles.pdf

Hurley, D.M., Lawrence, D.J., Bussey, B.J., Vondrak, R.R., Elphic, R.C., & Gladstone, G.R. (2012). Two-dimensional distribution of volatiles in the lunar regolith from space weathering simulations. *Geophysical Research Letters,* 39(L09203), 1-6.

Imhof, B., Urbina, D., Weiss, P., Sperl, M., Hoheneder, W., Waclavicek, R., Madakashira, H.K., Salini, J., Govindaraj, S., Gancet, J., Mohamed, M.P., Gobert, T., Fateri, M., Meurisse, A., Lopez, O., & Preisinger, C. (2017). Advancing Solar Sintering for Building a Base on the Moon. *69th IAC, Adelaide, Australia,* pp.1-17.

International Seabed Authority. (2000). Decision of the Assembly Relating to the Regulations on Prospecting and Exploration for Polymetallic Nodules in the Area, ISBA/6/A/18.

International Seabed Authority. (2001). Considerations relating to the regulations for prospecting and exploration for hydrothermal polymetallic sulphides and cobalt-rich ferromanganese crusts, ISBA/7/C/2.

International Seabed Authority. (2010). Regulations on Prospecting and exploration for polymetallic sulphides in the Area, ISBA/16/A/12/Rev.1.

International Seabed Authority. (2011). Environmental Management Plan for the Clarion-Clippterton Zone, ISBA/17/LTC/7.

International Seabed Authority. (2012a). Decision of the Council relating to an environmental management plan for the Clarion-Clipperton Zone, ISBA/18/C/22.

International Seabed Authority. (2012b). Regulations on Prospecting and Exploration for Cobalt-rich Ferromanganese Crusts in the Area, ISBA/18/A/11.

International Seabed Authority. (2013). Regulations on Prospecting and Exploration for Polymetallic Nodules in the Area, ISBA/19/C/17.

International Seabed Authority. (2015). Consolidated Regulations and Recommendations on Prospecting and Exploration. Revised Edition. Pp. 264.

International Seabed Authority. (2019). Draft Regulations on Exploitation of Mineral Resources in the Area, ISBA/25/C/WP.1.

International Seabed Authority. (2019b). Recommendations for the guidance of contractors on the relinquishment of areas under exploration contracts for polymetallic sulphides or cobalt-rich ferromangense crusts, ISBA/25/LTC/8.

International Seabed Authority. (2023a). Exploration Contracts. https://www.isa.org.jm/exploration-contracts/

International Seabed Authority. (2023b). The Legal and Technical Commission. https://www.isa.org.jm/organs/the-legal-and-technical-commission/.

Jaeckel, A. (2015). The International Seabed Authority and Marine Environmental Protection: A Case Study in Implementing the Precautionary Principle. Doctoral thesis (pp. 293). UNSW Australia.

Jaeckel, A. (2016). Deep seabed mining and adaptive management: The procedural challenges for the International Seabed Authority. *Marine Policy*, 70, 205–211.

Jaeckel, A. (2017). The International Seabed Authority and the Precautionary Principle: Balancing Deep Seabed Mineral Mining and Marine Environmental Protection. *Publications on Ocean Development*. 83, 1-382. Brill.

Jaeckel, A. (2020). Benefitting from the Common Heritage of Mankind: From Expectation to Reality. *The International Journal of Marine and Coastal Law*, 35, 660–681.

Jaeckel, A. (2022). Benefitting from the Common Heritage of Mankind: From Expectation to Reality. Valuing the Deep Sea for the Benefit of Humankind. *Renewable Resource Journal*, 37(3), 11-22.

Jaeckel, A., Ardron, J. A., & Gjerde, K. M. (2016). Sharing benefits of the common heritage of mankind – Is the deep seabed mining regime ready? *Marine Policy*, 70, 198-204. https://doi.org/10.1016/j.marpol.2016.03.009

Jakhu, R.S., Jasani, B., & McDowell, J.C. (2018). Critical issues related to registration of space objects and transparency of space activities. *Acta Astronautica*, 143, 406-420.

Japan. (2021). Space Resources Act. Act No. 83 of 2021. https://kanpou.npb.go.jp/old/20210623/20210623g00141/20210623g001410004f.html

Jenkins, M. C., Mungall, J. E., Zientek, M. L., Holick, P., & Butak, K. (2020). The nature and composition of the J-M Reef, Stillwater Complex, Montana, USA. *Economic Geology*, 115(8), 1799–1826.

Jones, D.O., Ardron, J.A., Colaço, A., & Durden, J.M. (2020). Environmental considerations for impact and preservation reference zones for deep-sea polymetallic nodule mining. *Marine Policy*, 118(103312), 1-9.

Jones, D.O., Kaiser, S., Sweetman, A.K., Smith, C.R., Menot, L., Vink, A., Trueblood, D., Greinert, J., Billet, D.S., Arbizu, P.M., Radziejewska, T., Singh, R., Ingole, B., Stratmann, T., Simon-Lledó, E., Durden, J.M, &, Clark, M.R. (2017). Biological responses to disturbance from simulated dee-sea polymetallic nodule mining. *PLoS ONE*, 12(2), e0171750.

Joyner, C. (1986). Legal Implications of the Concept of the Common Heritage of Mankind. *International & Comparative Law Quarterly*, 35(1), 190-199.

Jugo, P. (2009). Sulfide content at sulfide saturation in oxidized magmas. *Geology*, 37(5), 415–418.

Just, G.H., Smith, K., Joy, K.H., & Roy, M.J. (2020). Parametric review of existing regolith excavation techniques for lunar *In Situ* Resource Utilisation (ISRU) and recommendations for future excavation experiments. *Planetary and Space Science*, 180(104746), 1-12.

Kacmarzyk, M., & Musial, M. (2021). Parametric Study of Lunar Base Power Systems. *Energies*, 14(4), 1-31.

Kang, Y., & Liu, S. (2021). The Development History and Latest Progress of Deep-Sea Polymetallic Nodule Mining Technology. *Minerals*, 11(1132), 1-17.

Kealy, P.S., & Hook, S.J. (1993). Separating temperature and emissivity in thermal infrared multispectral scanner data: Implications for recovering land surface temperatures. *IEEE Transactions on Geoscience and Remote Sensing*. 31(6), 1155–1164.

Keane, J.T., Tikoo, S.M., & Elliott, J. (2022). Endurance: Lunar South Pole-Aitken Basin Traverse and Sample Return Rover. Mission Concept Study Report for the 2023–2032 Planetary Science and Astrobiology Decadal Survey. (pp. 296).

Kerr, R.A. (1998). Cheapest mission finds moon's frozen water. *Science*, 270(5357), 1628.

Khan, Z., Vranis, A., Zavorico, A., Fried, S., Manners, B. (2006). Power system Concepts for the Lunar Outpost: A Review of the Power Generation, Energy Storage,

Power Management, and Distribution (PMAD) System Required and Potential Technologies for Development of the Lunar Outpost. *AIP Conference Proceedings,* 813, 1083–1092.

Kiefer, W.S. (2004). Gravity evidence for an extinct magma chamber beneath Syrtis Major, Mars. A look at the magmatic plumbing system. *Earth Planet. Sci. Lett.*, 222(2), 349–361.

Kieffer, H.H. (2013). Thermal model for analysis of Mars infrared mapping. *Journal of Geophysical Research: Planets*, 118, 451–470.

Killen, R.M., Benkhoff, J., & Morgan, T.H. (1997). Mercury's polar caps and the generation of an OH exosphere. *Icarus,* 125, 195–211.

King, P. L., Ramsey, M. S., McMillan, P. F., & Swayze, G. (2004). Laboratory Fourier transform infrared spectroscopy methods for geologic samples. *Infrared Spectroscopy in Geochemistry, Exploration, and Remote Sensing*, 33, 57–91.

Kirsch, P., & Fraser, D. (1989). The Law of the Sea Preparatory Commission after Six Years: Review and Prospects. *Canadian Yearbook of International Law,* 26, 119-154.

Klingelhöfer, G., Morris, R.V., Bernhardt, B., Schröder, C., Rodionov, D.S., De Souza, P.A., Yen, A., Gellert, R., Evlanov, E.N., Zubkov, B., Foh, J., Bonnes, U., Kankeleit, E., Gütlick, P., Ming, D.W., Renz, F., Wdowiak, T., Squyres, S.W., & Arvidson, R.E. (2004). Jarosite and Hematite at Meridiani Planum From Opportunity's Mössbauer Spectrometer. *Science,* 306(5702), 1740–1745.

Kornuta, D., Abbud-Madrid, A., Atkinson, J., Barr, J., Barnhard, G., Bienhoff, D., Blair, B., Clark, V., Cyrus, J., deWitt, B., Dreyer, C., Finger, B., Goff, J., Ho, K. Kelsey, L., Keravala, J., Kutter, B., Metzger, P., Montgomery, L., Morrison, P., Neal, C., Otto, E., Roesler, G., Schier, J., Seifert, B., Sowers, G., Spudis, P., Sundahl, M., Zacny, K. and G. Zhu. (2019). Commercial lunar propellant architecture: A collaborative study of lunar propellant production. *Reviews in Human Space Exploration*, 129(100026), 1-77.

Kramer, W.R. (2014). Extraterrestrial environmental impact assessments – A foreseeable prerequisite for wise decisions regarding outer space exploration, research and development. *Space Policy,* 30, 215–222.

Kramer, W.R. (2020). A Framework for Extraterrestrial Environmental Assessment. *Space Policy,* 52(101385), 1-6.

Krujiff, M. (2000). The Peaks of Eternal Light on the Lunar South Pole: How they were found and what they look like. *In: Exploration and Utilisation of the Moon,* 462, 333-336.

Kumari, N., Bretzfelder, J.M., Ganesh, I., Lang, A., & Kring, D.A. (2022). Surface Conditions and Resource Accessibility at Potential Artemis Landing Sites 007 and 011. *The Planetary Science Journal,* 3(224), 1-23.

Lambach, D. (2021). The functional territorialization of the high seas. *Marine Policy*, 130, 104579.

Lamboray, B. (2019). Luxembourg's SpaceResources.lu Initiative: The Space Resources Value Chain and the Role of Robotics and Autonomous Systems. *CZ-LUX Robotic Day, March 13, 2019, Luxembourg*.

Land Matters. (2014). http://www.mylandmatters.org/Maps/Mining.html. Accessed 28 April 2022.

Landis, G.A., Bailey, S.G., Brinker, D.J., & Flood, D.J. (1990). Photovoltaic Power for a Lunar Base. *Acta Astronautica,* 22, 197–203.

Landis, M.E., Hayne, P.O., Williams, J.-P., Greenhagen, B.T., & Paige, D.A. (2022). Predicted Surface Volatile and Subsurface Water Ice Thermal Stability Zones at the Lunar Poles from Diviner Data. *53rd Lunar and Planetary Science Conference*, Ab# 1651.

Landis, M.E., Hayne, P.O., Williams, J.-P., Greenhagen, B.T., & Paige, D.A. (2022). Spatial Distribution and Thermal Diversity of Surface Volatile Cold Traps at the Lunar Poles, *The Planetary Science Journal.* 3(39), 1–13.

Lane, M. (1999). Midinfrared optical constants of calcite and their relationship to particle size effects in thermal infrared emission spectra of granular calcite. *Journal of Geophysical Research,* 104(E6), 14099–14108.

Lane, M. D., Bishop, J. L., Dyar, M. D., King, P. L., & Hyde, B. C. (2009). Iron sulfate and sulfide spectroscopy at thermal infrared wavelengths. In: *Workshop on modeling Martian hydrous environments.*

Lane, M., & Bishop, J. (2019). Mid-infrared (thermal) emission and reflectance spectroscopy: Laboratory spectra of geologic materials. In J. Bishop, J. Bell III, & J. Moersch (Eds.), *Part I–Theory of remote compositional analysis techniques and laboratory measurements* (pp. 42–67). Cambridge University Press.

Lane, M., & Christensen, P. R. (1998). Thermal infrared emission spectroscopy of salt minerals predicted for Mars. *Icarus*, 136(2), 528–536.

Le Gurun, G. (2014). Some Reflections on the Evolutionary Approach to the Establishment of the International Seabed Authority. In M. Lodge & M. Nordquist, Peaceful Order in the World's Oceans. pp. 249-264. Brill Nijhoff.

Le Vaillant, M., Barnes, S.J., Fisher, L., Fiorentini, M.I., & Caruso, S. (2014). Use and calibration of portable X-Ray fluorescence analysers: application to lithogeochemical exploration for komatiite-hosted sulphide deposits. *Geochemistry, Exploration, Environment, Analysis.* 14(3), 199.

Le Vaillant, M., Fiorentini, M. L., & Barnes, S. J. (2016). Review of lithogeochemical exploration tools for komatiite-hosted Ni-Cu-(PGE) deposits. *Journal of Geochemical Exploration*, 168, 1–19.

Lemelin, M., Blair, D.M., Roberts, C.E., Runyon, K.D., Nowka, D., & Kring, D.A. (2014). High-priority lunar landing sites for in situ and sample return studies of polar volatiles. *Planetary and Space Science*, 101, 149–161.

Lemelin, M., Li, S., Mazarico, E., Siegler, M.A., Kring, D.A., & Paige, D.A. (2021). Framework for Coordinated Efforts in the Exploration of Volatiles in the South Polar Region of the Moon. *The Planetary Science Journal,* 2(103), 1-17.

Lesher, C. M. (1989). Komatiite-associated nickel sulfide deposits. Chapter 5. In J. A. Whitney & A. J. Naldrett (Eds.), *Ore deposition associated with magmas* (Vol. 4, pp. 45–100). *Reviews in Economic Geology*.

Lévy, J.-P. (2014). International Seabed Authority: 20 Years. Pp. 150. International Seabed Authority.

Li, C. & Ripley, E.M. (2009). Sulfur Contents at Sulfide-Liquid or Anhydrite Saturation in Silicate Melts: Empirical Equations and Example Applications. Economic Geology, 104, 405–412.

Li, C., & Ripley, E.M. (2005). Empirical equations to predict the sulfur content of mafic magmas at sulfide saturation and applications to magmatic sulfide deposits. Mineralium Deposita, 40, 218–230.

Li, G.M., Wang, D.H., Jin, X.B., & Chen, G.Z. (2007). Electrolysis of solid MoS_2 in molten $CaCl_2$ for Mo extraction without emission. *Electrochemistry Communications*, 9, 1951–1957.

Li, S., Lucey, P.G., Milliken, R.E., Hayne, P.O., Fisher, E., Williams, J.-P., Hurley, D.M., & Elphic, R.C. (2018). Direct evidence of surface exposed water-ice in the lunar polar regions. *Earth, Atmospheric, and Planetary Sciences*, 115(36), 8907–8912.

Lillis, R.J., Dufek, J., Kiefer, W.S., Black, B.A., Manga, M.., Richardson, J.A., & Bleacher, J.E. (2015). The Syrtis Major volcano, Mars: A multidisciplinary approach to interpreting its magmatic evolution and structural development. *J. Geophys. Res. Planets*, 120, 1476–1496.

Liu, J., Li, S., Lv, Z., Fan, Y., He, J., & Song, J. (2023). Electro-desulfurization of metal sulfides in molten salts. *Separation and Purification Technology*, 310(123109), 1-10.

Liu, K., Zhang, L., Guo, X., & Huaiwei, N. (2021). Effects of sulfide composition and melt H_2O on sulfur content at sulfide saturation in basaltic melts. *Chemical Geology*, 559(119913), 1-8.

Liu, Y., Samaha, N.-T., & Baker, D. R. (2007). Sulfur concentration at sulfide saturation (SCSS) in magmatic silicate melts. *Geochimica et Cosmochimica Acta*, 71(7), 1783–1799.

Livengood, T., Lucey, P., Klaus, K, Kring, D.A., Patterson, W., & Sherwood, B. (2016). Lunar Polar Volatiles: Assessment of Existing Observations for Exploration. NASA Goddard Space Flight Center. (pp.11). https://www.lpi.usra.edu/science/kring/lunar_exploration/LunarPolarVolatiles.pdf

Lodge, M., Johnson, D., Le Gurun, G., Wengler, M., Weaver, P., & Gunn, V. (2014). Seabed mining: International Seabed Authority environmental management plan for the Clarion–Clipperton Zone. A partnership approach. *Marine Policy*, 49, 66–72.

Lodge, M.W. (2002). International Seabed Authority's Regulations on Prospecting and Exploration for Polymetallic Nodules in the Area. Journal of Energy & Natural Resources Law, 20(3), 270-295.

Lodge, M.W. (2011). Current Legal Developments: International Seabed Authority. *The International Journal of Marine and Coastal Law*, 26(3), 463-480.

Logan, L.M., Hunt, G.R., Salisbury, J.W., Balsamo, S.R. (1973). Compositional implications of Christiansen frequency minimums for infrared remote sensing applications. *Journal of Geophysical Research*, 78, 4983–5003.

Lomax, B.E., Conti, M., Khan, N., Bennett, N.S., Ganin, A.Y., & Symes, M.D. (2020). Proving the viability of an electrochemical process for the simultaneous extraction of oxygen and production of metal alloys from lunar regolith. *Planetary and Space Science*, 180(104748), 1–10.

Lorand, J.-P., & Alard, O. (2001). Platinum-group element abundances in the upper mantle: New constraints from in situ and whole-rock analyses of Massif Central xenoliths. *Geochimica et Cosmochimica Acta*, 65(16), 2789–2806.

Lowman Jr., P.D., Sharpe, B.L. and D.G. Shrunk. (2008). Moonbase Mons Malapert? Making the Case. Aerospace America, 46(10), 38-43.

Lu, X., Ma, R., Wang, C., & Yao, W. (2016). Performance analysis of a lunar based solar thermal power system with regolith thermal storage. *Energy*, 107, 227-233.

Lucey, P.G., Neumann, G.A., Riner, M.A., Mazarico, E., Smith, D.E., Zuber, M.T., Paige, D.A., Bussey, D.B., Cahill, J.T., McGovern, A., Isaacson, P., Corley, L.M., Torrence, M.H., Melosh, H.J., Head, J.W., & Song, E. (2014). The global albedo of the Moon at 1064 nm from LOLA. *JGR Planets*, 199(7), 1665–1679.

Luxembourg Space Agency. (2018). Opportunities for Space Resources Utilization. Future Markets & Value Chains: Study Summary. (pp.16). https://space-agency.public.lu/dam-assets/publications/2018/Study-Summary-of-the-Space-Resources-Value-Chain-Study.pdf.

Lyon, R.J.P. (1965). Analysis of rocks by spectral infrared emission (8 to 25 microns). *Economic Geology*, 60, 715–736.

Madureira, P., Brekke, H., Cherkashov, G., & Rovere, M. (2016). Exploration of polymetallic nodules in the Area: Reporting practices, data management and transparency. *Marine Policy*, 70, 101–107.

Maier, W. D. (2005). Platinum-group element (PGE) deposits and occurrences: Mineralization styles, genetic concepts, and exploration criteria. *Journal of African Earth Sciences*, 41(3), 165–191.

Maier, W. D., & Barnes, S.-J. (1999). Platinum-group elements in silicate rocks of the lower, critical and main zones at union section, Western Bushveld Complex. *Journal of Petrology*, 40(11), 1647–1671.

Maier, W. D., Peltonen, P., McDonald, I., Barnes, S. J., Barnes, S.-J., Hatton, C., & Viljoen, F. (2012). The concentration of platinum-group elements and gold in southern African and Karelian kimberlite-hosted mantle xenoliths: Implications for the noble metal content of the Earth's mantle. *Chemical Geology*, 302–303, 119–135.

Margulis, M.E., McKeon, N. Borras Jr., S.M. (2013). Land Grabbing and Global Governance: Critical Perspectives. *Globalizations*, 10(1), 1–23.

Matthews, J.J., & McMahon, S. (2018). Exogeoconservation: Protecting geological heritage on celestial bodies. *Acta Astronautica*, 149, 55–60.

Maturilli, A., & Helbert, J. (2014). Characterization, testing, calibration, and validation of the Berlin emissivity database. *Journal of Applied Remote Sensing*, 8, 1–12.

Maturilli, A., Helbert, J., & Moroz, L. (2008). The Berlin emissivity database (BED). *Planetary and Space Science*, 56(3–4), 420–425.

Maturilli, A., Helbert, J., Ferrari, S., Davidsson, B., & D'Amore, M. (2016). Characterization of asteroid analogues by means of emission and reflectance spectroscopy in the 1- to 100-µm spectral range. *Earth Planets and Space*, 68(1), 113–124.

Maturilli, A., Helbert, J., Witzke, A., & Moroz, L. (2006). Emissivity measurements of analogue materials for the interpretation of data from PFS on Mars Express and MERTIS on Bepi-Colombo. *Planetary and Space Science*, 54(11), 1057–1064.

Mavrogenes, J.A. & O'Neill, H.S.C. (1999). The relative effects of pressure, temperature and oxygen fugacity on the solubility of sulfide in mafic magmas. *Geochim. Cosmochim. Acta*, 63, 1173–1180.

Mazarico, E., Neumann, G.A., Smith, D.E., Zuber, M.T., & Torrence, M.H. (2011). Illumination conditions of the lunar polar regions using LOLA topography. *Icarus*, 211, 1066–1081.

McClure, B. (2022, January 6). Lunar libration: January 7 moon maximum for 2022. *EarthSky*. https://earthsky.org/astronomy-essentials/lunar-libration-see-more-than-50-of-moon/.

McDonough, W. W., & Sun, S. S. (1995). The composition of the Earth. *Chemical Geology*, 120(3–4), 223–253.

McKay, D.S., & Williams, R.J. (1979). A geologic assessment of potential lunar ores. Space Resources and Space Settlements, NASA SP–428, 243–255.

McMillan, P. (1985). Vibrational spectroscopy in the mineral sciences. In S. W. Kieffer & A. Navrotsky (Eds.), *Microscopic to macroscopic: Atomic environments to mineral thermodynamics* (Vol. 14, pp. 9–63). *Reviews in Mineralogy*.

McSween, H.Y., Wyatt, M.B., Gellert, R., Bell, J.F., Morris, R.V., Herkenhoff, K.E., Crumpler, L.S., Miliam, K.A., Stockstill, K.R., Tornabene, L.L., Arvidson, R.E., Bartlett, P., Blaney, D., Cabrol, N.A., Christensen, P.R., Clark, B.C., Crisp, J.A., Des Marais, D.J., Economou, T., Farmer, J.D., Farrand, W., Ghosh, A., Golombek, M., Gorevan, S., Greeley, R., Hamilton, V.E., Johnson, J.R., Joliff, B.L., Klingelhöfer, G., Knudon, A.T., McLennan, S., Ming, D., Moersch, J.E., Rieder, R., Ruff, S.W., Schröder, C., de Souza, P.A., Squyres, S.W., Wänke, H., Wang, A., Yen, A., & Zipfel, J. (2006). Characterization and petrologic interpretation of olivine-rich basalts at Gusev Crater, Mars. *JGR: Planets*, 111(E02S10), 1-17.

Merrie, A., Dunn, D.C., Metian, M., Boustany, A.M., Takei, Y., Elferink, A.O., Ota, Y., Christensen, V., Halpin, P.N., & Österblom, H. (2014). An ocean of surprises – Trends in human use, unexpected dynamics and governance challenges in areas beyond national jurisdiction. *Global Environmental Change*, 27, 19–31.

Metzger, P. (2021). System for Extracting Water from Lunar Regolith and Associated Method. U.S. Patent No. US 2021/0404338 A1.

Meurisse, A., & Carpenter, J. (2020). Past, present and future rationale for space resource utilization. *Planetary and Space Science*. 182(104853), 1-13.

Michelsen, H. A., Colket, M. B., Bengtsson, P. E., D'Anna, A., Desgroux, P., Haynes, B. S., et al. (2020). A review of terminology used to describe soot formation and evolution under combustion and pyrolytic condition. *ACS Nano*, 14(10), 12470–12490.

Miller, K.A., Thompson, K.F., Johnston, P., & Santillo, D. (2018). An Overview of Seabed Mining Including the Current State of Development, Environmental Impacts, and Knowledge Gaps. *Frontiers in Marine Science*, 4, 1-24.

Milliken, R., & Li, S. (2017). Remote detection of indigenous water in lunar pyroclastic deposits. *Nature Geoscience*, 10, 461-465.

Mitchell, J.K., Houston, W.N., Carrier III, W.D., & Costes, N.D. (1974). Apollo Soil Mechanics Experiment S-200. https://www.lpi.usra.edu/lunar/documents/NASA%20CR-134306.pdf

Mitrofaov, I.G., Sanin, A.B., Boynton, W.V., Chin, G., Garvin, J.B., Golovin, D., Evans, L.G., Harshman, K., Kozyrev, A.S., Litvak, M. L., Malakhov, A., Mazarizo, E., McClanahan, T., Milikh, G., Mokrousov, M., Nandikotkur, G., Neumann, G.A., Nuzhdin, I., Sagdeev, R., Shevchenko, V., Shvetsov, V., Smith, D.E., Starr, R., Tretyakov, V.I., Trombka, J., Varenikov, A., Vostruhkin, A., & Zuber, M.T. (2010). Hydrogen Mapping of the Lunar South Pole Using the LRO Neutron Detector Experiment LEND. *Science*, 330(6003), 483–486.

Moersch, J. E. (1992). Modeling particle size effects on the thermal emission spectra of minerals in the thermal infrared. M.S. thesis (pp. 1–77). Arizona State University.

Moersch, J.E., & Christensen, P.R. (1995). Thermal emission from particulate surfaces: A comparison of scattering models with measured spectra. *Journal of Geophysical Research*, 100, 7465–7477.

Molenaar, E.J. (2013). Area-based management tools. In Intersessional Workshops on the Conservation and Sustainable Use of Marine Biodiversity Beyond Areas of National

Jurisdiction (Oceans and the Law of the Sea division, 2013). https://go.nature.com/3m5jylf.

Mucha, J., Wasilewska-Blaszczyk, M., Kotlinski, R.A, & Maciąg, L. (2013). Variability and accuracy of polymetallic nodules abundances estimations in the IOM area-statistical and geostatistical approach. In *Tenth ISOPE Ocean Mining and Gas Hydrates Symposium, Szczecin, Poland, September 22-26, 2013*. Pp.27-31.

Murchie, S., Arvidson, R., Bedini, P., Beisser, K., Bibring, J.-P., Bishop, J., Boldt, J., Cavender, P., Choo, T., Clancy, R.T., Darlington, E.H., Des Marais, D.D., Espiritu, R., Fort, D., Green, R., Guinness, E., Hayes, J., Hash, C., Heffernan, K., Hemmler, J., Heyler, G., Humm, D., Hutcheson, J., Izenberg, N., Lee, R., Lees, J., Lohr, D., Malaret, E., Martin, T., McGovern, J.A., McGuire, P., Morris, R., Mustard, J., Pelkey, S., Rhodes, E., Robinson, M., Roush, T., Schaefer, E., Seagrave, G., Seelos, F., Silverglate, P., Slavney, S., Smith, M., Shyong, W.-J., Strohbehn, K., Taylor, H., Thompson, P., Tossman, B., Wirzburger, M., & Wolff, M. (2007). Compact Reconnaissance Imaging Spectrometer for Mars (CRISM) on Mars Reconnaissance Orbiter (MRO). *JGR: Planets,* 112(E5), 1-53.

Mustard, J.F., & Hays, J.E. (1997). Effects of hyperfine particles on reflectance spectra from 0.3 to 25 μm. *Icarus,* 145–163.

Naldrett, A. (1999). World-class Ni-Cu-PGE deposits: Key factors in their Genesis. *Mineralium Deposita*, 34(3), 27–240.

Naldrett, A. (2010). *Magmatic sulphide deposits: Geology, geochemistry, and exploration* (p. 728). Oxford University Press.

Naldrett, A. J., Wilson, A., Kinnaird, J., & Chunnett, G. (2009). PGE tenor and metal ratios within and below the Merensky Reef, Bushveld Complex: Implications for its genesis. *Journal of Petrology,* 50(4), 625–659.

Naldrett, T., Kinniard, J. A., Wilson, A. H., & Chunnett, G. (2008). Concentration of PGE in the Earth's crust with special reference to the Bushveld Complex. *Earth Science Frontiers*, 15(5), 264–297.

Nandan, S.N. (2006). Administering the Mineral Resources of the Deep Seabed. Chapter 5. In: Freestone, D., Barnes, D.M. (Eds.), *The Law of the Sea. Progress and Prospects*, pp 75-92. Oxford.

Nandan, S.N., Lodge, M.W., & Rosenne, S. (2002). The development of the regime for deep seabed mining. International Seabed Authority. pp. 1-73.

NASA. (2020). NASA's Plan for Sustained Lunar Exploration and Development. (p.13). https://www.nasa.gov/sites/default/files/atoms/files/a_sustained_lunar_presence_nspc_report4220final.pdf.

NASA. (2021). Sustained Phase Human Landing System (HLS) Program System Requirements Document, HLS-RQMT-006. https://govtribe.com/file/government-file/hls-rqmt-006-sustained-phase-dot-pdf.

NASA. (2022, August 19). NASA Identifies Candidate Regions for Landing Next Americans on Moon. https://www.nasa.gov/press-release/nasa-identifies-candidate-regions-for-landing-next-americans-on-moon.

Nash, D.B., Salisbury, J.W., Conel, J.E., Lucey, P.G., & Christensen, P.R. (1993). Evaluation of Infrared Emission Spectroscopy for Mapping the Moon's Surface Composition From Lunar Orbit. *Journal of Geophysical Research*, 98(E12):23535-23552.

National Aeronautics and Space Administration. (2020). The Artemis Accords: Principles for cooperation in the civil exploration and use of the Moon, Mars, comets and asteroids for peaceful purposes. https://www.nasa.gov/specials/artemis-accords/img/Artemis-Accords-signed-13Oct2020.pdf

National Research Council. (2001). Laying the Foundation for Space Solar Power: An Assessment of NASA's Space Solar Power Investment Strategy. Washington, D.C.: The National Academies Press. (Pp.94). https://doi.org/10.17226/10202.

National Research Council. (2007). The scientific context for exploration of the Moon. Washington, DC: The National Academies Press. (pp.120). https://doi.org/10.17226/11954.

Noda, H., Araki, H., Goossens, S., Ishihara, Y., Matsumoto, K., Tazawa, S., Kawano, N. and S. Sasaki, S. (2008). Illumination conditions at the lunar polar regions by Kaguya (SELENE) laser altimeter. *Geophysical Research Letters*, 35(L24203):1-5.

Nozette, S., Lichtenberg, C.L., Spudis, P., Bonner, R., Ort, W., Malaret, E., Robinson, M., & Shoemaker, E.M. (1996). The Clementine Bistatic Radar Experiment. *Science*, 274(5292):1495-1498.

Nozette, S., Rustan, P., Pleasance, L.P., Kordas, J.F., Leis, I.T., Park, H.S., Priest, R.E., Horan, D.M., Regeon, P., Lichtenberg, C.L., Shoemaker, E.M., Eliason, E.M., McEwen, A.S., Robinson, M.S., Spudis, P.D., Action, C.H., Buratti, B.J., Duxbury, T.C., Baker, D.N., Jakosky, B.M., Blamont, J.E., Corson, M.P., Resnick, J.H., Rollins, C.J., Davies, M.E., Lucey, P.G., Malaret, E., Massie, M.A., Pieters, C.M., Reisse, R.A., Smith, D.E., Soernson, T.C., Vorder Breugge, R.W., & Zuber, M.T.

(1994). The Clementine Mission to the Moon: Scientific Overview. *Science*, 266(5192), 1835–1839.

Nyquist, L.E., Boggard, D.D., Shih, C.-Y., Greshake, A., Stöffler, D., & Eugster, O. (2001). Ages and Geological Histories of Martian Meteorites. *Space Science Reviews*, 96, 105–164.

O'Brien, D. (2021). Is outer space a de jure common-pool resource. The Space Review. Accessed: March 3, 2023. https://www.thespacereview.com/article/4270/1

Ochoa, C. (2021). Contracts on the Seabed. *Yale Journal of International Law*, 46(1), 103-154.

Official newspaper of the Grand Duchy of Luxembourg. (2017). Law of July 20, 2017 on the exploration and use of space resources. https://legilux.public.lu/eli/etat/leg/loi/2017/07/20/a674/jo

Official newspaper of the Grand Duchy of Luxembourg. (2020). Law of December 15, 2020 on space activities. https://legilux.public.lu/eli/etat/leg/loi/2020/12/15/a1086/jo

Okada, T., Fukuhara, T., Tanaka, S., Taguchi, M., Imamura, T., Arai, T., et al. (2017). Thermal infrared imaging experiments of C-type asteroid 162173 Ryugu on Hayabusa2. *Space Science Reviews*, 208(1), 255–286.

Ortuño Crespo, G., Mossops, J., Dunn, D., Gjerde, K., Hazen, E., Reygondeau, G., Warner, R., Tittensor, D., & Halpin, P. (2020). Beyond static spatial management: Scientific and legal considerations of dynamic in the high seas. *Marine Policy*, 122(104012):1-7.

Osterloo, M. M., Anderson, F. S., Hamilton, V. E., & Hynek, B. M. (2010). Geologic context of proposed chloride-bearing materials on Mars. *Journal of Geophysical Research*, 115(E10012), 1–29.

Osterloo, M. M., Hamilton, V. E., Bandfield, J. L., Glotch, T. D., Baldridge, A. M., Christensen, P. R., et al. (2008). Chloride-bearing materials in the southern highlands of Mars. *Science*, 319(5870), 1651–1654.

Ostrom, E. (1990). Governing the Commons: The Evolution of Institutions for Collective Action. Cambridge University Press.

Ostrom, E. (1999). Design Principles and Threats to Sustainable Organizations that Manage Commons. Workshop in Political Theory and Policy Analysis, W99–6. Center for the Study of Institutions, Population and Environmental Change.

Ostrom, E. (2002). Common-Pool Resources and Institutions: Toward a Revised Theory. In B. Gardner & G. Rausser, (Eds.), *Handbook of agricultural economics*, 2:1315–1339. Elsevier.

Ostrom, E. (2010). Beyond Markets and States: Polycentric Governance of Complex Economic Systems. *American Economic Review*, 100(3):641-672.

Ostrom, E., Gardner, R., & Walker, J. (1994). Rules, Games, and Common-Pool Resources. University of Michigan Press.

Page, N. J., Zientek, M. L., Lipin, B. R., Raedeke, L. D., Wooden, J. L., Turner, A. R., et al. (1985). Geology of the Stillwater Complex exposed in the Mountain View area and on the west side of the Stillwater Canyon. In G. K. Czamanske & M. L. Zientek (Eds.), *The Stillwater Complex, Montana: Geology and guide. Special publication 92* (pp. 147–209).

Paige, D. A., Foote, M. C., Greenhagen, B. T., Schofield, J. T., Calcutt, S., Vasavada, A. R., et al. (2010). The lunar reconnaissance orbiter diviner lunar radiometer experiment. *Space Science Reviews*, 150(1–4), 125–160.

Paige, D. A., Lucey, P. G., Wyatt, M. B., Glotch, T. D., Allen, C. C., Arnold, J. A., et al. (2010). Global silicate mineralogy of the Moon from the Diviner lunar radiometer. *Science*, 329(5998), 1507–1509.

Paige, D.A., Siegler, M.A., Zhang, J.A., Hayne, P.O., Foote, E.J., Bennett, K.A., Vasavada, A.R., Greenhagen, B.T., Schofield, J.T., McClesse, D.J., Foote, M.C., Dejong, E., Bills, B.G., Hartford, W., Murray, B.C., Allen, CC., Snook, K., Soderblom, L.A., Calcutt, S., Taylor, F.W., Bowles, N.E., Bandfield, J.L., Elphic, R., Ghent, R., Glotch, T.D., Wyatt, M.B., Lucey, P.G. (2010). Diviner Lunar Radiometer Observations of Cold Traps in the Moon's South Polar Region. *Science*, 330(6003), 479-482.

Paige, D.A., Wood, S.A., & Vasavada, A.R. (1992). The Thermal Stability of Water Ice at the Poles of Mercury. *Science*, 258(5082), 643-646.

Palluconi, F. D., & Meeks, G. R. (1985). Thermal infrared multispectral scanner (TIMS): An investigator's guide to TIMS data (pp. 1–32). JPL Publication. Retrieved from https://ntrs.nasa.gov/api/citations/19850019974/downloads/19850019974.pdf

Palos, M.F., Serra, P., Fereres, S., Stephenson, K., & González-Cinca, R. (2020). Lunar ISRU energy storage and electricity generation. *Acta Astronautica*, 170, 412-420.

Paxson III, E.W. (1993). Sharing the Benefits of Outer Space Exploration.: Space Law and Economic Development. *Michigan Journal of International Law*, 14(3), 487-517.

Papike, J.J., Karner, J.M., Shearer, C.K., & Burger, P.V. (2009). Silicate mineralogy of martian meteorites. *Geochim. Cosmochim. Acta.* 73, 7443–7485.

Parianos, J., Lipton, I., & Nimmo, M. (2021) Aspects of Estimation and Reporting of Mineral Resources of Seabed Polymetallic Nodules: A Contemporaneous Case Study. *Minerals*, 11(200), 1-33.

Parviainen, T., Lehikoinen, A., Kuikka, S. and P. Happasaari. (2019). Risk frames and multiple ways of knowing: Coping with ambiguity in oil spill risk governance in the Norwegian Barents Sea. *Environmental Science and Policy*, 98, 95–111.

Patten, C., Barnes, S.-J., Mathes, E.A., & Jenner, F.E. (2013). Partition coefficients of chalcophile elements between sulfide and silicate melts and the early crystallization history of sulfide liquid: LA-CIP-MS analysis of MORB sulfide droplets. *Chemical Geology*. 358,170–188.

Peck, D. C., & Huminicki, M. A. E. (2016). Value of mineral deposits associated with mafic and ultramafic magmatism: Implications for exploration. *Ore Geology Reviews*, 72, 269–278.

Perring, C.S. (2015). Volcanological and Structural Controls on Mineralization at the Mount Keith and Cliffs Komatiite-Associated Nickel Sulfide Deposits, Agnew-Wiluna Belt, Western Australia–Implications for Ore Genesis and Targeting. *Economic Geology*, 110(7), 1669-1695.

Peters, M., & Kumar, M. (2013). Unique UK's licensing policy favours the state than the industry: Contradicting conventional wisdom. *Hungarian journal of legal studies*, 54(2), 200-204

Petty, G. W. (2006). *A first course in atmospheric radiation* (p. 459). Sundog Publishing.

Pfahl, A., Coventry, J., Röger, M., Wolderstetter, F., Vásquez-Arango, J.P., Gross, F., Arjomandi, M., Schwarzbözl, P., Geiger, M., & Lidke, P. (2017). Progress in heliostat development. *Solar Energy*, 152, 3-37.

Pierazzo, E., & Chyba, C.F. (1999). Amino acid survival in large cometary impacts. *Meteoritics & Planetary Science*. 34, 909–918.

Pieters, C.M., Goswami, J.N., Clark, R.N., Annadurai, M., Boardman, J., Buratti, B., Combe, J.-P., Dyar, M.D., Green, R., Head, J.W., Hibbits, C., Hicks, M., Isaacson, P., Klima, R., Kramer, G., Kumar, S., Livo, E., Lundeen, S., Malaret, E., McCord, T., Mustard, J., Nettles, J., Petro, N., Runyon, C., Staid, M., Sunshine, J., Taylor, L.A., Tompkins, S., & Varanasi, P. (2009). Character and Spatial Distribution of OH/H_2O on the Surface of the Moon Seen by M^3 on Chandrayaan-1. Science, 326(5952), 568-572.

Prem, P., Keresturi, A., Deutsch, A.N., Hibbitts, C.A., Schmidt, C.A., Grava, C., Honniball, C.I., Hardgrove, C.J., Pieters, C.M., Goldstein, D.B., Barker, D.C., Needham, D.H., Hurley, D.M., Mazarico, E., Dominguez, G., Patterson, G.W., Kramer, G.Y., Brisset, J., Gillis-Davis, J.J., Mitchell, J.L., Szalay, J.R., Halekas, J.S., Keane, J.T., Head, J.W.,…& Farrell, W.M. (2020). *Lunar Volatiles and Solar System Science*, 1-7, https://arxiv.org/pdf/2012.06317.pdf.

Race, M.S. (2011). Policies for scientific exploration and environmental protection: Comparison of the Antarctic and outer space treaties. *Science diplomacy: Antarctica, science, and the governance of international spaces*, Pp. 143-152.

Raclin, G.C. (1986). From Ice to Ether: The Adoption of a Regime to Govern Resource Exploitation in Outer Space. *Northwestern Journal of International Law & Business*, 7, 727-761.

Raedeke, L. D., & McCallum, I. S. (1980). A comparison of fractionation trends in the lunar crust and the Stillwater Complex. In *Conference on the lunar highlands crust* (Vol. 14, pp. 133–153). Pergamon Press.

Ramsey, M. (1996). Quantitative analysis of geological surfaces: A deconvolution algorithm for midinfrared remote sensing data, Ph.D. dissertation. Pp. 276. Arizona State University.

Ramsey, M. (2004). Quantitative geological surface processes extracted from infrared spectroscopy and remote sensing. In: Molecules to Planets: Infrared Spectroscopy in Geochemistry, Exploration Geochemistry and Remote Sensing. *Mineralogical Association of Canada*, 33, 1-17.

Ramsey, M., & Christensen, P.R. (1998). Mineral abundance determination: Quantitative deconvolution of thermal emission spectra. *Journal of Geophysical Research*, 103(B1), 577–596.

Rasera, J.N., Cilliers, J.J., Lamamy, J., & Hadler, K. (2020). The beneficiation of lunar regolith for space resouruce utilization: A review. *Planetary and Space Science,* 186(104879), 1-15.

Reina, P. (2022). UK Government Expands Offshore Oil Leases in North Sea. Energy News-Record, October 9, 2022. Available at: https://www.enr.com/articles/54953-uk-government-expands-offshore-oil-leases-in-north-sea. Accessed (February 24, 2023).

Reuss, F., Braun, B., Zacny, K., & Pinni, M. (2010). Lunar Base Site Preparation. (Ed.) Haym Benaroya. *In: Lunar Settlement.* CRC Press. p. 433-450.

Reyes, D.P., & Christensen, P.R. (1994). Evidence for Komatiite-type lavas on Mars from Phobos ISM data and other observations. *Geophysical Research Letters*, 21, 887–890.

Reynolds, G.H. (1995). The Moon Treaty: prospects for the future. *Space Policy*, 11(2):115–120.

Righter, K., Pando, K. & Danielson, L.R. (2009). Experimental evidence for sulfur-rich martian magmas: Implications for volcanisms and surficial sulfur sources. *Earth and Planet. Sci.* 43, 1709–1723.

Rio Declaration on Environment and Development. (1992). 31 ILM 874.

Ripley, E. M., & Li, C. (2013). Sulfide saturation in mafic magmas: Is external sulfur required for magmatic Ni-Cu-(PGE) ore genesis? *Economic Geology*, 108(1), 45–58.

Ripley, E. M., Wernette, B. W., Ayre, A., Li, C., Smith, J. M., Underwood, B. S., & Keays, R. R. (2017). Multiple S isotope studies of the Stillwater Complex and country rocks: An assessment of the role of crustal S in the origin of PGE enrichment found in the J-M Reed and related rocks. *Geochmica et Cosmochmica Acta*, 214, 226–245.

Rivard, B., Feng, J., Gallie, E. A., & Francis, H. (2001). Ore detection and grade estimation in the Sudbury mines using thermal infrared reflectance spectroscopy. *Geophysics*, 66(6), 1691–1698.

Roberts, J., Chircop, A. and S. Prior. (2010). Area-based management on the high seas: possible application of the IMO's particularly sensitive sea area concept. *International Journal of Marine and Coastal Law*, 25, 483–522.

Robinson, M.S., et. al. (2010). Lunar Reconnaissance Orbiter Camera (LROC) Instrument Overview. *Space Science Reviews*, 150, 81–124.

Rodenbeck, C.T., Jaffe, P.I., Strassner II, B.H., Hausgen, P.E., McSpadden, J.O., Kazemi, H., Shinohara, N., Tierney, B.B., & DePuma, C.B. (2021). Microwave and Millimeter Wave Power Beaming. *IEEE Journal of Microwaves*, 1(1), 229–259.

Rogers, A. D., & Christensen, P. R. (2007). Surface mineralogy of Martian low-albedo regions from MGS-TES data: Implications for upper crustal evolution and surface alteration. *Journal of Geophysical Research*, 112(E1), 1–18.

Rudnick, R. L., & Gao, S. (2003). Composition of the continental crust. In H. D. Holland & K. K. Turekian (Eds.), *Treatise on Geochemistry* (1st ed., pp. 1–64). Pergamon.

Ruff, S. W., & Farmer, J. D. (2016). Silica deposits on Mars with features resembling hot spring biosignatures at El Tatio in Chile. *Nature Communications*, 7(13554), 1–10.

Ruff, S. W., & Hamilton, V. E. (2017). Wishtone to Watchtower: Amorphous alteration of plagioclase-rich rocks in Gusev crater, Mars. *American Mineralogist*, 102(2), 235–251.

Ruff, S. W., Christensen, P. R., Barbera, P. W., & Anderson, D. L. (1997). Quantitative thermal emission spectroscopy of minerals: A laboratory technique for measurement and calibration. *Journal of Geophysical Research*, 102(B7), 14899–14913.

Ruff, S. W., Christensen, P. R., Blaney, D. L., Farrand, W. H., Johnson, J. R., Michalski, J. R., et al. (2006). The rocks of Gusev Crater as viewed by the mini-TES instrument. *Journal of Geophysical Research*, 111(E12), 1–36.

Ruff, S. W., Christensen, P. R., Glotch, T. D., Blaney, D. L., Moersch, J. E., & Wyatt, M. B. (2008). The mineralogy of Gusev crater and Meridiani Planum derived from the Miniature Thermal Emission Spectrometers on the Spirit and Opportunity rovers. In J. F. Bell III (Ed.), *The Martian surface: Composition, mineralogy, and physical properties* (pp. 315–338). Cambridge University Press.

Ruff, S. W., Hamilton, V. E., Rogers, D., Edwards, C. S., & Horgan, B. H. N. (2022). Olivine and carbonate-rich bedrock in Gusev crater and the Nili Fossae region of Mars may be altered ignimbrite deposits. *Icarus*, 380, 114974.

Ruff, S.W., Christensen, P.R., Barbera, P.W., & Anderson, D.L. (1997). Quantitative thermal emission spectroscopy of minerals: A laboratory technique for measurement and calibration. *Journal of Geophysical Research*. 102(B7), 14899–14913.

Ruppert, S., Ross, A., Vlassak, J.J., & Elvis, M. (2021). Tall Towers on the Moon. arXiv preprint arXiv:2103.00612. p. 1-12.

Salisbury, J. M., & Walter, L. S. (1989). Thermal infrared (2.5–13.5 μm) spectroscopic remote sensing of igneous rock types on particulate planetary surfaces. *Journal of Geophysical Research*, 94(B7), 9192–9202.

Salisbury, J. W. (1993). Mid-infrared spectroscopy: Laboratory data. Remote geochemical analysis: Elemental and mineralogical composition (pp. 79–98).

Salisbury, J. W., & D'Aria, D. M. (1992). Emissivity of terrestrial materials in the 8–14 μm atmospheric window. *Remote Sensing of Environment*, 42(2), 83–106.

Salisbury, J. W., & Estes, J. (1985). The effect of particle size and porosity on spectra in the mid-infrared. *Icarus*, 64(3), 586–588.

Salisbury, J. W., Walter, L. S., Vergo, N., & D'Aria, D. M. (1991). *Infrared (2.1–25 μm) spectra of minerals.* Johns Hopkins University Press.

Salisbury, J.W., & Eastes, J.W. (1985). The effect of particle size and porosity on spectral contrast in the mid-infrared. *Icarus*, 64, 586–588.

Salisbury, J.W., & Wald, A. (1992). The role of volume scattering in reducing spectral contrast of Reststrahlen bands in spectra of powdered minerals. *Icarus*, 96, 121–128.

Salisbury, J.W., & Walter, L.S. (1989). Thermal infrared (2.5–13.5 μm) Spectroscopic Remote Sensing of Igneous Rock types on Particulate Planetary Surfaces. *Journal of Geophysical Research*, 94(B7), 9192–9202.

Salisbury, J.W., Walter, L.S., & Vergo, N. (1987). Mid-infrared (2.1-25 μm) reflectance spectra of powdered stony meteorites. *Icarus*, 92, 280–297.

Salter, E., & Ford, J. (2000). Environmental Pollution Challenges and Associated Planning and Management Issues Facing Offshore Oil and Gas Field Development in the UK. *Journal of Environmental Planning and Management*, 43(2), 253–276.

Schlüter, L., & Cowley, A. (2020). Review of techniques for In-Situ oxygen extraction on the Moon. *Planetary and Space Science*, 181(104753), 1-17.

Schlüter, L., Cowley, A., Pennec, Y., & Roux, M. (2021). Gas purification for oxygen extraction from lunar regolith. *Acta Astronautica*, 179, 371-381.

Schmidt-Tedd, B, & Soucek, A. (2020). Registration of Space Objects. In: *Oxford Research Encyclopedia of Planetary Science.* https://doi.org/10.1093/acrefore/9780190647926.013.95.

Schorghofer, N. (2008). The lifetime of ice on main belt asteroids. *The Astrophysical Journal*, 682, 697–705.

Schorghofer, N., & Taylor, G.J. (2007). Subsurface migration of H_2O at lunar cold traps. *Journal of Geophysical Research*, 112(E02010), 1-11.

Schultz, P.H., Hermalyn, B., Colaprete, A., Ennico, K., Shirley, M., & Marshall, W.S. (2010). The LCROSS Cratering Experiment. *Science*, 330, 468-472.

Schwind, M. (1986). Open Stars: An Examination of the United States Push to Privatize International Telecommunications Satellites. *Suffolk Transnational Law Journal*, 10, 87.

Sebenius, J.L. (1984). Negotiating the Law of the Sea Cambridge: Harvard University Press.

Sequeira, H., Skura, J., Thompson, T.W., Thomson, B.J., Ustinov, E.A., & Winters, H.L. (2010). Initial results for the north pole of the Moon from Mini-SAR, Chandrayaan-1 mission. *Geophysical Research Letters*, 37(L06204), 1-6.

Sercel, J.C., Longman, A., & Small, J. (2021). Systems and Methods for Radiant Gas Dynamic Mining of Permafrost for Propellant Extraction. U.S. Patent No. 11,143,026 B2.

Shackelford, S.J. (2009). The Tragedy of the Common Heritage of Mankind. *Stanford Environmental Law Journal,* 28(1), 109-169.

Sharpe, B.L., & Schrunk, D.G. (2003). Malapert Mountain: Gateway to the Moon. *Advances in Space Research,* 31(11), 2467–2472.

Shaw, M.G., Humbert, M.S., Brooks, G.A., Rhamdhani, A., Duffy, A.R., & Pownceby, M.I. (2021). Mineral Processing and Metal Extraction on the Lunar Surface – Challenges and Opportunities. *Mineral Processing and Extractive Metallurgy Review*. 43(7):865–891.

Shearer, C., & Tahu, G. (2010). Lunar Pole Volatiles Explorer (LPVE). NASA Mission Concept Study. (Pp. 50). https://nap.nationalacademies.org/resource/13117/App%20G%2006_Lunar_Polar_Volatiles_Explorer.pdf

Sherwood, B. (2018). Principles of a Practical Moon Base. *69th International Astronautical Congress.* IAC-18.A3.1.6.x46496. (p.1–13).

Shirley, K. A., & Glotch, T. D. (2019). Particle size effects on mid-infrared spectra of lunar analog minerals in a simulated lunar environment. *Journal of Geophysical Research: Planets*, 124(4), 970–988.

Singh, P.A., & Araujo, F.C.B. (2023). The Past, Present and Future of Ocean Governance: Snapshots from Fisheries, Area-Based Management Tools and International Seabed Mineral Resources. In M. Bavinck, M. Hadjimichael, & A.-K. Hornidge (Eds.), *Ocean Governance*. Springer. (pp.113–135). https://doi.org/10.1007/978-3-031-20740-2.

Slack, J. F., Kimball, B. E., Shedd, K. B., & Cobalt, C. F. (2017). Critical mineral resources of the United States–Economic and environmental geology and prospects for future supply. In K. J. Schulz, J. H. DeYoung Jr, R. R. Seal II, & D. C. Bradley (Eds.). *U.S. Geological survey professional paper 1802*. (pp.F1–F40).

Sladek-Nowlis, J., & Friedlander, A. (2004). Design and Designation of Marine Reserves. In: J. Sobel & C. Dahlgren (Eds.), *Marine Reserves: A Guide to Science, Design and Use*. Washington DC: Island Press. pp. 128-163.

Smith, C.R., Gaines, S., Friedlander, A.., Morgan, C., Thurnherr, A., Mincks, S., Watling, L., Rogers, A., Clark, M., Baco-Taylor, A., Bernardino, A., De Leo, F., Dutriuex, P., Riser, A., Kittinger, J., Padilla-Gamino, J., Prescott, R., & Srsen, P. (2008). Preservation Reference Areas for Nodule Mining in the Clarion-Clipperton Zone: Raitionale and Recommendations to the International Seabed Authority. In *Workshop to Design Marine Protected Areas for Seamounts and the Abyssal Nodule Province in Pacific High Seas*, October 23-26, 2007, University of Hawaii at Manoa.

Smith, D.E., Zuber, M.T., Jackson, G.B., Cavanaugh, J.F., Neumann, G.A., Riris, H., Sun, X., Zellar, R.S., Coltharp, C., Connelly, J., Katz, R.B., Kleyner, I., Liiva, P., Matuszeski, A., Mazarico, E.M., McGarry, J.F., Novo-Gradac, A.-M., Ott, M.N., Peters, C., Ramos-Izquierdo, L.A., Ramsey, L., Rowlands, D.D., Schmidt, S., Scott III, V.S., Shaw, G.B., Smith, J.C., Swinski, J.-P., & Torrence, M.H. (2010b). The lunar orbiter laser altimeter investigation on the lunar reconnaissance orbiter mission. *Space Science Reviews*, 150(1-4), 209-241.

Smith, D.E., Zuber, M.T., Neumann, G.A., Lemoine, F.G., Mazarico, E., Torrence, M.H., McGarry, J.F., Rowlands, D.D., Head, J.W., Duxbury, T.H., Aharonson, O., Lucey, P.G., Robinson, M.S., Barnouin, O.S., Cavanaugh, J.F., Sun, X., Liiva, P., Mao, D.-D., Smith, J.C., & Bartels, A.E. (2010a). Initial observations from the Lunar Orbiter Laser Altimeter (LOLA). *Geophysical Research Letters*, 37(18), 37(L18204):1-6.

Song, X., Wang, Y., & Chen, L. (2011). Magmatic Ni-Cu-(PGE) deposits in magmatic plumbing systems: Features, formation and exploration. *Geoscience Frontiers*. 2(3), 375–384.

Soong, R., & Farmer, V. C. (1978). The identification of sulphide minerals by infra-red spectroscopy. *Mineralogical Magazine*, 42(322), M17– M20.

Sowers, G., & Dreyer, C.B. (2019). Ice Mining in Lunar Permanently Shadowed Regions. *New Space*, 7(4):235-244.

Sparenberg, O. (2019). A historical perspective on deep-sea mining for manganese nodules, 1965–2019. *The Extractive Industries and Society*, 6:842–854.

Speyerer, E.J., & Robinson, M.S. (2013). Persistently illuminated regions at the lunar poles: Ideal sites for future exploration. *Icarus*, 222(1), 122-136.

Speyerer, E.J., Robinson, M.S., Denevi, B.C., & the LROC Science Team. (2011). Lunar Reconnaissance Orbiter Camera Global Morphological Map of the Moon. *42nd Lunar and Planetary Science Conference, No. 2387*.

Spudis, P.D., Bussey, D.B.J., Baloga, S.M., Butler, B.J., Carl, D., Carter, L.M., Chakraborty, M., Elphic, R.C., Gillis-Davis, J.J., Goswami, J.N., Heggy, E., Hillyard, M., Jensen, R., Kirk, R.L., LaVallee, D., McKerracher, P., Neish, C.D., Nozette,S., Nylund, S., Palsetia, M., Patterson, W., Robinson, M.S., Raney, R.K., Schulze, R.C., Sequeira, H., Skura, J., Thompson, T.W., Thomson, B.J., Ustinov, E.A., & Winters, H.L. (2010). Initial results for the north pole of the Moon from Mini-SAR, Chandrayaan-1 mission. *Geophysical Research Letters,* 37(L06204), 1-6.

Spudis, P.D., Bussey, D.B.J., Baloga, S.M., Cahill, J.T.S., Glaze, L.S., Patterson, G.W., Raney, R.K., Thompson, T.W., Thomson, B.J., & Ustinov, E.A. (2013). Evidence for water ice on the Moon: results for anomalous polar craters from the LRO Mini-RF imaging radar. *J. Geophysical Research,* 118(10), 2016–2029.

Squyres, S.W., Arvidson, R.E., Bell III, J.F., Bruckner, J., Cabrol, N.A., Calvin, W., … & Yen, A. (2004). The Spirit rover's Athena science investigation at Gusev crater, Mars. *Science,* 305(5685), 794–799.

Stoica, A., Ingham, M., Tamppari, L., Mitchell, K., & Quadrelli, M. (2014). TransFormers for Extreme Environments. NIAC Phase 1 Final Report. (pp.72). https://www.nasa.gov/sites/default/files/files/Stoica_2013_PhI_Transformers.pdf.

Taylor, L.A., & Meek, T.T. (2005). Microwave sintering of lunar soil: properties, theory, and practice. *Journal of Aerospace Engineering*, 18(3), 188–196.

Taylor, S. R., & McClennan, S. M. (1985). The continental crust: Its composition and evolution and examination of the geochemical record preserved in sedimentary rocks (p. 312). Blackwell Scientific Publication.

The Hague International Space Resources Working Group. (2019). Building Blocks for the Development of an International Framework on Space Resources Activities. https://www.universiteitleiden.nl/binaries/content/assets/rechtsgeleerdheid/instituut-voor-publiekrecht/lucht--en-ruimterecht/space-resources/hisrgwg_building-blocks-for-space-resource-activities.pdf.

Todd, S. G., Keith, D. W., Le Roy, L. W., Schissel, D. J., Mann, E. L., & Irvine, T. N. (1982). The J-M platinum-palladium reef of the Stillwater Complex, Montana: I. Stratigraphy and petrology. *Economic Geology*, 77(6), 1454–1480.

Toklu, Y., & Järvstråt, N. (2003). Design and construction of a self sustainable lunar colony with in-situ resource utilization. *CE: The Vision for the Future Generation in Research and Applications,* pp. 623–628.

Trigwell, S., Captain, J., Weis, K., & Quinn, J. (2012). Electrostatic beneficiation of lunar regolith: applications in in situ resource utilization. *Journal of Aerospace Engineering,* 26, 30-36.

Tronchetii, F. (2010). Commercial Exploitation of Natural Resources of the Moon and Other Celestial Bodies: What Role for the Moon Agreement? In: *Proceedings of the International Institute of Space Law*, 53, 614–624.

Tronchetti, F. 2008. *The Korean Journal of Air & Space Law and Policy*, 23(1), 131–168.

UNCLOS, United Nations Convention on the Law of the Sea. (1982). 1833 UNTS 397. https://www.un.org/depts/los/convention_agreements/texts/unclos/unclos_e.pdf.

UNEP-WCMC (2019). A Marine Spatial Planning Framework for Areas Beyond National Jurisdiction. Technical document produced as part of the GEF ABNJ Deep Seas Project. Cambridge (UK): UN Environment Programme World Conservation Monitoring Centre. (pp. 1-45.)

UNEP-WCMC and Seascape Consultants Ltd. (2019). Learning form experience: Case studies of Area-Based Planning in ABNJ. Technical document Produced as part of the GEF ABNJ Deep Seas Project. Cambridge (UK):UN Environment World Conservation Monitoring Centre. (pp. 1-88).

United Arab Emirates. (2019). Federal Law No. (12) of 2019 on the Regulation of the Space Sector. https://www.moj.gov.ae/assets/2020/Federal%20Law%20No%2012%20of%202019%20on%20THE%20REGULATION%20OF%20THE%20SPACE%20SECTOR.pdf.aspx

United Nations Agreement Governing the Activities of States on the Moon and Other Celestial Bodies. (1979). 1363 UNTS 3.

United Nations Agreement on the Rescue of Astronauts, the Return of Astronauts and the Return of Objects Launched into Outer Space. (1968). 672 UNTS 119.

United Nations Committee on the Peaceful Uses of Outer Space. (2020). Building blocks for the development of an international framework on space resources activities, A/AC.105/C.2/L.315. https://documents-dds-ny.un.org/doc/UNDOC/LTD/V20/008/95/PDF/V2000895.pdf?OpenElement

United Nations Committee on the Peaceful Uses of Outer Space. (2022). Report of the Legal Subcommittee on its sixtieth session held in Vienna from 31 May to 11 June 2021, A/AC.105/1260. https://documents-dds-ny.un.org/doc/UNDOC/GEN/V22/022/49/PDF/V2202249.pdf?OpenElement

United Nations Convention on International Liability for Damaged Caused by Space Objects. (1972). 961 UNTS 187.

United Nations Convention on the Registration of Objects Launched into Outer Space. (1975). 1023 UNTS 15.

United Nations General Assembly, Committee on the Peaceful Uses of Outer Space. (2022). Report of the Legal Subcommittee on its sixty-first session, held in Vienna from 28 March to 8 April 2022, UN Doc A/AC.105/1260. https://www.unoosa.org/oosa/oosadoc/data/documents/2022/aac.105/aac.1051260_0.html

United Nations General Assembly. (1970). Declaration of Principles Governing the Sea-Bed and the Ocean Floor, and the Subsoil Thereof, beyond the Limits of National Jurisdiction, UN Doc A/RES/2749, http://www.un-documents.net/a25r2749.htm

United Nations General Assembly. (1994). Agreement Relating to the Implementation of Part XI of the United Nations Convention on the Law of the Sea of 10 December 1982, UN Doc A/RES/48/263. https://treaties.un.org/doc/source/docs/A_RES_48_263-E.pdf.

United Nations Treaty on Principles Governing the Activities of States in the Exploration and Use of Outer Space, Including the Moon and Other Celestial Bodies. (1967). 610 UNTS 205.

United States Commercial Space Launch Competitiveness Act, H.R. 2262, 114th Cong. (2015). https://www.congress.gov/bill/114th-congress/house-bill/2262/text

Valle, B. (2023). Guyana to complete new oil contract model by Q2 as auction looms. Reuters, February 14, 2023. Available at: https://www.reuters.com/business/energy/guyana-kicks-off-oil-conference-exxon-mulls-adding-more-blocks-2023-02-14/. Accessed (February 24, 2023).

Vanoutryve, B., De Rosa, D., Fisackerly, R., Houdou, B., Carpenter, J., Philippe, C., Pradier, A., Jojaghaian, A., Espinasse, S., & Gardini, B. (2010). An analysis of illumination and communication conditions near lunar south pole based on Kaguya data. *Proceedings of International Planetary Probe Workshop, Barcelona.* (pp. 1-7).

Vasavada, A. R., Paige, D. A., & Wood, S. E. (1999). Near-Surface Temperatures on Mercury and the Moon and the Stability of Polar Ice Deposits. *Icarus*, 141(2), 179-193.

Vaughan, D., & Corkhill, C. (2017). Mineralogy of sulfides. *Elements*, 13(2), 81–87.

Vaughan, D., & Lennie, A. R. (1991). The iron sulphide minerals: Their chemistry and role in nature. *Science Progress*, 75(3/4), 371–388.

Vondrak, R.R. (1992).. Lunar Base Activities and the Lunar Environment. *2nd Conference on Lunar Bases and Space Activities*, 337-345.

Waldron, R.D. (1990). Lunar Base Power Requirements. *In: Engineering, Construction, and Operations in Space II, ASCE*, 1288–1297.

Wall, M. (2020, December 3). NASA will buy moon dirt from these 4 companies. Space.com. https://www.space.com/nasa-will-buy-moon-dirt-masten-ispace-lunar-outpost

Wänke, H., Dreibus, G., & Wright, I. P. (1994). Chemistry and accretion history of Mars. *Transactions of the Royal Society of London. A*, 349, 285–293.

Watson, K., Murray, B.C. and H. Brown. (1961). The behavior of volatiles on the lunar surface. *Journal of Geophysical Research*, 66(9), 3033–3045.

Watson, K., Murray, B.C., & Brown, H. (1961a). On the possible presence of ice on the Moon. *Journal of Geophysical Research*, 66(5), 1598–1600.

Wedding, L.M., Friedlander, A.M., Kittinger, J.N., Watling, L., Gaines, S. D., Bennett, M., Hardy, S.M., & Smith, C.R. (2013). From principles to practice: a spatial approach to systematic conservation planning in the deep sea. *Proc. R. Soc. B*, 280(20131684), 1-10.

Wedding, L.M., Reiter, S.M., Smith, C.R., Gjerde, K.M., Kittinger, J.N., Friedlander, A.M., Gaines, S.D., Clark, M.R., Thurnherr, A.M., Hardy, S.M., & Crowder, L.B. (2015). Managing mining of the deep seabed. *Science*, 349(6244), 144–145.

Weeden, B.C., & Chow, T. (2012). Taking a common-pool resources approach to space sustainability: A framework and potential policies. *Space Policy*, 28, 166–172.

Wenrich, M.L., & Christensen, P.R. (1996). Optical constants of minerals derived from emission spectroscopy: Application to quartz. *JGR: Solid Earth*, 101(B7), 15921–15931.

West, M. D., & Clarke, J. D. A. (2010). Potential Martian mineral resources: Mechanisms and terrestrial analogues. *Planetary and Space Science*, 58(4), 574–582.

Williams, J. P., Paige, D. A., Greenhagen, B. T., & Sefton-Nash, E. (2017). The global surface temperature of the Moon as measured by the diviner lunar radiometer experiment. *Icarus*, 283, 300–325.

Williams, J.-P., Greenhagen, B.T., Paige, D.A., Schörghofer, D., Sefton-Nash, E., Hayne, P.O., Lucey, P.G., Siegler, M.A., Aye, K.M. (2019). Seasonal Polar Temperatures on the Moon. *JGR Planets*, 124(10), 2502-2521.

Wolfrum, R. (1995). The Decision-Making Process According to Sec. 3 of the Annex to the Implementation Agreement: A model to be Followed for Other International Economic Organisations? *Heidelberg Journal of International Law*, 55, 310-328.

Wood, M.C. (1999). International Seabed Authority: The First Four Years. *Max Planck Yearbook of United Nations Online*, 3(1), 173-241.

Wood, M.C. (2007). The International Seabed Authority: Fifth to Twelfth Sessions (1999-2006). *Max Planck Yearbook of United Nations Law*, 11, 47-98

World Commission on Environment and Development. (1987). Report of the World Commission on Environment and Development: Our Common Future. https://sustainabledevelopment.un.org/content/documents/5987our-common-future.pdf

Wykes, J. L., O'Neill, H. S., & Mavrogenes, J. A. (2015). The effect of FeO on the sulfur content at sulfide saturation (SCSS) and the selenium content at selenide saturation of silicate melts. *Journal of Petrology*, 56(7), 1407–1424.

Yang, F., Xu, Y., Chan, K.L., Zhang, X., Hu, G., & Li, Y. (2019). Study of Chang'E-2 microwave radiometer data in the lunar polar region. *Advances in Astronomy,* 3940837.

Yang, K., Yao, H., Ma, W., Li, Y., & He, G. (2022). A step-by-step relinquishment method for cobalt-rich crusts: A case study on Caiqi Guyot, Pacific Ocean. *Marine Georesources & Geotechnology*, 40(9), 1139–1150.

Zacny, K., Bar-Cohen, Y., Brennan, M., Briggs, G., Cooper, G., Davis, K., et al. (2008). Drilling systems for extraterrestrial subsurface exploration. *Astrobiology*, 8(3), 665–706.

Zacny, K., Betts, B., Hedlund, M., Long, P., Gramlich, M., Tura, K., et al. (2014). PlanetVac: Pneumatic regolith sampling system. *In 2014 IEEE Aerospace Conference*. (pp. 1–7). IEEE.

Zacny, K., Paulsen, G., McKay, C. P., Glass, B., Dav., A., Davila, A. F., et al. (2013). Reaching 1m deep on Mars: The icebreaker drill. *Astrobiology*, 13(12), 1166–1198.

Zalik, A. (2015). Trading on the offshore: territorialization and the ocean grab in the international seabed. In Ervine, K. & G. Fridel (Eds.). Beyond Fair Trade, pp.173–190. London, Palgrave Macmillan.

Zalik, A. (2018). Mining the seabed, enclosing the Area: ocean grabbing, proprietary knowledge and the geopolitics of the extractive frontier beyond national jurisdiction. *International Social Science Journal,* 68(229-230), 343–359.

Zelenyi, L.M., Zakharov, A.V., Kuznetsov, I.A., & Shekhovtsova, A.V. (2021). Moondust As a Risk Factor in Lunar Exploration. *Herald of the Russian Academy of Sciences,* 91:637–646.

Zhang, J.A., & Paige, D.A. (2009). Cold-trapped organic compounds at the poles of the Moon and Mercury: Implications for origins. *Geophysical Research Letters,* 36(L16203), 1-5.

Zhang, T., Xu, K., Yao, Z., Ding, X., Zhao, Z., Hou, X., et al. (2019). The progress of extraterrestrial regolith-sampling robots. *Nature Astronomy,* 3(6), 487–497.

Zientek, M. L. (2012). Magmatic ore deposits in layered intrusions–descriptive model for reef-type PGE and contact-type Cu-Ni-PGE deposits. *U.S. Geological Survey Open-File Report 2012-1010* (pp. 1–48).

Zientek, M. L., Czamanske, K., & Irvine, T. N. (1985). Stratigraphy and nomenclature for the Stillwater Complex. In G. K. Czamanske & M. L. Zientek (Eds.), *The Stillwater Complex, Montana: Geology and guide. Special publication 92* (pp. 21–38).

Zientek, M. L., Loferski, P. J., Parks, H. L., Schulte, R. F., & Seal II, R. R. (2017). Platinum-group elements, chap. N of Schulz. In K. J. Schulz, J. H. DeYoung Jr, R. R. Seal II, & D. C. Bradley (Eds.), *Critical mineral resources of the United States—economic and environmental geology and prospects for future supply (pp. N1–N91). U.S. Geological Survey. Professional Paper 1802*. https://doi.org/10.3133/pp1802N

APPENDIX A

SUPPLEMENTAL FIGURES AND TEXT FOR CHAPTER 2

Supporting Information for **Thermal infrared Emission Spectroscopy of Graybody Minerals (Sulfide): Implications for Extraterrestrial Exploration for Magmatic Ore Deposits.**

Kevin M. Hubbard,[1†] Christopher W. Haberle[2], Linda T. Elkins-Tanton[1], Phillip R. Christensen[1] and Steven Semken[1]

[1]Arizona State University – School of Earth and Space Exploration.
[2]Northern Arizona University – Department of Astronomy and Planetary Science.
[†]Corresponding author. E-mail: kmhubz1@gmail.com

Text S1.

Because a blackbody does not produce reflected energy, it is unaffected by energy from the environmental chamber. However, fluctuations in environmental temperature can produce errors in emissivity for non-blackbody emitters, particularly low-emissivity materials such as pyrrhotite. For example, Ruff et al. (1997) demonstrate that a systematic error of the environmental temperature (0.3°C) produces an emissivity error of ~0.5% for a synthetic graybody. Thus, the stability of our sample was monitored to ensure that the environment remained isothermal. The environmental temperature was monitored by sampling the chamber temperature every ten seconds during a measurement session using a Keithley multimeter. Figure S1 shows the distribution of 1562 temperature measurements of the environmental chamber collected over nine days when a sample (quartz, forsterite, or sulfide) was present in the chamber. The temperature measurements were collected using a thermocouple connected to a Keithley multimeter every ten seconds.

Despite the sample heater operating at a temperature set point (393.15K) much higher than any other experiment previously conducted in the ASU spectral laboratory, the chamber's average temperature of 300.00K had a standard deviation of only 0.4 K,

demonstrating that the chamber effectively remains an isothermal source of energy regardless of the fact that the new sample heater emits a significant amount of energy.

To further illustrate the temperature conditions within the blackbody chamber during measurement, Figure S2 shows the environmental temperature during three back-to-back measurements of the J–M Reef sulfide sample. Between measurements, the sample was removed from the sample cup and left to equilibrate with the lab environment before being re-poured into the sample cup. This was done to ensure that the environmental chamber was at the same temperature each time before inserting a sample into the chamber and to ensure that the sample was at the same temperature before the pre-heating step described in the manuscript.

The average temperature of the environment during each sulfide measurement was 27.16 °C, 27.27 °C, and 27.24 °C. Combining all three measurements, the mean and standard deviation is 27.22 ± 0.4°C respectively, revealing the stability of the environmental chamber when using the new sample heater.

The average temperature of the environment during each sulfide measurement was 27.16 °C, 27.27 °C, and 27.24 °C. Combining all three measurements, the mean and standard deviation is 27.22 ± 0.4°C respectively, revealing the stability of the environmental chamber when using the new sample heater.

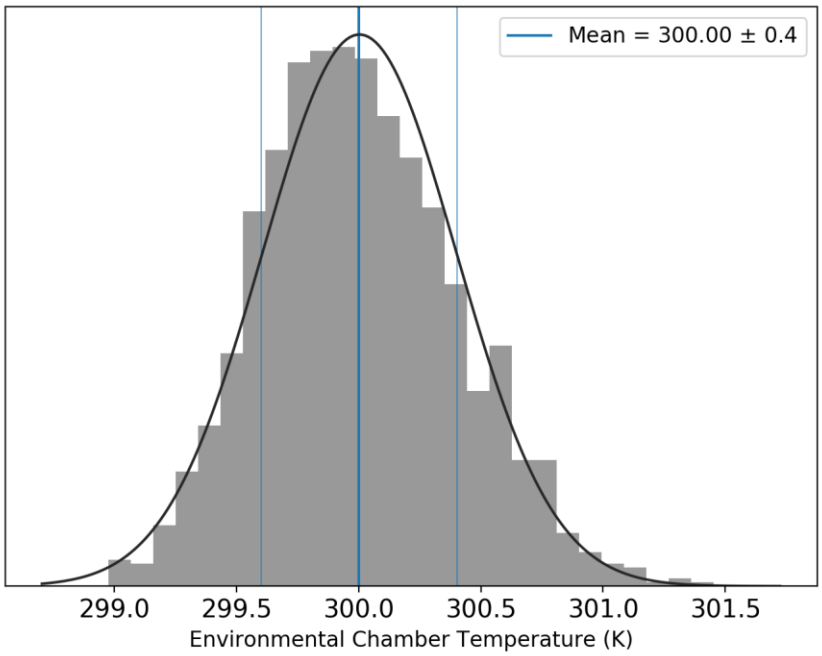

Figure S2.1 – The distribution of the environmental chamber temperature during measurements over the course of nine days. The figure demonstrates that regardless of the sample, the temperature of the chamber remains stable.

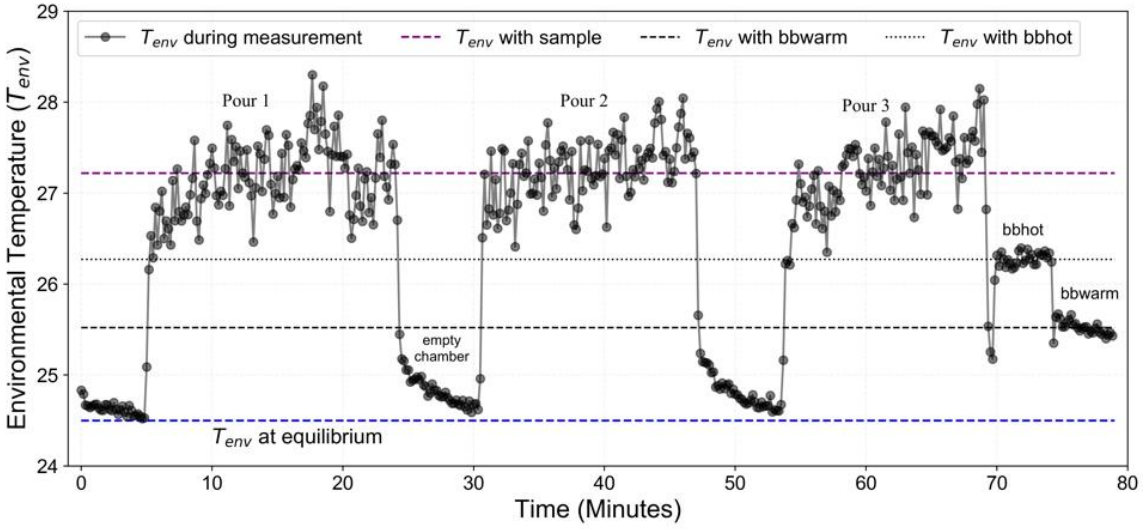

Figure S2..2 - Monitoring the environmental temperature (T_{env}) throughout the course of a measurement session. The session mean temperature (purple dashed line) and standard deviation for all three pyrrhotite measurements is 27.2°C +/- 0.4°C. The average temperature of the sample chamber during each pyrrhotite measurement is 27.27°C (Pour 1), 27.24°C (Pour 2), and 27.22°C (Pour 3), revealing the stability of the environmental temperature when using the new sample heater. The horizontal blue dashed line represents the chamber temperature at equilibrium, the dotted and dashed gray lines

represent the average temperature of the chamber during measurement of the warm and hot blackbody target.

APPENDIX B

SUPPLEMENTAL FIGURES AND TEXT FOR CHAPTER 4

Table S4.1 – Number of pixels within each block for each data set used to construct the Lunar Mining Map Tool. The average maximum summer temperature data was compiled by Williams et al. (2019) derived from 10 years of Diviner data. The Earth visibility and illumination data are derived from data obtained by the Lunar Orbiter Laster Altimeter (LOLA) and compiled by Mazarico et al. (2011). The slope layer was produced by ASU personnel from resampled, interpolated data from LOLA.

Average Maximum Summer Temperature*										
Number of Pixels	0	1	2	3	4	5	6	7	8	9
Count	39	157	201	296	5968	249	70033	157	287	210755
Average Percent Earth Visibility										
Number of Pixels	16	20	25							
Count	211	15429	272502							
Average Percent Illumination										
Number of Pixels	16	20	25							
Count	211	15429	272502							
Average Slope										
Number of Pixels	1156	1190	1225							
Count	63292	144251	80599							

*While a nearly all of the blocks in the Lunar Mining Map Tool contain either 4, 6, or 9 DIVINER pixels to estimate their potential to harbor water ice, a small percentage (< 0.6%) of blocks contain between 0 and 3 pixels as well as five, seven, and eight pixels. These blocks are all located at -80°S latitude and are likely a result of the maps construction.

APPENDIX C

AUTHOR PERMISSION FOR USE OF PUBLISHED MATERIAL FOR CHAPTER 2

Linda Elkins-Tanton, Philip Christensen, Chris Haberle, and Steven Semken has granted permission for the use of co-authored materials in this dissertation.

APPENDIX D

AUTHOR PERMISSION FOR USE OF PUBLISHED MATERIAL FOR CHAPTER 5

Kevin Hubbard <kmhubba1@asu.edu>

Use of a figure in your 2018 paper

Kathryn Miller <kmiller@greenpeace.org> Fri, Mar 3, 2023 at 1:13 PM
To: Kevin Hubbard <kmhubba1@asu.edu>

Hi Kevin,

Thanks for your email. I'm delighted to hear that you would like to use the figure, yes, you are permitted to use this under the Creative Commons licence. So, as long as you include a citation to the original paper as you would for a text citation, together with a link to the Creative Commons site then you're good to go. Please let me know if you need any more assistance regarding the citation or content of the paper.

I hope all goes well with your research – it sounds very interesting.

With best wishes,
Kathryn

Kathryn Miller
Science consultant
Greenpeace Research Laboratories
College of Life and Environmental Sciences
University of Exeter
Devon EX4 4RN
UK

[Quoted text hidden]

Kevin Hubbard <kmhubba1@asu.edu>

Permission to reuse content from your paper published in Marine Georesources & Geotechnology

yangkh@sio.org.cn <yangkh@sio.org.cn> Mon, Apr 3, 2023 at 8:50 PM
To: Kevin Hubbard <kmhubba1@asu.edu>

It is OK. Wish you all the best!

Kehong Yang

At 2023-04-04 06:01:46, "Kevin Hubbard" <kmhubba1@asu.edu> wrote:

> Hello,
>
> My name is Kevin Hubbard, a PhD Candidate at Arizona State University. In one of the chapters in my dissertation, I am writing about potential ways to govern mining on the Moon and use seabed mining as an analog. In my paper, I point out the International Seabed Authority's relinquishment process as a potential way to manage mining on the Moon. Your paper has great schematics depicting the relinquishment process Thus, I was hoping that you all would grant me permission to reuse the figures that I have attached here to help me describe the process of relinquishment. I will make sure that the figures are properly cited.
>
> I also reached out to the publisher. and it appears that it is okay to reuse the figures, so long as I submit another request before publishing the work elsewhere, but I wanted to reach out to you all just in case.
>
> All the best, and thank you for your time,
> Kevin Hubbard